CENTRO INTERNACIONAL DE ESTUDOS
DE DOUTORAMENTO E AVANZADOS
DA USC (CIEDUS)

TESIS DOCTORAL

SUPRAMOLECULAR STRATEGIES FOR INTRACELLULAR DELIVERY AND DESIGN OF NEW THERMORESPONSIVE MATERIALS

Héctor Fernández Caro

ESCUELA DE DOCTORADO INTERNACIONAL

PROGRAMA DE DOCTORADO EN CIENCIA Y TECNOLOGÍA QUÍMICA

SANTIAGO DE COMPOSTELA

AÑO 2020

USC
UNIVERSIDADE
DE SANTIAGO
DE COMPOSTELA

DECLARACIÓN DEL AUTOR DE LA TESIS

SUPRAMOLECULAR STRATEGIES FOR INTRACELLULAR DELIVERY AND DESIGN OF NEW THERMORESPONSIVE MATERIALS

Para defensas telemáticas

D. Héctor Fernández Caro

Presento mi Tesis, siguiendo el procedimiento adecuado al Reglamento, y declaro que:

1) La Tesis abarca los resultados de la elaboración de mi trabajo.
2) De ser el caso, en la Tesis se hará referencia a las colaboraciones que tuvo este trabajo.
3) La Tesis es la versión definitiva presentada para su defensa y coincide con la versión enviada en formato electrónico.
4) Confirmo que la Tesis no incurre en ningún tipo de plagio de otros autores ni de trabajos presentados por mí para la obtención de otros títulos.

Y me comprometo a presentar el ejemplar impreso de la Tesis en el plazo de un mes desde que la EDIUS me lo requiera, así como del Compromiso Documental de Supervisión en el caso que el original no esté depositado en la Escuela.

En Santiago de Compostela, ... de ..... de 2020

Fdo. Héctor Fernández Caro

USC
UNIVERSIDADE
DE SANTIAGO
DE COMPOSTELA

AUTORIZACIÓN DEL DIRECTOR/ TUTOR DE LA TESIS

SUPRAMOLECULAR STRATEGIES FOR INTRACELLULAR DELIVERY AND DESIGN OF NEW THERMORESPONSIVE MATERIALS

D. Juan Ramón Granja Guillán
D. Javier Montenegro García

INFORMAN:

Que la presente Tesis se corresponde con el trabajo realizado por D. Héctor Fernández Caro, bajo nuestra dirección, y autorizamos su presentación, considerando que reúne los requisitos exigidos en el Reglamento de Estudios de Doctorado de la USC, y que como directores de esta no incurre en las causas de abstención establecidas en la Ley 40/2015.

En Santiago de Compostela, ... de ..... de 2020

Fdo. Juan Ramón Granja Guillán

Fdo. Javier Montenegro García

USC
UNIVERSIDADE
DE SANTIAGO
DE COMPOSTELA

Agradecimientos

En primer lugar, me gustaría expresar mi enorme agradecimiento a los directores de esta Tesis doctoral, Javier Montenegro y Juan R. Granja. Gracias por darme esta oportunidad y permitir que todo esto haya sido posible.

A Javier Montenegro, por darme la oportunidad de formar parte de este proyecto. Gracias por trasmitirnos día tras día tu pasión por la investigación, por tus multiples enseñanzas para poder desarrollar investigación de alta calidad y por tu apoyo a nivel personal en los momentos difíciles. Todavía recuerdo mis inicios cuando me enseñabas a hacer mis primeras columnas cromatográficas. Sin duda, todo lo conseguido ha sido fruto de innumerables horas de trabajo, esfuerzo y aprendizaje. Gracias por confiar en mí.

A Juan R. Granja, por tus innumerables enseñanzas, ideas para mejorar el desarrollo de los proyectos y discusiones científicas en los seminarios. Por transmitirnos tu enorme rigor científico y por enseñarnos y demostrarnos los valores que debe cumplir un excelente investigador y profesor. Por enseñarnos que de los errores también se aprende. Muchas gracias.

Agradecer a la Xunta de Galicia la concesión de mi beca predoctoral (ED481A-2017/047) que me ha permitido desarrollar esta Tesis doctoral y por haberme dado la oportunidad de realizar una estancia predoctoral en Northwestern University. Además, también me gustaría dar las gracias a todas las instituciones que han financiado la labor investigadora del grupo durante estos años.

A Alejandro Méndez, por todo lo que me has enseñado. Por poseer esa capacidad para reconducir los proyectos y para hacer que lo difícil parezca fácil. A Irene Lostalé, por enseñarme a hacer los primeros experimentos en células y explicarme todo lo necesario para poder entender la parte biológica de los proyectos. A Julián Bergueiro, por confiar en mí y permitirme aprender de tí, día tras día, en los distintos proyectos que compartimos. Muchas gracias.

A los doctores Manuel Amorín, Rebeca García-Fandiño y al prof. Luis Castedo. Por las interesantes discusiones científicas durante los seminarios de grupo. A Patricia Lago, por tu por tu ayuda y amabilidad a la hora de resolver cualquier tipo de gestión.

Al prof. Nathan Gianneschi por haberme brindado la oportunidad de realizar una estancia en su grupo de investigación en Northwestern University, Evaston, Illinois. A Andrea S. Carlini, Mollie A. Touve, Matthew P. Thompson, Wei Cao, Mary F. Cassidy, Spencer Burton, Claudia Battistella, Hao Sun, Chris Forman, Wonmin Choi y al resto del grupo por haberme ayudado a crecer como investigador y acompañarme en esta gran experiencia.

Al prof. Jose Luis Mascareñas por sus ideas, consejos y ayuda en el desarrollo del proyecto. A Miguel Martínez-Calvo por su ayuda en la preparación de los transportadores y, también, a Jesús Mosquera. Al prof. Jonathan R. Nitschke y su grupo de investigación por la preparación de la caja supramolecular.

A Rebeca Menaya-Vargas por su ayuda con los cultivos celulares y su enorme interés y dedicación para que todo salga siempre a la perfección.

A la RIAIDT de la Universidad de Santiago de Compostela por poner a mi disposición sus medios técnicos para el correcto desarrollo de esta Tesis doctoral. En especial me gustaría destacar a Esteban Guitián por todos los análisis de espectrometría de masas realizados. Además, me gustaría agradecer a todo el personal técnico del CIQUS, en especial a Arcadio, Laura, Pablo y Noela.

Me gustaría agradecerle enormemente a todas/os y cada una/o de mis compañeras/os de laboratorio, que después de todo este tiempo, tengo el placer de, a muchas/os, poder llamarlas/os amigas/os.

A Ale, creo que ninguna palabra puede agradecer todo lo que has hecho por mí durante estos años, ya no solo todo lo que me has enseñado en el laboratorio, sino como amigo, me has hecho reir, has sabido comprenderme y animarme en todo momento. Eres una persona y un amigo impresionante y te deseo todo lo mejor porque te lo mereces.

A Alfonso, gracias por recorrer este duro camino conmigo. Pienso en el pasado y recuerdo millones de buenos momentos, chistes, risas, viajes, fiestas, festivales, conversaciones en el desierto. Pero, sin duda, lo que nos ha hecho ser grandes amigos es el mantenernos unidos y animarnos en los malos momentos. Muchas gracias por todo, mago.

A Marisa, por enseñarme y cuidarme desde que llegué al laboratorio y ayudarme a confiar en el péptido. Marisa, confía en el péptido. A Juanillo, por enseñarme en los inicios y querer siempre lo mejor para mí. A Iván, por todos esos abrazos y animos reconfortantes, por las gominolas a últimas horas de la tarde.

A Jose Juan ¨Josete¨, por ayudarme cuando las cosas no salían, por hacerme reir día a día, por aconsejarme como a un hijo, por tu forma de aplicar matemáticas. A Marta, por acompañarme en este camino y permitirme observar en primera persona la gran investigadora en la que te has convertido. A Irene, por ayudarnos siempre en todo lo necesario, por tus bromas.

A Alberto, por tus millones de consejos, por ayudarme con el proyecto inicial y con muchas otras cosas, por contarnos miles de veces la misma historia, haciéndonos creer, a veces, que tu eras el protagonista, por los partidos de padel mañaneros. A Álvaro, por ser parte del grupo, por nuestras comiditas y cafecitos, por proporcionarnos siempre cualquier reactivo.

A Julián, por crear en menos de un segundo millones de ideas para millones de nuevos proyectos, por confiar en mí para los nuevos proyectos, por tener siempre un chiste malo para compartir. A Geert, por llegar al laboratorio todos los días con una sonrisa. También a Mariette, gracias por tu enorme generosidad. A Rebe, por tus ganas de aprender y por suministrarme chocolate en tiempos de escritura. También, a Jose María.

A Lamas, por todos los grandes momentos compartidos, por demostrarnos como se hace un buen revés en tenis. A Nacho, por las clases prácticas, por las risas y bromas compartidas, por tus inesperados lanzamientos de pipas. A Giulia, por todas las conversaciones, por enseñarnos italiano, por organizar las mejores cenas y fiestas. A Martín Calvelo, por todas las anécdotas graciosas que vivimos, por formar parte del equipo trámite.

A Evita, por todas las conversaciones de camino al trabajo, aunque, a veces, te quedases dormida, por tu apoyo y tus enseñanzas. A Ángel, por tu bondaz, tu esfuerzo y dedicación que me han enseñado que todo esfuerzo, al final, tiene su recompensa. A Vicky, por irradiar esa alegría característica. A Fede, por tu generosidad, espero que todo vaya increíble en tu nueva etapa. A Alicia, por ser una magnifica vecina de vitrina. A Iria, por ayudarme en los inicios. A los más jóvenes, Sandra, Marcos, Ezequiel, Antía, Charlene etc. estoy seguro que os irá muy bien. A Richard, Ghibom y a Sahnawaz, por todos los momentos compartidos.

Además, también, a todos los compañeros de otros grupos de investigación, en especial a Jaime, por animarme día tras día, por esperarme mientras acababa los experimentos antes de ir a entrenar, por ser el gran capitán. También a Felipe, por recibirme siempre con una sonrisa y algo nuevo que contar, por compartir tu sabiduría. A Tomás Pose, por animarme siempre a

superar mis limites, por los maratones nocturnos a la ciudad de la cultura y vuelta. A Jacobo, a David y a Marc, por todas las charlas siempre divertidas. A Bea, por tratarme siempre tan bien.

A todas las demás personas que han contribuído en mayor o menor medida al desarrollo de este período de mi vida y no los haya citado anteriormente. Todas estas personas han aportado su granito de arena, tanto dentro como fuera del laboratorio, en esta Tesis. Muchísimas gracias a todos.

Entrando en un ámbito más personal, me gustaría agradecerle todos los animos recibidos y experiencias vividas a todos mis amigos/as durante estos años.

A mis amigos que conocí hace ya muchos años en la universidad y todavía forman parte de mi vida. En especial voy a destacar a los pilares básicos en mi vida:

A Andrea, por acompañarme en mi desarrollo como investigador y, a la vez, personal, por hacer evaporarse todos los problemas con un par de palabras, por tu empuje y motivación durante todos estos años.

A Bustelo, por ser el claro ejemplo de optimismo y transmitírselo a toda la gente que te rodea. Tengo suerte de tenerte cerca.

A Martín, por acudir al rescate siempre que lo necesito y hacerme reir hasta más no poder.

A Reims, por comprenderme y aconsejarme, a Rocío, a Nerea y a Andrea López por su apoyo continuado.

A mis amigos de toda la vida, en especial a Rica. Siempre dispuestos a aconsejarme, ayudarme y vivir nuevas experiencias. Por muchos años que pasen conservamos nuestra amistad y eso es un auténtico tesoro. A mis compañeros/amigos del equipo de fútbol, que me permitisteis liberar todas las tensiones del doctorado y llegar a formar parte de vuestra ¨familia¨. A Carliños, por tratarme tan bien y enseñarme tanto inglés.

A Jorge, por convertirte en una pieza muy importante en mi vida, por recorrer el mundo conmigo, por querer siempre lo mejor para mí, por regarlarme siempre los mejores consejos.

A Sara, gracias por transmitirme todos los días tus ganas de vivir y tu alegría, por convertirte en la perfecta compañera de aventuras, experiencias y viajes, por tirar de mi cuando las cosas no salen bien, por hacer que este baile valga la pena. Gracias por todo lo vivido, ha sido apasionante. Me alegra pensar todo lo que nos queda por vivir. Agradecer, también, a Ana, César y Anita todo el apoyo que me habéis brindado y por tratarme siempre tan bien.

Por último, me gustaría dedicarle unas líneas a mi familia por apoyarme y animarme en todo momento. A mis abuelos, en especial a mi abuela Lola, que me demuestra día a día que la edad no importa sino las ganas de vivir. A mi sobrino Álvaro, que desde que llegó a la familia, nos ha proporcionado un enorme soplo de aire fresco. A Luis. A mi hermana, Jessica, siempre dispuesta a ayudarme y, sin duda, uno de mis grandes apoyos en la vida. A mis padres, por avanzar en tiempos en los que sólo estudiaban algunos privilegiados, por prometerse, hasta conseguirlo, que sus hijos, al revés que ellos, podrían ir a la universidad y por formar esta familia de la cual estoy tan orgulloso. Gracias por tanto.

USC
UNIVERSIDADE
DE SANTIAGO
DE COMPOSTELA

USC
UNIVERSIDADE
DE SANTIAGO
DE COMPOSTELA

Abbreviations

δ	chemical shift (ppm)
ζ	zeta
λ_{em}	emission wavelength
λ_{ex}	excitation wavelength
Aa	amino acid
Abs	absorbance
Ac	acetyl
Ad	adamantane
ACPPs	activable cell-penetrating peptides
ACN	acetonitrile
AFM	atomic force microscope
Ahx	6-aminohexanoic acid
Ala	alanine
anti-EGFR	anti-epidermal growth factor receptor
Arg	arginine
ATRP	atom transfer radical polymerization
AuNPs	gold nanoparticles
BCECF	2′,7′-Bis(2-carboxyethyl)-5(6)-carboxyfluorescein
BCECF-AM	2′,7′-Bis(2-carboxyethyl)-5(6)-carboxyfluorescein acetoxymethyl ester
Boc	*tert*-Butoxycarbonyl
br s	broad singlet
^{13}C-NMR	^{13}C nuclear magnetic resonance
CA	calixarene
calcd	calculated
CB	cucurbituril
β-CD	*β*-cyclodextrin
CD	circular dichroism
CDs	cyclodextrins
β-CD@AuNPs	*β*-cyclodextrin-modified AuNPs
CD@AuNPs	cyclodextrin-modified AuNPs

CDP	cyclodextrin-containing polymer
CF	carboxyfluorescein
CP	cyclic peptide
CPPs	cell-penetrating peptides
CPT	camptothecin
CRISPR	clustered regularly interspace short palindromic repeats
CTC	2- chlorotrityl chloride
d	doublet
DCM	dichloromethane
DLS	dynamic light scattering
DNA	deoxyribonucleic acid
DMEM	Dulbecco's Modified Eagle Medium
DMSO	dimethylsulfoxide
DIEA	N, N-Diisopropylethylamine
DMF	N, N-Dimethylformamide
DP	degree of polymerization
DYN	dynasore
E_9	nona-L-glutamic acid
EDC	1-ethyl-3-(3-dimethylaminopropyl)carbodiimide hydrochloride
EDTA	ethylenediaminetetraacetic acid
EBPs	elastin-based polymers
EBPPA	elastin-based side-chain helical poly(phenylacetylene)
ELPs	elastin-like polypeptides
EPR	enhanced permeability and retention
EYPG	egg yolk phosphatidylglycerol
Fab′	antigen-binding fragment
FBS	fetal bovine serum
FDA	food and drug administration
FITC	fluorescein isothiocyanate
Fmoc	9- Fluorenylmethoxycarbonyl
FRET	fluorescence resonance energy transfer
FSC	forward scatter channel
Gln	glutamine

Gly	glycine
Glu	glutamic acid
GSH	glutathione
^{1}H-NMR	proton nuclear magnetic resonance
HEPES	4-(2-hydroxyethyl)-1-piperazineethanesulfonic acid
HFIP	1,1,1,3,3,3-hexafluoro-2-propanol
His	histidine
HKR	HEPES-Krebs-Ringer buffer
HPLC-MS	high-performance liquid chromatography coupled with mass spectrometry
HPTS	8-hydroxypyrene-1,3,6-trisulfonic acid (pyranine)
HR-MS	high-resolution mass spectrometry
ICP-MS	inductively coupled plasma mass spectrometry
J	coupling constant
K_a	affinity constant
K_d	dissociation constant
LCST	lower critical solution temperature
Leu	leucine
Lys	lysine
m	multiplet
MeOH	methanol
MES	2-(N-morpholino)ethanesulfonic acid
mRNA	messenger RNA
MS	mass spectrometry
MTT	(3-(4,5- dimethylthiazol-2-yl)-2,5-diphenyltetrazolium bromide) tetrazolium;
Mtt	4-methyltrityl
N-HATU	N-[(Dimethylamino)-1H1,2,3-triazolo[4,5-b]pyridine 1ylmethylene]-N-methylmethanaminium-hexafluorophosphate N-oxide;
N-HBTU	N-[(1HBenzotriazol-1-yl)-(dimethylamino)methylene]-N-methylmethanaminium hexafluorophosphate N-oxide
NHS	N-hydroxysuccinimide

NMR	nuclear magnetic resonance
NPs	nanoparticles
O2Oc	8-amino-3,6-dioxaoctanoic acid
PAMAM	polyamidoamine dendrimers
Pbf	2,2,4,6,7-Pentamethyldihydrobenzofuran-5-sulfonyl
PBS	phosphate-buffered saline
Phe	phenylalanine
pDNA	plasmid DNA
PEG	polyethylene glycol
PEI	polyethyleneimine
PNAs	peptide nucleic acids
PNA-AuNPs	polyvalent nucleic acid capped AuNPs
PNIPAM	poly(*N*-isopropylacrylamide)
POEG	poly(oligoethyleneglycol)
Ppm	parts per million
Pro	proline
PyAOP	(7-Azabenzotriazol-1-yloxy) tripyrrolidinophosphonium hexafluorophosphate;
PVCL	poly(N-vinlycaprolactam)
RAFT	reversible addition−fragmentation chain-transfer
R_4	tetraarginine
R_8	octaarginine
RGD	arginine-glycine-aspartic acid peptide
RP-HPLC	reversed-phase high-performance liquid chromatography
R_t	retention time
s	singlet
SD	standard deviation
Ser	serine
SCID	severe combined immunodeficiency
SCPNs	self-assembling cyclic peptide nanotubes
siRNA	small interfering RNA
sgRNA	single guide RNA
shRNA	small hairpin RNA

SPNs	supramolecular nanoparticles
SPPS	solid-phase peptide synthesis
t	triplet
TAMRA	5-carboxytetramethyl rhodamine
T_{CP}	cloud point temperature
TEM	transmission electron microscopy
TF	transcription factor
TFA	trifluoroacetic acid
TFE	trifluoroethanol
TFRC	transferrin receptor
TGA	thermogravimetric analysis
TIS	triisopropylsilane
TNF	tumor necrosis factor
TRAIL	tumor necrosis factor-related apoptosis-inducing ligand
UCST	upper critical solution temperature
uHPLC	ultra-high performance liquid chromatography
UV-vis	ultraviolet-visible
Val	valine

USC
UNIVERSIDADE
DE SANTIAGO
DE COMPOSTELA

Summary

Synthetic organic chemistry has played a key role in the development of novel strategies for obtaining chemically functional compounds. Despite the great advance that organic synthesis has undergone in the last decades, covalent strategies present intrinsic limits for achieving structures with larger dimensions such as architectures commonly found in Nature, such as those formed by the assembling of proteins. The preparation of these complex molecules by only using strategies based on the formation of covalent bonds is almost unapproachable from the point of view of time and human effort required together with the lack of appropriated synthetic strategies. Additionally, certain collective phenomena such as self-organization require the coordinated interaction between different chemical entities, which is outside the scope of traditional covalent chemistry. Accordingly, a novel discipline coined supramolecular chemistry emerged in the 70-80's. This field was first defined by Jean-Marie Lehn as ¨the chemistry beyond the molecule¨. This discipline focuses on the study of interactions between different chemical entities through non-covalent interactions, which include Van de Waals forces, hydrogen or halogen bonding, ion-ion/dipole, dipole-dipole, cation or anion π interactions, or π-π interactions. This strategy allows the construction of extremely complex three-dimensional structures from synthetically simple precursors. Furthermore, the use of supramolecular chemistry confers to these structures many different advantages such as reversibility, self-healing, or adaptive response to different stimuli. For the preparation of novel supramolecular systems mainly two processes have been explored the molecular recognition and self-assembly. Molecular recognition has been defined as the specific binding of a guest entity to a complementary host molecule to generate a host-guest complex by using non-covalent interactions. Importantly, in some examples, host-guest binding constants have reached values almost comparable to covalent bonds. However, these host-guest complexes still maintain the advantages that offer the use of supramolecular chemistry. A relevant example in this sense is the molecular recognition of biotin by the protein, streptavidin. On the other hand, self-assembly has been defined as a process by which a non-organized system of molecular components, or a part of a molecule, as a consequence of non-covalent interactions, spontaneously generates an organized structure. Nature has also used molecular self-assembly to achieve complex and functional structures such as the double helix structure of DNA, the assembly of the tobacco mosaic virus, or the construction of lipid membranes. Since the day of its inception to nowadays, supramolecular systems have gained momentum in the development of functional materials, such as diverse delivery and thermoresponsive systems.

In this Ph.D. dissertation, we have applied supramolecular strategies to promote intracellular delivery of diverse molecules and design potential thermoresponsive systems. Host-guest chemistry has been exploited to encapsulate and deliver different anionic probes such as pyranine, as well as anionic peptides with low self-delivery efficiency. Finally, we have designed potential thermoresponsive supramolecular materials based on self-assembling cyclic peptide nanotubes (SCPNs).

During the last decades, new promising therapeutic and diagnostic molecules have been synthesized. However, some of these molecules presented limitations to cross the cellular membrane. To overcome this problem, a wide range of cell delivery systems have been described to promote the intracellular internalization of different entities such as therapeutic nucleic acids, proteins, or small molecules such as drugs or fluorescent probes. Different examples of delivery systems commonly used to internalize biologically important

macromolecules and small molecules are liposomes, polymers, or metal nanoparticles. A relevant example of promising delivery vehicles is cell-penetrating peptides (CPPs). These peptides are small-sized peptides that showed impressive capabilities for internalizing a wide variety of membrane-impermeable therapeutic and diagnostic macromolecules and also small molecules into the cell cytosol. CPPs with different physicochemical properties have been described such as cationic, hydrophobic, or amphipathic. Some relevant examples of widely studied CPPs are penetratin, TAT, octaarginine, MPG, or PEP-1. During the last decades, different designs and structural modifications have been explored to improve the translocation capabilities of these molecules. An innovative strategy used to prepare new CPPs has been the formation of dynamic bonds such as oxime, hydrazone, or disulfide bonds. This strategy allowed to prepare a library of CPPs in a short period of time, larger quantities, and high yields. For instance, in our group, we have used the alcoxyamine group for attaching different electrophilic aldehydes and to achieve the easy modulation of the properties of the model CPP. Moreover, our group has also explored the hydrazide group for the incorporation of different hydrophobic aldehydes such as oleic acid into the CPP scaffold. It was found that this modification importantly improved the translocation of a pseudohelical model peptide. The incorporation of the cargo into the delivery system has been achieved mainly by applying covalent or non-covalent supramolecular strategies. Covalent attachment of the cargo has been traditionally used for the preparation of the drug-delivery system entity. On the other hand, supramolecular methodologies have shown important advantages such as improvement of cargo release and reduction of the synthetic effort. For instance, cell-penetrating peptides have been non-covalently attached to therapeutic proteins such as Cas9 ribonucleoprotein, nucleic acids such as siRNA or plasmid DNA, and small molecules such as drugs or probes.

In the first chapter of this thesis, we have developed a novel generation of highly efficient and biocompatible supramolecular vehicles for the transport of molecular probes inside living cells. Negatively charged molecular probes such as pyranine or Alexa dyes are of interest for probing the intracellular space. However, the inefficient transport of these promising molecules across the plasma membrane, due to the repulsive interactions between molecular probes and the cellular membrane, currently remains a fundamental limitation. To overcome this problem, we have demonstrated that a hybrid system composed of a membrane-impermeable supramolecular cage and a covalently anchored tetraarginine peptide can be exploited for the cytosolic delivery of negatively charged fluorophores to different cell lines (HeLa and Vero cells). The supramolecular cage **C** used for the preparation of these carriers shows a trisbipyridyl structure and, in a previous report by prof. Nitschke group, demonstrated to encapsulate with high-affinity different anions of large sizes, such as pyranine, in an aqueous environment. Based on these previous results, we prepared acetylated and fluorescently labeled (TAMRA) R_4 peptides by using solid-phase peptide synthesis, and then the cationic supramolecular cage **C** was coupled by standard conditions for amide bond formation to generate delivery agents $^{Ac}\boldsymbol{R_4}\mathbf{C}$ and $^{Tm}\boldsymbol{R_4}\mathbf{C}$. Fluorescence experiments showed supramolecular complexation between these hybrid vectors and pyranine probe, with calculated dissociation constants of K_d = 189 nM and K_d = 12.6 µM, respectively. In previous reports by the group of prof. Matile, *in vitro U*-tube experiments showed the ability of different molecules to act as carriers. In this experiment, chloroform was placed at the bottom of a *U*-tube, and two different aqueous buffers were added at both sides of the organic phase (*cis* and *trans* buffers). Then, the transference from *cis* to *trans* buffer was monitored. To assess transport across the model apolar organic solvent -chloroform-, we carried out *in vitro U*-tube experiments in the presence of naturally occurring phospholipids. Time-dependent fluorescence measurements indicated that the peptide-cage carrier $^{Ac}\boldsymbol{R_4}\mathbf{C}$ favored the transport of pyranine probe from *cis* to *trans* aqueous

phase. After a period of 12 h, the *trans* aqueous phase contained 4 times more pyranine dye when the peptide carrier was used in comparison with control experiments. This indicated that the peptide-cage carrier $^{Ac}\boldsymbol{R_4}\mathbf{C}$ acts as a carrier of the pyranine probe across the bulk apolar layer. Delivery experiments with pyranine-complexed to $^{Ac}\boldsymbol{R_4}\mathbf{C}$ and $^{Tm}\boldsymbol{R_4}\mathbf{C}$ showed cytosolic release in HeLa and Vero cells. Competition assays in the presence of a competing molecular probe (TAMRA) showed that $^{Tm}\boldsymbol{R_4}\mathbf{C}$ was able to selectively internalize pyranine into the cytosol by endocytosis. This mechanism of entry was confirmed by experiments in the presence of endocytosis inhibitors and by observing pyranine-carrier colocalization by confocal microscopy experiments. We confirmed the integrity of the cellular membrane in the pyranine transport by nuclear staining. In these experiments, after the transport experiments with the probe, we incubated the cells with DAPI and also with propidium iodide, probes that would cause nuclear staining when the cellular membrane is damaged. Moreover, competition experiments also ensured non-membrane permeabilization. Finally, we extrapolated this strategy to the delivery of multiple anionic probes, namely carboxyfluorescein and Alexa Fluors 488, 546, and 568, and we also confirmed their release in the cytosolic medium by confocal microscopy experiments. On the other hand, the modification of the physiological intracellular pH has been described to be related to the emergence of different pathologies such as cancer. For instance, cancer cells present a slightly acidic pH compared to normal cells. Therefore, the meticulous study of the intracellular pH would allow a better understanding of important cellular processes and diseases. A wide range of molecules can be used to carry out intracellular pH measurements. For instance, pyranine presents wonderful properties and can be used as a pH indicator. However, aggressive strategies, such as electroporation, have to be used for the intracellular delivery of this molecule. Therefore, in this chapter, we finally decided to use the previously synthesized carriers to efficiently internalize pyranine and to track the intracellular pH. Using confocal microscopy experiments, we confirmed the efficiency of the developed methodology to carry out the ratiometric intracellular pH tracking using the pyranine probe. Interestingly, we were able to discriminate the pH of different cellular compartments such as the neutral pH of cytosol (pH: 7.5), the moderately acidic pH of the early endosomes (pH: 7.0), and the more acidic pH of late endosomes (pH: 6.5).

In the second chapter, we have explored supramolecular nanoparticles for the delivery of hydrophilic peptides. The term supramolecular nanoparticles (SNPs) has normally been used to define nanoparticles constructed mainly by non-covalent interactions. Supramolecular interactions have been used for the functionalization with different moieties which provide different functionalities to the system. The scaffolds used to construct these materials can be soft or hard, which have relevant consequences not only in their properties but also in their therapeutic effect. Supramolecular nanoparticles based on soft materials have been used for the intracellular delivery of not only therapeutic nucleic acids but also small molecules such as drugs. Interestingly, examples of SNPs that have already reached clinical trials have been reported. Moreover, co-delivery using SPNs of different cargos, such as small drugs and nucleic acids, has been also explored. On the other hand, metallic nanoparticles have been widely used and studied in Nanotechnology. For instance, these particles have been used in the development of novel drug delivery vehicles. During the last decades, gold nanoparticles (AuNPs) have shown applications in catalysis, as sensors, in biomedicine, etc. For the development of efficient and non-toxic therapeutics, multicomponent functionalization of the nanoparticle surface is fundamental. Furthermore, the incorporation of reversibility by supramolecular interactions has emerged as an innovative approach for the design of novel multicomponent nanoparticles. A relevant example is the combination of AuNPs and supramolecular macrocycles. The use of supramolecular interactions allowed the preparation of complex systems by easy mixing of the

different building blocks. Moreover, this methodology avoids difficult synthetic steps and complicated purifications of the final materials. During the last years, AuNPs functionalized with macrocyclic hosts such as cucurbiturils or cyclodextrins (CDs) have been prepared. For instance, CDs present a highly hydrophobic internal cavity, which makes these entities wonderful hosts for a wide range of hydrophobic molecules such as hydrophobic drugs. During the last decades, the use of metallic host-guest based-nanoparticles for therapeutic applications has emerged as a great deal of interest in the scientific community. The formation of host-guest complexes has been traditionally used in the solubilization and integration of different hydrophobic drugs such as cisplatin prodrugs, doxorubicin, paclitaxel, or methotrexate into nanoparticle systems. However, most of these strategies have explored the release and exchange of hydrophobic host cargos. To the best of our knowledge, the release and dynamic exchange between hydrophilic peptide guests and host decorated nanoparticles has not yet been investigated. In this project, one of the main challenges is the chemical complexity of peptides, which can lead to unspecific interactions such as electrostatic or van der Waals contacts. On the other hand, the covalent and electrostatic coating has been traditionally used for the coating of nanoparticle surfaces with hydrophilic peptides. However, examples using supramolecular host-guest recognition are still limited.

The second chapter of this manuscript covers the development of a supramolecular strategy for the incorporation of hydrophilic peptides and PEG polymers into ***β*-CD@AuNPs** by using host-guest supramolecular processes. We prepared beta-cyclodextrin anchored gold nanoparticles (***β*-CD@AuNPs**) and characterized them by TEM, DLS, UV-Visible, and TGA experiments. TGA experiments indicated a loading of an average of 20 *β*-CDs per nanoparticle, while TEM and DLS supported the generation of low-polydisperse nanoparticles of a size of 2-3 nm and hydrodynamic diameter of approximately 8 nm. A library of hydrophilic cell-penetrating peptides (tetra- and octa-arginine) bearing mono (**AdR$_4$** and **AdR$_8$**) and divalent (**Ad$_2$R$_4$** and **Ad$_2$R$_8$**) adamantane guests were generated by exploiting the alcoxyamine-aldehyde condensation between peptide alcoxyamine and guest aldehyde. In this work, we chose the adamantane **(Ad)** guest because of its high affinity constant to *β*-CD hosts. On the other hand, mono- and divalent **Ad** guests were used to explore the dynamic exchange by multivalent or statistical effects. *ζ*-potential experiments supported the incorporation of these mono and divalent peptides into ***β*-CD@AuNPs** promoted by specific host-guest processes. Furthermore, control peptides without guest motives did not show relevant coating of the ***β*-CD@AuNPs.** The *ζ*-potential titration curves were used to provide an estimative idea of the binding affinities, which were found in a plausible range for the individual Ad-CD interaction. Additionally, the interpretation of the apparent binding constants obtained indicate that the predominant process is a statistical rebinding or internanoparticle interactions. Competition experiments in the presence of free *β*-CD showed a drop in the positive *ζ*-potential of the nanoparticles which indicated thermodynamic reversibility. On the other hand, biocompatible polymers such as polyethylene glycol (PEG) have been used for the prevention of nanoparticle surface coating with different proteins of the biological environment. Here, we decided to synthesized and characterized hydrophilic mono (**AdPEG**) and divalent (**Ad$_2$PEG**) PEG moieties using the previously described synthetic approach to incorporate another functionality into the nanosystem. Furthermore, we constructed multicomponent nanoparticles composed of guest-functionalized polyarginine peptide and PEG. Size and *ζ*-potential experiments in the presence of a mixture of monovalent/divalent polyarginine and PEG suggested that electrostatic stabilization is the main actor in the stabilization, while PEG might have a detrimental effect by hampering the development of high potential values. Only in electrostatic stability zones, the addition of PEG resulted in the favorable modulation of size. Finally, we hypothesized

whenever peptide host-guest exchange could be carried out by valency competition. We demonstrated that the complexation of membrane-impermeable polyglutamic peptides (**AdE_9**) with ***β*-CD@AuNPs** promotes the intracellular delivery of these peptides. Moreover, confocal microscopy experiments and cell cytometry assays confirmed the exchange of the anionic peptide **AdE_9** with peptides with a divalent guest such as **Ad_2R_8** inside living cells.

The last chapter of this thesis was focused on the development of thermoresponsive supramolecular nanotubular systems. During the last decades, stimuli-responsive systems, also named as ¨smart materials¨, have attracted a great deal of interest due to their ability to respond to a wide range of stimuli such as pH, ionic strength, light, magnetic or electric field, or temperature. Between them, thermoresponsive materials, which can adapt to changes in the environmental temperature, have demonstrated numerous biomedical applications such as gene therapy or drug delivery. Elastin, which is a structural protein, has been found to present thermoresponsive properties. Tropoelastin was defined as the un-cross-linked precursor of elastin and its primary structure is composed of repeating pentapeptide sequences. The most commonly found peptide sequence is $Val_1Pro_2Gly_3Val_4Gly_5$ or VPGVG. During the last decades, elastin-like polypeptides (ELPs) and elastin-based polymers (EBPs) have been synthesized. Investigating this type of materials a lower critical solution temperature (LCST) behavior or an upper critical solution temperature (UCST) behavior and multiple applications, such as thermoresponsive drug delivery vehicles, have been found. On the other hand, self-assembling cyclic peptide nanotubes (SCPNs) represent one of the most relevant examples of supramolecular entities. For instance, SCPNs have been prepared using *D,L*-α-cyclic peptides (*D,L*-α-CPs), which consist of an even number of amino acids with alternating chirality. The self-assembly of cyclic peptides is based on the stacking of multiple subunits through the formation of a hydrogen bond network. Since the discovery of the CP nanotubes, different structural modifications have been carried out and also a wide range of applications have been described. SCPNs have demonstrated capabilities as analogues of membrane ion channels or as ion sensors. Furthermore, these supramolecular entities have been used not only as drug delivery vehicles but also as antibacterial or antiviral agents. During the last decades, our group has designed and synthesized a wide range of cyclic peptides structures of different sizes able to self-assemble into nanotubes acquiring high expertise in this field. Recently, in our group, self-assembly of cyclic peptides have been achieved inside vesicles. More recently, the formation of nanosheets has been found under physiological conditions and these entities were characterized as bilayers of self-assembling cyclic peptide nanotubes. To provide stimuli-responsiveness to these supramolecular systems, cyclic peptides have been functionalized with polymers leading to the construction of nanotubes based on polymer-cyclic peptide hybrids. These hybrid materials have shown to respond to environmental stimuli such as temperature or pH. However, the attachment of thermosensitive artificial polymers to cyclic peptides lack of an easy synthetic approach that allows the controlled modification of the transition temperatures and a detailed study of the self-assembly of SCPNs with the variation of the temperature. Furthermore, when used for biomedical applications, these cyclic peptide-polymer hybrids are normally cytotoxic. Therefore, the attachment of peptide thermoresponsive moieties, such as elastin, into cyclic peptides would allow constructing not only thermoresponsive supramolecular materials in an easier and more tunable approach but also fully biocompatible systems.

Therefore, in the third chapter of this dissertation, we have studied the different possibilities to design elastin-modified cyclic peptides with potential capabilities to self-assemble by pH changes into cyclic peptide nanotubes. These cyclic peptides consisted of eight amino acid

residues with alternating chirality (*D/L*-α-CP) decorated with the thermosensitive elastin moiety. We designed three different base cyclic peptide scaffolds incorporating different pH-responsive residues to promote the self-assembly at basic pH (**CP1.1** and **CP1.2**), at neutral pH (**CP2.1** and **CP2.2**), and at acidic pH (**CP3.1** and **CP3.2**). In this design, we decided to incorporate the elastin moiety to the cyclic peptide scaffold in two different orientations: the natural elastin segment [**H**-(V-P-G-V-G-)OH] and the, also thermoresponsive, reversed structure [**H**-(G-V-G-P-V-)OH]. Moreover, we also designed the control peptides without the elastin moiety **CP1**, **CP2,** and **CP3**. In this thesis, we synthesized two different elastin-modified cyclic peptides **CP1.1** and **CP3.1** both peptides incorporating the natural elastin segment (**H**-V-P-G-V-G-OH). We hypothesized that **CP1.1** would be able to self-assemble into nanotubular structures at basic pH while **CP3.1** at acidic pH. In **CP1.1**, we incorporated into the base cyclic peptide sequence (**CP1**) three pH-responsive residues (2 His and 1 Lys) to achieve the self-assembly into cyclic peptide nanotubes at basic pH. In this cyclic scaffold, the basification of the aqueous media would promote the deprotonation of the histidine side chains ($pK_a \approx 6.0$) that would lead to the emergence of histidine-histidine hydrogen bonds. Furthermore, the Lys side chains ($pK_a \approx 10.5$) at basic pH would be deprotonated and the cationic electrostatic repulsions would be minimized. In **CP3.1,** to achieve the nanotube formation at acidic pH, we incorporated three Glu residues to the cyclic peptide sequence (**CP3**). The acidification of the aqueous media would promote the protonation of the Glu side chains ($pK_a \approx 4.2$) that would lead to hydrogen bond formation. For the preparation of these two different elastin-modified cyclic peptides (**CP1.1** and **CP3.1**), we carried out a full solid-phase peptide synthesis. Using this synthetic strategy the growth of the elastin-based fragment and the synthesis and cyclization of the *D, L*-fragment were implemented on a trityl resin. Furthermore, we have studied the self-assembly and the thermoresponsiveness of these elastin-modified cyclic peptides. We studied the self-assembly of **CP1.1** at basic pH by circular dichroism (CD) experiments. However, we could not correlate the obtained CD signal with cyclic peptide self-assembly at basic pH. We also investigated, by using turbidimetry experiments, the thermoresponsiveness of **CP1.1** and, unfortunately, we did not find temperature-responsive behavior at different temperatures and/or pH. On the other hand, we also explored the self-assembly capabilities of **CP3.1** under previously reported purification conditions.

Resumen

La química orgánica sintética ha jugado un papel clave en el desarrollo de nuevas estrategias para obtener compuestos químicamente funcionales. A pesar del gran avance que ha experimentado la síntesis orgánica en las últimas décadas, las estrategias covalentes presentan limitaciones para lograr estructuras de mayor dimensión, tales como arquitecturas comúnmente encontradas en la naturaleza, como las estructuras formadas por las proteínas ensambladas. La preparación de estas moléculas complejas utilizando exclusivamente estrategias basadas en la formación de enlaces covalentes es casi inaccesible desde el punto de vista del tiempo y el esfuerzo humano requerido y debido a la falta de estrategias sintéticas apropiadas. Además, ciertos fenómenos colectivos como la autoorganización requieren la interacción coordinada entre diferentes entidades químicas, lo que está fuera del alcance de la química covalente tradicional. En consecuencia, una novedosa disciplina denominada química supramolecular emergió en los años 70-80 y fue definida por primera vez por Jean-Marie Lehn como "la química más allá de la molécula". Esta disciplina se centra en el estudio de las interacciones entre diferentes entidades químicas a través de interacciones no covalentes, que incluyen las fuerzas de Van de Waals, enlaces de hidrógeno o halógeno, iones/dipolos, dipolos-dipolos, interacciones π catión o anión, o interacciones π-π. Esta estrategia permite la construcción de estructuras tridimensionales extremadamente complejas a partir de precursores sintéticamente simples. Además, el uso de la química supramolecular confiere a estas estructuras diversas ventajas, como la reversibilidad, la auto-reparación o la respuesta adaptativa a diferentes estímulos. Para la preparación de nuevos sistemas supramoleculares se han explorado principalmente dos procesos, el reconocimiento y el autoensamblaje molecular. El reconocimiento molecular se ha definido como la unión específica de una entidad anfitrión (host) a una molécula huésped (guest) complementaria para generar un complejo anfitrión-huésped (host-guest) mediante el uso de interacciones no covalentes. Es importante destacar que, en algunos ejemplos, las constantes de asociación del enlace anfitrión-huésped han alcanzado valores casi comparables a los enlaces covalentes. Sin embargo, estos complejos anfitrión-huésped aún mantienen las ventajas que ofrece el empleo de interacciones supramoleculares. Un ejemplo relevante en este ámbito es el reconocimiento molecular de la biotina por el bolsillo de unión de la proteína estreptavidina. Por otro lado, el autoensamblaje se ha definido como un proceso mediante el cual un sistema no organizado de componentes moleculares, o una parte de una molécula, como consecuencia de interacciones no covalentes, genera espontáneamente una estructura organizada. La naturaleza también ha utilizado el autoensamblaje molecular para lograr estructuras complejas y funcionales, como la estructura de doble hélice del ADN, el ensamblaje del virus del mosaico del tabaco o la construcción de membranas lipídicas. Desde el día de su creación hasta nuestros días, los sistemas supramoleculares han tenido un papel destacado en el desarrollo de materiales funcionales, como sistemas para transporte intracelular y sistemas termorresponsivos.

En esta Tesis doctoral, hemos empleado estrategias supramoleculares para promover el transporte intracelular de diversas moléculas y diseñar potenciales sistemas termorresponsivos. La química anfitrión-huésped ha sido empleada para encapsular y transportar al interior celular diferentes sondas aniónicas, como la piranina, y, también, péptidos aniónicos con baja eficiencia de transporte a través de la membrana plasmática. Finalmente, hemos diseñado potenciales materiales supramoleculares termorresponsivos basados en nanotubos formados por péptidos cíclicos (SCPNs).

Durante las últimas décadas, se han sintetizado nuevas moléculas terapéuticas y de diagnóstico. Sin embargo, algunas de estas moléculas presentaron dificultades para cruzar la membrana celular. Para superar este problema, se han preparado un amplio rango de sistemas de transporte para promover la internalización celular de diferentes entidades, como ácidos nucleicos, proteínas o moléculas pequeñas, como fármacos o sondas fluorescentes. Diferentes ejemplos de sistemas de transporte comúnmente empleados para internalizar macromoléculas biológicamente importantes y moléculas pequeñas son liposomas, polímeros o nanopartículas metálicas. Un ejemplo relevante entre los distintos vehículos de transporte intracelular son los péptidos penetrantes de células (CPPs). Estas moléculas son péptidos de pequeño tamaño que han mostrado impresionantes capacidades para transportar al interior celular una amplia variedad de macromoléculas y moléculas de pequeño tamaño con carácter terapéutico y de diagnóstico impermeables a la membrana celular. Se han descrito CPPs con diferentes propiedades físico-químicas, como los CPPs catiónicos, hidrófobicos o anfipáticos. Algunos ejemplos relevantes de CPPs ampliamente estudiados son penetratina, TAT, octa-arginina, MPG o PEP-1. Durante las últimas décadas, se han explorado diferentes diseños y modificaciones estructurales para mejorar las capacidades de translocación de estas moléculas. Una estrategia innovadora utilizada para preparar nuevos CPPs ha sido la formación de enlaces dinámicos como enlaces oxima, hidrazona o disulfuro. Esta estrategia permitió preparar una quimioteca de CPPs en un corto período de tiempo, obteniendo cantidades elevadas de peptido y con altos rendimientos. Por ejemplo, en nuestro grupo de investigación, hemos utilizado el grupo alcoxiamina para unir diferentes aldehídos electrofílicos y lograr, de forma sencilla, la modulación de las propiedades de un CPP modelo. Además, nuestro grupo también ha explorado el grupo hidrazida para la incorporación de diferentes aldehídos hidrófobos, como el ácido oleico, en la estructura de un CPP. Se demostró que esta modificación mejoró significativamente la translocación de un péptido modelo pseudohelicoidal. La incorporación del cargo al sistema de transporte se ha logrado principalmente mediante la formación de enlaces covalentes o mediante estrategias supramoleculares no covalentes. La unión covalente entre el vehículo y el cargo se ha utilizado tradicionalmente para la preparación de sistemas de transporte intracelular de fármacos. Por otro lado, las metodologías supramoleculares han mostrado importantes ventajas como la mejora en la liberación del cargo y la reducción del esfuerzo sintético. Por ejemplo, los péptidos penetrantes de celulas se han unido de forma no covalente a proteínas terapéuticas, como la ribonucleoproteína Cas9, a ácidos nucleicos, como siRNA o plásmidos de DNA y a moléculas pequeñas, como fármacos o sondas fluorescentes.

En el primer capítulo de esta Tesis, hemos desarrollado una nueva generación de vehículos supramoleculares altamente eficientes y biocompatibles para el transporte de sondas moleculares al interior celular. Distintas sondas moleculares cargadas negativamente, como la piranina, son de elevado interés para visualizar el espacio intracelular. Sin embargo, el transporte ineficiente de estas moléculas a través de la membrana plasmática, debido a las interacciones repulsivas existentes entre las sondas moleculares y la membrana plasmática, sigue siendo una limitación fundamental para su aplicación. Para superar este problema, hemos demostrado que un sistema híbrido compuesto por una caja supramolecular impermeable a la membrana y un péptido de tetraarginina anclado covalentemente puede emplearse para el transporte citosólico de fluoróforos cargados negativamente en diferentes líneas celulares (células HeLa y Vero). La caja supramolecular **C** utilizada para la preparación de estos transportadores presenta una estructura de trisbipiridilo y, en publicaciones previas del grupo del prof. Nitschke, demostró encapsular con alta afinidad diferentes aniones de gran tamaño, como la piranina, en medio acuoso. En base a estos resultados previos, preparamos péptidos $\boldsymbol{R_4}$ acetilados y marcados con un fluoroforo (TAMRA) mediante el uso de la síntesis de péptidos

en fase sólida y luego acoplamos la caja supramolecular catiónica **C** empleando condiciones estándar para la formación de enlaces amida para generar los transportadores $^{Ac}\boldsymbol{R_4}\mathbf{C}$ y $^{Tm}\boldsymbol{R_4}\mathbf{C}$. Experimentos de fluorescencia demostraron la complejación supramolecular entre estos vectores híbridos y la sonda de piranina, con constantes de disociación calculadas de K_d = 189 nM y K_d = 12.6 µM, respectivamente. En publicaciones previas del grupo del prof. Matile experimentos *in vitro* empleando tubos en *U* mostraron la capacidad de diferentes moléculas para actuar como transportadores. En estos experimentos, se colocó cloroformo en el fondo de un tubo en *U* y se añadieron dos buffers acuosos diferentes a ambos lados de la fase orgánica (buffers *cis* y *trans*). Luego, se monitorizó la transferencia del buffer *cis* al *trans*. Para evaluar el transporte a través del disolvente orgánico apolar -cloroformo-, llevamos a cabo experimentos *in vitro* con tubos en *U* en presencia de fosfolípidos naturales. Medidas de fluorescencia a distintos tiempos indicaron que el transportador $^{Ac}\boldsymbol{R_4}\mathbf{C}$ transporta piranina desde la fase acuosa *cis* a la *trans*. Después de un período de 12 h, la fase acuosa *trans* contenía 4 veces más piranina cuando se usó el transportador peptídico en comparación con los experimentos control. Esto indicó que $^{Ac}\boldsymbol{R_4}\mathbf{C}$ actúa como un transportador de piranina a través de la capa apolar de cloroformo. Experimentos de transporte intracelular de piranina empleando $^{Ac}\boldsymbol{R_4}\mathbf{C}$ y $^{Tm}\boldsymbol{R_4}\mathbf{C}$ mostraron liberación citosólica de la sonda en células HeLa y Vero. Los ensayos de competición en presencia de otra sonda molecular (TAMRA) mostraron que $^{Tm}\boldsymbol{R_4}\mathbf{C}$ fue capaz de internalizar selectivamente piranina al citosol celular por endocitosis. Este mecanismo de entrada se confirmó mediante experimentos en presencia de inhibidores de endocitosis y observando la colocalización del transportador y la piranina mediante experimentos de microscopía confocal. Confirmamos la integridad de la membrana celular tras el transporte de piranina mediante tinción nuclear. En este ensayo, después de los experimentos de transporte con la sonda, incubamos las células con DAPI y también con yoduro de propidio, sondas que causan tinción nuclear cuando se daña la membrana celular. Además, los experimentos de competición también confirmaron que no se permeabiliza la membrana durante el transporte de piranina. Finalmente, empleamos esta estrategia para el transporte de múltiples sondas aniónicas, tales como carboxifluoresceína y los Alexa Fluors 488, 546 y 568, y confirmamos también su liberación al citosol celular mediante experimentos de microscopía confocal. Por otro lado, se ha descrito que la modificación del pH fisiológico intracelular está relacionada con la aparición de diferentes patologías como el cáncer. Por ejemplo, las células cancerosas presentan un pH ligeramente ácido en comparación con las células normales. Por lo tanto, el estudio meticuloso del pH intracelular permitiría comprender mejor los procesos celulares importantes y también las enfermedades. Se puede utilizar un amplio rango de moléculas para llevar a cabo medidas del pH intracelular. Por ejemplo, la piranina presenta excelentes propiedades y puede usarse como indicador de pH. Sin embargo, para el transporte intracelular de esta molécula es necesario utilizar estrategias agresivas, como la electroporación. Por lo tanto, en este capítulo, finalmente decidimos usar los transportadores sintetizados previamente para internalizar eficientemente la piranina y medir el pH intracelular. Usando experimentos de microscopía confocal, confirmamos la eficiencia de la metodología desarrollada y llevamos a cabo medidas ratiometricas del pH intracelular utilizando piranina como sonda. Curiosamente, pudimos distinguir el pH de diferentes compartimentos celulares como el pH neutro del citosol (pH: 7.5), el pH ligeramente ácido de los endosomas tempranos (pH: 7.0) y el pH más ácido de los endosomas tardíos (pH: 6.5).

En el segundo capítulo, hemos empleado nanopartículas supramoleculares para el transporte intracelular de péptidos hidrofílicos. El término nanopartículas supramoleculares (SNPs) se ha usado normalmente para definir nanopartículas construidas principalmente por interacciones no covalentes. Las interacciones supramoleculares se han utilizado para la

funcionalización con diferentes entidades que proporcionan diferentes funcionalidades al sistema. Los materiales utilizados para construir estos sistemas pueden ser blandos o duros, lo que tiene consecuencias relevantes no solo en sus propiedades sino también en su efecto terapéutico. Las nanopartículas supramoleculares basadas en materiales blandos se han utilizado para el transporte intracelular no solo de ácidos nucleicos terapéuticos sino también de moléculas pequeñas como los fármacos. Curiosamente, se han publicado ejemplos de SNPs que han alcanzado ensayos clínicos. Además, también se han preparado SPNs que permiten el transporte intracelular simultáneo de diferentes cargos, como fármacos y ácidos nucleicos. Por otro lado, las nanopartículas metálicas han sido ampliamente utilizadas y estudiadas en nanotecnología. Por ejemplo, estas partículas se han utilizado en el desarrollo de nuevos vehículos de transporte de fármacos. Durante las últimas décadas, las nanopartículas de oro (AuNPs) han mostrado aplicaciones en catálisis, como sensores, en biomedicina, etc. Para el desarrollo de terapias altamente eficientes y con baja toxicidad, la incorporación de varios componentes en la superficie de las nanopartículas es fundamental. Además, el empleo de interacciones supramoleculares se ha convertido en un enfoque innovador para el diseño de nuevas nanopartículas multicomponente. Un ejemplo relevante es la combinación de AuNPs y macrociclos supramoleculares. El uso de interacciones supramoleculares permite la preparación de sistemas complejos simplemente mezclando los diferentes componentes. Además, esta metodología evita pasos sintéticos difíciles y purificaciones complicadas de los materiales finales. Durante los últimos años, se han preparado AuNPs funcionalizadas con anfitriones macrocíclicos como cucurbiturilos o ciclodextrinas (CDs). Por ejemplo, las CDs contienen una cavidad interna altamente hidrofóbica, lo que hace que estas entidades sean excelentes anfitriones para un amplio rango de moléculas hidrofóbicas, como los fármacos hidrofóbicos. Durante las últimas décadas, el uso de nanopartículas metálicas, basadas en química anfitrión-huésped, con aplicaciones terapéuticas ha suscitado un gran interés en la comunidad científica. La formación de complejos anfitrión-huésped se ha utilizado tradicionalmente en la solubilización e integración en nanopartículas de diferentes fármacos hidrofóbicos como los profármacos de cisplatino, doxorrubicina, paclitaxel o metotrexato. Sin embargo, la mayoría de estas estrategias han explorado la liberación e intercambio de cargos hidrofóbicos. Hasta donde sabemos, aún no se ha investigado la liberación y el intercambio dinámico entre péptidos huésped hidrofílicos y nanopartículas decoradas con anfitriones. En este proyecto, uno de los principales desafíos es la complejidad química de los péptidos, que puede conducir a interacciones inespecíficas como, por ejemplo, interacciones electrostáticas o de van der Waals. Por otro lado, tradicionalmente para la funcionalización de la superficie de las nanopartículas con péptidos hidrofílicos se han empleado enlaces covalente e interacciones electrostáticas. Sin embargo, ejemplos que utilizan el reconocimiento supramolecular anfitrión-huésped siguen siendo limitados.

El segundo capítulo de esta Tesis, se desarrolló una estrategia supramolecular para la incorporación de péptidos y polímeros hidrofílicos en ***β*-CD@AuNPs** mediante el empleo de procesos supramoleculares anfitrión-huésped. Preparamos nanopartículas de oro ancladas a *β*-ciclodextrinas (***β*-CD@AuNPs**) y las caracterizamos mediante experimentos de TEM, DLS, UV-Visible y TGA. Los experimentos de TGA indicaron que estas poseen un promedio de 20 *β*-CD por nanopartícula, mientras que experimentos de TEM y DLS demostraron la preparación de nanopartículas de un tamaño de 2-3 nm y un diámetro hidrodinámico de aproximadamente 8 nm. Se sintetizó una quimioteca de péptidos penetrantes de células hidrófilicos (tetra y octa-arginina) modificados con adamantanos, mono (**AdR_4** y **AdR_8**) y divalentes (**Ad$_2$R$_4$** y **Ad$_2$R$_8$**) empleando la condensación alcoxiamina-aldehído entre el grupo alcoxiamina del péptido y el grupo aldehído del huésped. En este trabajo, elegimos el adamantano (**Ad**) como huésped

debido a su elevada constante de afinidad por el anfitrión, *β*-CD. Por otro lado, los huéspedes mono y divalentes se utilizaron para explorar el intercambio dinámico de péptidos en la superficie de las ***β*-CD@AuNPs** mediante efectos estadísticos o multivalentes. Experimentos de potencial ***ζ*** confirmaron la incorporación de estos péptidos mono y divalentes en las ***β*-CD@AuNPs** mediante interacciones específicas anfitrión-huésped. Además, los péptidos control sin huésped no recubrieron de forma relevante las ***β*-CD@AuNPs.** Los resultados de los experimentos de potencial ***ζ*** se utilizaron para proporcionar una idea estimada de las constantes de asociación anfitrión-huésped, que se encontraron en un rango adecuado para la interacción individual Ad-CD. Además, la interpretación de las constantes de asociación aparentes calculadas indica que el proceso predominante es una unión estadística o interacciones entre partículas. Además, los experimentos de competición en presencia de *β*-CD libre mostraron un descenso en el potencial ***ζ*** de las nanopartículas que indica reversibilidad termodinámica. Por otro lado, los polímeros biocompatibles como el polietilenglicol (PEG) se han utilizado para prevenir el recubrimiento de la superficie de nanopartículas con diferentes proteínas del medio biológico. Aquí, decidimos sintetizar y caracterizar cadenas de PEG hidrofílicos mono (**AdPEG**) y divalentes (**Ad$_2$PEG**), utilizando la metodología sintética descrita anteriormente, para incorporar otra funcionalidad en el nanosistema. Construimos nanopartículas multicomponente compuestas por péptidos de poliarginina y cadenas de PEG funcionalizados con el huésped adamantano. Los experimentos de tamaño y potencial ***ζ*** en presencia de una mezcla de poliarginina y PEG monovalentes/divalentes sugirieron que la estabilización electrostática es la causante de la estabilización del sistema, mientras que el PEG podría tener un efecto negativo al obstaculizar el alcance de valores elevados de potencial. Exclusivamente en zonas de estabilidad electrostática, la adición de PEG dio como resultado una modulación favorable del tamaño. Por último, planteamos la hipótesis de que el intercambio de péptidos sobre las ***β*-CD@AuNPs**, mediante interacciones anfitrión-huésped, podría llevarse a cabo empleando péptidos que presentasen una valencia superior. Demostramos que la formación de complejos entre péptidos poliglutámicos impermeables a la membrana (**AdE$_9$**) y ***β*-CD@AuNPs** promueve el transporte intracelular de estos péptidos. Además, los experimentos de microscopía confocal y los ensayos de citometría celular confirmaron el intercambio de estos péptidos aniónicos **AdE$_9$** por péptidos divalentes como **Ad$_2$R$_8$** en el interior de células vivas.

El último capítulo de esta Tesis se ha centrado en el desarrollo de nuevos sistemas nanotubulares supramoleculares termorresponsivos. Durante las últimas décadas, los sistemas que responden a los estímulos, también llamados "materiales inteligentes", han atraído un gran interés debido a su capacidad para responder a una amplia gama de estímulos, como el pH, la fuerza iónica, la luz, el campo magnético o eléctrico o la temperatura. Entre ellos, los materiales termorresponsivos, que poseen la capacidad de adaptarse a los cambios de la temperatura ambiental, han demostrado numerosas aplicaciones biomédicas, como en terapia génica o en la administración de fármacos. Se ha demostrado que la elastina, que es una proteína estructural, presenta propiedades termorresponsivas. La tropoelastina se definió como el precursor de la elastina y su estructura primaria está compuesta por secuencias repetidas de pentapéptidos. La secuencia peptídica más comúnmente encontrada es $Val_1Pro_2Gly_3Val_4Gly_5$ o VPGVG. Durante las últimas décadas, se han sintetizado polipéptidos tipo elastina (ELP) y polímeros basados en elastina (EBP). Al investigar este tipo de materiales, se ha encontradon comportamientos LCST (temperatura de solución crítica inferior) o comportamientos UCST (temperatura de solución crítica superior) y múltiples aplicaciones, como por ejemplo como vehículos termorresponsivos para la internalización celular de fármacos. Por otro lado, los nanotubos constituidos por péptidos cíclicos (SCPNs) representan uno de los ejemplos más relevantes de entidades

supramoleculares. Por ejemplo, SCPNs se han preparado utilizando *D,L*-α-ciclopéptidos (*D,L*-α-CP) que consisten en un número par de aminoácidos con quiralidad alternante. El autoensamblaje de péptidos cíclicos se basa en el apilamiento de múltiples subunidades mediante la formación de una red de enlaces de hidrógeno. Desde el descubrimiento de los SCPNs, se han llevado a cabo diferentes modificaciones estructurales y también se han descrito una amplia variedad de aplicaciones. Los SCPNs han demostrado capacidades como análogos de canales de iones de membrana o como sensores de iones. Además, estas entidades supramoleculares se han utilizado no solo como vehículos de administración de fármacos sino también como agentes antibacterianos o antivirales. Durante las últimas décadas, nuestro grupo de investigación ha diseñado y sintetizado un amplio rango de estructuras de péptidos cíclicos de diferentes tamaños capaces de autoensamblarse en nanotubos adquiriendo una alta experiencia en este campo. Recientemente, en nuestro grupo, se ha logrado demostrar el autoensamblaje de péptidos cíclicos dentro de vesículas. Más recientemente, la formación de nanohojas se ha demostrado en condiciones fisiológicas y se caracterizaron como bicapas de SCPNs. Para proporcionarle a estos sistemas supramoleculares la capacidad para responder a distintos estímulos, péptidos cíclicos se han funcionalizado con polímeros que conducen a la construcción de nanotubos basados en híbridos de péptidos cíclicos y polímeros. Estos materiales híbridos han demostrado responder a estímulos ambientales como la temperatura o el pH. Sin embargo, la unión de los polímeros artificiales termorresponsivos a péptidos cíclicos carece de una estrategia sintética fácil que permita la modificación controlada de las temperaturas de transición y un estudio detallado del autoensamblaje de los SCPNs con la variación de la temperatura. Además, cuando se usan en aplicaciones biomédicas, estos híbridos cíclicos péptido-polímero normalmente producen toxicidad celular. Por lo tanto, la unión de cadenas peptídicas termorresponsivas, como la elastina, a péptidos cíclicos permitiría construir no solo materiales supramoleculares termorresponsivos de una forma más sencilla sino también sistemas plenamente biocompatibles.

Por lo tanto, en el tercer capítulo de esta Tesis doctoral, hemos estudiado las diferentes posibilidades para diseñar péptidos cíclicos modificados con elastina con potenciales capacidades para autoensamblarse en nanotubos de péptidos cíclicos mediante variaciones en el pH del medio. Estos péptidos cíclicos están constituidos por ocho aminoácidos con quiralidad alternante (*D/L*-α-CP) decorados con una cadena de elastina, que confiere capacidades termorresponsivas al sistema. Diseñamos tres péptidos cíclicos base diferentes que poseen diferentes aminoácidos sensibles al pH para promover el autoensamblaje a pH básico (**CP1.1** y **CP1.2**), a pH neutro (**CP2.1** y **CP2.2**) y a pH ácido (**CP3.1** y **CP3.2**). En este diseño, decidimos incorporar una cadena de elastina a los péptidos cíclicos en dos orientaciones diferentes: el segmento de elastina natural [**H**-(V-P-G-V-G-)OH] y la estructura inversa, también termorresponsiva (**H**-(G-V-G-P-V-)OH). Además, también diseñamos los péptidos de control sin la cadena de elastina **CP1**, **CP2** y **CP3**. En esta Tesis, sintetizamos dos péptidos cíclicos diferentes modificados con elastina **CP1.1** y **CP3.1**, en ambos péptidos incorporamos el segmento natural de elastina [**H**-(V-P-G-V-G-)OH]. Aquí planteamos la hipótesis de que **CP1.1** podría autoensamblarse en estructuras nanotubulares a pH básico, mientras que **CP3.1** a pH ácido. En **CP1.1**, incorporamos a la secuencia de péptido cíclico base (**CP1**) tres residuos sensibles al pH (2 His y 1 Lys) para lograr el autoensamblaje en nanotubos de péptidos cíclicos a pH básico. En este peptido cíclico, la basificación del medio acuoso promovería la desprotonación de las cadenas laterales de histidina ($pK_a \approx 6.0$) que conduciría a la aparición de enlaces de hidrógeno histidina-histidina. Además, las cadenas laterales de Lys ($pK_a \approx 10.5$) a pH básico estarían desprotonadas, por lo tanto, las repulsiones electrostáticas catiónicas se minimizarían. En **CP3.1**, para lograr la formación de nanotubos a pH ácido, incorporamos tres

residuos de Glu a la secuencia base del péptido cíclico (**CP3**). En este péptido, la acidificación del medio acuoso produciría la protonación de las cadenas laterales de Glu ($pK_a \approx 4.2$) que conduciría a la formación de enlaces de hidrógeno. Para la preparación de estos dos péptidos cíclicos diferentes modificados con elastina (**CP1.1** y **CP3.1**), utilizamos exclusivamente la síntesis de péptidos en fase sólida. Usando esta estrategia sintética, el crecimiento del fragmento de elastina y la síntesis y ciclación del fragmento D, L se llevaron a cabo en la resina clorotritilo. Además, hemos estudiado el autoensamblaje y la capacidad de respuesta térmica de estos péptidos cíclicos modificados con elastina. Estudiamos el autoensamblaje de **CP1.1** a pH básico mediante experimentos de dicroísmo circular (CD). Sin embargo, no pudimos correlacionar la señal de CD obtenida con el autoensamblaje de péptidos cíclicos a pH básico. También investigamos, mediante experimentos de turbidimetría, la capacidad de respuesta térmica de **CP1.1** y, desafortunadamente, no encontramos comportamiento termorresponsivo a diferentes temperaturas y/o pH. Por otro lado, también llevamos a cabo la exploración de las capacidades de autoensamblaje de **CP3.1** en condiciones de purificación previamente descritas.

USC
UNIVERSIDADE
DE SANTIAGO
DE COMPOSTELA

General Introduction

USC
UNIVERSIDADE
DE SANTIAGO
DE COMPOSTELA

1. Supramolecular chemistry

Jean-Marie Lehn defined supramolecular chemistry as the "chemistry beyond the molecule".[1] Due to their important discoveries in this area, Lehn[1], Cram[2], and Pedersen[3] received the Nobel prize in 1987. Supramolecular chemistry focuses on the design and preparation of complex systems that held together chemical components by non-covalent interactions.[4,5,6] Instead of networks of covalent bonds, the driving force for the assembly of supramolecular systems relies on a gamut of non-covalent forces, such as ion-ion/dipole, dipole-dipole, hydrogen and halogen bonding, cation or anion-π interactions, van der Waals forces or π-π interactions.[6, 7]

The emergence of supramolecular chemistry allowed to obtain complex structures that present functional groups oriented in a precise direction of the three-dimensional space. The preparation of these complex ensembles by the formation of covalent bonds results extremely challenging from the point of view of time and human resources.[8] Moreover, supramolecular chemistry provided a possibility of manipulating supramolecular building blocks at a molecular level, allowing the "bottom-up" synthesis of complex molecular architectures with controlled size and shape.[9] Due to the use of non-covalent interactions, supramolecular materials have shown reversibility, allowing convenient complex dissociation and association at a low energy cost.[10] Interestingly, this type of systems has also shown adaptive behavior in response to external stimuli that can trigger the structure variation of supramolecular materials.[11]

2. Molecular recognition and self-assembly

Supramolecular systems are mainly assembled by molecular recognition or self-assembly. In both cases, the interaction between the molecules occurs based on their structural information. This is constituted mainly of two elements: chemical complementarity, which implies the correct distribution of the matching in shape and chemical groups in the molecule, and the preorganization, which refers to the adequate conformational disposition of the interacting units. The main difference between both processes is related to the complexity of the obtained supramolecular systems. Molecular recognition is focused on simple processes in which only a few molecules are interacting, while self-assembly deals with more complex systems, generally involving an infinite number of molecules. Molecular recognition is defined as the specific binding of a guest molecule to a complementary host entity to generate a host-

[1] J.-M. Lehn, *Angew. Chem. Int. Ed.* **1988**, *27*, 89-112.
[2] D. J. Cram, *Angew. Chem. Int. Ed.* **1988**, *27*, 1009-1020.
[3] C. J. Pedersen, *Angew. Chem. Int. Ed.* **1988**, *27*, 1021-1027.
[4] J.-M. Lehn, *Chem. Soc. Rev.* **2017**, *46*, 2378-2379.
[5] J.-M. Lehn, *Eur. Rev.* **2009**, *17*, 263-280.
[6] J. W. Steed, D. R. Turner, K. Wallace, *Core Concepts in Supramolecular Chemistry and Nanotechnology*, Jon Wiley & Sons, Chichester, **2007**.
[7] J. D. Badjić, A. Nelson, S. J. Cantrill, W. B. Turnbull, J. F. Stoddart, *Acc. Chem. Res.* **2005**, *38*, 723-732.
[8] D. N. Reinhoudt, *Science* **2002**, *295*, 2403-2407.
[9] V. Balzani, A. Credi, M. Venturi, *Chem. Eur. J.* **2002**, *8*, 5524-5532.
[10] K. Liu, Y. Kang, Z. Wang, X. Zhang, *Adv. Mater.* **2013**, *25*, 5530-5548.
[11] B. Rybtchinski, *ACS Nano* **2011**, *5*, 6791-6818.

guest complex by the use of non-covalent interactions. On the other hand, molecular self-assembly is defined as the construction of systems without guidance from an outside source.[6,12]

3. Molecular self-assembly

Self-assembly is a process by which a non-organized system of molecular components, or a part of a molecule, spontaneously generates an organized structure as a consequence of non-covalent interactions.[13] The molecules involved in this type of process are programmed chemical entities. Therefore, these molecules include functional complementary groups that direct the organization of matter towards the generation of architectures with a pre-defined topology and properties.[14] Molecular self-assembly has been also the strategy selected by nature to construct complex and functional architectures.[15] In fact, the most sophisticated examples of self-assembly can be found in natural systems, such as the double helix structure of DNA, the assembly of the tobacco mosaic virus, the folding of proteins to obtain their three-dimensional structure that determines its biological function or the formation of lipid membranes.[16] The implementation of self-assembly in synthetic chemistry allowed to construct a wide range of complex structures with different topologies such as spheres,[17] helicates,[18] barrels,[19] nanowires,[20] cubes[21] , or nanotubes.[22]

4. Host-guest chemistry

4.1. General principles

An important phenomenon studied by supramolecular chemistry is the formation of inclusion complexes. Here, a host molecule can interact with a guest entity in order to form a host-guest complex, as shown in Figure 1.[23] The driving force is the formation of non-covalent supramolecular interactions such as van der Waals forces.[24] The geometrical fitting of the guest to the host pocket is therefore an essential factor in maximizing these stabilizing interactions while minimizing sterical repulsion. The stability of the host-guest complex at a given temperature and solvent is typically measured by the thermodynamic equilibrium formation constant (K_a), or the dissociation constant (K_d, being $K_d = K_a^{-1}$). K_a is expressed as the concentration of formed host-guest complex divided by concentrations of free host and guest (Figure 1, right). In some cases, host-guest binding constants can reach magnitudes almost

[6] J. W. Steed, D. R. Turner, K. Wallace, *Core Concepts in Supramolecular Chemistry and Nanotechnology*, Jon Wiley & Sons, Chichester, **2007**.
[12] D. Rasale, A. Das, *Int. J. Mol. Sci.* **2015**, *16*, 10797-10820.
[13] Whitesides, G. M.; Grzybowski, B. *Science* **2002**, *295*, 2418-2421.
[14] Hosseini, M. W. *Chem. Commun.* **2005**, 5825-5829.
[15] Lehn, J.-M. *Proc. Natl. Acad. Sci. U. S. A.* **2002**, *99*, 4763-4768.
[16] Whitesides, G. M.; Mathias, J. P.; Seto, C. T. *Science* **1991**, *254*, 1312-1319.
[17] A. R. Stefankiewicz, J. K. M. Sanders, *Science* **2010**, *328*, 1115-1116.
[18] M. Boiocchi, L. Fabbrizzi, *Chem. Soc. Rev.* **2014**, *43*, 1835-1847.
[19] Y. Lim, M. Lee, *J. Mater. Chem.* **2011**, *21*, 11680-11685.
[20] C. Qian, F. Kim, L. Ma, F. Tsui, P. Yang, J. Liu, *J. Am. Chem. Soc.* **2004**, *126*, 1195-1198.
[21] A. Stephenson, M. D. Ward, *Dalton Trans.* **2011**, *40*, 10360-10369.
[22] Chapman, R.; Danial, M.; Koh, M. L.; Jolliffe, K. A.; Perrier, S. *Chem. Soc. Rev.* **2012**, *41*, 6023-6041.
[23] S. M. Mantooth, B. G. Munoz-Robles, M. J. Webber, *Macromol. Biosci.* **2019**, *19*, 1800281.
[24] C. B. Rodell, J. E. Mealy, J. A. Burdick, *Bioconjug. Chem.* **2015**, *26*, 2279-2289.

comparable to covalent bonds. A clear example in this sense is the molecular recognition of biotin by the binding pocket of streptavidin protein,[25] with a $K_d \sim 4 \times 10^{-14}$ M^{-1}.

Figure 1. Interaction between a cavitand host (red) and a fitting guest (blue) to give a host-guest complex, where k_{on} and k_{off} are the formation and dissociation rate constants respectively. The binding constant (K_a) determines the speciation of free host, free guest, and host-guest complex.[23]

4.2.Multivalency

In supramolecular chemistry, multivalency typically describes multiple non-covalent interactions that occur between a multivalent host and a multivalent guest. This results, generally, in enhanced binding affinities and specificities,[26] which plays a pivotal role in intercellular adhesion[27] or protein-carbohydrate recognition.[28] Depending on the spacing and flexibility of the multivalent motives, a multivalent guest can bind to a multivalent host in an intramolecular or intermolecular fashion. Intramolecular binding typically leads to relatively high association constants with respect to monovalent binding and the formation of well-defined complexes. In contrast, intermolecular binding might lead to the formation of large aggregates that often precipitate from solution. Binding shows association constants comparable to those of the corresponding monovalent interactions, while irreversible precipitation and aggregation lead to decreased dissociation rates and consequently to an apparent binding enhancement (Figure 2A).[29]

In addition to its importance in relevant biological processes, multivalent interactions are the foundation of several technologies in nanomedicine and material sciences. For example, viral infections typically proceed by an initial binding to membrane receptors which subsequently triggers cell endocytosis and starts the infection. Viral inhibitors can be designed by including multiple copies of the antigen into a multivalent platform, which shows higher affinities towards the host cell and therefore prevents virus binding by multivalent competition. As example, Nazario Martin and col. demonstrated that giant multivalent glycofullerenes are potent inhibitors of Ebola virus infection showing subnanomolar half-maximum inhibitory concentrations. These multivalent compounds demonstrated inhibition of lectin-mediated viral infections in cellular experiments. Interestingly, the half-maximum inhibitory concentrations overpassed by three orders of magnitude (two if the number of mannoses is considered) those exhibited by hexakis adducts showing 12 mannoses (Figure 2B).[30] On the other hand, materials with enhanced adhesion can be designed by covering large surfaces with host-guest pairs, yielding underwater "velcros". For example, multivalent interactions arising between a host

[25] N. M. Green, *Methods Enzymol.* **1990**, *184*, 51-67.
[26] M. J. W. Ludden, D. N. Reinhoudt, J. Huskens, *Chem. Soc. Rev.* **2006**, *35*, 1122-1134.
[27] Y. Zhang, S. Sivasankar, W. J. Nelson, S. Chu, *Proc. Natl. Acad. Sci.* **2009**, *106*, 109-114.
[28] T. K. Dam, R. Roy, S. K. Das, S. Oscarson, C. F. Brewer, *J. Biol. Chem.* **2000**, *275*, 14223-14230.
[29] A. Mulder, J. Huskens, D. N. Reinhoudt, *Org. Biomol. Chem.* **2004**, *2*, 3409-3424.
[30] A. Muñoz, D. Sigwalt, B. M. Illescas, J. Luczkowiak, L. Rodríguez-Pérez, I. Nierengarten, M. Holler, J. Remy, K. Buffet, S. P. Vincent, et al., *Nat. Chem.* **2016**, *8*, 50-57.

(curcubit[7]uril) decorated silicon and guest (Fc) functionalized silicon strongly enhanced the adhesion between these two surfaces (Figure 2C).[31]

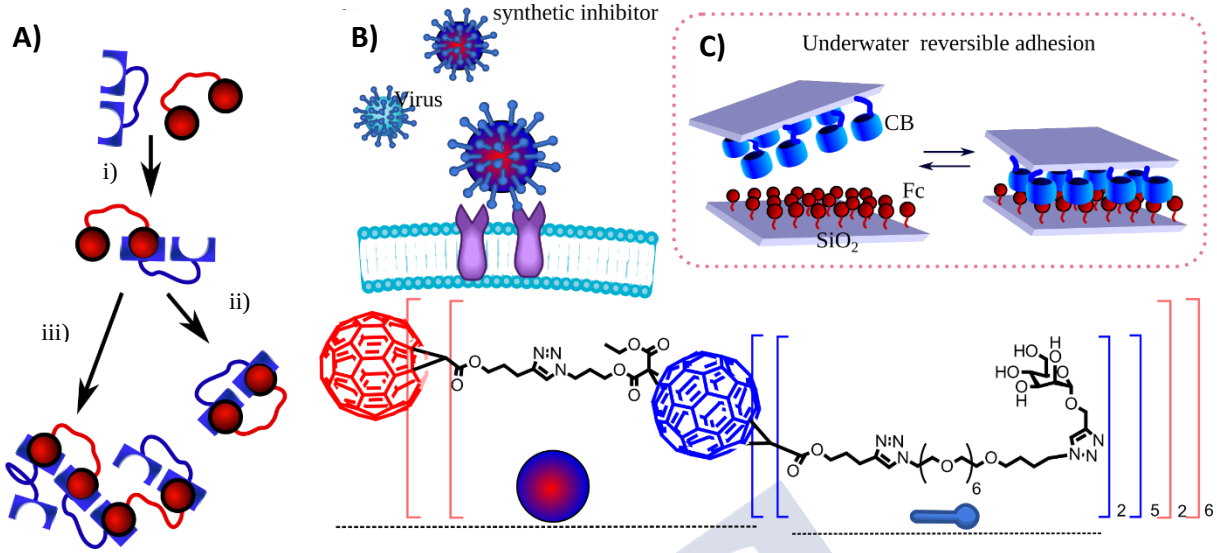

Figure 2. A) Intramolecular vs intermolecular multivalent binding: i) initial monovalent binding; ii) intramolecular binding; iii) intermolecular binding with the formation of aggregates.[29] Examples of technological applications of multivalency: B) Development of viral inhibitors (i.e. Ebola).[30] C) Underwater velcros operating by multiple interactions between a curcubit[7]uril silicon surface and a Fc-functionalized silicon surface.[31]

4.3.Examples of cavitands

During the past few decades, a wide range of macrocyclic hosts and their derivatives have been developed.[32] From those, the *cavitand* family has been defined as "hosts possessing permanent intramolecular cavities",[33] such as the example structures depicted in Figure 3. These can form *cavitates* (the host-guest complex) with multiple guests, which might be inert or stimuli-responsive molecules, including molecules with biological activity such as drugs or biomolecules (i.e. cholesterol[34]).[35,36] Some archetypical examples are shown in Figure 3.

[31] Y. Ahn, Y. Jang, N. Selvapalam, G. Yun, K. Kim, *Angew. Chem. Int. Ed.* **2013**, *52*, 3140-3144.
[32] Z. Liu, S. K. M. Nalluri, J. F. Stoddart, *Chem. Soc. Rev.* **2017**, *46*, 2459-2478.
[33] J. W. Steed, J. L. Atwood, *Supramolecular Chemistry*, John Wiley & Sons, New York, **2000**.
[34] J. Nishijo, S. Moriyama, S. Shiota, *Chem. Pharm. Bull.* **2003**, *51*, 1253-1257.
[35] A. S. Braegelman, M. J. Webber, *Theranostics* **2019**, *9*, 3017-3040.
[36] X. Ma, Y. Zhao, *Chem. Rev.* **2015**, *115*, 7794-7839.

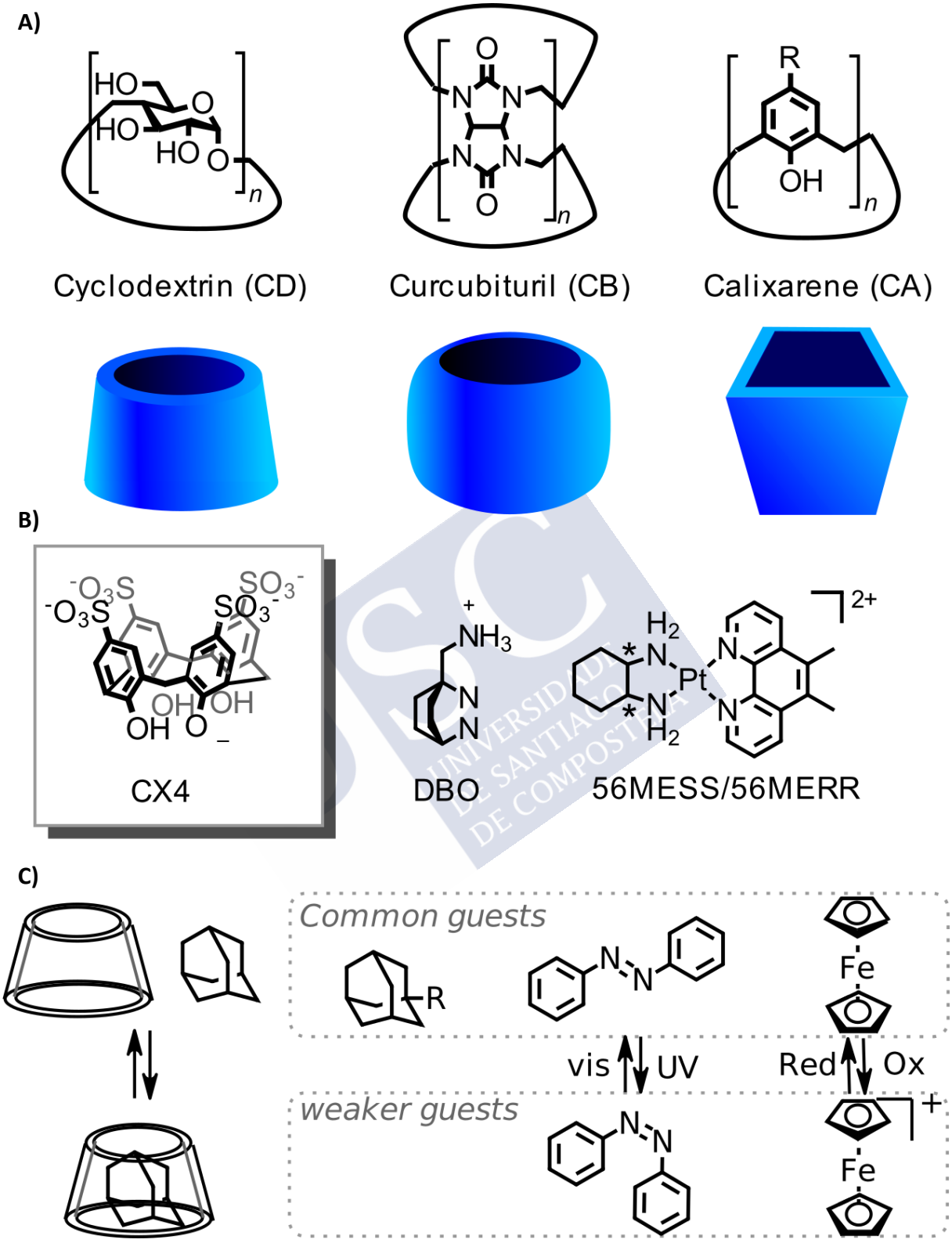

Figure 3. A) Schematic representations and chemical structures of classical cavitand host entities cyclodextrin, cucurbituril and calixarene.[36] B) Chemical structure of p-sulfonatocalix[4]arene (CX4) and guest entities DBO[47] and platinum(II)-based anticancer drugs (56 MESS/56MERR).[53] C) Host-guest complexes between cyclodextrin and adamantane guest. The right side shows some common guest exploited in the construction reversible cavitates.[64,65,66]

4.3.1. Cucurbiturils

Cucurbiturils (CB[*n*]s) are macrocyclic host entities prepared by acid-catalyzed reaction of glycoluril units with formaldehyde.[37] Each glycoluril subunit is bonded to its adjacent subunit by two methylene bridges. The most common CB[*n*] cavitands are composed of 5, 6, 7, 8, and 10 glycoluril subunits.[38] The molecular structure of these macrocycles defines a hydrophobic cavity with polar carbonyl groups surrounding the upper and lower rims. Due to the dipole defined by the carbonyl groups, CBs present a certain level of water solubility, with CB[5] and CB[7] showing solubilities of 30-20 mM while CB[6] and CB[8] are soluble only at less than 20 μM concentrations.[39] Therefore, in aqueous solutions, CBs can host hydrophobic molecules of suitable size in their pocket.[40] An illustrative example is the complexation between CB[7] and a diamantane quaternary diammonium ion derivative, showing an extremely high binding affinity (K_{eq} = 7.2 x 10^{17} M^{-1} in D_2O).[41]

4.3.2. Calixarenes

Calixarenes are another family of cavitands synthesized by the reaction of phenol units and formaldehyde catalyzed by a base.[42,43] Each subunit is attached by forming a methylene bridge in the meta-2,6 position to its adjacent subunit. These macrocycles are named calix[*n*]arenes due to their morphology resembles a calix and consist of [*n*] meta-arene rings linked by methylene groups in their structure.[43] The most generally used CAs are formed by 4, 5, 6, or 8 phenolic subunits.[44] CAs and derivatives have shown their ability to form host-guest complexes with a variety of guest molecules.[45,46] For example, Nau *et al*. reported the inclusion properties of the positively charged and fluorescent bicyclic diazoalkane (DBO) which, as expected, forms a very stable complex in water with p-sulfonatocalix[4]arene **CX4** (K_a = 60000 M^{-1}) owing to the complementarity of the spherical shape of the azoalkane and the CA cavity and the stabilizing electrostatic interactions between the protruding ammonium head group and the sulfonate groups at the upper rim (Figure 3).[47,48] Because of their good complexation capabilities, CA hosts have been used in sensing and biomedical applications.[49,50,51,52] For instance, the group of the prof. Aldrich-Wright showed the ability of *p*-sulfonatocalix[4]arenes

[37] K. I. Assaf, W. M. Nau, *Chem. Soc. Rev.* **2015**, *44*, 394-418.
[38] S. J. Barrow, S. Kasera, M. J. Rowland, J. del Barrio, O. A. Scherman, *Chem. Rev.* **2015**, *115*, 12320-12406.
[39] J. Lagona, P. Mukhopadhyay, S. Chakrabarti, L. Isaacs, *Angew. Chem. Int. Ed.* **2005**, *44*, 4844-4870.
[40] J. Murray, K. Kim, T. Ogoshi, W. Yao, B. C. Gibb, *Chem. Soc. Rev.* **2017**, *46*, 2479-2496.
[41] L. Cao, M. Šekutor, P. Y. Zavalij, K. Mlinarić-Majerski, R. Glaser, L. Isaacs, *Angew. Chem. Int. Ed.* **2014**, *53*, 988-993.
[42] C. D. Gutsche, B. Dhawan, K. H. No, R. Muthukrishnan, *J. Am. Chem. Soc.* **1981**, *103*, 3782-3792.
[43] C. D. Gutsche, L.-G. Lin, *Tetrahedron* **1986**, *42*, 1633-1640.
[44] L. Baldini, F. Sansone, A. Casnati, R. Ungaro, Calixarenes in Molecular Recognition. In *Supramolecular Chemistry: From Molecules to Nanomaterials*, John Wiley & Sons, Chichester, **2012**.
[45] A. F. Danil de Namor, R. M. Cleverley, M. L. Zapata-Ormachea, *Chem. Rev.* **1998**, *98*, 2495-2526.
[46] R. N. Dsouza, U. Pischel, W. M. Nau, *Chem. Rev.* **2011**, *111*, 7941-7980.
[47] H. Bakirci, A. L. Koner, M. H. Dickman, U. Kortz, W. M. Nau, *Angew. Chem. Int. Ed.* **2006**, *45*, 7400-7404.
[48] W. M. Nau, G. Ghale, A. Hennig, H. Bakirci, D. M. Bailey, *J. Am. Chem. Soc.* **2009**, *131*, 11558-11570.
[49] L. Baldini, A. Casnati, F. Sansone, R. Ungaro, *Chem. Soc. Rev.* **2007**, *36*, 254-266.
[50] E. V. Ukhatskaya, S. V. Kurkov, S. E. Matthews, T. Loftsson, *J. Pharm. Sci.* **2013**, *102*, 3485-3512.
[51] R. Kumar, A. Sharma, H. Singh, P. Suating, H. S. Kim, K. Sunwoo, I. Shim, B. C. Gibb, J. S. Kim, *Chem. Rev.* **2019**, *119*, 9657-9721.
[52] V. Bagnacani, V. Franceschi, M. Bassi, M. Lomazzi, G. Donofrio, F. Sansone, A. Casnati, R. Ungaro, *Nat. Commun.* **2013**, *4*, 1721.

to complex platinum(II)-based anticancer complexes, such as [(5,6-dimethyl-1,10-phenanthroline)(1*R*,2*R*-diaminocyclohexane) platinum(II)]$^{2+}$ (56MERR) and ([(5,6-dimethyl-1,10-phenanthroline) (1S,2S-diaminocyclohexane)platinum(II)]$^{2+}$ (56MESS, Figure 3). The authors found that this host-guest complexation effectively protected drugs from being degraded by GSH and remarkably decreased the diffusion rate of metal complexes while maintaining their anticancer activity.[53]

4.3.3. Cyclodextrins

Cyclodextrins (CDs) are cyclic oligomers of D-glucopyranoside units linked by α-1,4-glycosidic bonds (Figure 3).[54] These molecules are easily synthesized by a simple enzymatic degradation of starch by microorganisms such as *bacillus macerans*. The most commonly used CDs are the *α*-, *β*- and *γ*- CDs, composed of six, seven, and eight glucopyranose units respectively. These cavitands present the geometric molecular structure of a shallow truncated cone, where the primary and secondary hydroxyl groups are segregated in opposed primary (narrow) and secondary (wider) rims, respectively. The external side of the CDs is highly polar due to the hydroxyl groups, which makes them soluble in water. On the other hand, the internal cavity of CDs is hydrophobic, which makes these macrocycles excellent hosts for multiple non-polar molecules.[55,56] In this sense, a combination of several factors, such as the hydrophobic effect or van der Waals interactions between the internal cavity of the CDs and the guests are involved in the formation of the cyclodextrin-guest complex.[57]

Because of the low toxicity of cyclodextrin cavitands, they have been used as excipients for pharmaceutical applications to improve the formulation of hydrophobic drugs.[58] These supramolecular complexes can improve water solubility, bioavailability, physicochemical stability, and half-time. As a representative example, piroxicam[59] is an anti-inflammatory drug with poor water solubility. However, the corresponding complex with *β*-CD increased five-fold the apparent solubility,[60] reducing gastrointestinal irritation and allowing faster drug absorption and the onset of the analgesic effect.[61] Other drug examples include steroids, prostaglandins, antibiotics, or nitroglycerin. Interestingly, CDs have also been used to reduce the unpleasant smell or taste of pharmaceuticals.[62] In addition to hydrophobic drugs, a wide variety of host-guest complexes have been characterized.[63] Some remarkable examples are guests with a high affinity constant, such as adamantane[64] ($K_a \sim 10^5$ M^{-1}). Furthermore, stimuli-sensitive guests are also well known, including light-sensitive (azobenzene[65]) and redox-sensitive (ferrocene[66])

[53] A. M. Krause-Heuer, N. J. Wheate, M. J. Tilby, D. G. Pearson, C. J. Ottley, J. R. Aldrich-Wright, *Inorg. Chem.* **2008**, *47*, 6880-6888.
[54] M. Wakao, K. Fukase, S. Kusumoto, *J. Org. Chem.* **2002**, *67*, 8182-8190.
[55] G. Crini, *Chem. Rev.* **2014**, *114*, 10940-10975.
[56] S. Li, W. C. Purdy, *Chem. Rev.* **1992**, *92*, 1457-1470.
[57] E. M. M. Del Valle, *Process Biochem.* **2004**, *39*, 1033-1046.
[58] M. E. Davis, M. E. Brewster, *Nat. Rev. Drug Discov.* **2004**, *3*, 1023-1035.
[59] G. Wenz, *Clin. Drug Investig.* **2000**, *19*, 21-25.
[60] M. E. Brewster, T. Loftsson, *Adv. Drug Deliv. Rev.* **2007**, *59*, 645-666.
[61] S. Jacob, A. B. Nair, *Drug Dev. Res.* **2018**, *79*, 201-217.
[62] S. Carneiro, F. Costa Duarte, L. Heimfarth, J. Siqueira Quintans, L. Quintans-Júnior, V. Veiga Júnior, Á. Neves de Lima, *Int. J. Mol. Sci.* **2019**, *20*, 642.
[63] K. A. Connors, *Chem. Rev.* **1997**, *97*, 1325-1358.
[64] D. Taura, Y. Taniguchi, A. Hashidzume, A. Harada, *Macromol. Rapid Commun.* **2009**, *30*, 1741-1744.
[65] D. Wang, W. Zhao, Q. Wei, C. Zhao, Y. Zheng, *ChemPhotoChem* **2018**, *2*, 403-415.
[66] H. Gu, S. Mu, G. Qiu, X. Liu, L. Zhang, Y. Yuan, D. Astruc, *Coord. Chem. Rev.* **2018**, *364*, 51-85.

guests. Because synthetic hosts and guests are easily available, they have been implemented into a variety of scaffolds (e.g. polymers, dendrimers, surfaces) in order to build systems with implemented functionality such as delivery and sensing, as will be discussed in Chapter 2.

4.3.4. Coordination cages

Coordination cages have been defined as three-dimensional architectures with the ability to act as host entities in solution. These molecules have been prepared by self-assembly in solution of the organometallic precursors to achieve complex supramolecular structures.[67,68] During the last decades, Fujita´s, Raymond´s, or Nitschke´s groups, among others, have made important contributions to the design, synthesis, and study of the host-guest capabilities of these entities.

As a structural example, the group of prof. Nitschke has prepared three-dimensional covalent receptors by forming dynamic covalent imine bonds (C=N) and coordinative nitrogen-metal bonds (N→M) during the self-assembly.[69] Interestingly, these cationic cages have been applied for anion binding in an aqueous environment. For instance, metal-free covalent water-soluble cages were prepared through the borohydride reduction of metal-organic assemblies previously synthesized by using subcomponent self-assembly (Figure 4). Interestingly, these supramolecular cages demonstrated to be capable of encapsulating large anions with high affinity in aqueous environment.[69] An important aspect of coordination cages in comparison with the cavitands described above is that the cavity size can be enlarged in a feasible fashion through molecular design. In an impressive example, Fujita's group reported the self-assembly of Goldberg polyhedra-like structures composed of up to 60 metallic atoms and 120 ligands (Figure 4).[70] Moreover, these scaffolds can be designed to undergo adaptative guest recognition in processes that mimic enzyme pocket adaptation.[71] As a consequence, the use of coordination cages as nanocontainers for the delivery of molecules of biological interest has been proposed.[72]

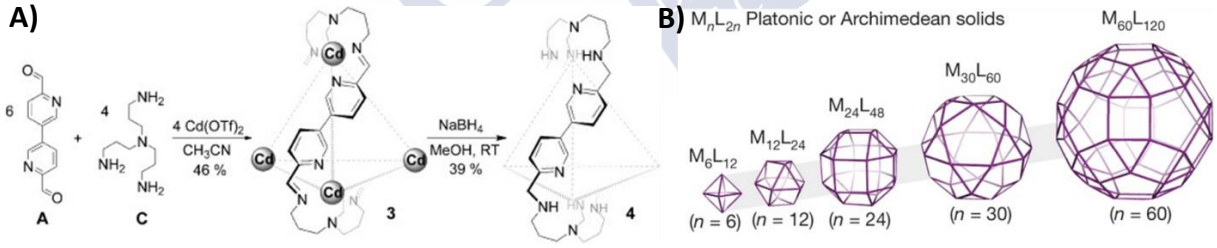

Figure 4. A) Example of the strategy developed by prof. Nitschke's group for the preparation of a metal-organic cage (**3**) by subcomponent self-assembly and subsequent obtainment of the corresponding metal-free covalent cage (**4**) after $NaBH_4$ reduction. Reprinted and adapted from ref. 69 with permission from John Wiley and Sons. Copyright 2014 Wiley-VCH Verlag GmbH & Co. KGaA, Weinheim. B) Goldberg polyhedra-like structures developed by prof. Fujita´s group. Reprinted and adapted with permission from ref. 70. Copyright 2016 Springer Nature.

[67] T. R. Cook, P. J. Stang, *Chem. Rev.* **2015**, *115*, 7001-7045.
[68] R. Chakrabarty, P. S. Mukherjee, P. J. Stang, *Chem. Rev.* **2011**, *111*, 6810-6918.
[69] J. Mosquera, S. Zarra, J. R. Nitschke, *Angew. Chem. Int. Ed.* **2014**, *53*, 1556-1559.
[70] D. Fujita, Y. Ueda, S. Sato, N. Mizuno, T. Kumasaka, M. Fujita, *Nature* **2016**, *540*, 563-566.
[71] Y. Tamura, H. Takezawa, M. Fujita, *J. Am. Chem. Soc.* **2020**, *142*, 5504-5508.
[72] A. Casini, B. Woods, M. Wenzel, *Inorg. Chem.* **2017**, *56*, 14715-14729.

Chapter I:
Supramolecular caging for cytosolic delivery of anionic probes

USC
UNIVERSIDADE
DE SANTIAGO
DE COMPOSTELA

Introduction

USC
UNIVERSIDADE
DE SANTIAGO
DE COMPOSTELA

1. The cellular membrane as a selective natural barrier

The cellular membrane is primarily responsible for the protection and the strict control of the exchange of molecules between the cellular interior and the extracellular environment.[73] This selective natural barrier is mainly formed by two components: lipids and proteins. Membrane lipids have a hydrophobic tail and a hydrophilic head that are oriented to form a protective barrier, the lipid bilayer. In addition to lipids, the cellular membrane contains different types of proteins. These membrane proteins can act, for example, as transporters (controlling the exchange of different molecules between the cellular interior and its environment) or as receptors (being responsible for cell signaling).[74]

The transport of different substances inside of the cells can be performed by using a variety of mechanisms that can be mainly classified in passive diffusion, facilitated diffusion, and active transport. Transport by passive diffusion allows the cells to transport different substances across the cell membrane in favor of an electrochemical or a concentration gradient. Therefore, this mechanism does not require energy from the cell. An important point is that this mechanism only allows the transport of hydrophobic small molecules across the cell membrane. To improve the transport of biologically important hydrophilic molecules for the cell such as ions or sugars, cells use facilitated diffusion. This mechanism occurs helped by different membrane proteins and it does not require energy from the cell.[75]

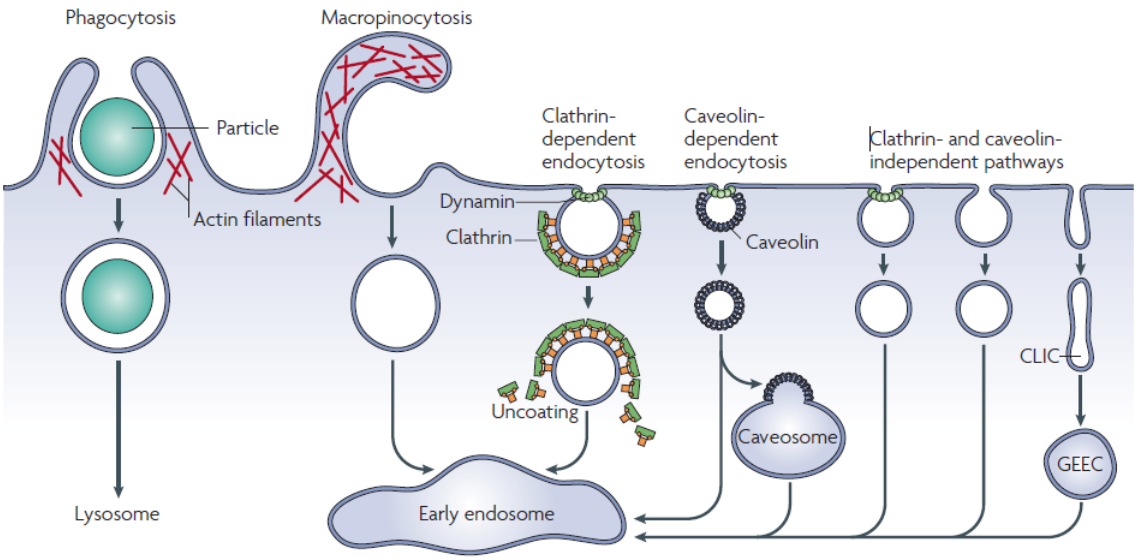

Figure 5. Schematic representation of the different endocytic pathways. Reprinted with permission from ref. 77. Copyright 2007 Springer Nature.

Active transport allows cells to transport extracellular molecules against an electrochemical or a concentration gradient, a mechanism that demands energy consumption by the cell. An important type of active transport is endocytosis, which allows the cell to transport fluids and solutes from its surroundings to the cell interior. Endocytosis is a phenomenon where there is a conformational change of the cell membrane to introduce different extracellular substances

[73] J. Lombard, *Biol. Direct* **2014**, *9*, 32.
[74] A. Uzman, B. Alberts, A. Johnson, J. Lewis, M. Raff, K. Roberts, P. Walter, *Molecular Biology of the Cell*, 4th edition, Garland Science, New York, **2003**.
[75] N. J. Yang, M. J. Hinner, *Methods Mol. Biol.* **2015**, *1266*, 29-53.

through the formation of small transport vesicles. Endocytosis can be classified into two major classes: phagocytosis and pinocytosis. Phagocytosis is an important process that allows the cell to internalize large particles and occurs exclusively in specialized cells such as neutrophils and macrophages. However, pinocytosis is a mechanism that allows the non-specialized cells to transport a variety of extracellular molecules and fluids through the cell membrane. Furthermore, pinocytosis can be also classified in different internalization pathways such as macropinocytosis, caveolin-dependent endocytosis, clathrin-dependent endocytosis, and clathrin and caveolin-independent endocytosis (Figure 5).[76,77]

This meticulous control of the transport through the cell membrane importantly influences the delivery of therapeutics as the effectiveness of drugs and other bioactive compounds depends on their effective delivery. The main reason is that the site of action of many molecules is placed in the cell interior. Thus, the drug needs to cross the plasma membrane to accomplish its pharmaceutical effect. For this reason, in the last years, many innovative cell delivery systems have emerged to improve the transport across the cell membrane of large hydrophilic molecules. Over the last twenty years, cell-penetrating peptides have emerged as an innovative approach to improve the intracellular delivery of different therapeutic and diagnostic cargoes such as drugs, imaging agents, nucleic acids, proteins, etc.[78]

2. Cell-penetrating peptides

In 1988, it was discovered that the TAT protein of the human immunodeficiency virus (HIV-1), consisting of 86 amino acids, had the ability to cross the cell membrane.[79,80] After studying this phenomenon, it was discovered that the sequence that provided these transport capabilities was a small peptide (RKKRRQRRR) called TAT.[81] In 1994, translocation capabilities were also found in the homeodomain of Antennapedia.[82] It was discovered that these transport properties were provided also by a small peptide which was called Penetratin (RQIKIWFQNRRMKWKK).[83] Following these preliminary findings, the scientific community was fascinated by the transport capabilities of these peptide sequences and began to develop modifications of these sequences designing new structures with penetrating capabilities, these peptides were named as cell-penetrating peptides (CPPs).[84]

Cell-penetrating peptides (CPPs) are small-sized peptides (usually less than 30 amino acids) capable of transporting a wide range of membrane-impermeable therapeutic agents into the cell interior. An important characteristic of these peptides is that they have the ability to transport molecules with low cellular toxicity at low micromolar concentrations. Different classifications have emerged for the wide variety of CPPs, for example, CPPs can be easily classified according to their physical-chemical properties in different types:

[76] G. J. Doherty, H. T. McMahon, *Annu. Rev. Biochem.* **2009**, *78*, 857-902.
[77] S. Mayor, R. E. Pagano, *Nat. Rev. Mol. Cell Biol.* **2007**, *8*, 603-612.
[78] F. Heitz, M. C. Morris, G. Divita, *Br. J. Pharmacol.* **2009**, *157*, 195-206.
[79] A. D. Frankel, C. O. Pabo, *Cell* **1988**, *55*, 1189-1193.
[80] M. Green, P. M. Loewenstein, *Cell* **1988**, *55*, 1179-1188.
[81] E. Vivès, P. Brodin, B. Lebleu, *J. Biol. Chem.* **1997**, *272*, 16010-16017.
[82] D. Derossi, A. H. Joliot, G. Chassaing, A. Prochiantz, *J. Biol. Chem.* **1994**, *269*, 10444-10450.
[83] D. Derossi, G. Chassaing, A. Prochiantz, *Trends Cell Biol.* **1998**, *8*, 84-87.
[84] J. D. Ramsey, N. H. Flynn, *Pharmacol. Ther.* **2015**, *154*, 78-86.

Cationic CPPs: This type of CPPs is characterized by their content of mainly cationic residues such as arginine and lysine, which confer a high net positive charge to the CPP. Some examples in this category are TAT, penetratin, or polyarginines.

Hydrophobic CPPs: These peptides mainly consist of hydrophobic amino acids. An example of a hydrophobic peptide is K-FGF (AAVLLPVVLLAAP).

Amphipathic CPPs: these peptides contain two different regions, a hydrophobic domain, and hydrophilic and cationic domain.[85] This class of CPPs normally can form stable non-covalent complexes with different cargos inducing the internalization in the cell. An amphipathic peptide, **Pep-1** (KETWWETWWTEWSQPKKKRKV) has been applied for delivering a wide number of cargos. For instance, this peptide can form non-covalent interactions with other peptides and protein cargos to allow their membrane translocation. Another example of this category is the **MPG** (GALFLGFLGAAGSTMGAWSQPKKKRKV), a peptide that has been discovered able to form stable complexes with different nucleic acids.[86] Moreover, amphipathic proline-rich peptides $(VXLPPP)_n$ have been prepared and also showed good membrane translocation capabilities.[87,88]

Many studies have been published regarding the mechanism of uptake of the CPPs. This topic has generated great controversy. Normally, these peptides are translocated inside of the cell following different endocytic pathways. It is known that there is a high influence of the concentration of the peptide and the characteristics of the cargo delivered and the type of CPP.[89]

A powerful strategy for the synthesis of new cell-penetrating peptides is the incorporation of dynamic bonds, such as oximes, hydrazones, or disulfides. Dynamic bonds are responsive to different external stimuli and, during their internalization pathway, these bonds are sensitive to the environment. From the synthetic point of view, dynamic bonds are also interesting as they lead to the final products with high yields, with the generation of a water molecule as the only side product, and in short periods of time.[90] Recently, in our research group, we have designed new penetrating peptides that contain dynamic bonds.[91] First, we synthesized cationic peptides containing amino acids modified with an alcoxyamine group. These peptides were then reacted with different aldehydes resulting in new oxime amphiphilic peptides. These amphiphilic cationic peptides were able to transport a variety of anionic DNA molecules in vesicle transport experiments.[91] Subsequently, we applied the same strategy to synthesize an amphiphilic pseudo-helical parent peptide, which was easily reacted with different hydrophobic and hydrophilic electrophiles (Figure 6).[92] In this work, we explored the capacity of DNA transport in vesicles of this type of peptides and the difference that exists depending on the hydrophilicity of the electrophiles used. Moreover, we studied the modification of the membrane translocation capabilities of the peptides in cells with the modulation of their amphiphilicity.[92] In our research group, dynamic linkages, such as hydrazone bonds, have also been applied to synthesize

[85] D. Raucher, J. S. Ryu, *Trends Mol. Med.* **2015**, *21*, 560-570.
[86] M. C. Morris, S. Deshayes, F. Heitz, G. Divita, *Biol. Cell* **2008**, *100*, 201-217.
[87] A. D. Frankel, C. O. Pabo, *Cell* **1988**, *55*, 1189-1193.
[88] Y. A. Fillon, J. P. Anderson, J. Chmielewski, *J. Am. Chem. Soc.* **2005**, *127*, 11798-11803.
[89] A. Rioboo, I. Gallego, J. Montenegro, *An. Química* **2019**, *115*, 9-21.
[90] C. Gehin, J. Montenegro, E. K. Bang, A. Cajaraville, S. Takayama, H. Hirose, S. Futaki, S. Matile, H. Riezman, *J. Am. Chem. Soc.* **2013**, *135*, 9295-9298.
[91] J. M. Priegue, J. Montenegro, J. R. Granja, *Small* **2014**, *10*, 3613-3618.
[92] M. Pazo, H. Fernández-Caro, J. Priegue, I. Lostalé-Seijo, J. Montenegro, *Synlett* **2017**, *28*, 924-928.

dynamic penetrating peptides with hydrophobic tails which formed complexes by non-covalent interactions and, then, triggered the transport of plasmid DNA[93] and Cas9[94] in cells.

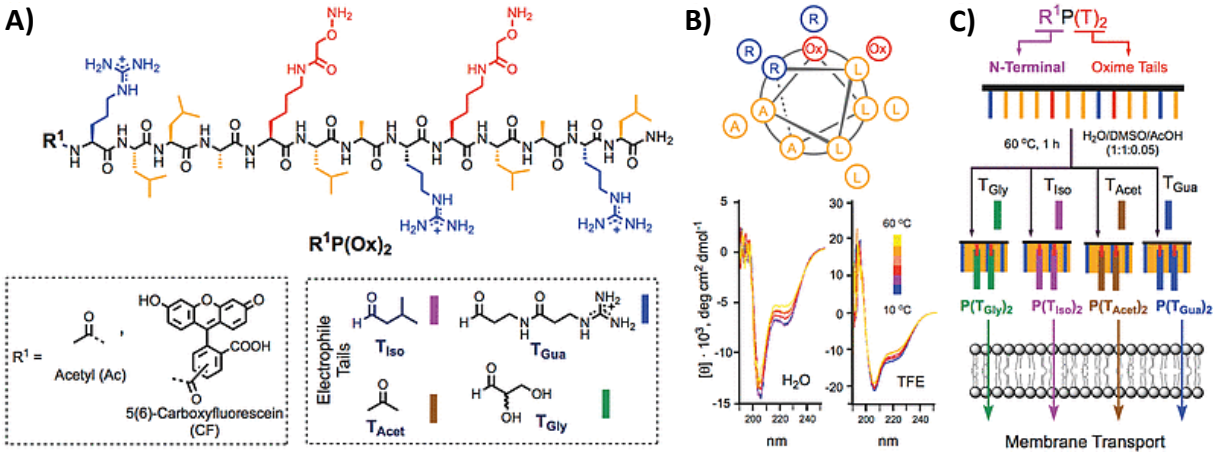

Figure 6. A) Chemical structure of the amphiphilic peptide showing two alcoxyamine reactive groups where the different electrophilic aldehydes were attached. B) Top-view helical diagram and circular dichroism spectra of the parent peptide. C) Schematic representation of peptide functionalization with the different aldehydes to afford oxime-modulated peptides for membrane transport applications. Reprinted from ref. 92 under the terms of the Creative Commons CC-BY-NC-ND license.

3. Cell delivery of biologically active macromolecules

Proteins and nucleic acids have emerged as excellent therapeutics for the treatment of a variety of diseases.[95,96] Macromolecular therapeutics, such as nucleic acids or recombinant proteins, have to efficiently cross the cellular membrane due to their site of action is located in the cytosol or the cell nucleus. Unfortunately, the cytosolic delivery of nucleic acids and proteins is inefficient mainly because of endosomal entrapment and enzymatic digestion.[97,98] Therefore, the delivery of macromolecules into cells and tissues remains a major challenge, and new delivery systems to overcome these limitations are needed. During the last years, different methods can be differentiated to deliver therapeutic macromolecules into the cell interior including physical and mechanical methods and chemical covalent and non-covalent methods.

[93] I. Louzao, R. García-Fandiño, J. Montenegro, *J. Mater. Chem. B* **2017**, *5*, 4426-4434.
[94] I. Lostalé-Seijo, I. Louzao, M. Juanes, J. Montenegro, *Chem. Sci.* **2017**, *8*, 7923-7931.
[95] J. Nguyen, F. C. Szoka, *Acc. Chem. Res.* **2012**, *45*, 1153-1162.
[96] Y. Zhang, J. J. Røise, K. Lee, J. Li, N. Murthy, *Curr. Opin. Biotechnol.* **2018**, *52*, 25-31.
[97] V. Torchilin, *Drug Discov. Today Technol.* **2008**, *5*, 95-103.
[98] M. L. Read, A. Logan, L. W. Seymour, *Adv. Genet.* **2005**, *53*, 19-46.

3.1.Physical and mechanical methods

Several physical and mechanical strategies have been developed to achieve direct cytosolic delivery of macromolecules such as DNA or proteins.[99,100]

Mechanical methods, such as **microinjection**, are a typical powerful strategy. Microinjection is one of the most direct and simplest methods to incorporate DNA into the nucleus or the cytosol of cells. In this technique, the release of the biomolecule is carried out using a needle on a single cell. This strategy is carried out when a precise and accurate delivery of the macromolecule is necessary. However, this methodology does not show good results when a high number of cell transfection is required.[101]

Physical methods, such as **electroporation** have been also widely applied. This technique induces short high voltage electric cycles to the cell suspensions. This voltage produces transient pores in the cell membrane and the soluble desired proteins can cross the cell membrane by simple diffusion.[102] The main advantage of this technique is that it can be applied to different cell lines and a large number of cells can be transfected. However, the main limitation of electroporation methods is the important cytotoxicity induced by the high voltage cycles and the damage produced to the cell membrane. Moreover, this technique is limited to *in vitro* usage.[103]

3.2. Chemical covalent methods

During the last years, macromolecules, such as DNA or proteins, have been covalently linked to different delivery systems including cell-penetrating peptides,[104] gold nanoparticles,[105] polymers,[106] and strain-promoted thiols.[107]

3.2.1. Cell-penetrating peptides

The covalent attachment of macromolecules to cell-penetrating peptides has been applied to deliver different therapeutic macromolecules such as proteins or nucleic acids.[104]

Delivery of proteins. Different CPPs such as TAT peptide, Penetratin, Transportan, etc. have demonstrated, in different *in vitro* examples, their abilities to efficiently deliver proteins.[108,109] For instance, it has been demonstrated that TAT peptide has the ability to deliver large proteins such as *β*-galactosidase. The *in vivo* administration of the covalent conjugate

[99] M. S. Al-Dosari, X. Gao, *AAPS J.* **2009**, *11*, 671.
[100] S. Du, S. S. Liew, L. Li, S. Q. Yao, *J. Am. Chem. Soc.* **2018**, *140*, 15986-15996.
[101] S. Mehier-Humbert, R. H. Guy, *Adv. Drug Deliv. Rev.* **2005**, *57*, 733-753.
[102] M. Chiper, K. Niederreither, G. Zuber, *Adv. Healthc. Mater.* **2018**, *7*, e1701040.
[103] A. Fu, R. Tang, J. Hardie, M. E. Farkas, V. M. Rotello, *Bioconjug. Chem.* **2014**, *25*, 1602-1608.
[104] D. Kalafatovic, E. Giralt, *Molecules* **2017**, *22*, 1929.
[105] D. A. Giljohann, D. S. Seferos, W. L. Daniel, M. D. Massich, P. C. Patel, C. A. Mirkin, *Angew. Chem. Int. Ed.* **2010**, *49*, 3280-3294.
[106] R. Duncan, *Nat. Rev. Drug Discov.* **2003**, *2*, 347-360.
[107] N. Chuard, G. Gasparini, D. Moreau, S. Lörcher, C. Palivan, W. Meier, N. Sakai, S. Matile, *Angew. Chem. Int. Ed.* **2017**, *56*, 2947-2950.
[108] S. G. Patel, E. J. Sayers, L. He, R. Narayan, T. L. Williams, E. M. Mills, R. K. Allemann, L. Y. P. Luk, A. T. Jones, Y. H. Tsai, *Sci. Rep.* **2019**, *9*, 6298.
[109] M. Mäe, Ü. Langel, *Curr. Opin. Pharmacol.* **2006**, *6*, 509-514.

between β-galactosidase and TAT has shown an efficient delivery not only in the different tissues of the mice but also in the brain.[110] To successfully reach its intracellular target and produce its therapeutic effect the protein should not remain trapped inside of the endosome.[111] To promote protein delivery, the use of covalently attached endosomolytic peptides has also been reported.[112] The covalent conjugation between proteins and CPPs can be achieved by expressing CPP-fusion proteins.[113] In addition, the CPP can be covalently linked to the side chain of a lysine of the protein or to a thiol of a cysteine to achieve specific modifications.[114,115]

Delivery of nucleic acids. CPPs have also demonstrated their abilities to efficiently deliver bioactive nucleic acids. 5´-thiol functionalized siRNA has been covalently attached to Transportan and Penetratin peptides modified with terminal cysteines. This complex CCP-siRNA showed an efficient knockdown of mammalian cells.[116] Moreover, peptide nucleic acids (PNAs) have been also covalently attached to different CPPs to improve their translocation capabilities.[117,118] The use of covalent bonds with CPPs has been successfully applied for the cellular delivery of a variety of therapeutic macromolecules. However, this strategy has also drawbacks such as modification of the chemical properties of the cargo, which can lead to changes in its biological activity.[119] In addition, this strategy is not as compatible with the functional delivery of large biomolecules such as pDNA and the synthesis and purification of the corresponding conjugates results tedious as it normally requires multiple steps.[120]

3.2.2. Metal nanoparticle conjugates

Gold nanoparticles (AuNPs) have also been applied to deliver macromolecules by covalent strategies. The group of prof. Chad Mirkin prepared a type of polyvalent nucleic acid capped AuNPs (pNA-AuNPs) by covalently functionalizing AuNPs with thiol-modified oligonucleotides for siRNA-based gene silencing.[121] The incorporation of the oligonucleotides on the surface of these AuNPs showed protection of the cargo and inhibition of its degradation by nucleases. Interestingly, these pNA-AuNPs were efficiently internalized in more than fifty different cell lines.[105,122] More recently, to target specific cells, this group modified the pNA-

[110] S. R. Schwarze, A. Ho, A. Vocero-Akbani, S. F. Dowdy, *Science* **1999**, *285*, 1569-1572.
[111] P. Lönn, A. D. Kacsinta, X. S. Cui, A. S. Hamil, M. Kaulich, K. Gogoi, S. F. Dowdy, *Sci. Rep.* **2016**, *6*, 32301.
[112] M. Li, Y. Tao, Y. Shu, J. R. LaRochelle, A. Steinauer, D. Thompson, A. Schepartz, Z. Y. Chen, D. R. Liu, *J. Am. Chem. Soc.* **2015**, *137*, 14084-14093.
[113] J. Jo, S. Hong, W. Y. Choi, D. R. Lee, *Sci. Rep.* **2014**, *4*, 4378.
[114] S. B. Gunnoo, A. Iyer, W. Vannecke, K. W. Decoene, T. Hebbrecht, J. Gettemans, M. Laga, S. Loverix, I. Lasters, A. Madder, *Chem. Commun.* **2018**, *54*, 11929-11932.
[115] D. A. Shannon, E. Weerapana, *Curr. Opin. Chem. Biol.* **2015**, *24*, 18-26.
[116] A. Muratovska, M. R. Eccles, *FEBS Lett.* **2004**, *558*, 63-68.
[117] Y. Wolf, S. Pritz, S. Abes, M. Bienert, B. Lebleu, J. Oehlke, *Biochemistry* **2006**, *45*, 14944-14954.
[118]S. Abes, J. J. Turner, G. D. Ivanova, D. Owen, D. Williams, A. Arzumanov, P. Clair, M. J. Gait, B. Lebleu, *Nucleic Acids Res.* **2007**, *35*, 4495-4502.
[119] G. Guidotti, L. Brambilla, D. Rossi, *Trends Pharmacol. Sci.* **2017**, *38*, 406-424.
[120] T. Lehto, K. Kurrikoff, Ü. Langel, *Expert Opin. Drug Deliv.* **2012**, *9*, 823-836.
[121] D. S. Seferos, A. E. Prigodich, D. A. Giljohann, P. C. Patel, C. A. Mirkin, *Nano Lett.* **2009**, *9*, 308-311.
[105] D. A. Giljohann, D. S. Seferos, W. L. Daniel, M. D. Massich, P. C. Patel, C. A. Mirkin, *Angew. Chem. Int. Ed.* **2010**, *49*, 3280-3294.
[122] P. C. Patel, D. A. Giljohann, W. L. Daniel, D. Zheng, A. E. Prigodich, C. A. Mirkin, *Bioconjug. Chem.* **2010**, *21*, 2250-2256.

AuNPs with monoclonal antibody-DNA conjugates (Figure 7, left). Importantly, higher cell selectivity and gene knockdown were achieved in cells that overexpress the target antigen.[123]

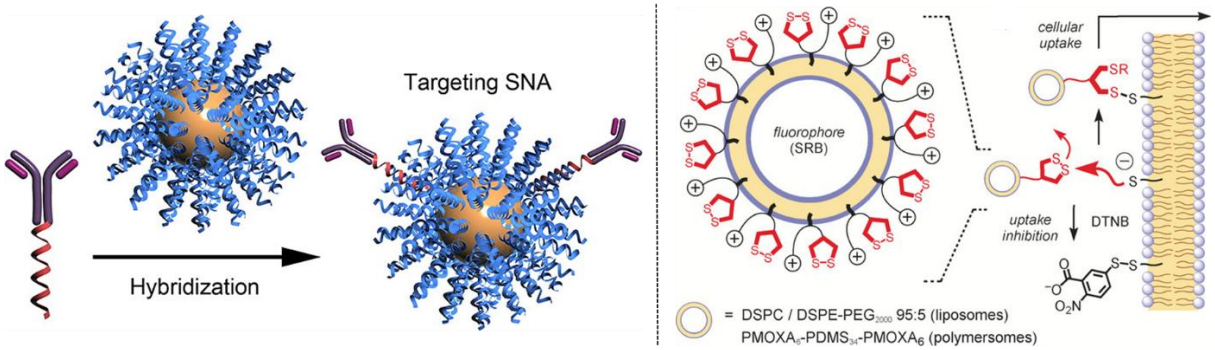

Figure 7. Left: Hybridization of pNA-AuNPs using monoclonal antibody-DNA conjugates. Reprinted with permission from ref. 123. Copyright 2012 American Chemical Society. Right: Strain-promoted thiols strategy applied to deliver liposomes and polymersomes inside living cells. Reprinted from ref. 107 with permission from John Wiley and Sons. Copyright 2017 Wiley-VCH Verlag GmbH & Co. KGaA, Weinheim.

3.2.3. Strain-promoted thiols

Strain-promoted thiols are a recently developed strategy from the group of the prof. Matile.[107] The application of this strategy allowed the delivery of polymersomes and liposomes into HeLa Kyoto cells.[107] Based on previous work from this group on strained cyclic disulfides, the transferrin receptor (TFRC) was found to be related to the cellular internalization of the corresponding penetrating peptides.[124] Recently, cationic amphiphiles were modified with cyclic disulfides to obtain liposomes and polymersomes and, after disulfide exchange with cellular exofacial thiols, the highly strained disulfides lead to an efficient cytosolic release of these giant substrates (Figure 7, right).[107]

3.2.4. Polymer-drug conjugates

Polymer-drug conjugates are attractive molecules to deliver drugs inside cells. The incorporation of different macromolecules, such as proteins, into polymeric scaffolds, has emerged as an innovative approach to overcome endosomal entrapment. For instance, the limitations of protein therapeutics such as fast clearance, low stability, and high immunogenicity can be solved by PEGylation.[125] Conjugation of PEG with protein therapeutics reduce immunogenicity, by shielding its antigenic epitopes, and improving its therapeutic safety. Moreover, protein PEGylation demonstrated to avoid opsonization and digestion by proteolytic enzymes. Furthermore, molecular mass increase helps to reduce plasma clearance and therefore the dosage frequency.[126] During the last years, several **PEGylated proteins** such

[123] K. Zhang, L. Hao, S. J. Hurst, C. A. Mirkin, *J. Am. Chem. Soc.* **2012**, *134*, 16488-16491.
[107] N. Chuard, G. Gasparini, D. Moreau, S. Lörcher, C. Palivan, W. Meier, N. Sakai, S. Matile, *Angew. Chem. Int. Ed.* **2017**, *56*, 2947-2950.
[124] D. Abegg, G. Gasparini, D. G. Hoch, A. Shuster, E. Bartolami, S. Matile, A. Adibekian, *J. Am. Chem. Soc.* **2017**, *139*, 231-238.
[125] P. Caliceti, F. M. Veronese, *Adv. Drug Deliv. Rev.* **2003**, *55*, 1261-1277.
[126] I. Ekladious, Y. L. Colson, M. W. Grinstaff, *Nat. Rev. Drug Discov.* **2019**, *18*, 273-294.

as enzymes, antibodies, growth factors, or cytokines have been developed. Moreover, different PEG-protein conjugates, such as Adagen® (a PEG-adenosine deaminase conjugate), have been approved as therapies for a wide range of indications. For instance, Adagen® has been approved for the treatment of severe combined immunodeficiency disease (SCID).[127] Furthermore, while the antigen-binding fragment (Fab′) of antibodies demonstrated innovative therapeutic capabilities, normally shows short circulation times. Recently, a PEGylated anti-tumour necrosis factor (TNF) Fab′, named certolizumab pegol (Cimzia®), has been approved and showed extended circulation half-life.[128]

On the other hand, **PEGylation of nucleic acids**, such as aptamer therapeutics, have been also carried out. Generally, these molecules suffer from cleavage by nucleases a situation that importantly reduces its half-life. A notable example is the approved drug for macular degeneration, pegaptanib sodium (Macugen®).[129,130] PEGylation of this aptamer showed an important increase in half-life. All these advances demonstrate the impact that PEGylation has produced in the development of novel therapeutic agents.

3.3.Chemical non-covalent supramolecular methods

Supramolecular methods can use different non-covalent interactions to conjugate the delivery system with the macromolecular cargo such as electrostatic interactions or hydrophobic forces. During the last decades, macromolecular cargos, such as nucleic acids or proteins, have been studied in non-covalent delivery systems using different carriers such as cell-penetrating peptides,[131] synthetic polymers,[132] dynamic amphiphiles,[133] and gold nanoparticles.[134]

3.3.1. Cell-penetrating peptides

The formation of non-covalent interactions between macromolecules and CPP has emerged as an innovative approach to overcome endosomal entrapment.[131] This strategy has the advantage that the modification of the cargo is not required so there will not be any modification of its biological activity.

CPPs have demonstrated nucleic acid delivery capabilities driven by non-covalent interactions. For instance, amphiphilic CPPs, such as MPG peptide, are able to establish hydrophobic and electrostatic interactions with anionic nucleic acids. MPG peptide was demonstrated to form stable complexes with the DNA cargo and these nanocomplexes were internalized and the cargo was efficiently delivered inside the cells.[135] As we have previously commented, a recent example of the application of CPPs for the transport of plasmid DNA to the cellular interior, driven by non-covalent interactions, was developed in our research group

[127] S. N. S. Alconcel, A. S. Baas, H. D. Maynard, *Polym. Chem.* **2011**, *2*, 1442-1448.
[128] E. D. Deeks, *Drugs* **2013**, *73*, 75-97.
[129] A. D. Keefe, S. Pai, A. Ellington, *Nat. Rev. Drug Discov.* **2010**, *9*, 537-550.
[130] P. L. Turecek, M. J. Bossard, F. Schoetens, I. A. Ivens, *J. Pharm. Sci.* **2016**, *105*, 460-475.
[131] M. Chang, Y.-W. Huang, R. Aronstam, H.-J. Lee, *Curr. Pharm. Biotechnol.* **2014**, *15*, 267-275.
[132] D. W. Pack, A. S. Hoffman, S. Pun, P. S. Stayton, *Nat. Rev. Drug Discov.* **2005**, *4*, 581-593.
[133] A. Fuertes, M. Juanes, J. R. Granja, J. Montenegro, *Chem. Commun.* **2017**, *53*, 7861-7871.
[134] Y. Ding, Z. Jiang, K. Saha, C. S. Kim, S. T. Kim, R. F. Landis, V. M. Rotello, *Mol. Ther.* **2014**, *22*, 1075-1083.
[135] S. Deshayes, M. Morris, F. Heitz, G. Divita, *Adv. Drug Deliv. Rev.* **2008**, *60*, 537-547.

(Figure 8).[93] In this work, a helical penetrating peptide was synthesized bearing two hydrazides incorporated in the peptide linear sequence. This model peptide was reacted with a series of hydrophobic aldehydes, obtaining with a reduced synthetic effort, a peptide library with different amphiphilic properties. This strategy allowed good transfection results in comparison with common transfection agents such as Lipofectamine 2000.[93] Furthermore, over the last years, different peptide sequences have been discovered capable of transporting oligonucleotides inside living cells. Highlights include, for example, KALA amphiphilic peptides,[136] peptides stearylated at the N-terminal positions,[137] or tetralisin functionalizations with guanidinocarbonylpyrrole groups.[138]

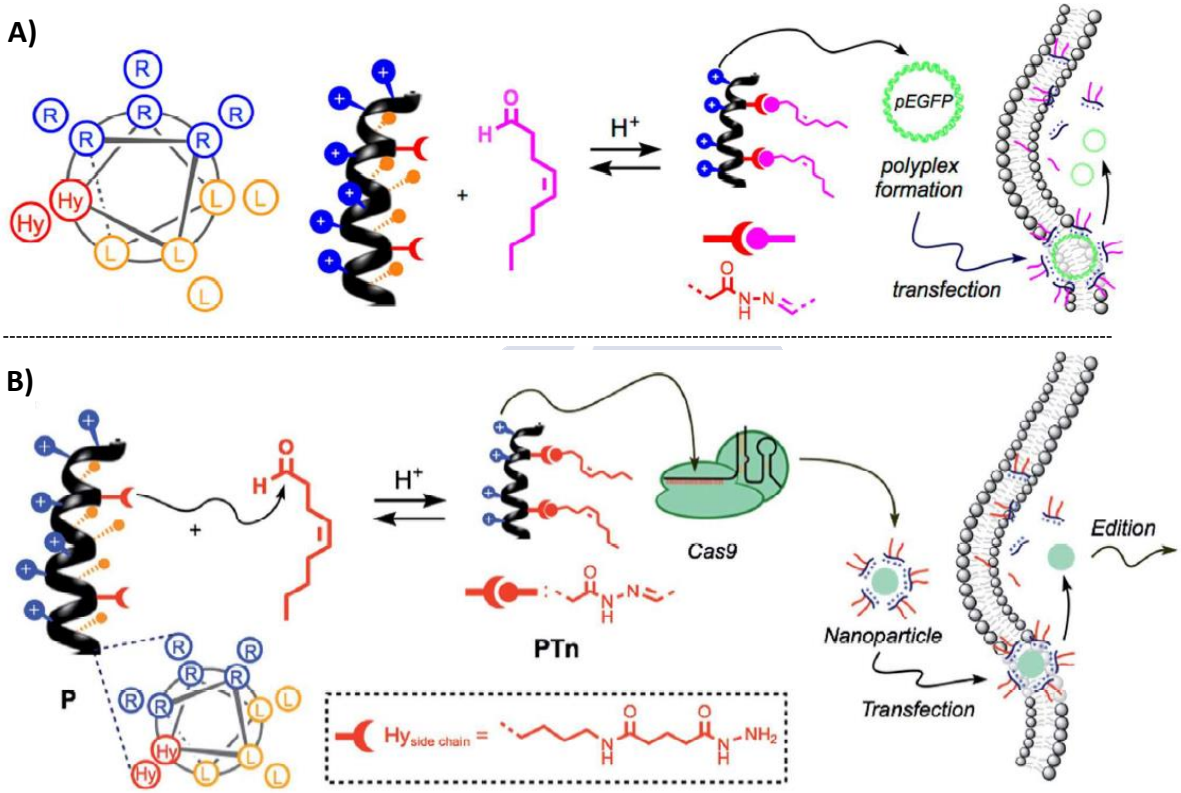

Figure 8. Schematic representation of an amphiphilic helical peptide bearing two reactive hydrazide groups, functionalization with hydrophobic aldehydes and, subsequent, complexation, transport, and delivery of A) a plasmid DNA and B) Cas9 ribonucleoprotein inside living cells. A) Reproduced from Ref. 93 with permission from The Royal Society of Chemistry. B) Reprinted from Ref. 94 under the terms of the Creative Commons Attribution-NonCommercial 3.0 Unported Licence. Published by The Royal Society of Chemistry.

CPPs have also shown protein delivery capabilities driven by non-covalent interactions. For example, it has been found that the amphiphilic peptide, Pep-1, is able to efficiently deliver a wide range of proteins.[139] Recently, the system Cas9 ribonucleoprotein has attracted high attention due to the therapeutic opportunities of gene edition. However, this system has some

[93] I. Louzao, R. García-Fandiño, J. Montenegro, *J. Mater. Chem. B* **2017**, *5*, 4426-4434.
[136] T. B. Wyman, F. Nicol, O. Zelphati, P. V. Scaria, C. Plank, F. C. Szoka, *Biochemistry* **1997**, *36*, 3008-3017.
[137] S. Futaki, W. Ohashi, T. Suzuki, M. Niwa, S. Tanaka, K. Ueda, H. Harashima, Y. Sugiura, *Bioconjug. Chem.* **2001**, *12*, 1005-1011.
[138] M. Li, S. Schlesiger, S. K. Knauer, C. Schmuck, *Angew. Chem. Int. Ed.* **2015**, *54*, 2941-2944.
[139] E. Gros, S. Deshayes, M. C. Morris, G. Aldrian-Herrada, J. Depollier, F. Heitz, G. Divita, *Biochim. Biophys. Acta* **2006**, *1758*, 384-393.

difficulties for crossing the cell membrane and several strategies have been developed up to date.[140,141,142] As we have previously commented, a prominent example in the field of this potentially therapeutic protein delivery into the cell interior is the method recently developed in our research group (Figure 8).[94] In this work, the internalization of the Cas9 protein was again carried out by using a penetrating peptide with two tails of oleic acids. In this case, a complex is formed between the amphiphilic peptide functionalized with the aldehydes and the Cas9 protein, subsequently, this complex is internalized and released to the cell cytosol, where Cas9 is released and carries out its function.[94]

As we have previously mentioned, one of the main limitations for the delivery of macromolecules is the endosomal entrapment. A prominent strategy to avoid this problem is to design new endosomolytic peptides.[143] Recently, the group of prof. Futaki designed an interesting peptide with penetrating and endosomolytic capabilities.[144] In this work, one amino acid of the hydrophobic part of a lytic spider venom peptide was replaced by glutamate (Figure 9). The modified peptide reaches the cellular endosomes without any lytic activity. However, once in the endosome, the glutamate residue gets protonated and the peptide recovers its lytic capabilities and is able to disrupt the cell endosome. This methodology was used in the cytosolic release of antibodies.[144] More recently, in Futaki´s group, new endosomolytic peptides with improved properties have been designed.[145]

[140] S. Ramakrishna, A. B. Kwaku Dad, J. Beloor, R. Gopalappa, S. K. Lee, H. Kim, *Genome Res.* **2014**, *24*, 1020-1027.
[141] J. A. Zuris, D. B. Thompson, Y. Shu, J. P. Guilinger, J. L. Bessen, J. H. Hu, M. L. Maeder, J. K. Joung, Z.-Y. Chen, D. R. Liu, *Nat. Biotechnol.* **2015**, *33*, 73-80.
[142] M. Wang, J. A. Zuris, F. Meng, H. Rees, S. Sun, P. Deng, Y. Han, X. Gao, D. Pouli, Q. Wu, et al., *Proc. Natl. Acad. Sci.* **2016**, *113*, 2868-2873.
[94] I. Lostalé-Seijo, I. Louzao, M. Juanes, J. Montenegro, *Chem. Sci.* **2017**, *8*, 7923-7931.
[143] A. El-Sayed, S. Futaki, H. Harashima, *AAPS J.* **2009**, *11*, 13-22.
[144] M. Akishiba, T. Takeuchi, Y. Kawaguchi, K. Sakamoto, H. H. Yu, I. Nakase, T. Takatani-Nakase, F. Madani, A. Gräslund, S. Futaki, *Nat. Chem.* **2017**, *9*, 751-761.
[145] Y. Azuma, H. Imai, Y. Kawaguchi, I. Nakase, H. Kimura, S. Futaki, *Angew. Chem. Int. Ed.* **2018**, *57*, 12771-12774.

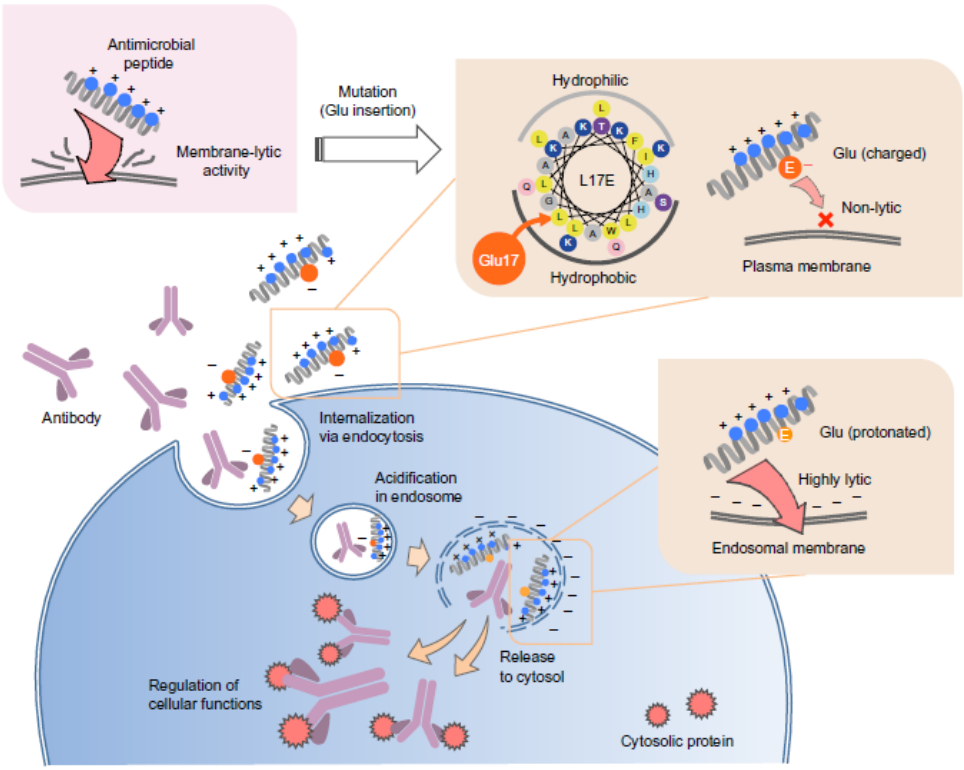

Figure 9. Schematic representation of the mechanism of internalization of a non-lytic penetrating and endosomolytic peptide derived from a lytic spider venom peptide used for the delivery of antibodies into the cell cytosol. Reproduced with permission from ref. 144. Copyright 2017 Springer Nature.

3.3.2. Synthetic polymers

Synthetic polymers can also be employed for the transport and release of nucleic acids into the cellular interior.[132] Certain positively charged polymers interact, through electrostatic forces, with DNA and RNA anionic cargos. The resulting complex internalizes into cells following endocytic pathways and the cargo is released to the cell cytosol. Some prominent polymers in this field that have been used for the transport of nucleic acids are polyethylenimine[146] (PEI) and polyamidoamine dendrimers (PAMAM).[147]

In recent years, our research group developed new dynamic polyhydrazones to trigger the transport of nucleic acids into the cell interior. In collaboration with the group of Dr. Fernández-Trillo, the hydrazone-containing amphiphilic polymers were applied in the delivery of siRNA in human HeLa cells (Figure 10).[148] Subsequently, this idea was extended to different nucleic acids such as plasmid DNA[149] and mRNA.[150]

[132] D. W. Pack, A. S. Hoffman, S. Pun, P. S. Stayton, *Nat. Rev. Drug Discov.* **2005**, *4*, 581-593.
[146] B. Brissault, A. Kichler, C. Guis, C. Leborgne, O. Danos, H. Cheradame, *Bioconjug. Chem.* **2003**, *14*, 581-587.
[147] A. U. Bielinska, C. Chen, J. Johnson, J. R. Baker, *Bioconjug. Chem.* **1999**, *10*, 843-850.
[148] J. M. Priegue, D. N. Crisan, J. Martínez-Costas, J. R. Granja, F. Fernandez-Trillo, J. Montenegro, *Angew. Chem. Int. Ed.* **2016**, *55*, 7492-7495.
[149] J. M. Priegue, I. Lostalé-Seijo, D. Crisan, J. R. Granja, F. Fernández-Trillo, J. Montenegro, *Biomacromolecules* **2018**, *19*, 2638-2649.
[150] M. Juanes, O. Creese, P. Fernández-Trillo, J. Montenegro, *Med. Chem. Commun.* **2019**, *10*, 1138-1144.

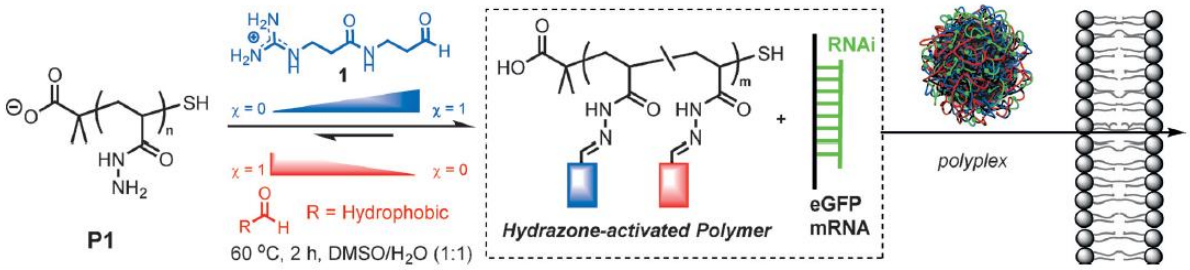

Figure 10. Post-polymerization functionalization with hydrophobic and cationic aldehydes, complexation with the payload (siRNA), and intracellular delivery. Reprinted from ref. 148 with permission from John Wiley and Sons. Copyright 2016 Wiley-VCH Verlag GmbH & Co. KGaA, Weinheim.

3.3.3. Dynamic amphiphiles

Another strategy to incorporate various biomacromolecules into the cell such as DNA for therapeutic purposes is the use of dynamic amphiphiles. Dynamic amphiphiles are amphiphiles which have a hydrophilic head and a hydrophobic tail with a dynamic covalent bridge between them (Figure 11).[133] A remarkable example in this area was designed by Jean-Marie Lehn in which an amphiphile formed by a hydrophobic part (cholestenone) and a cationic and hydrophilic part (guanidinium) connected by a hydrazone bond was synthesized (Figure 11, left). This type of molecules was applied as a vector to internalize luciferase-expressing plasmid DNA.[151]

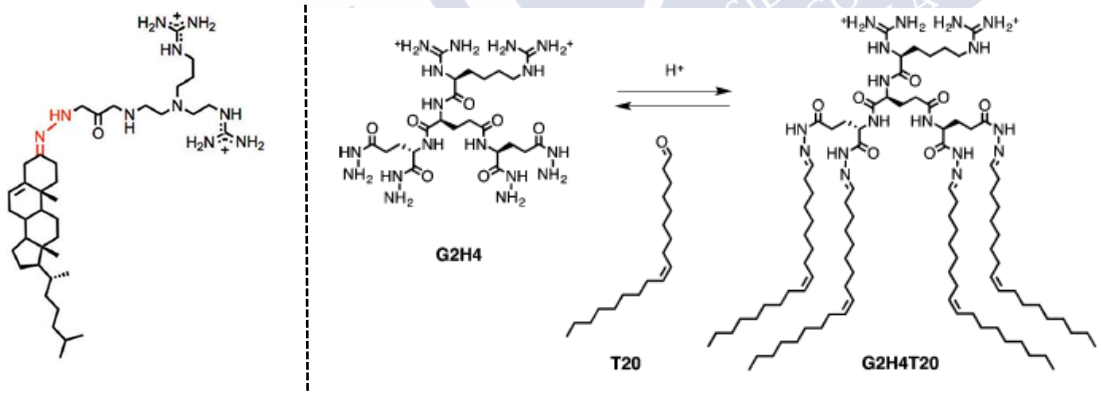

Figure 11. Left. Example of dynamic amphiphile applied to transport luciferase-expressing plasmid DNA.[151] Right. Synthesis of amphiphile through the use of dynamic bonds.[90]

As we have previously mentioned, the group of prof. Matile developed a new synthetic strategy, based on dynamic bonds, to facilitate the synthesis of amphiphile dendron libraries. These compounds were shown to be capable of inducing the transport of various anions through model membranes.[152] Subsequently, this group expanded this strategy to living cells and demonstrated the transport of siRNA in human cells with high efficiency.[90] A library of

[133] A. Fuertes, M. Juanes, J. R. Granja, J. Montenegro, *Chem. Commun.* **2017**, *53*, 7861-7871.
[151] A. Aissaoui, B. Martin, E. Kan, N. Oudrhiri, M. Hauchecorne, J. P. Vigneron, J. M. Lehn, P. Lehn, *J. Med. Chem.* **2004**, *47*, 5210-5223.
[152] T. Takeuchi, J. Montenegro, A. Hennig, S. Matile, *Chem. Sci.* **2011**, *2*, 303-307.
[90] C. Gehin, J. Montenegro, E. K. Bang, A. Cajaraville, S. Takayama, H. Hirose, S. Futaki, S. Matile, H. Riezman, *J. Am. Chem. Soc.* **2013**, *135*, 9295-9298.

dendronized amphiphiles was prepared by reacting a collection of cationic hydrazides with a variety of hydrophobic aldehydes tails (Figure 11, right). These compounds showed excellent results in the transfection of siRNA in human primary fibroblasts and HeLa cells with higher efficiency than the siRNA routine transfection agents (i.e. Lipofectamine RNAiMAX).[90]

3.3.4. Metal nanoparticles

Gold nanoparticles (AuNPs) have emerged as an excellent non-covalent delivery vehicle for nucleic acids.[134] It has been proven that cationic AuNPs have the ability to interact with nucleic acids that are negatively charged.[153] For instance, the quaternary ammonium–functionalized AuNPs (Figure 12, left) developed by Rotello *et al.* have been applied for cellular delivery of plasmid DNA.[154] Interestingly, the formation of the DNA-AuNP complex, in which DNA is bent and wrapped on the surface of the AuNP, has been demonstrated to protect DNA from its digestion by nucleases.[155] AuNPs have also been applied as an important strategy for intracellular transport of genome editing tools such as CRISPR/Cas9 (Figure 12, right).[156] AuNPs were modified with cationic arginines on their surface and the resulting cationic AuNPs showed their ability to form a complex with Cas9 protein modified with sgRNA and a glutamate peptide tag. Interestingly, the group of prof. Rotello found that these nanoassemblies cross the cell membrane and, using this strategy, high efficiency of transfection and gene editing at target genes were achieved.[156]

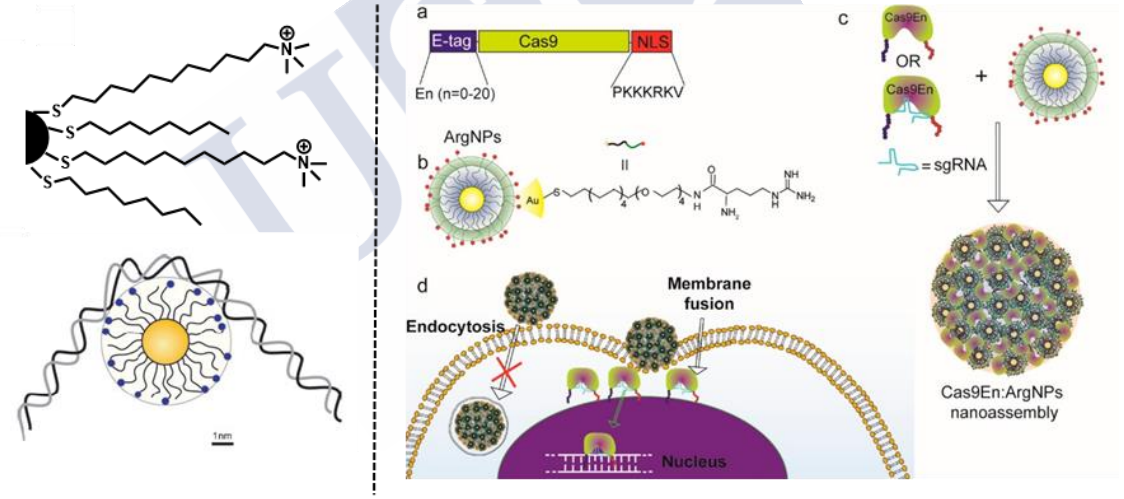

Figure 12. Left: Quaternary ammonium–functionalized AuNPs and interaction with the DNA. Reprinted with permission from ref. 155. Copyright 2005 John Wiley and Sons. Right: Schematic representation of AuNPs modified with arginine moieties, the formation of the nanoassembly with Cas9 protein modified with sgRNA and a glutamate peptide tag and transport across the cellular membrane. Reprinted with permission from ref. 156. Copyright 2017 American Chemical Society.

[90] C. Gehin, J. Montenegro, E. K. Bang, A. Cajaraville, S. Takayama, H. Hirose, S. Futaki, S. Matile, H. Riezman, *J. Am. Chem. Soc.* **2013**, *135*, 9295-9298.
[134] Y. Ding, Z. Jiang, K. Saha, C. S. Kim, S. T. Kim, R. F. Landis, V. M. Rotello, *Mol. Ther.* **2014**, *22*, 1075-1083.
[153] C. M. McIntosh, E. A. Esposito, A. K. Boal, J. M. Simard, C. T. Martin, V. M. Rotello, *J. Am. Chem. Soc.* **2001**, *123*, 7626-7629.
[154] K. K. Sandhu, C. M. McIntosh, J. M. Simard, S. W. Smith, V. M. Rotello, *Bioconjug. Chem.* **2002**, *13*, 3-6.
[155] G. Han, C. T. Martin, V. M. Rotello, *Chem. Biol.* **2006**, *67*, 78-82.
[156] R. Mout, M. Ray, G. Yesilbag Tonga, Y. W. Lee, T. Tay, K. Sasaki, V. M. Rotello, *ACS Nano* **2017**, *11*, 2452-2458.

4. Cell delivery of small molecules

Small molecules have a strong potential as intracellular probes and drugs for the treatment of a wide range of diseases.[157,158,159] However, many small molecules, such as drugs, have their site of action located in the cytosol, in the cell nucleus, or intracellular organelles. As examples, reverse transcriptase inhibitors or statins can be highlighted.[160,161] Moreover, some drugs suffer from cell efflux mediated by P-glycoproteins (P-gp) or multidrug resistance proteins (MRP).[162] Therefore, to achieve the desired effect, small molecules have to be able to cross the cell membrane, to be efficiently delivered into the cell cytosol, and to avoid the cellular efflux.

Hydrophilic small drugs with intracellular targets, such as doxorubicin, have emerged as valuable anticancer drugs. Doxorubicin is a widely administer anticancer drug whose mechanism of cell damage is related to inhibition of the DNA-topoisomerase II complex.[163] Unfortunately, its hydrophilic character makes its cytosolic delivery very inefficient and the efflux pumping, by multidrug resistance proteins (MRPs) and P-glycoproteins (P-gp), makes mandatory to administrate a high dose of doxorubicin to reach the proper anticancer effect.[164] Therefore, the efficient delivery of small hydrophilic drugs into cells and tissues remains a major challenge, and new delivery methods are needed to overcome these problems.

Hydrophilic anionic small fluorescent molecules are relevant intracellular probes such as sulfonated Alexas, pyranine, or carboxyfluorescein (Figure 13). Moreover, pyranine has shown excellent properties as a pH indicator. Unfortunately, the negative net charge at physiological pH of these hydrophilic anionic small molecules makes their cytosolic delivery very inefficient.[165] Therefore, the delivery of small hydrophilic fluorescent molecules into cells and tissues remains a major challenge, and new delivery systems to overcome these limitations are needed.

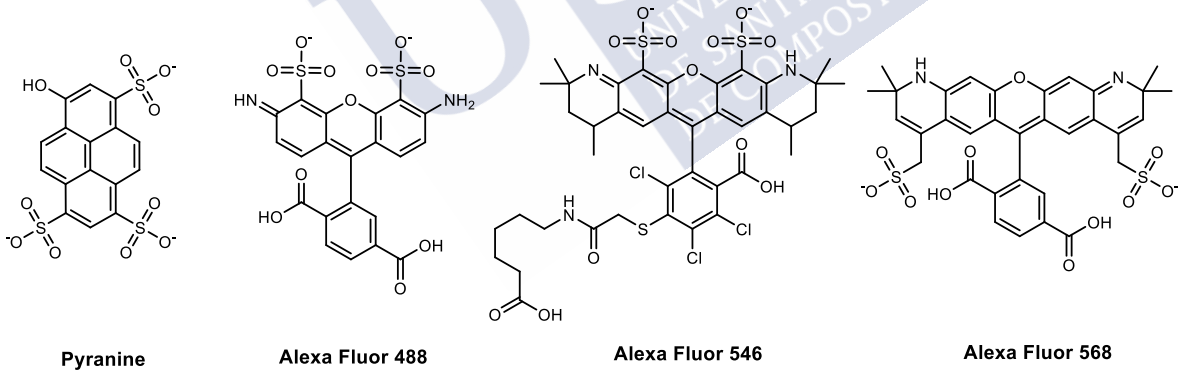

Figure 13. Examples of hydrophilic and anionic fluorescent probes which do not pass through the cellular membrane at low micromolar concentration.

[157] S. Weggen, M. Rogers, J. Eriksen, *Trends Pharmacol. Sci.* **2007**, *28*, 536-543.
[158] M. Vogler, D. Dinsdale, M. J. S. Dyer, G. M. Cohen, *Cell Death Differ.* **2009**, *16*, 360-367.
[159] N. K. Devaraj, S. Hilderbrand, R. Upadhyay, R. Mazitschek, R. Weissleder, *Angew. Chem. Int. Ed.* **2010**, *49*, 2869-2872.
[160] W. Lewis, B. J. Day, W. C. Copeland, *Nat. Rev. Drug Discov.* **2003**, *2*, 812-822.
[161] C. Stancu, A. Sima, *J. Cell. Mol. Med.* **2001**, *5*, 378-387.
[162] M. M. Gottesman, *Annu. Rev. Med.* **2002**, *53*, 615-627.
[163] S. Darwish, S. Mozaffari, K. Parang, R. Tiwari, *Tetrahedron Lett.* **2017**, *58*, 4617-4622.
[164] A. Nasrolahi Shirazi, R. Tiwari, B. S. Chhikara, D. Mandal, K. Parang, *Mol. Pharm.* **2013**, *10*, 488-499.
[165] G. Y. Wiederschain, *Biochem.* **2011**, *76*, 1276-1276.

During the last years, different methods have been explored for the delivery of small hydrophilic molecules to the cell interior including physical and mechanical methods, cell-penetrating peptides (CPPs), supramolecular methods, or by transitory reduction of charge.

4.1.Physical and mechanical methods

Physical and mechanical methods have been applied to cytosolic deliver small molecules such as anionic probes. For example, microinjection has been used when the number of cells to transfect is small. Moreover, the use of strong hypotonic stress to the cells has been also applied.[166] Furthermore, small molecules, such as anticancer drugs or fluorophores, have been incorporated inside the cell by electropermeabilization. This technique uses short high-voltage cycles to produce transitory permeabilization of the cell membrane to allow small molecules to cross the cell membrane by simple diffusion.[167,168]

4.2.Covalent methods using cell-penetrating peptides

The covalent attachment to a CPP constitutes an alternative strategy for the cytosolic delivery of small molecules. Different approaches have been developed where the CPP is covalently attached to small anticancer drugs such as doxorubicin or methotrexate[169] and also to fluorophores.[170] Traditionally, the covalent bond formation was one of the most used methods. To incorporate the cargo into the peptide by covalent bonding, one of the possible strategies is based on the anchoring of the cargo into the cysteine or the lysine side chain of one of the peptide residues.[171] Among the different types of covalent bonding between the cargo and the CPP, it is necessary to highlight the disulfide bond, as this bond has the advantage of being sensitive to the cytosolic glutathione, which allows the dynamic disconnection of the cargo inside the cells. An exceptional example was described by the group of prof. Paul Wender, in which a CPP was connected to luciferin by a disulfide bond. The cargo-luciferin complex can cross the plasma membrane and once inside the cell, glutathione reduces the disulfide bond causing the release of the luciferin that triggers luciferase activity and light emission (Figure 14).[172]

[166] B. S. Gan, E. Krump, L. D. Shrode, S. Grinstein, *Am. J. Physiol.* **1998**, *275*, C1158-C1166.
[167] M.-P. Rols, *Biochim. Biophys. Acta* **2006**, *1758*, 423-428.
[168] A. Pena, J. Ramirez, G. Rosas, M. Calahorra, *J. Bacteriol.* **1995**, *177*, 1017-1022.
[169] K. M. Stewart, K. L. Horton, S. O. Kelley, *Org. Biomol. Chem.* **2008**, *6*, 2242-2255.
[170] Z. Qian, P. G. Dougherty, D. Pei, *Chem. Commun.* **2015**, *51*, 2162-2165.
[171] M. Zorko, U. Langel, *Adv. Drug Deliv. Rev.* **2005**, *57*, 529-545.
[172] L. R. Jones, E. A. Goun, R. Shinde, J. B. Rothbard, C. H. Contag, P. A. Wender, *J. Am. Chem. Soc.* **2006**, *128*, 6526-6527.

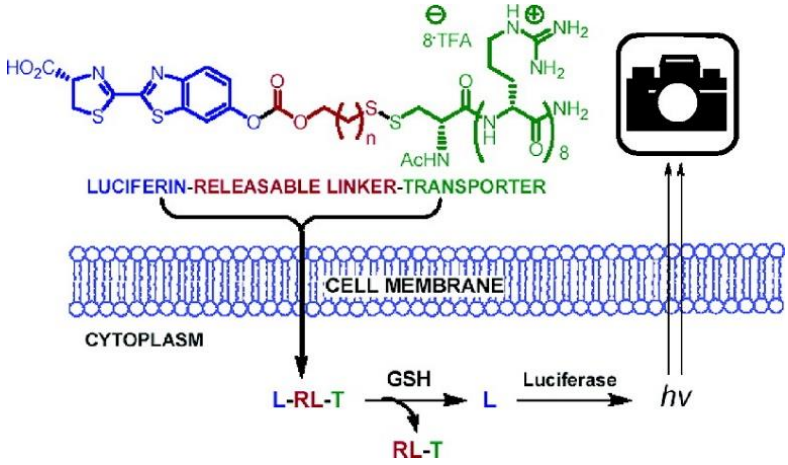

Figure 14. Schematic illustration showing intracellular transport of luciferin covalently attached to a cell-penetrating peptide through a releasable linker and, the subsequent, intracellular release of the cargo mediated by glutathione. Reprinted with permission from 172. Copyright 2006 American Chemical Society.

CPPs have been used to improve the internalization of a wide range of drugs (Figure 15). For example, the prodrug 5-aminolevulinic acid was attached to penetratin for cell delivery.[173] Furthermore, cyclosporine A-CPP conjugates were also synthesized and it was found that this conjugate is able to pass through the stratum corneum and to carry out its therapeutic effect.[174] Some of these covalent conjugates were also applied *in vivo*, showing good properties to cross the brain membrane. For example, the attachment of benzylpenicillin to a CPP importantly increased the drug delivered into the brain in comparison with the drug alone.[175]

Interestingly, the covalent attachment of CPPs to anticancer drugs also showed to overcome anticancer-drug resistance in cells.[176] These conjugates showed the ability to avoid the efflux pump proteins, such as in the case of the covalent conjugation of doxorubicin to TAT which has shown high cytotoxicity against doxorubicin-resistant cell lines.[177] A methotrexate-CPP conjugate has also shown internalization and toxicity against cell lines resistant to this anticancer drug.[178]

A prominent strategy based on activable cell-penetrating peptides (ACPPs) was developed by the group of prof. Roger Tsien (Figure 15, right).[179] A fusion peptide was prepared by a combination of a cationic CPP and an anionic amino acid sequence that acts as an inhibitor of the penetrating activity. A consensus peptide sequence recognized by proteases that are overexpressed in tumors cells was incorporated between the cationic and the anionic sequences. Therefore, proteases cleavage of the inhibitor sequence triggers selective penetration of the cargo such as a fluorophore to selectively label tumor cells.[179] Imaging agents have been

[173] L. Bourré, F. Giuntini, I. M. Eggleston, M. Wilson, A. J. MacRobert, *Br. J. Cancer* **2009**, *100*, 723-731.
[174] J. B. Rothbard, S. Garlington, Q. Lin, T. Kirschberg, E. Kreider, P. L. McGrane, P. A. Wender, P. A. Khavari, *Nat. Med.* **2000**, *6*, 1253-1257.
[175] C. Rousselle, P. Clair, J. Temsamani, J. M. Scherrmann, *J. Drug Target.* **2002**, *10*, 309-315.
[176] S. B. Fonseca, M. P. Pereira, S. O. Kelley, *Adv. Drug Deliv. Rev.* **2009**, *61*, 953-964.
[177] J. F. Liang, V. C. Yang, *Bioorganic Med. Chem. Lett.* **2005**, *15*, 5071-5075.
[178] M. Lindgren, K. Rosenthal-Aizman, K. Saar, E. Eiríksdóttir, Y. Jiang, M. Sassian, P. Östlund, M. Hällbrink, Ü. Langel, *Biochem. Pharmacol.* **2006**, *71*, 416-425.
[179] T. Jiang, E. S. Olson, Q. T. Nguyen, M. Roy, P. A. Jennings, R. Y. Tsien, *Proc. Natl. Acad. Sci.* **2004**, *101*, 17867-17872.

incorporated into these peptides for their use as tumor tissues labelling probes *in vivo*[180,181] and for guided surgery.[182,183]

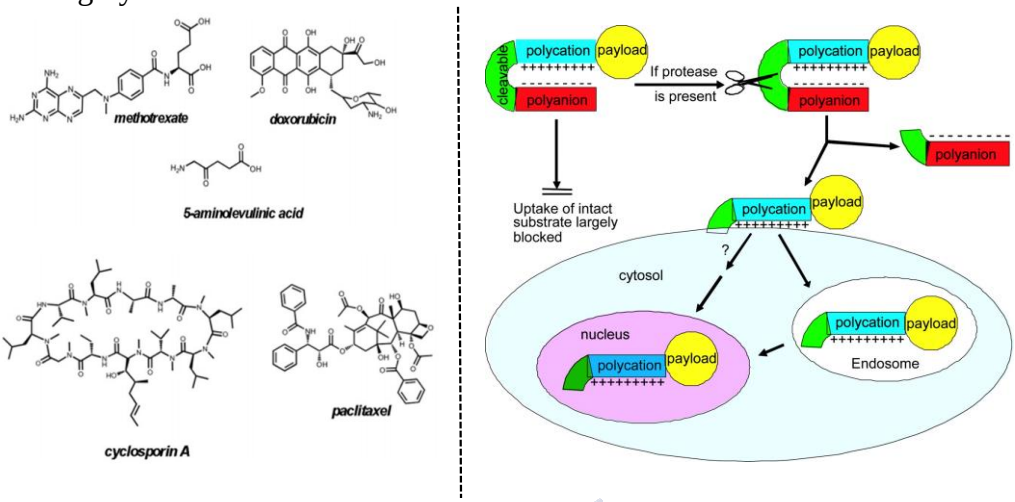

Figure 15. Left: Examples of drugs delivered into cells by applying covalent attachment to CPPs. Reproduced from Ref. 169 with permission from The Royal Society of Chemistry. Right: Schematic illustration of the mechanism of internalization of activable cell-penetrating peptides (ACPPs). Reprinted from ref. 179 Copyright 2004 National Academy of Sciences.

Moreover, this strategy has been extended to the field of chemotherapy by the incorporation of an anticancer drug such as doxorubicin. This idea allowed to increase the specificity in tumors that overexpress enzymes such as MMPs (matrix metalloproteinases).[184] Although there are many examples of CPP-molecular conjugates by covalent bonds, this strategy has also some limitations such as alterations of the biological effect of the cargo and sometimes tedious synthetic steps. For this reason, during the last decades, different supramolecular strategies have been developed to overcome some of the limitations of the covalent attachment.

4.3.Non-covalent supramolecular methods

Supramolecular strategies can use different non-covalent interactions, such as host-guest encapsulation, electrostatic interactions, or hydrophobic forces, to incorporate small molecules, such as drugs or probes, into efficient delivery vehicles. During the last years, multiple supramolecular strategies have emerged for the cytosolic delivery of a wide range of small molecules including peptides,[185] ionophores,[186] liposomes,[187] macrocyclic capsules,[188] supramolecular nanoparticles[188] or stimuli-responsive vesicles.[189]

[180] T. A. Aguilera, E. S. Olson, M. M. Timmers, T. Jiang, R. Y. Tsien, *Integr. Biol.* **2009**, *1*, 371-381.
[181] E. S. Olson, T. A. Aguilera, T. Jiang, L. G. Ellies, Q. T. Nguyen, E. H. Wong, L. A. Gross, R. Y. Tsien, *Integr. Biol.* **2009**, *1*, 382-393.
[182] Q. T. Nguyen, R. Y. Tsien, *Nat. Rev. Cancer* **2013**, *13*, 653-662.
[183] Q. T. Nguyen, E. S. Olson, T. A. Aguilera, T. Jiang, M. Scadeng, L. G. Ellies, R. Y. Tsien, *Proc. Natl. Acad. Sci. U. S. A.* **2010**, *107*, 4317-4322.
[184] N. Q. Shi, W. Gao, B. Xiang, X. R. Qi, *Int. J. Nanomedicine* **2012**, *7*, 1613-1621.
[185] S. J. Song, S. Lee, K. S. Ryu, J. S. Choi, *Bioconjug. Chem.* **2017**, *28*, 2266-2276.
[186] P. R. Brotherhood, A. P. Davis, *Chem. Soc. Rev.* **2010**, *39*, 3633-3647.
[187] U. Bulbake, S. Doppalapudi, N. Kommineni, W. Khan, *Pharmaceutics* **2017**, *9*, 12.
[188] M. J. Webber, R. Langer, *Chem. Soc. Rev.* **2017**, *46*, 6600-6620.
[189] W. C. de Vries, D. Grill, M. Tesch, A. Ricker, H. Nüsse, J. Klingauf, A. Studer, V. Gerke, B. J. Ravoo, *Angew. Chem. Int. Ed.* **2017**, *56*, 9603-9607.

4.3.1. Cell-penetrating peptides

Non-covalent conjugates between cell-penetrating peptides and small molecules constitute an excellent method to accomplish the cytosolic delivery of small molecules. Despite covalent conjugation has been extensively used, the preparation of the corresponding peptide conjugates sometimes requires multiple steps. In contrast, the procedure to cellular delivery by non-covalent interactions using penetrating peptides represents a much more simple and straightforward idea.

An elegant example of non-covalent delivery of fluorophores has been developed in the group of prof. Tampé (Figure 16, left).[190] A peptide consisting of six N-terminal histidines was connected by a linker (GGGS) to the typical penetrating peptide TAT (RKKRRQRRR). On the other hand, a fluorescent multivalent chelator made of a multivalent derivative of the N-nitrilotriacetic acid (trisNTA) was modified with different fluorophores, such as Alexa Fluor 647. The trisNTA was able to coordinate with the histidine amino acids and when mixed together the trisNTA and the peptide His_6-TAT in the presence of Ni (II), a complex was formed. This complex was able to cross the cell membrane and the fluorescent multivalent chelator was released inside of the cell.[190] Another example of non-covalent delivery of fluorophores with amphiphilic cell-penetrating peptides was shown with a non-covalent complex including thermally activated delayed fluorescence (TADF) moieties.[191] In this work, the authors designed an amphiphilic cell-penetrating peptide, $F_6G_6(rR)_3R_2$, that was able to form supramolecular complexes with TADF compounds such as 4CzIPN, NAI-DPAC, and BTZ-DMAC (Figure 16, right). These fluorescent molecules and the peptide self-assembled into fluorescent nanoparticles, these NPs were able to easily cross the cell membrane and to allow the acquisition of time-resolved luminescence images.[191] Furthermore, amphipathic peptides forming nanoribbons coated with a second layer of cell-penetrating peptides were also able to deliver fluorophores inside of the cell.[192]

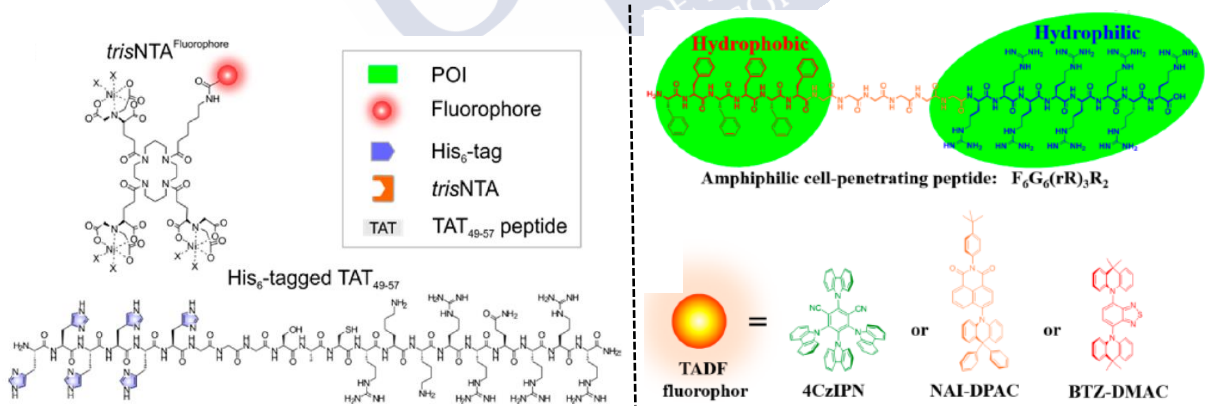

Figure 16. Left: Chemical structure of trisNTA fluorophore and His_6-tagged TAT cell-penetrating peptide. Reprinted with permission from ref. 190. Copyright 2018 American Chemical Society. Right: Chemical structure of amphiphilic CPP and the different TADF fluorophores. Reprinted and adapted with permission from ref. 191. Copyright 2018 American Chemical Society.

[190] R. Wieneke, N. Labòria, M. Rajan, A. Kollmannsperger, F. Natale, M. C. Cardoso, R. Tampé, *J. Am. Chem. Soc.* **2014**, *136*, 13975-13978.
[191] Z. Zhu, D. Tian, P. Gao, K. Wang, Y. Li, X. Shu, J. Zhu, Q. Zhao, *J. Am. Chem. Soc.* **2018**, *140*, 17484-17491.
[192] Y. Lim, E. Lee, M. Lee, *Angew. Chem. Int. Ed.* **2007**, *46*, 3475-3478.

On the other hand, amphiphilic peptides, using non-covalent interactions, were shown to transport drugs such as curcumin or doxorubicin.[185,193] For example, amphiphilic peptide nanorods were recently used to encapsulate curcumin and subsequently to deliver this molecule in cancer cell lines and zebrafish models.[185] Moreover, a new amphiphilic peptide was recently shown to self-assemble to form pH-responsive micelles that were able to entrap and deliver doxorubicin in cells.[193]

4.3.2. Ionophores

Another supramolecular method for the transport of small molecules is the ionophores. This family of synthetic molecules gets inspiration from a variety of naturally occurring products that are able to complex ions in a very tight and efficient manner and promote their translocation across lipid bilayers.[194] To carry out such a challenging task, natural ionophores present a structure that is generally cyclic or bent-shaped, in which the external surface of the molecules presents a strong hydrophobic character, which grants a good partitioning into the fatty-acid rich membrane lumen. The hydrophilic region of ionophores is rich in coordinating heteroatoms responsible for the interaction with the ions, normally being able to mimic the hydration sphere of the ion that is translocated.[195,196] Various research groups have modified natural molecules to design new transporters. In this group, **prodigiosins** are a class of molecules based on 4-methoxy-bipyrrole with different substituents (Figure 17).[197] In recent years, it has been found that this type of molecules can function as H^+/Cl^- [198] and Cl^-/HCO_3^- [199] exchanger antiporters.

To achieve segregation between an external lipophilic surface and a coordination-rich inner cavity, researchers have employed multipodal scaffolds to obtain a prearranged tridimensional disposition of key functional groups.[200] In this regard, the **cholapods,** which are a family of steroids derived from cholic acid, have been designed (Figure 17B). In these molecules, one of the hydrophobic faces is preserved and groups capable of complexing anions such as squaramides, thioureas, or ureas are incorporated into various positions of the polycyclic ring.[186] Interestingly, cholapods with high efficiency for the transport of Cl^- in model vesicles have been discovered.[201] Also applying this strategy, the functionalization with three ureas or

[185] S. J. Song, S. Lee, K. S. Ryu, J. S. Choi, *Bioconjug. Chem.* **2017**, *28*, 2266-2276.
[193] J. Liang, W. Wu, X. Xu, R. Zhuo, X. Zhang, *Colloids Surfaces B Biointerfaces* **2014**, *114*, 398-403.
[194] A. Roy, D. Saha, A. Mukherjee, P. Talukdar, *Org. Lett.* **2016**, *18*, 5864-5867.
[195] J. Rutkowski, B. Brzezinski, *Biomed Res. Int.* **2013**, *2013*, 162513.
[196] P. A. Gale, *Acc. Chem. Res.* **2011**, *44*, 216-226.
[197] J. L. Sessler, L. R. Eller, W. S. Cho, S. Nicolaou, A. Aguilar, J. T. Lee, V. M. Lynch, D. J. Magda, *Angew. Chem. Int. Ed.* **2005**, *44*, 5989-5992.
[198] K. Tanigaki, T. Sato, Y. Tanaka, T. Ochi, A. Nishikawa, K. Nagai, H. Kawashima, S. Ohkuma, *FEBS Lett.* **2002**, *524*, 37-42.
[199] J. T. Davis, P. A. Gale, O. A. Okunola, P. Prados, J. C. Iglesias-Sánchez, T. Torroba, R. Quesada, *Nat. Chem.* **2009**, *1*, 138-144.
[200] N. Busschaert, M. Wenzel, M. E. Light, P. Iglesias-Hernández, R. Pérez-Tomás, P. A. Gale, *J. Am. Chem. Soc.* **2011**, *133*, 14136-14148.
[186] P. R. Brotherhood, A. P. Davis, *Chem. Soc. Rev.* **2010**, *39*, 3633-3647.
[201] S. J. Edwards, H. Valkenier, N. Busschaert, P. A. Gale, A. P. Davis, *Angew. Chem. Int. Ed.* **2015**, *54*, 4592-4596.

thioureas has been carried out using tris(2-aminoethyl)amine, and the resulting compounds showed good efficiency as bicarbonate transporters.[202]

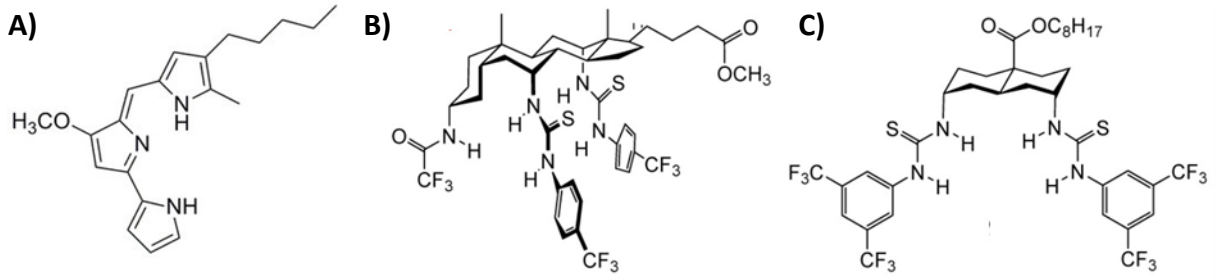

Figure 17. Chemical structures of different examples of ionophores: A) Prodigiosin.[197] B) Example of cholapod.[186] C) Representative example of trans-decalin derivative.[204]

Other transporters of high interest are difunctionalized **trans-decalins** in the 4,8-diaxial positions. In this type of molecules, the hydrophobic moiety of the core molecule is maintained while in the other part is modified with two thiourea or urea groups with aromatic substituents.[203] Interestingly, one of the trans-decalin derivatives was the most effective transporter for the Cl^- anion in model vesicles (Figure 17).[204] This transporter consists of a modified trans-decalin with two aryl-thiourea groups in which the aromatic rings are functionalized with two CF_3 groups in positions 3 and 5.[204] More recently, we should highlight that these transport systems are starting to be considered *in vitro* for the treatment of cystic fibrosis, in which these artificial molecules could have the potential to mimic Cl^- transporting channels (CFTR proteins) absent or malfunctioning in the patients that suffer from this disease.[205,206]

4.3.3. Liposomes

Liposomes are one of the most used drug delivery systems. Classical liposomes consist of spherical vesicles with an internal aqueous core that is surrounded by one or more lipid bilayers in the external layer. From the pharmaceutical point of view, these entities are capable of incorporating both hydrophobic (in the bilayer) and hydrophilic molecules (in the aqueous space).[207] When classical liposomes were administered following the intravenous pathway, it was found that they suffer from a fast clearance, having short circulation times. However, clearance was reduced carrying out the PEGylation of the liposome. A few years ago, the PEGylated liposomal doxorubicin (Doxil®) was FDA approved and showed an increase in the drug levels and reduction of cardiomyocyte damage in comparison with doxorubicin alone. Another example of using a PEGylated liposomal system, in this case, for irinotecan delivery is Onivyde™.[187] Recently, multifunctional liposomes (Figure 18, left) have emerged to improve

[202] N. Busschaert, P. A. Gale, C. J. E. Haynes, M. E. Light, S. J. Moore, C. C. Tong, J. T. Davis, W. A. Harrell, *Chem. Commun.* **2010**, *46*, 6252-6254.
[203] S. Hussain, P. R. Brotherhood, L. W. Judd, A. P. Davis, *J. Am. Chem. Soc.* **2011**, *133*, 1614-1617.
[204] H. Valkenier, L. W. Judd, H. Li, S. Hussain, D. N. Sheppard, A. P. Davis, *J. Am. Chem. Soc.* **2014**, *136*, 12507-12512.
[205] K. A. Muraglia, R. S. Chorghade, B. R. Kim, X. X. Tang, V. S. Shah, A. S. Grillo, P. N. Daniels, A. G. Cioffi, P. H. Karp, L. Zhu, et al., *Nature* **2019**, *567*, 405-408.
[206] P. A. Gale, J. T. Davis, R. Quesada, *Chem. Soc. Rev.* **2017**, *46*, 2497-2519.
[207] T. O. B. Olusanya, R. R. H. Ahmad, D. M. Ibegbu, J. R. Smith, A. A. Elkordy, *Molecules* **2018**, *23*, 907.
[187] U. Bulbake, S. Doppalapudi, N. Kommineni, W. Khan, *Pharmaceutics* **2017**, *9*, 12.

the pharmaceutical properties of liposomes. This kind of liposomes can incorporate different functionalities in the same entity such as targeting ligands (antibody or carbohydrates), imaging agents, hydrophilic or hydrophobic drugs, therapeutic nucleic acids, etc.[208] For instance, an innovative approach has been recently developed in the group of prof. Alexander Kros.[209] In this work, a pair of complementary coiled-coil lipopeptides were designed and incorporated into liposomes. The fusion of the coiled-coil peptides allowed the release of the anticancer drug, doxorubicin, encapsulated inside the liposomes in cells, and zebrafish models.[209]

4.3.4. Host-guest delivery systems

Host-guest processes are a powerful tool to develop new carriers for the encapsulation and the delivery of small molecules. As we have previously commented, classical host molecules such as cyclodextrins, cucurbiturils, or calixarenes have been applied to deliver a variety of therapeutic molecules.[188] **Cyclodextrins** (CDs) have been shown to be suitable delivery carriers for different cargos due to their high bioavailability and low cytotoxicity. For instance, *β*-CDs have been demonstrated not only to recognize a variety of substrates but also to promote the delivery of different anticancer drugs such as doxorubicin[210] or paclitaxel.[211] For example, host-guest molecular recognition between *β*-CDs and paclitaxel has been recently used to deliver this antitumoral drug in living cells and also *in vivo* (Figure 18, right).[212] Kim and co-workers have designed a system constituted by poly-paclitaxel and poly-CDs conjugated by ester bonds to a polymer chain. Moreover, a peptidic targeting ligand was also incorporated into the system. Once inside the cell, intracellular enzymes cleave the ester bonds and the cyclodextrin/paclitaxel complexes are released from the polymers. Finally, these complexes dissociate and the free paclitaxel produces its tumor cytotoxic effect.[212]

[208] M. Riaz, M. Riaz, X. Zhang, C. Lin, K. Wong, X. Chen, G. Zhang, A. Lu, Z. Yang, *Int. J. Mol. Sci.* **2018**, *19*, 195.
[209] J. Yang, A. Bahreman, G. Daudey, J. Bussmann, R. C. L. Olsthoorn, A. Kros, *ACS Cent. Sci.* **2016**, *2*, 621-630.
[188] M. J. Webber, R. Langer, *Chem. Soc. Rev.* **2017**, *46*, 6600-6620.
[210] H. Hyun, S. Lee, W. Lim, D. Jo, J. S. Jung, G. Jo, S. Y. Kim, D. Lee, S. Um, D. H. Yang, et al., *J. Ind. Eng. Chem.* **2019**, *70*, 145-151.
[211] J. Jing, A. Szarpak-Jankowska, R. Guillot, I. Pignot-Paintrand, C. Picart, R. Auzély-Velty, *Chem. Mater.* **2013**, *25*, 3867-3873.
[212] R. Namgung, Y. Mi Lee, J. Kim, Y. Jang, B. H. Lee, I. S. Kim, P. Sokkar, Y. M. Rhee, A. S. Hoffman, W. J. Kim, *Nat. Commun.* **2014**, *5*, 3702.

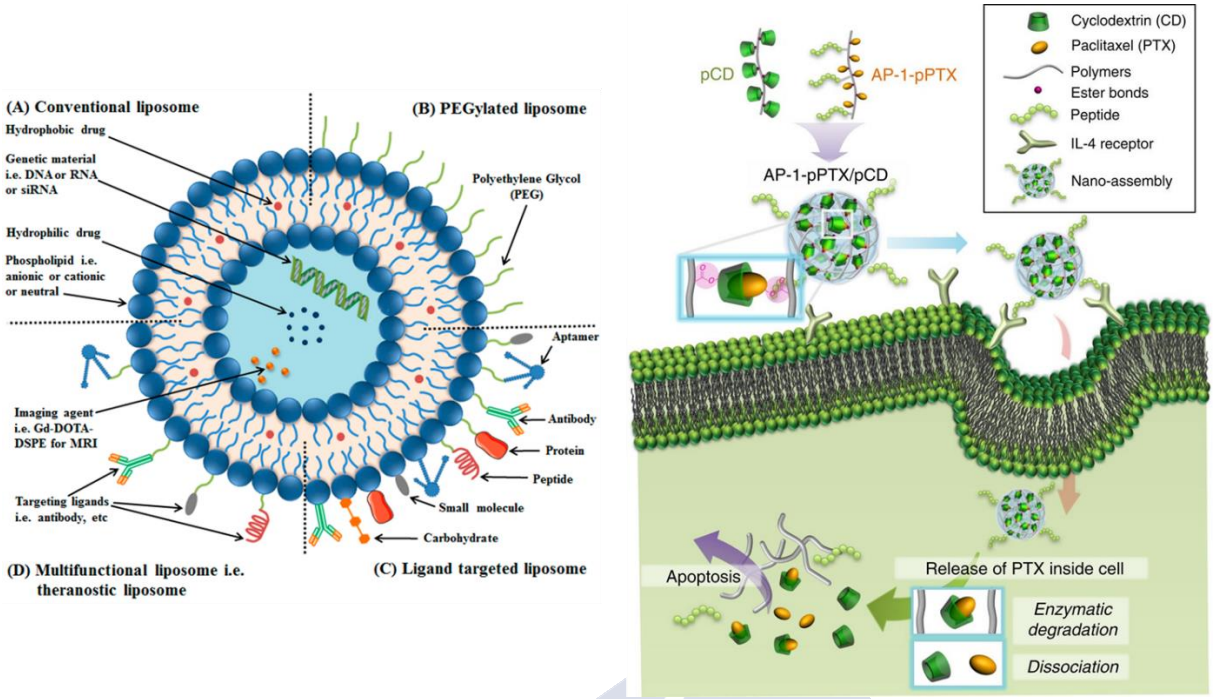

Figure 18. Left. Schematic representation showing the different types of liposomes: A) Conventional liposomes, B) PEGylated liposomes, C) Ligand targeted liposomes and D) Multifunctional liposomes such as theranostic liposomes. Reprinted from ref. 208 under the terms of the Creative Commons CC BY license. Right. Schematic illustration of the mechanism of internalization and paclitaxel release from the supramolecular host-guest nano-assembly. Reprinted with permission from ref. 212. Copyright 2014 Springer Nature.

4.3.5. Redox and pH-responsive encapsulating vesicles

Redox-responsive nanocontainers have been shown to deliver hydrophilic cargos such as pyranine or phalloidin. These nanocontainers consist of a shell formed by a redox-responsive polymer attached by host-guest processes to a cyclodextrin core through an adamantane moiety (Figure 19, left). The encapsulation of different cargos was achieved by disulfide bonds that were incorporated into the polymeric shell as redox cleavable functions. In this work, the authors showed that these nanocontainers were able to release different molecular payloads in the cell interior and driven by the redox trigger.[189]

On the other hand, pH-responsive core-shell nanoparticles have also been described to deliver fluorescent probes and small molecular drugs simultaneously (Figure 19, right).[213] These nanoparticles consist of a shell formed by the negatively charged pyranine with a core of positively charged carboxymethylhexanoyl chitosan. The electrostatic interactions between the shell and core polymers produce the assembly into pH-responsive nanoparticles. Interestingly, the encapsulation of the antitumoral drug camptothecin into these NPs for pH-controlled drug release was achieved. The authors were able to develop a theranostic system with potential therapeutic and diagnosis capabilities.[213]

[189] W. C. de Vries, D. Grill, M. Tesch, A. Ricker, H. Nüsse, J. Klingauf, A. Studer, V. Gerke, B. J. Ravoo, *Angew. Chem. Int. Ed.* **2017**, *56*, 9603-9607.
[213] H. S. Chou, M. H. Hsiao, W. Y. Hung, T. Y. Yen, H. Y. Lin, D. M. Liu, *J. Mater. Chem. B* **2014**, *20*, 6580-6589.

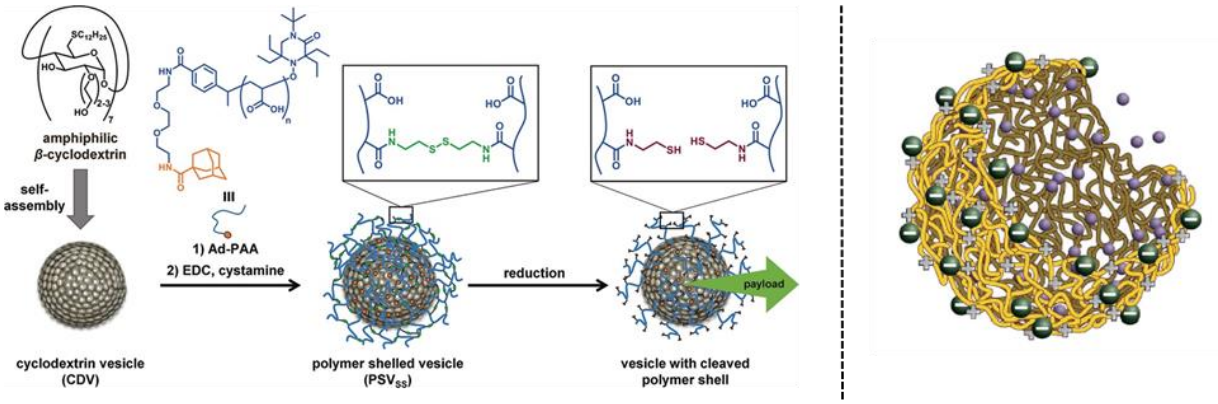

Figure 19. Left. Preparation of redox-responsive nanocontainer and redox-triggered payload release. Reprinted ref. 189 with permission from John Wiley and Sons. Copyright 2017 Wiley-VCH Verlag GmbH & Co. KGaA, Weinheim. Right: Schematic representation of pH-responsive core-shell nanoparticles. Reproduced from Ref. 213 with permission from The Royal Society of Chemistry.

4.4.Transitory reduction of charge

Transitory reduction of charge is one of the most widely applied methods to trigger the intracellular release of small hydrophilic molecules. This strategy is based on increasing the hydrophobicity of the molecule by forming hydrophobic esters at phosphoric or carboxylic acids, among others. The resulting molecule, with higher hydrophobic properties, can cross the cell membrane and, after the action of intracellular enzymes, the hydrophilic molecule is released.[214,215] The main limitations of this strategy are the required synthetic modification of the active molecule and the need for efficient intracellular hydrolysis of the corresponding ester.

A few decades ago, the prodrug strategy has been developed.[216] This strategy is based on the modification of active drugs that after suffering an intracellular cleavage, by enzymes or chemicals, will lead to the release of the active drug. This methodology has been applied to increase the efficiency of a wide range of drugs.[217] For instance, cidofovir is a highly hydrophilic drug, used as therapy for herpesviruses, which have strong limitations to cross the plasma membrane. However, when the phosphate group of this molecule is modified by esterification with a hydrophobic molecule, the resulting molecule can be internalized by simple diffusion, and subsequently, the ester enzymatic hydrolysis of the ester inside the cell allows the recovery of the active principle. Importantly, the administration of the prodrug of cidofovir causes a four-fold activity enhancement compared to the unmodified drug (Figure 20).[218] In addition to bioactive molecules and drugs, this strategy has also been applied for different fluorescent probes.[219] In recent years, fluorescein derivatives have been used to carry out intracellular pH measurements by fluorescence methods. One of the most used compounds is 2´,7´-Bis(2-carboxyethyl)-5(6)-carboxyfluorescein (BCECF) (Figure 20).[220] This small highly

[214] P. Ozkan, R. Mutharasan, *Biochim. Biophys. Acta* **2002**, *1572*, 143-148.
[215] J. Rautio, H. Kumpulainen, T. Heimbach, R. Oliyai, D. Oh, T. Järvinen, J. Savolainen, *Nat. Rev. Drug Discov.* **2008**, *7*, 255-270.
[216] J. Rautio, N. A. Meanwell, L. Di, M. J. Hageman, *Nat. Rev. Drug Discov.* **2018**, *17*, 559-587.
[217] K. M. Huttunen, H. Raunio, J. Rautio, *Pharmacol. Rev.* **2011**, *63*, 750-771.
[218] E. De Clercq, H. J. Field, *Br. J. Pharmacol.* **2006**, *147*, 1-11.
[219] L. D. Lavis, T.-Y. Chao, R. T. Raines, *Chem. Sci.* **2011**, *2*, 521-530.
[220] N. Boens, W. Qin, N. Basarić, A. Orte, E. M. Talavera, J. M. Alvarez-Pez, *J. Phys. Chem. A* **2006**, *110*, 9334-9343.

hydrophilic molecule at physiological pH shows huge problems to cross the plasma membrane and therefore, to carry out the measurement of intracellular pH. Therefore, the transitory reduction of charge strategy was applied and BCECF acetoxymethyl ester (BCECF-AM) was synthesized (Figure 20).[221] This molecule showed stronger lipophilicity and the ability to cross the membrane by passive diffusion. Again, after crossing the plasma membrane, the intracellular esterases hydrolyze the ester bonds and the fluorescent form is released. Nevertheless, this methodology has the limitation of the acid-catalyzed hydrolysis of the ester bond.[221] In addition, BCECF suffers from photobleaching and this effect can cause the release of toxic products such as oxygen radicals.[222]

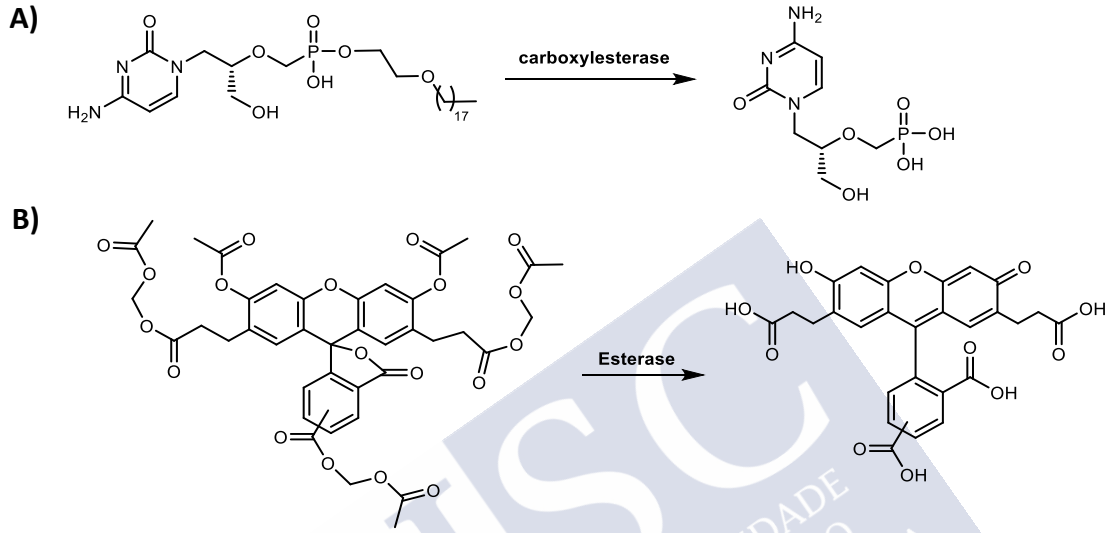

Figure 20. Intracellular hydrolysis of membrane-permeable cidofovir ester (A) or BCECF-AM (B) into active molecule cidofovir[218] (A) or BCECF[221] (B).

5. Methods of intracellular pH measurement

The regulation of cellular pH is crucial to maintain a wide range of cellular processes such as organelles activity, enzyme functions, cellular proliferation, the degradation of the proteins, etc.[223,224] The pH in mammalian cells is heterogeneously distributed in slightly acidic pH in endosomes and lysosomes and a slightly basic pH in the cytosol and the mitochondria. The appearance of abnormalities in the physiological cellular pH values has been strictly related to aberrant cellular activity and with different pathologies such as cancer or Alzheimer's disease.[225] For example, it has been demonstrated that cancer cells present aberrant acidic pH values.[226,227] Due to the importance of maintaining a correct physiological cellular pH, the study of the intracellular pH has emerged as an excellent opportunity for sensor development and a variety of strategies have been studied to track the intracellular pH.

[221] C. J. Bachmeier, W. J. Trickler, D. W. Miller, *J. Pharm. Sci.* **2004**, *93*, 932-942.
[222] I. D. Weiner, L. L. Hamm, *Am. J. Physiol.* **1989**, *256*, F957-F964.
[223] J. R. Casey, S. Grinstein, J. Orlowski, *Nat. Rev. Mol. Cell Biol.* **2010**, *11*, 50-61.
[224] J. Srivastava, D. L. Barber, M. P. Jacobson, *Physiology* **2007**, *22*, 30-39.
[225] M. H. Lee, J. H. Han, J. H. Lee, N. Park, R. Kumar, C. Kang, J. S. Kim, *Angew. Chem. Int. Ed.* **2013**, *52*, 6206-6209.
[226] A. Hulikova, A. L. Harris, R. D. Vaughan-Jones, P. Swietach, *J. Cell. Physiol.* **2013**, *228*, 743-752.
[227] B. A. Webb, M. Chimenti, M. P. Jacobson, D. L. Barber, *Nat. Rev. Cancer* **2011**, *11*, 671-677.

5.1.Conventional methods

Many conventional strategies have been used to measure the intracellular pH such as NMR spectroscopy or pH-sensitive microelectrodes.[228] More recently, absorbance spectroscopy and fluorescence microscopy have been also applied.[229] It has also been shown that the combination of UV-Vis microspectroscopy and pH indicators, such as bromothymol blue or bromocresol green, allows single-cell pH imaging (Figure 21).[230] In this assay, the color of the solution of bromothymol blue in PBS changes from yellow to blue with the increase of the pH from 4.0 to 7.5. On the other hand, the color of the solution of bromocresol green in PBS solutions is also modified from yellow to blue with the increase of the pH value from 3.0 to 7.5. Using this methodology, the authors were able to distinguish normal cells from cancer cells. After the incubation of the cells with the pH indicator in PBS, under the bright-field microscope, the cancer cells showed yellow and bright color because of their acidic pH and, in contrast, the healthy cells showed blue and dark color due to their neutral pH.[230]

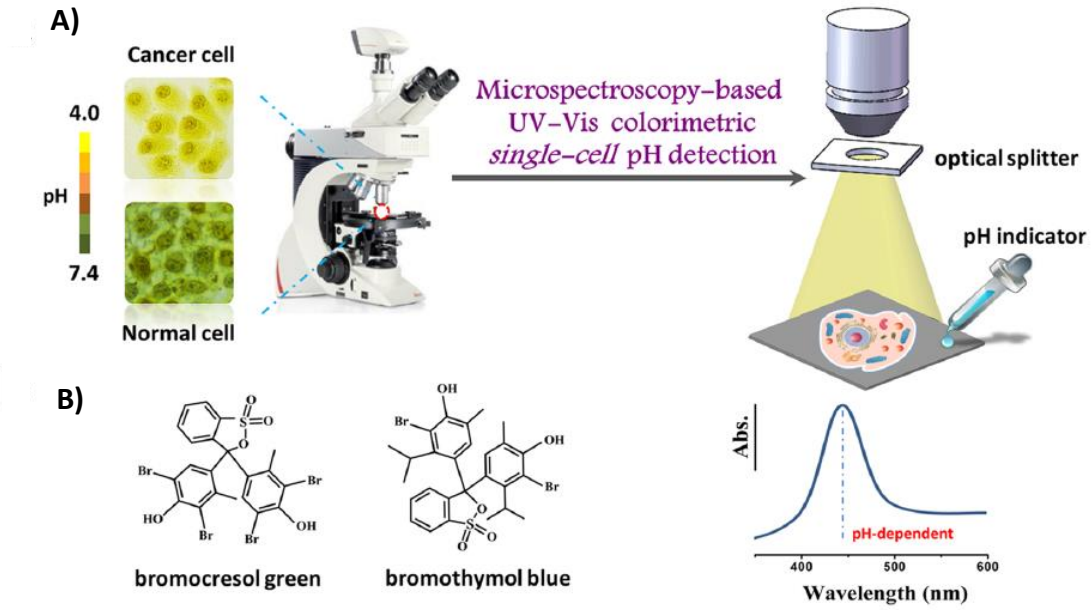

Figure 21. A) Schematic representation of single-cell pH imaging and detection by a combination of UV-Vis microspectroscopy and pH indicators. B) Chemical structures of pH indicators. Reprinted from ref. 230 under the terms of Creative Commons CC BY license. Copyright 2017 Springer Nature.

[228] S. Chen, Y. Hong, Y. Liu, J. Liu, C. W. T. Leung, M. Li, R. T. K. Kwok, E. Zhao, J. W. Y. Lam, Y. Yu, et al., *J. Am. Chem. Soc.* **2013**, *135*, 4926-4929.
[229] H. S. Chou, M. H. Hsiao, W. Y. Hung, T. Y. Yen, H. Y. Lin, D. M. Liu, *J. Mater. Chem. B* **2014**, *20*, 6580-6589.
[230] H. Hou, Y. Zhao, C. Li, M. Wang, X. Xu, Y. Jin, *Sci. Rep.* **2017**, *7*, 1759.

5.2.Fluorometric strategies

Fluorometric techniques have emerged as the method of choice to perform cellular pH measurements. These techniques have many advantages such as spatiotemporal resolution and high sensitivity.[231,232] Recently, different strategies, such as polyethylene glycol-phospholipid (PEG-lipid) probe conjugates, pH-sensitive nanocapsules, or nanoparticle conjugates, have emerged to facilitate the measurement of pH in different cellular compartments. Moreover, a variety of fluorescent molecules attached to both small molecules or proteins have been also developed.

Recently, a prominent strategy to obtain the cell surface pH imaging has been developed by attaching a polyethylene glycol-phospholipid (PEG-lipid) to a pH-sensitive probe fluorescein isothiocyanate (FITC).[233] The PEG-lipid part of the molecule is able to insert into the cell membrane and the pH probe FITC allows the visualization of the cell surface at the different pHs from weakly basic to acidic pH (Figure 22A).[233] Furthermore, the group of prof. Parak developed pH-sensitive capsules to measure the lysosomal pH modifications after stimulation.[234] These capsules consist of a pH-sensitive fluorophore loaded into the cavity of layer-by-layer polyelectrolyte capsules and, when incubated with cells, remain entrapped inside lysosomes showing yellow fluorescence. After the addition of agents that increase the pH inside the lysosome, such as chloroquine, the capsules located inside of the lysosome showed a fluorescence change from yellow to red which reports the pH change in this organelle (Figure 22B).[234]

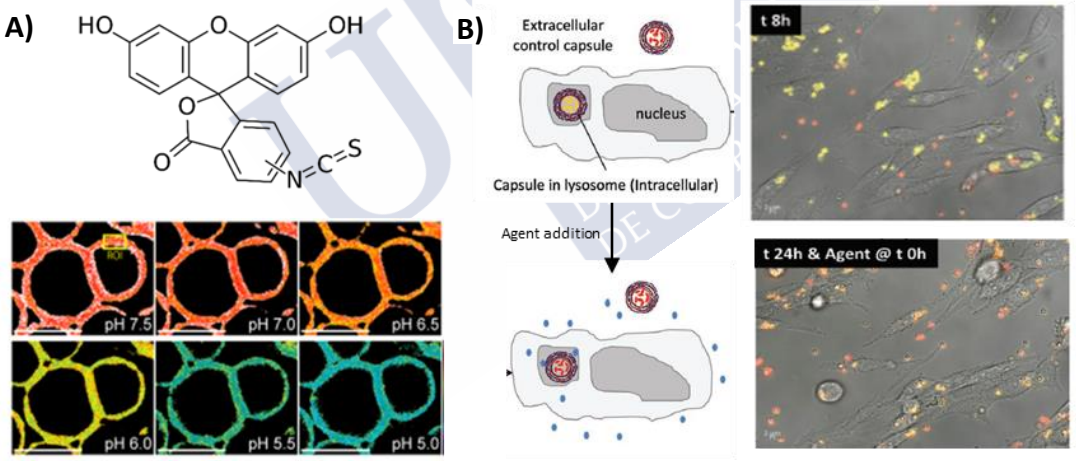

Figure 22. A) Chemical structure of pH-sensitive FITC probe and ratiometric visualization of the pH of the cell surface applying FITC-PEG-lipid. Reprinted from ref. 233 under the terms of Creative Commons CC BY license, Copyright 2017 Springer Nature. B) Left, schematic representation showing the behavior of the pH-sensitive capsules inside of the lysosome before and after the addition of an agent that increases the pH of the lysosome such as chloroquine. Right, overlay of confocal micrographs, before and after the addition of chloroquine, showing the change of the fluorescence of the capsules from yellow to red with the induced-pH change inside the lysosome. Reprinted and adapted from ref. 234 with permission from John Wiley and Sons. Copyright 2012 Wiley-VCH Verlag GmbH & Co. KGaA, Weinheim.

[231] B. Turkowyd, D. Virant, U. Endesfelder, *Anal. Bioanal. Chem.* **2016**, *408*, 6885-6911.
[232] M. Fernández-Suárez, A. Y. Ting, *Nat. Rev. Mol. Cell Biol.* **2008**, *9*, 929-943.
[233] R. Ohgaki, Y. Teramura, D. Hayashi, L. Quan, S. Okuda, *Sci. Rep.* **2017**, 17484.
[234] P. RiveraGil, M. Nazarenus, S. Ashraf, W. J. Parak, *Small* **2012**, *8*, 943-948.

A variety of **functionalized nanoparticles** have been developed for measuring intracellular pH.[235] For instance, the group of prof. Long has prepared a pH-sensitive probe used for both Raman/fluorescence imaging of the cellular pH.[236] The system consists of AuNPs functionalized with a double-strand DNA, which was modified by two complementary strands of DNA (DNA-1 and DNA-2). The DNA-1 was modified with a Raman signaling molecule and DNA-2 was modified with a cyanine probe (Cy5). Cy5 fluorescence of DNA-2 was quenched by the fluorescence resonance energy transfer (FRET) effect with the Raman signaling molecule by the AuNP. In acidic pH of cancer cells, the DNA-1 undergoes a conformational change which promotes that the Raman signaling molecules move closer to the surface of AuNPs, which increased the Raman signal. Simultaneously, DNA-2 modified with Cy5 was released from the AuNPs, which increase the fluorescence signal. Using this technique, at acidic pH, the authors were able to turn ‘‘on’’ both Raman and fluorescence signals.[236]

Furthermore, a variety of **fluorescent molecules**, from small compounds to pH-sensitive fluorescent proteins, have also recently been prepared for facilitating the measurement of pH in the different cellular compartments.[237] As it was previously mentioned**, BCECF** (2′,7′-Bis(2-carboxyethyl)-5(6)-carboxyfluorescein) is one of the most used fluorescent dyes to measure cellular pH (Figure 23A). This molecule has the perfect characteristics to carry out the pH measurement of the cytosol (which is usually between 6.8 and 7.4) due to its pK_a being 7.0. Moreover, as we have previously mentioned, to avoid the invasive loading of the cells with the dye, BCECF acetoxymethyl esters were developed showing higher membrane transport capabilities. Furthermore, **Carboxy-SNARF-1** (C.SNARF-1) is also one of the most applied probes to measure cellular pH (Figure 23B). This molecule is a near-infrared ratiometric probe with excitation wavelengths such as 514 or 536 nm. Therefore, this probe reduces the cytotoxicity produced by the irradiation of cells. Moreover, the C.SNARF-1 acetoxymethyl ester has been also developed to facilitate its transport across the cell membrane.

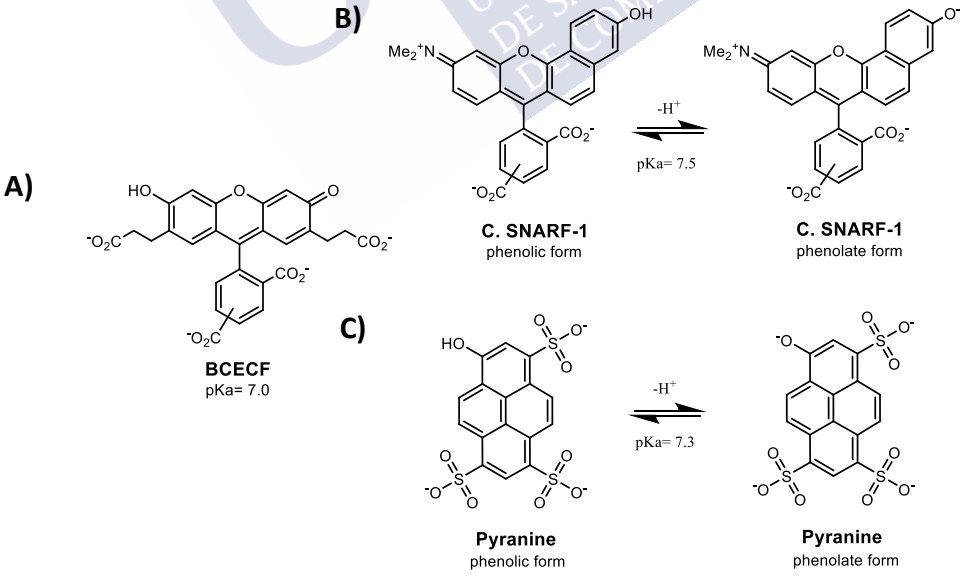

Figure 23. Chemical structures of commonly used pH-sensitive probes: A) BCECF, B) C.SNARF-1 and C) Pyranine (HPTS).

[235] Y. Xing, Y. Zhou, L. Fan, Y. Yang, Y. Zhang, X. Deng, C. Dong, S. Shuang, *Talanta* **2019**, *205*, 120021.
[236] Y. Cao, R. C. Qian, D. W. Li, Y. T. Long, *Chem. Commun.* **2015**, *51*, 17584-17587.
[237] A. Méndez-Ardoy, J. J. Reina, J. Montenegro, *Chem. Eur. J.* **2020**, *26*, 7516-7536.

HPTS (8-Hydroxypyrene-1,3,6-trisulfonic acid), also named as **pyranine** (Figure 23C), is an interesting small molecule to track intracellular pH. This molecule presents exceptional properties such as physical and chemical stability, high retention inside cells, and water solubility. Pyranine has also high pH sensitivity and may be applied for intracellular ratiometric pH measurements because it presents two pH-dependent excitation maxima at 450 nm (deprotonated form) and 405 nm (protonated form). This molecule has been applied as a pH indicator for cells or tissues. However, pyranine can not be efficiently transported across cell membranes, mainly because of their negative charge at physiological pH. Different invasive techniques such as microinjection and electroporation, have been applied to internalize pyranine into the cells. However, these methods produce cell damage that may modify the precise pH measurement.[238,239,240,166] Therefore, the development of a simple strategy to deliver these anionic hydrophilic smalls probes into cells remains as a major challenge. Such a method will also allow highly precise and efficient intracellular pH tracking.

[238] J. Han, K. Burgess, *Chem. Rev.* **2010**, *110*, 2709-2728.
[239] I. Johnson and M. Spence, *Molecular probes handbook: a guide to fluorescent probes and labeling technologies*, 11th edition, Life Technologies, Carlsbad, **2010**.
[240] C. C. Overly, K. D. Lee, E. Berthiaume, P. J. Hollenbeck, *Proc. Natl. Acad. Sci.* **1995**, *92*, 3156-3160.
[166] B. S. Gan, E. Krump, L. D. Shrode, S. Grinstein, *Am. J. Physiol.* **1998**, *275*, C1158-C1166.

Objectives

USC
UNIVERSIDADE
DE SANTIAGO
DE COMPOSTELA

Based on previous results on cage complexation of planar anionic molecules,[69] we decided to explore the potential caging strategy for the transitory masking of the hydrophilicity of planar probes and to achieve their delivery in the cytosol. The supramolecular nature of the approach will allow us to deliver these probes into the cell cytosol driven by the different concentrations of the probe between the extracellular and the intracellular environment and the high concentration of different anions present in the cell interior (Figure 24).

The specific objectives of this first chapter would be:

- Conjugation of a membrane-impermeable supramolecular cationic cage with different cell-penetrating peptides of different lengths, which would donate cell membrane transport capabilities to the supramolecular cage and evaluation of their cytotoxicity.
- Study of the interaction between the supramolecular cage and the pyranine probe by titration experiments, to understand the transport mechanism of the probe by *U*-tube experiments.
- Intracellular cytosolic delivery of pyranine in different cell lines using the previously synthesized peptide-cage carriers.
- Study of the mechanism of transport of these supramolecular complexes inside living cells by ensuring the non-permeabilization of the cell membrane and by using endocytosis inhibitors.
- Evaluation of the specificity of the approach by competition assays with different cargos.
- Extension of the approach to study interaction with the cage and cellular delivery efficiency of different anionic probes (CF and Alexa Fluor´s).
- Cell pH tracking by using peptide-cage carrier and pyranine as a pH-sensitive probe.

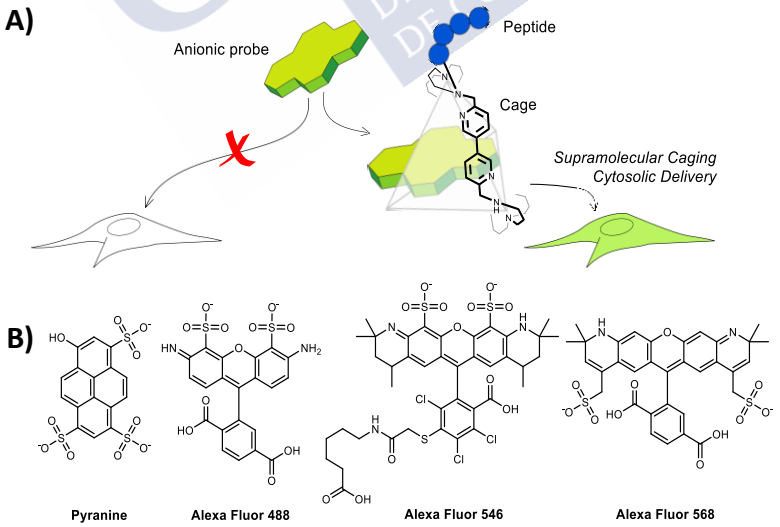

Figure 24. A) Objective: development of a peptide-cage carrier that consists of a peptide (blue spheres) and a positively charged supramolecular cage that is capable of delivering membrane-impermeable planar anionic probes into living cells and release them from endosomes. B) Examples of highly valuable fluorescent probes which are not able to cross cell membranes at low micromolar concentrations.

[69] J. Mosquera, S. Zarra, J. R. Nitschke, *Angew. Chem. Int. Ed.* **2014**, *53*, 1556-1559.

USC
UNIVERSIDADE
DE SANTIAGO
DE COMPOSTELA

Results and discussions

The results of this chapter have been published in:

H. Fernández-Caro, I. Lostalé-Seijo, M. Martínez-Calvo, J. Mosquera, J. L. Mascareñas, J. Montenegro, *Chem. Sci.* **2019**, *10*, 8930-8938.

USC
UNIVERSIDADE
DE SANTIAGO
DE COMPOSTELA

1. Antecedents

The group of prof. Nitschke has recently developed a cationic supramolecular cage (Figure 25) that showed the ability to interact by host-guest molecular recognition with the pyranine probe in aqueous environment with a K_d of 1.2 nM.[69] Later, in collaboration with Prof. Mascareñas group, a pyranine-peptide guest was designed by connecting a typical cell-penetrating peptide (octaarginine) to a polyanionic oligoglutamic terminated with a pyranine moiety. This peptide was not able to cross the cell membrane due to the anionic character of the pendant. However, when the supramolecular cage was incorporated, the cationic cage formed a host-guest complex with the anionic pyranine, masking its negative charge and promoting the cellular internalization of the membrane-impermeable pyranine-peptide (Figure 25).[241]

More recently, in a fruitful collaboration between the group of prof. Mascareñas and the group of prof. Liz-Marzán, the supramolecular interaction pyranine-cage was further explored to switch the cellular uptake of gold nanoparticles (AuNPs) (Figure 25).[242] In this work, AuNPs were functionalized with pyranine moieties. Due to their high negative charge, these AuNPs did not cross through the cell membrane. However, after the formation of the host-guest complex between the cage and the pyranine, their negative charge was masked and the cellular internalization of the pyranine-modified AuNPs was achieved. Interestingly, it was found that the cellular uptake of the pyranine-modified AuNPs could be reversibly turned on and off with the addition of the supramolecular cage.[242]

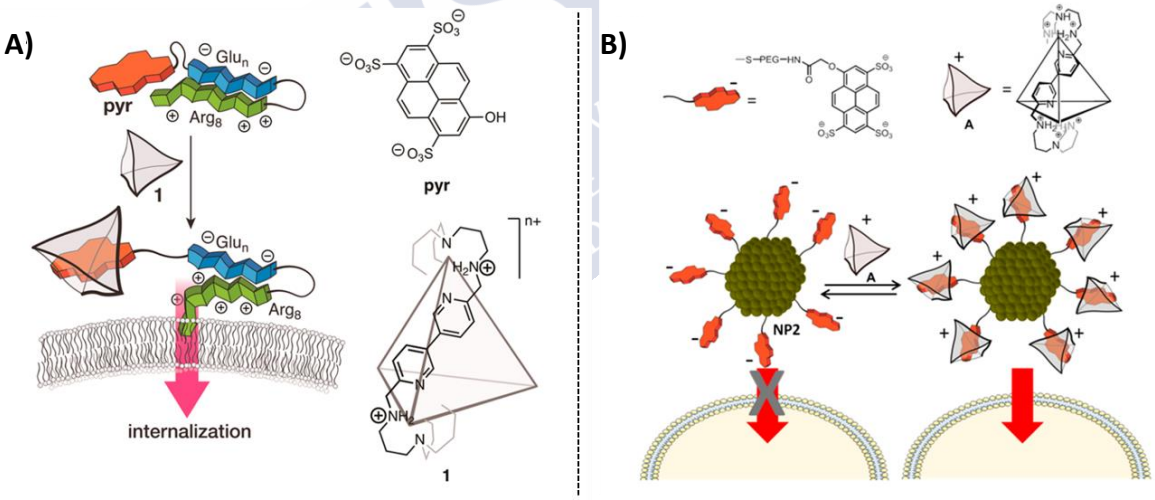

Figure 25. Schematic representations showing the intracellular delivery of membrane-impermeable A) pyranine-functionalized peptide and B) pyranine-modified AuNPs triggered by the addition of the cationic supramolecular cage. A) Reprinted with permission from ref. 241. Copyright 2017 American Chemical Society. B) Reprinted with permission from ref. 242. Copyright 2018 American Chemical Society.

[69] J. Mosquera, S. Zarra, J. R. Nitschke, *Angew. Chem. Int. Ed.* **2014**, *53*, 1556-1559.
[241] J. Rodríguez, J. Mosquera, J. R. Couceiro, J. R. Nitschke, M. E. Vázquez, J. L. Mascareñas, *J. Am. Chem. Soc.* **2017**, *139*, 55-58.
[242] J. Mosquera, M. Henriksen-Lacey, I. García, M. Martínez-Calvo, J. Rodríguez, J. L. Mascareñas, L. M. Liz-Marzán, *J. Am. Chem. Soc.* **2018**, *140*, 4469-4472.

2. Design and synthesis

2.1.Synthesis of the cage C and initial cellular internalization experiments

First, in collaboration with the group of prof. Nitschke, we followed the procedure reported in the literature for the synthesis and the purification of the supramolecular cage **C** (Figure 4A).[69] Following the described procedure, the 3,3'-bipyridine-6,6'-dicarboxaldehyde was reacted with tris(2-aminoethyl)amine and cadmium(II) trifluoromethanesulfonate ($Cd(OTf)_2$) in acetonitrile solution. The resulting Cd^{II}-templated cage was then reduced using sodium borohydride ($NaBH_4$), leading to the demetallated cage **C.** Once, we have prepared the cationic cage **C**, we wondered if the cage **C** alone would have the ability to promote the cellular internalization of pyranine and, also, if pyranine alone would be able to cross the cell membrane at different concentrations (Figure 26). To study this phenomenon, we decided to carry out preliminary control experiments using confocal microscopy.

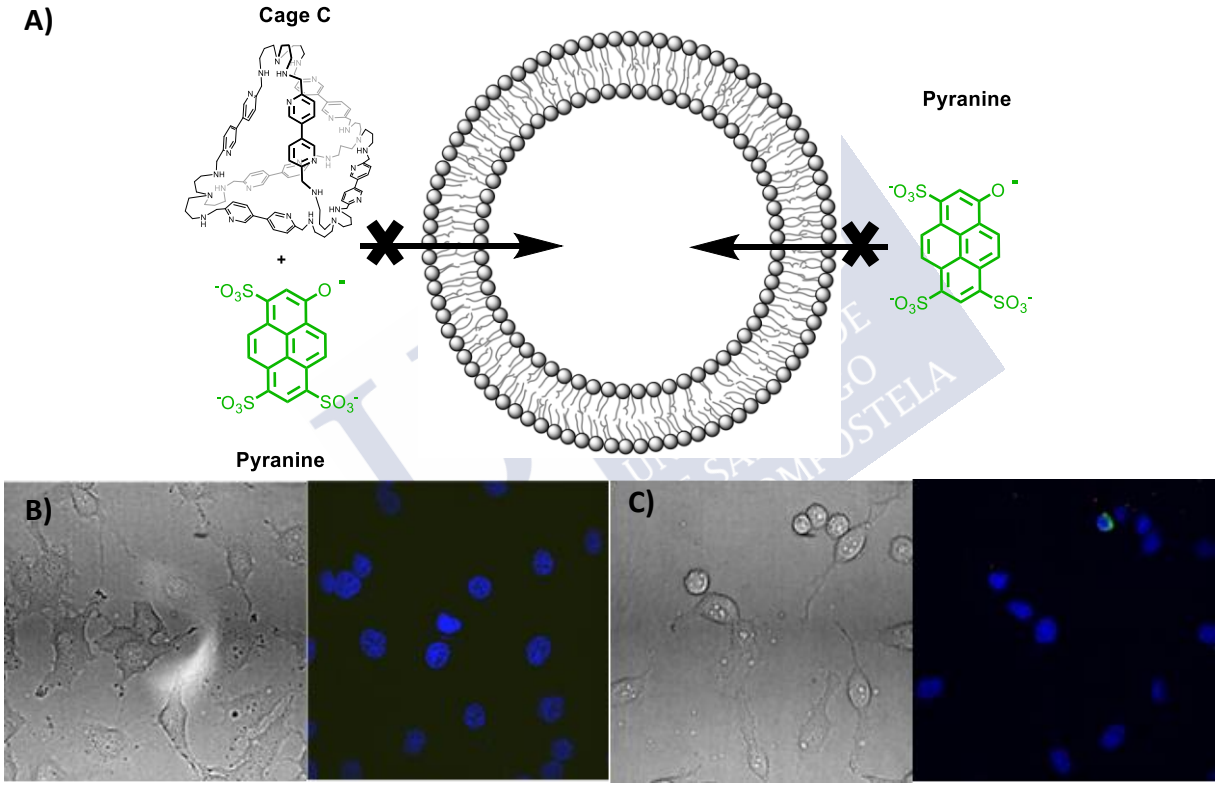

Figure 26. A) Schematic representation of the control experiments showing neither internalization of the complex pyranine and cage **C** nor pyranine alone inside cells. B and C) Control transport experiments in HeLa cells. Confocal micrographs of HeLa cells incubated with: B) Pyranine (5 µM) C) Pyranine (5 µM) and only cage **C** (5µM). Nuclei stained with Hoechst (blue). DIC on the left and merge of fluorescence channels [Pyranine emission (green) + Hoechst 33342 emission (blue)] on the right.

First, we decided to evaluate the potential of the cage **C** to internalize pyranine. For this, we co-incubated different concentrations of the cage **C** and pyranine with HeLa cells. To carry out this internalization experiment, we treated HeLa cells with Hoechst 33342 for 30 min (for nucleus staining), we washed (HKR buffer, 1x), and then cells were incubated with the different concentrations of cage and pyranine, for instance, 5 µM of pyranine and 5 µM of cage **C** (Figure 26), in HKR buffer for 30 min at 37 ºC. Cells were finally washed (HKR buffer, 3x) and

[69] J. Mosquera, S. Zarra, J. R. Nitschke, *Angew. Chem. Int. Ed.* **2014**, *53*, 1556-1559.

observed under the confocal microscope. In the confocal micrographs (Figure 26), we did not observe any pyranine (green) fluorescence inside the cells. This result demonstrated that the supramolecular cage **C** does not promote the intracellular delivery of pyranine. On the other hand, we also evaluated the ability of pyranine alone to cross the cell membrane at different concentrations. Following the same procedure, HeLa cells incubated with 5 μM of pyranine alone did not show any green fluorescence inside the cells (Figure 26).

2.2. Initial design and synthesis of the peptide-cage hybrids ^{Tm}AC and ^{Tm}***R*$_8$**C

After verifying by confocal experiments that the supramolecular cage **C** alone is not able to internalize pyranine at different concentrations, we then decided to covalently attach to one of the vertices of the cage different cationic peptides with excellent internalization abilities and high aqueous solubility. We hypothesized that these peptide pendants would promote the cellular internalization and also would increase the solubility of the cage in the aqueous environment.

With this purpose, first, we decided to covalently attach to the cage a typical cell-penetrating peptide octaarginine (**R$_8$**). This peptide (Figure 27) has been intensively studied and demonstrated to be able to improve the solubility and to promote the cellular translocation of different therapeutically active molecules.[169] We also decided to incorporate the amphiphilic peptide **A** (Figure 27) to the cage.[109] Furthermore, we incorporated the TAMRA fluorophore at the N-terminus of both peptides (Figure 27) to follow the distribution of the peptide in cellular experiments by confocal microscopy without causing any interference with the pyranine emission.

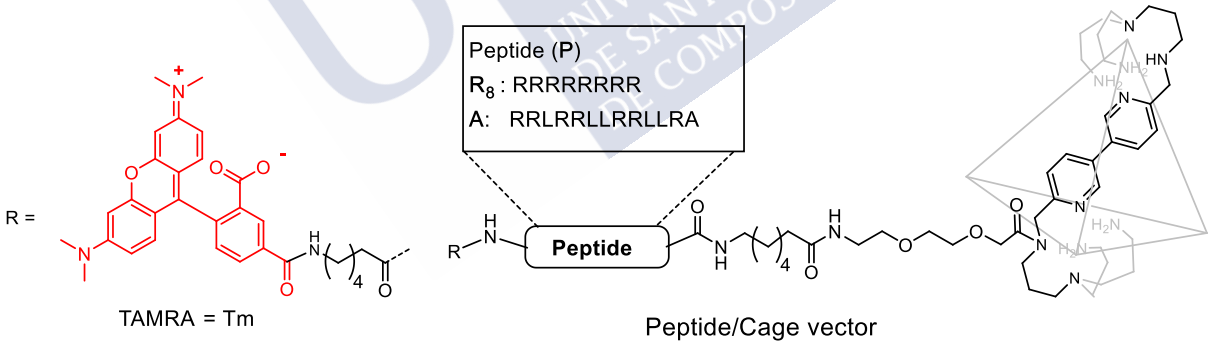

Figure 27. Chemical structure of the peptide-cage hybrids ^{Tm}***R*$_8$**C and ^{Tm}**AC**.

To promote the intracellular delivery of pyranine, we synthesized two different peptide-cage hybrids ^{Tm}***R*$_8$**C and ^{Tm}**AC** in which the **Tm** superindex denotes the incorporation of TAMRA fluorophore at the N-terminus of the peptides (Figure 27). The synthetic strategy was divided into two steps, first, we synthesized ^{Tm}**A** and ^{Tm}***R*$_8$** with a free carboxylic acid group at their terminal carboxylic ends and, in the second step, in collaboration with the group of the prof. Mascareñas, we attached the supramolecular cage **C** (Figure 28). To carry out the first step, SPPS by manual Fmoc solid-phase was applied by using a 2-chlorotrityl chloride resin.[243] This resin was employed to obtain the corresponding free C-terminal group for the subsequent

[169] K. M. Stewart, K. L. Horton, S. O. Kelley, *Org. Biomol. Chem.* **2008**, *6*, 2242-2255.
[109] M. Mäe, Ü. Langel, *Curr. Opin. Pharmacol.* **2006**, *6*, 509-514.
[243] M. Alhassan, O. Al Musaimi, J. M. Collins, F. Albericio, B. G. de la Torre, *Green Chem.* **2020**, *22*, 2840-2845.

attachment of the cage **C**. Importantly, we incorporated two different linkers, first, 8-amino-3,6-dioxaoctanoic acid (O2Oc) and then, 6-aminohexanoic acid (Ahx), before both peptide sequences. We hypothesized that the incorporation of both linkers would decrease the steric hindrance and the electrostatic interactions and would increase the yield of the reaction with the cationic cage in the last step. The first coupling was carried out in CH_2Cl_2 using DIEA as the base. For the following couplings, we used *N*-HBTU as activator, DIEA as base, and DMF as solvent. The deprotection of the temporal Fmoc protecting group was performed by treating the resin with 20% piperidine in DMF. To couple the fluorophore at the N-terminus we used three equivalents of 5(6)-Carboxytetramethylrhodamine (TAMRA) with 3 equivalents of *N*-HATU and 5 equivalents of DIEA in DMF (0.2 M) for 60 min. The cleavage/deprotection step was performed by treatment of the resin-bound peptide for 2 h with the following cleavage cocktail: 900 mL TFA, 50 mL CH_2Cl_2, 25 mL H_2O, and 25 mL TIS. Peptides were precipitated with Et_2O and purified by RP-HPLC. The peptides were characterized by HPLC-MS.

Once we have synthesized and characterized ^{Tm}**A** and ^{Tm}***R*$_8$** with the free terminal carboxylic groups, we proceed with the second synthetic step, the coupling of the supramolecular cage. To synthesize ^{Tm}**AC** and ^{Tm}***R*$_8$C**, we first dissolved ^{Tm}**A** and ^{Tm}***R*$_8$** peptides in DMF (0.1 mM, 100 mL) and then *N*-HATU (1 equiv.) and DIEA (10 equiv.) were added to the solution. This mixture was added to a 0.1 mM solution of the cage **C** (1 equiv.) and the reaction was left stirring overnight. The resulting product was purified by RP-HPLC and the peptide-cage peptides were characterized by mass spectrometry.

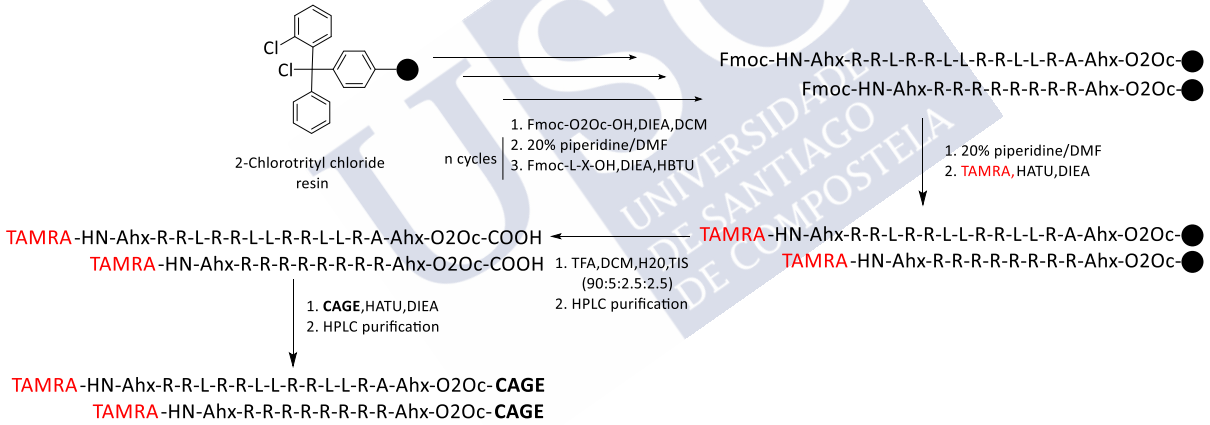

Figure 28. Scheme for the synthesis of ^{Tm}**AC** and ^{Tm}***R*$_8$C**.

2.3.Preliminary internalization experiments using ^{Tm}AC and ^{Tm}*R*$_8$C

Once we had synthesized and characterized the peptides ^{Tm}**AC** and ^{Tm}***R*$_8$C**, we addressed if these peptide-cage hybrids would be able to internalize pyranine inside cells. To study the internalization of this probe, we decided to carry out preliminary transport experiments using low micromolar concentrations of both pyranine and the different peptides. First, we carried out pyranine transport experiments using ^{Tm}**AC**. We incubated HeLa cells with Hoechst 33342 for 30 min, washed (HKR buffer, 1x), and then we co-incubated the cells with 5 µM of ^{Tm}**AC** and 5 µM Pyranine in HKR buffer for 30 min at 37 ºC. The cells were finally washed (HKR buffer, 3x) and then observed under the confocal microscope. Unexpectedly, we found high cellular toxicity of the ^{Tm}**AC** peptide which can be appreciated in the confocal images **(**Figure 29**)** by the morphological cellular alterations such as nuclear profiling. Moreover, we also found that this peptide forms aggregates in the presence of pyranine in the cellular environment.

Then, we carried out pyranine transport experiments with $^{Tm}\boldsymbol{R_8}$**C** following the same procedure as before but, in this case, using 5 µM of $^{Tm}\boldsymbol{R_8}$**C** and 5 µM Pyranine. However, we found again high cytotoxicity of $^{Tm}\boldsymbol{R_8}$**C** which was evident by the cellular morphological alterations and the lower number of cells observed (Figure 29). Moreover, as the previous hybrid, this peptide is also forming aggregates in the presence of pyranine in the cellular medium.

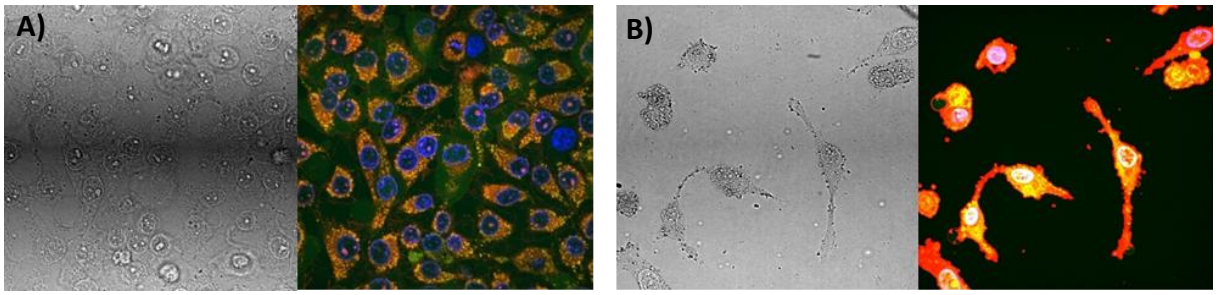

Figure 29. Transport experiments in HeLa cells with ^{Tm}**AC** and $^{Tm}\boldsymbol{R_8}$**C**. Confocal micrographs of HeLa cells incubated with: A) 5 µM of ^{Tm}**AC** and 5 µM Pyranine B) 5 µM of $^{Tm}\boldsymbol{R_8}$**C** and 5 µM Pyranine. DIC on the left and merge channels [Pyranine emission (green) + TAMRA emission (red) + Hoechst 33342 emission (blue)] on the right.

2.4.Re-design and synthesis of the peptide cage-hybrids $^{Ac}\boldsymbol{R_4}$**C**/$^{Tm}\boldsymbol{R_4}$**C**

Taking into account the high cellular toxicity and high ability to form aggregates when incubated with pyranine of previously designed peptides ^{Tm}**AC** and $^{Tm}\boldsymbol{R_8}$**C**. We re-designed our peptide-cage hybrid and we decided to covalently attach a shorter tetraarginine peptide to one of the vertices of the cage instead of the octapeptide (Figure 30). We hypothesized that this shorter cationic peptide would avoid cytotoxicity and aggregation problems.

Therefore, we synthesized two **R$_4$-cage** hybrids, $^{Ac}\boldsymbol{R_4}$**C** and $^{Tm}\boldsymbol{R_4}$**C** (super indexes: **Ac** for the acetylated hybrid and **Tm** for the TAMRA labeled derivative). Again, we prepared the labeled version with the aim of following the distribution of the peptide in cellular experiments using confocal microscopy. On the other hand, the acetylated version $^{Ac}\boldsymbol{R_4}$**C** (Figure 30) was prepared to evaluate the influence of the fluorophore in the internalization.

The synthesis of both $^{Ac}\boldsymbol{R_4}$**C** and $^{Tm}\boldsymbol{R_4}$**C** was carried out following the strategy previously described for ^{Tm}**AC** and $^{Tm}\boldsymbol{R_8}$**C**. For the preparation of $^{Ac}\boldsymbol{R_4}$, the acetylation of the N-terminal group was performed under standard Fmoc removal conditions (20% piperidine in DMF) followed by treatment with a solution of acetic anhydride and 2,6-lutidine (1: 1, 1 mL) for 30 min. Moreover, these peptide-cage vectors were purified and characterized by HPLC-MS showing that only one peptide was attached to a single cage.

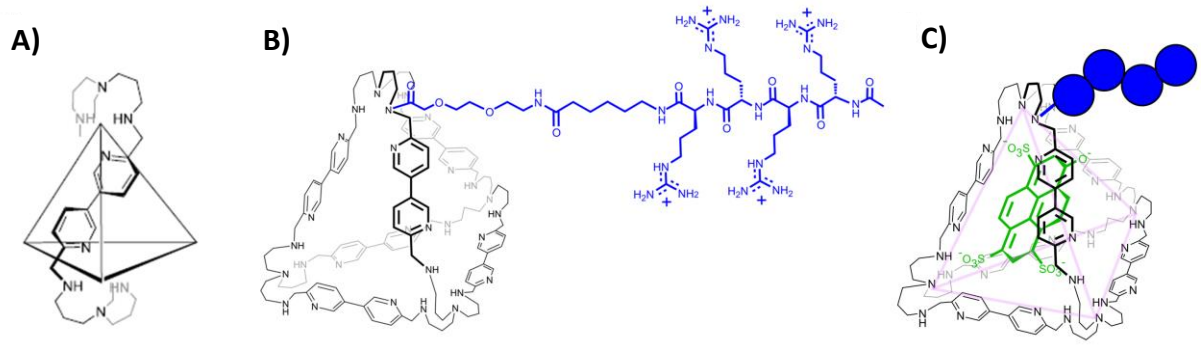

Figure 30. A) Structure of the supramolecular cage **C**.[69] For clarity, only one of the edges of the structure is shown. B) Chemical structure of $^{Ac}\boldsymbol{R}_4\mathbf{C}$ as a representative example of the attachment of the peptide to C. Only one peptide is attached to the cage. C) Schematic representation of the peptide-cage hybrid with a pyranine molecule inside the cage.

3. Evaluation of the cellular toxicity of $^{Ac}\boldsymbol{R}_4\mathbf{C}$ and $^{Tm}\boldsymbol{R}_4\mathbf{C}$

Once we have synthesized and characterized $^{Ac}\boldsymbol{R}_4\mathbf{C}$ and $^{Tm}\boldsymbol{R}_4\mathbf{C}$, we found that these peptide-cage hybrids showed excellent aqueous solubility even in the presence of pyranine. Therefore, we decided to carry out the MTT assay to evaluate the toxicity of these peptides in different cell lines (HeLa and Vero cells). First, we incubated different equimolar concentrations of pyranine and $^{Tm}\boldsymbol{R}_4\mathbf{C}$ or $^{Ac}\boldsymbol{R}_4\mathbf{C}$ and pyranine alone for 1 hour with HeLa cells and we found high cell viability at the different concentrations (Figure 31). We also extended the incubation time to 24 hours in HeLa cells with the same conditions showing neither cytotoxicity at low concentrations (Figure 31). Furthermore, we also carried out these cytotoxicity studies in Vero cells as another different cell line, and no cytotoxicity was found (Figure 52).

In addition, we also decided to evaluate the toxicity of $^{Ac}\boldsymbol{R}_4\mathbf{C}$ in the absence of pyranine. Interestingly, we found that $^{Ac}\boldsymbol{R}_4\mathbf{C}$ in the absence of pyranine at high concentrations such as 20 μM showed cytotoxicity. However, when we co-incubated $^{Ac}\boldsymbol{R}_4\mathbf{C}$ with pyranine at high concentrations (20 μM), the cytotoxicity was reduced (Figure 31). This result suggests that the supramolecular encapsulation of pyranine decreases the cytotoxicity of the peptide-cage carrier perhaps as a consequence of the reduced cationic character of the complex.

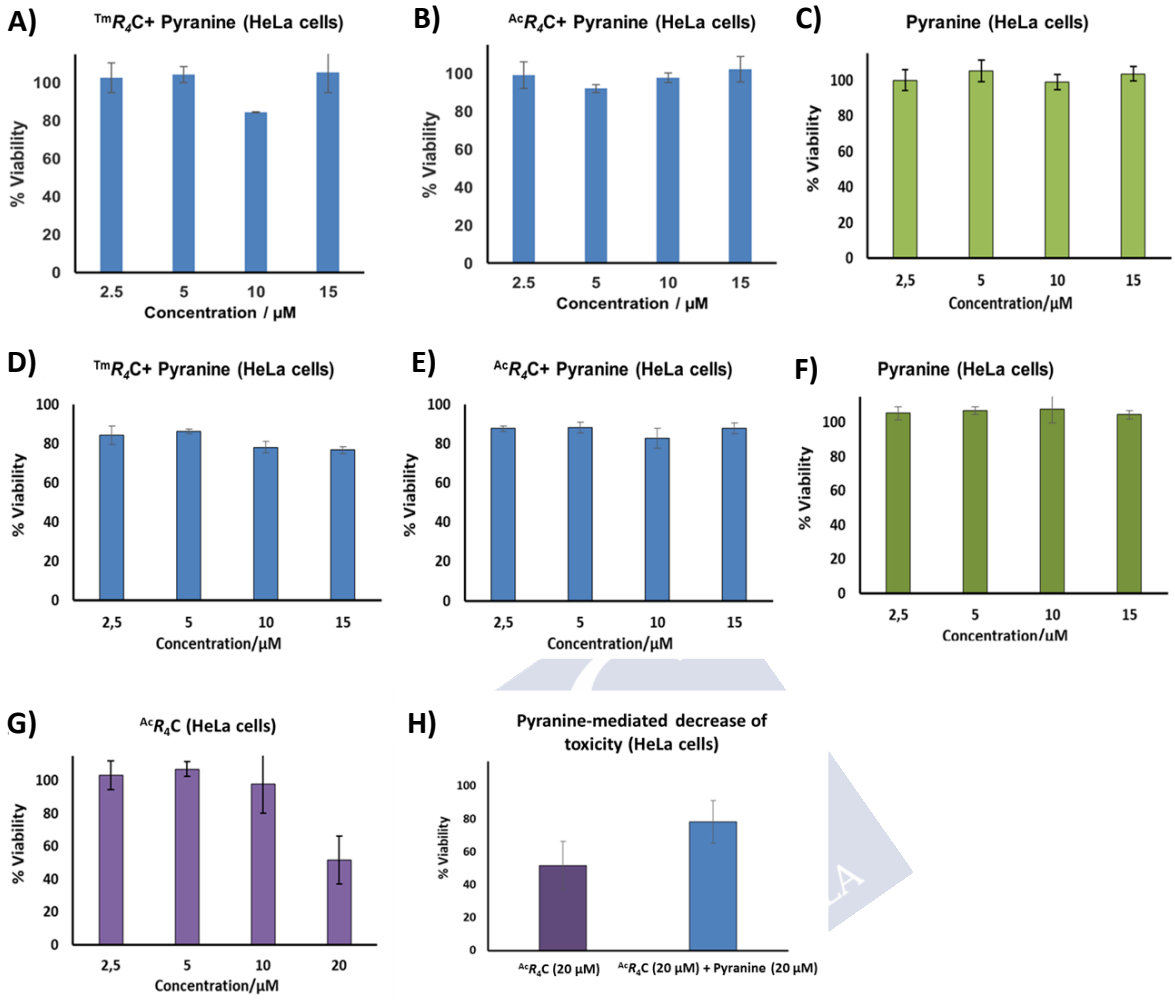

Figure 31. Viability assay in HeLa cells at different **equimolar** concentrations of pyranine and $^{Tm}\boldsymbol{R}_4\mathbf{C}$ (A, D) or $^{Ac}\boldsymbol{R}_4\mathbf{C}$ (B, E) and only pyranine (C, F), after 1 hour incubation time (A, B, C) and after 24 hours incubation time (D, E, F) in HKR at 37 ºC. G) Viability of $^{Ac}\boldsymbol{R}_4\mathbf{C}$ at different concentrations. H) Viability comparison between $^{Ac}\boldsymbol{R}_4\mathbf{C}$ at 20 µM and $^{Ac}\boldsymbol{R}_4\mathbf{C}$ at 20 µM in presence of 20 µM of pyranine showing the decrease of toxicity produced by pyranine. Error bars represent the standard deviation of four replicates.

4. *In vitro* experiments

4.1. Study of the interaction between the supramolecular cage C and pyranine probe

Once we demonstrated that the new peptide-cage carriers ($^{Ac}\boldsymbol{R}_4\mathbf{C}$/$^{Tm}\boldsymbol{R}_4\mathbf{C}$) are not cytotoxic, we decided to study the supramolecular interaction between the supramolecular cage anchored to the peptide and the pyranine probe. Titration experiments of the pyranine probe with increasing concentrations of the peptide-cage carriers in phosphate buffer at pH 7 were carried out.

In previous results of the group of prof. Nitschke, it was shown that the K_d between the cage alone and pyranine was 1.2 nM.[69] Following the same procedure, first, we decided to study the interaction between the pyranine and the cage with the acetylated peptide attached (^{Ac}***R*$_4$C**). The supramolecular cage has the ability to quench pyranine. Therefore, we expect to observe a decrease in the fluorescence signal of pyranine with increasing concentrations of ^{Ac}***R*$_4$C** if the cage-pyranine interaction occurs. In this experiment, we found a decrease in the fluorescence signal of pyranine with the increase of the concentration of ^{Ac}***R*$_4$C** (Figure 32). This result demonstrated that there was an interaction between the pyranine and the cage. In comparison with the cage alone, the K_d of pyranine for the cage increases with the presence of the peptide from 1.2 nM[69] to 189 nM. This result suggests that the interaction between the cage and pyranine is hindered by the presence of the cationic peptide.

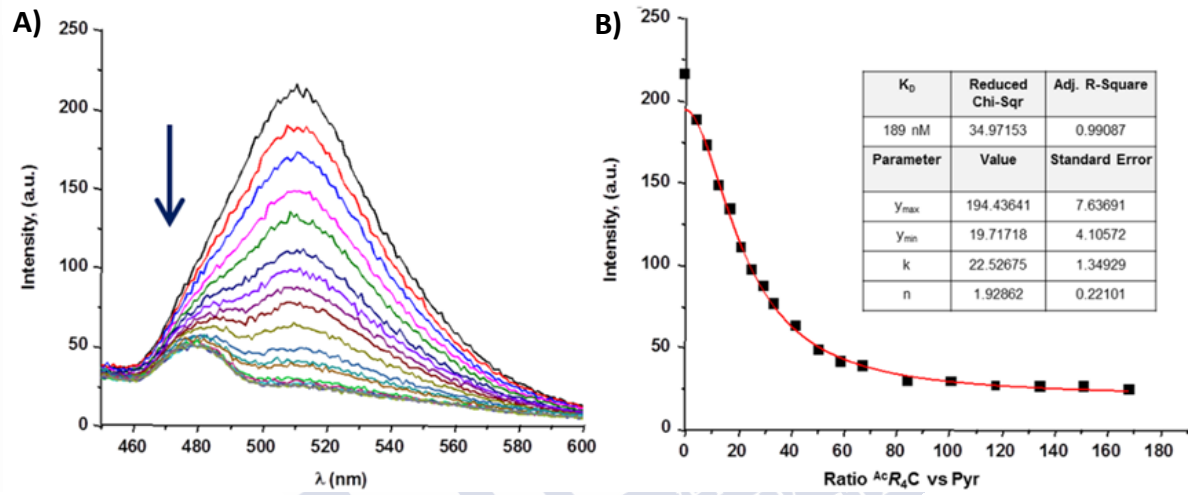

Figure 32. A) Fluorescence titration of pyranine with the peptide/cage ^{Ac}***R*$_4$C** in phosphate buffer (pH 7). Arrow indicates the decrease of pyranine fluorescence with increasing amounts of the peptide. B) 510 nm fluorescence emission and curve fit for the titration of pyranine with ^{Ac}***R*$_4$C** in phosphate buffer pH 7. The best fit to the data using nonlinear analysis with Origin 8.5 to the Hill 1 equation. The small peak observed in A) at about 480 nm at the higher concentrations of peptide corresponds to the Raman scattering of water for an excitation wavelength of 415 nm.

Subsequently, we carried out the same experiment but with the TAMRA labeled peptide, ^{Tm}***R*$_4$C** (Figure 33). This experiment showed that there is an interaction between pyranine and cage and that the dissociation constant is K_d = 12.6 μM. Interestingly, in comparison with the acetylated peptide the dissociation constant increases from 189 nM to 12.6 μM. We first hypothesized that the interaction between TAMRA and the cage could be related to the increase of the K_d. However, we did not observe any interaction between both entities by fluorescence titrations (Figure 43). We then suggested that TAMRA could be producing a steric effect or the labeled carrier could be adopting a new supramolecular structure which is difficulting pyranine-cage interaction.

[69] J. Mosquera, S. Zarra, J. R. Nitschke, *Angew. Chem. Int. Ed.* **2014**, *53*, 1556-1559.

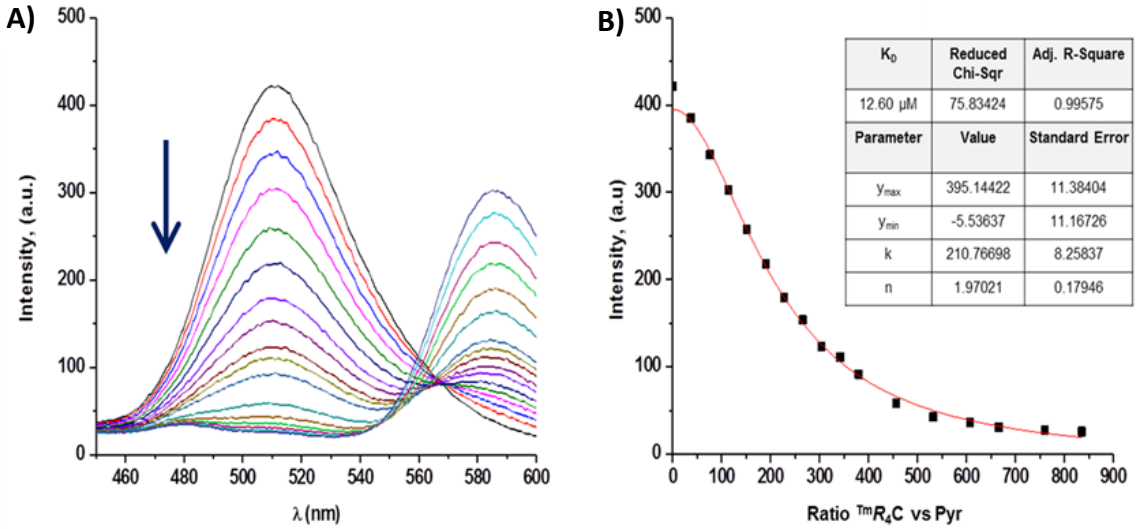

Figure 33. A) Fluorescence titration of pyranine with the peptide/cage $^{Tm}\boldsymbol{R}_4\mathbf{C}$ in phosphate buffer (pH 7). Arrow indicates the decrease of pyranine fluorescence with increasing amounts of the peptide. The right peak in A corresponds to the TAMRA emission from $^{Tm}\boldsymbol{R}_4\mathbf{C}$. B) 510 nm fluorescence emission and curve fit for the titration of pyranine with $^{Tm}\boldsymbol{R}_4\mathbf{C}$ in phosphate buffer pH 7. The best fit to the data using nonlinear analysis with Origin 8.5 to the Hill 1 equation.

4.2. Study of the mechanism of transport by *U*-tube experiments

Once we discovered the interaction capabilities of peptide-cage hybrids with pyranine, we decided to study the potential of $^{Ac}\boldsymbol{R}_4\mathbf{C}$ to transport pyranine *in vitro*. With this purpose, we carried out transport experiments in a *U*-tube. The group of prof. Matile, as well as other groups, applied transport experiments in *U*-tubes to ensure the ability of molecules to act as carriers.[244,245] Additionally, this group also showed the high difficulty for the transport of pyranine using polyarginine carriers in the *U*-tube experiments.[246]

To study the potential of $^{Ac}\boldsymbol{R}_4\mathbf{C}$ to transport pyranine in a *U*-tube, we followed the described methodology by placing at the bottom of the *U*-tube the organic phase ($CHCl_3$) and, then, adding at both sides of the organic phase, two aqueous buffers (*cis* and *trans*). In the *cis* buffer, we added a mixture of $^{Ac}\boldsymbol{R}_4\mathbf{C}$, pyranine, and a physiological counterion, in this case, the anionic lipid called egg yolk phosphatidylglycerol (EYPG). The organic phase was stirred and aliquots were collected at different times from the *trans* buffer. These aliquots were then diluted and fluorescence measurements were carried out. These fluorescence values allowed us to quantify the pyranine transport through the organic phase $CHCl_3$ with the time (Figure 34). This experiment showed the ability of $^{Ac}\boldsymbol{R}_4\mathbf{C}$ to importantly increase the transport of pyranine through the organic phase. This result was shown by simple naked eye observation (Figure 34) and also by fluorescence measurements (Figure 34).

[244] T. Takeuchi, V. Bagnacani, F. Sansone, S. Matile, *ChemBioChem*, **2009**, *10*, 2793-2799.
[245] P. Breccia, M. Van Gool, R. Pérez-Fernández, S. Martín-Santamaría, F. Gago, P. Prados, J. de Mendoza, *J. Am. Chem. Soc.* **2003**, *125*, 8270-8284.
[246] N. Sakai, S. Matile, *J. Am. Chem. Soc.* **2003**, *125*, 14348-14356.

Control *U*-tube experiments following the same procedure and using only pyranine, the cage (**C**) with pyranine, and the tetraarginine peptide (^{Ac}***R*$_4$**) with pyranine showed only the increase of pyranine transport with ^{Ac}***R*$_4$**C** (Figure 34**)**. Importantly, we found that while ^{Ac}***R*$_4$**C** promotes a strong increase in the pyranine transference, the acetylated peptide without cage (^{Ac}***R*$_4$**) did not. This result clearly shows the importance of the interaction between the cage and pyranine for the carrier mechanism.

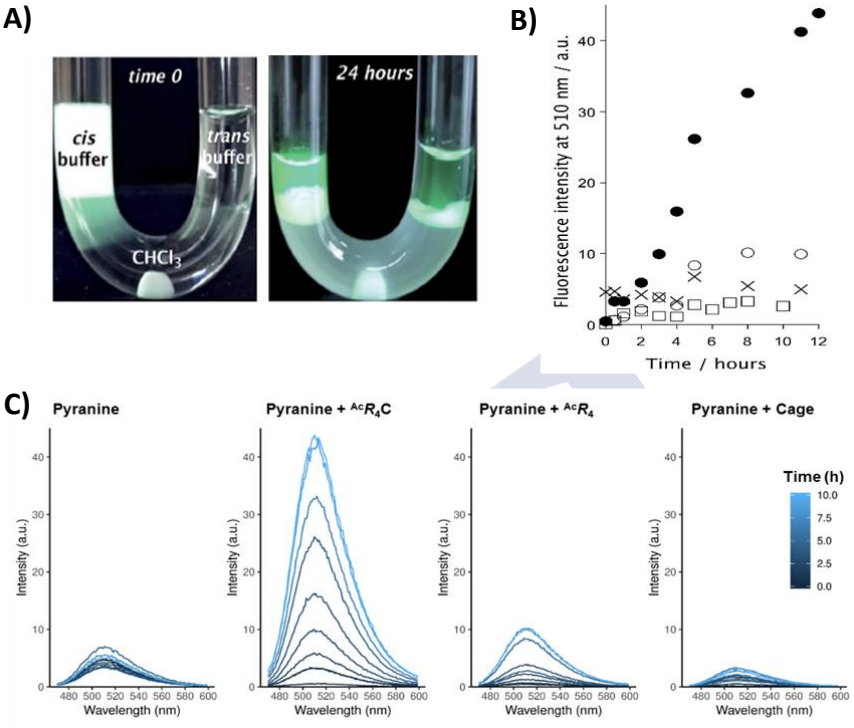

Figure 34. U-tube experiments. A) Pictures at time 0 and after 24 hours. B) Transport of pyranine as a function of time from the *cis* buffer (0.5 mL, ^{Ac}***R*$_4$**C: 80 μM, EYPG: 10 mM and pyranine: 200 μM) into the *trans* buffer (0.5 mL) across the chloroform phase (1 mL). Buffer: 10 mM $Na_mH_nPO_4$, 100 mM NaCl, pH 7.4. Pyranine + ^{Ac}***R*$_4$**C (●), pyranine + ^{Ac}***R*$_4$** (○), pyranine + cage **C** (□), pyranine (×). C) Pyranine fluorescence emission spectra of the aliquots taken from the *U*-Tube *trans* buffer at different times. From left to right: Pyranine alone (200 μM). Pyranine (200 μM) + ^{Ac}***R*$_4$**C (80 μM). Pyranine (200 μM) + ^{Ac}***R*$_4$** (80 μM). Pyranine (200 μM) + Cage **C** alone (80 μM). Data previously represented as a function of time in B).

5. Intracellular cytosolic delivery of pyranine

After demonstrating the interaction between pyranine and the supramolecular cage of both ^{Ac}***R*$_4$**C/^{Tm}***R*$_4$**C** and the ability of ^{Ac}***R*$_4$**C** to transport this probe *in vitro* by *U*-tube experiments, we decided to carry out cell internalization experiments.

First, we studied the cellular internalization of ^{Tm}***R*$_4$**C** alone to demonstrate that this peptide has the ability to translocate the cellular membrane and to reach the cellular cytosol. To ensure the low cytotoxicity, we performed these cell transport experiments at **5 μM of ^{Tm}*R*$_4$C** due to this concentration previously showed high cellular viability by MTT assays (Figure 31)**.** To carry out this experiment, we first treated HeLa cells with Hoechst 33342 for 30 min, washed (HKR buffer, 1x), and then incubated the cells with ^{Tm}***R*$_4$**C (5 μM)** in HKR buffer for 30 min at 37 ºC. The cells were finally washed (HKR buffer, 3x) and then observed under the confocal

microscope. Confocal microscopy images (Figure 35) showed a really efficient internalization of $^{Tm}\boldsymbol{R}_4\mathbf{C}$ at low concentrations (5 µM). $^{Tm}\boldsymbol{R}_4\mathbf{C}$ alone showed cytosolic distribution but also showed accumulation in the cell nucleolus (Figure 35), as previously described for other arginine-rich peptides.[247]

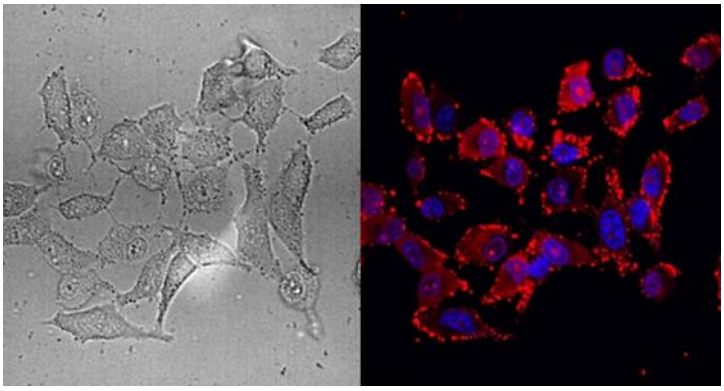

Figure 35. $^{Tm}\boldsymbol{R}_4\mathbf{C}$ internalization experiment in HeLa cells. Confocal micrographs of HeLa cells incubated with $^{Tm}\boldsymbol{R}_4\mathbf{C}$ (5 µM). DIC on the left and merge of fluorescence channels [TAMRA emission (red) + Hoechst 33342 emission (blue)] on the right.

Once we demonstrated the ability of $^{Tm}\boldsymbol{R}_4\mathbf{C}$ to cross the cell membrane and to be efficiently delivered into the cell cytosol of HeLa cells and taking into account that $^{Tm}\boldsymbol{R}_4\mathbf{C}$ has shown good affinities with pyranine, we decided to perform cell transport experiments of this probe. To reach our specific objective of delivering pyranine in the cell cytosol. Our peptide-cage carrier would have to encapsulate the pyranine probe, to translocate de cellular membrane and to release this probe in the cell cytosol (Figure 36).

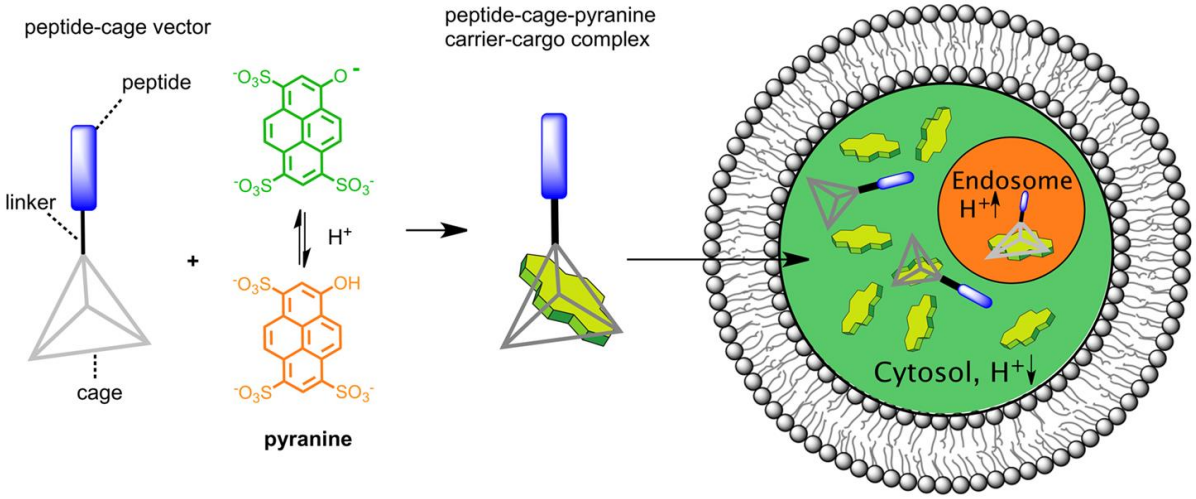

Figure 36. Schematic representation of the strategy to deliver pyranine into the cellular cytosol mediated by a peptide-cage vector.

[247] R. M. Martin, G. Ter-Avetisyan, H. D. Herce, A. K. Ludwig, G. Lättig-tünnemann, M. C. Cardoso, *Nucleus*, **2015**, *6*, 314-325.

To achieve an efficient pyranine delivery in cells, first, we performed dose-response transport experiments with increasing concentrations of pyranine (Figure 37) in order to find the best concentration of carrier/pyranine for the best transport efficiency. To carry out this experiment, we decided to use the same concentration of $^{Tm}\boldsymbol{R_4}$**C** (5 µM) than in the previous experiment because it was shown to have good translocation efficiency at this concentration. Then, we used increasing concentrations of the **pyranine** (2,5 µM, 5 µM, and 10 µM). In this experiment, HeLa cells were incubated with the different concentrations in HKR buffer for 30 min at 37 ºC. The cells were finally washed (HKR buffer, 3x) and then observed under the confocal microscope.

In this dose-response experiment, we found that $^{Tm}\boldsymbol{R_4}$**C** (5 µM) was able to transport pyranine to the cell cytosol at 2.5 µM and 5 µM concentration. The best transport efficiency was showed at $^{Tm}\boldsymbol{R_4}$**C** (5 µM) and **pyranine** (5 µM). Moreover, we found that when we increased the pyranine concentration to 10 µM, the transport of pyranine was inhibited and extracellular aggregation was observed (Figure 37).

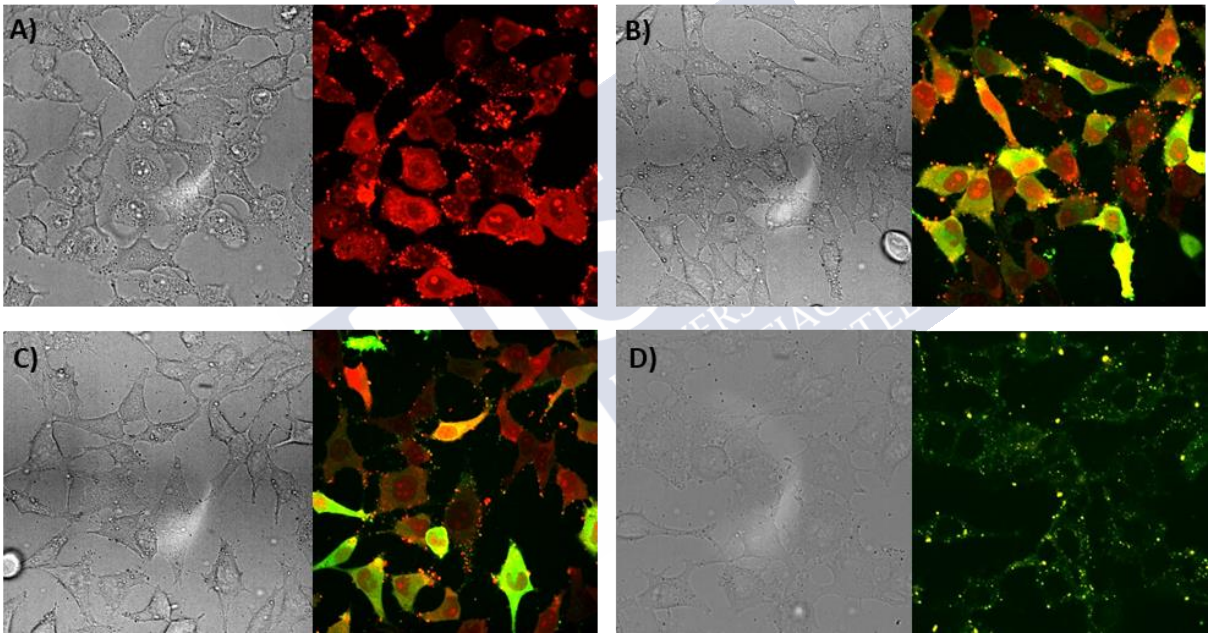

Figure 37. Dose-response transport experiments of pyranine in HeLa cells with $^{Tm}\boldsymbol{R_4}$**C**. Confocal micrographs of HeLa cells incubated with: A) $^{Tm}\boldsymbol{R_4}$**C** (5 µM), B) $^{Tm}\boldsymbol{R_4}$**C** (5 µM) and Pyranine (2.5 µM), C) $^{Tm}\boldsymbol{R_4}$**C** (5 µM) and Pyranine (5 µM), D) $^{Tm}\boldsymbol{R_4}$**C** (5 µM) and Pyranine (10 µM). DIC on the left and merge channels [Pyranine emission (green) + Tm emission (red)] on the right.

Since the results of the dose-response experiment suggested that the best transport efficiency was reached at equimolar concentrations of $^{Tm}\boldsymbol{R_4}$**C** (5 µM) and **pyranine** (5 µM) in HeLa cells (Figure 37C)**,** we decided to carry out further cell internalization experiments in a different cell line such as Vero cells, achieving also efficient cytosolic delivery of pyranine with $^{Tm}\boldsymbol{R_4}$**C** (Figure 38).

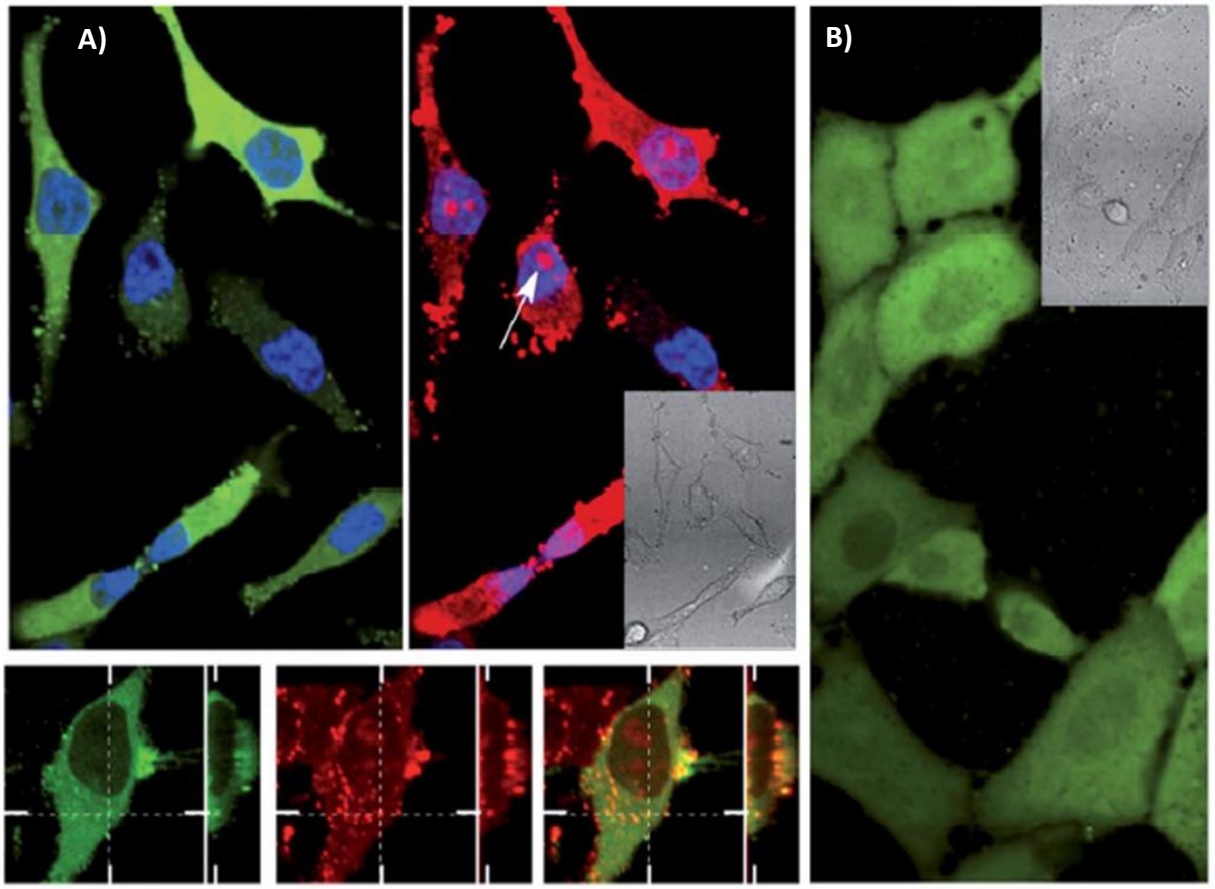

Figure 38. Pyranine transport experiments in HeLa (A) and Vero (B) cells. A) Top: confocal micrographs of HeLa cells co-incubated with pyranine (5 μM, green) and $^{Tm}\boldsymbol{R}_4\mathbf{C}$ (5 μM, red) for 30 min in HKR buffer. Nuclei were stained with Hoechst (blue). The white arrow shows the nucleolar accumulation of the peptide-cage carrier. Bottom: confocal micrographs and the orthogonal projection of the same HeLa cells showing pyranine (green) and $^{Tm}\boldsymbol{R}_4\mathbf{C}$ (red) cytosolic distribution and partial endosomal co-localization. B) Internalization of pyranine (15 μM, green) in the presence of $^{Tm}\boldsymbol{R}_4\mathbf{C}$ (15 μM) in Vero cells, after incubation for 30 min in HKR.

Moreover, we carried out control transport experiments in HeLa cells using the tetra-arginine peptide without the supramolecular cage **C** ($^{Tm}\boldsymbol{R}_4$). These experiments would allow us to confirm the key role of the supramolecular cage in the intracellular transport of pyranine. In this experiment, we followed the same procedure as before but using $^{Tm}\boldsymbol{R}_4$ instead of $^{Tm}\boldsymbol{R}_4\mathbf{C}$. Interestingly, we found that $^{Tm}\boldsymbol{R}_4$ does not promote any pyranine internalization (Figure 39A). Therefore, we showed that the supramolecular cage has a key role to promote the pyranine transport inside of the cell. In addition, as we have previously mentioned, we also demonstrated that neither the cage **C** alone co-incubated with pyranine nor pyranine alone is able to enter the cellular cytosol (Figure 26B and C).

Once we showed the ability of $^{Tm}\boldsymbol{R}_4\mathbf{C}$ to deliver pyranine, we studied the intracellular transport of pyranine using the acetylated version of the peptide-cage hybrid ($^{Ac}\boldsymbol{R}_4\mathbf{C}$). Interestingly, we found that $^{Ac}\boldsymbol{R}_4\mathbf{C}$ is also able to deliver pyranine probe into the cytosol of both HeLa (Figure 39B) and Vero cells (Figure 39D). Moreover, as expected, we also showed that the acetylated peptide without the cage **C** ($^{Ac}\boldsymbol{R}_4$) does not promote intracellular delivery of pyranine inside cells (Figure 39C).

After discovering the ability of both $^{Tm}\boldsymbol{R_4}$**C** and $^{Ac}\boldsymbol{R_4}$**C** to promote intracellular delivery of pyranine. We hypothesized if $^{Ac}\boldsymbol{R_4}$**C** would be able to capture free pyranine previously dissolved in the cellular medium and internalize this probe inside of the cells. With this purpose, we decided to carry out the sequential addition of both components, the pyranine, and then the peptide. In this experiment, we first incubated Vero cells for ten minutes only with pyranine, and then we added dropwise the peptide-cage hybrid $^{Ac}\boldsymbol{R_4}$**C** to Vero cells in a final concentration of 10 µM followed by an incubation for 30 minutes at 37 ºC. Interestingly, we found that $^{Ac}\boldsymbol{R_4}$**C** is able to capture and to internalize pyranine dissolved in the extracellular medium (Figure 39D).

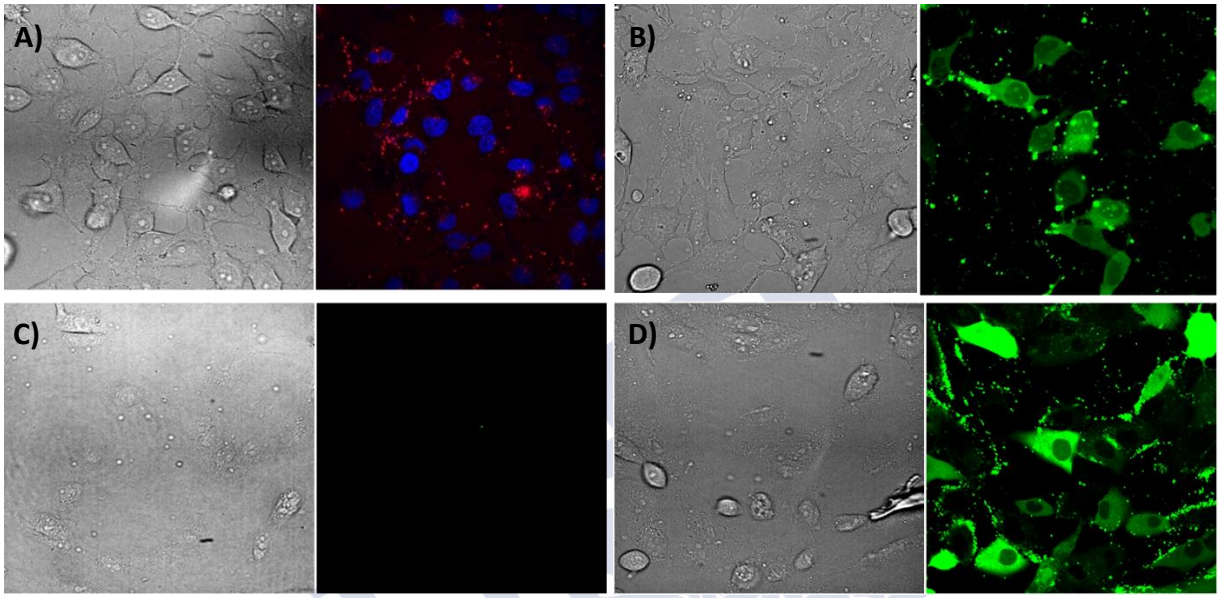

Figure 39. Experiments in HeLa (A and B) and Vero (C and D) cells. A) Confocal micrographs of HeLa cells incubated with $^{Tm}\boldsymbol{R_4}$ (5 µM) and Pyranine (5 µM). Nuclei were stained with Hoechst. DIC on the left and merge of fluorescence channels [Pyranine emission (green) + TAMRA emission (red) + Hoechst 33342 emission (blue)] on the right. B) Confocal micrographs of HeLa cells incubated with $^{Ac}\boldsymbol{R_4}$**C** (5 µM) and Pyranine (5 µM; green) for 30 min in HKR. C) Confocal micrographs of Vero cells incubated with Pyranine (10 µM, green) and $^{Ac}\boldsymbol{R_4}$ (10 µM) in HKR for 30 min. D) Sequential addition of pyranine and $^{Ac}\boldsymbol{R_4}$**C** to Vero cells. B, C, and D) DIC on the left and Pyranine emission (green) on the right.

6. Demonstration of cellular membrane integrity cytosolic delivery of pyranine

Once we showed that both $^{Ac}\boldsymbol{R_4}$**C** and $^{Tm}\boldsymbol{R_4}$**C** can promote the intracellular transport of pyranine with high efficiency and reproducibility, we decided to study the mechanism of transport of the supramolecular complex inside living cells. To this aim, we carried out two different experiments using nuclear staining agents to demonstrate membrane integrity during pyranine internalization and also competition experiments.

6.1.Membrane integrity by nuclear staining

First, we decided to demonstrate that the internalization of pyranine is not mediated by membrane permeabilization or by any cellular membrane damage. With this purpose, we carried out pyranine transport experiments but subsequently, we incubated the cells with two different dyes, DAPI or propidium iodide. Both dyes would produce nuclear staining in the case of membrane permeabilization. In the first experiment, we used DAPI (4',6-diamidino-2-phenylindole) which is a fluorescent probe with the ability to bind DNA. This dye will produce a blue (λ_{ex} = 405 nm and λ_{em} = 450/50 nm) nuclear fluorescence in the case of membrane permeabilization (Figure 40A). First, we carried out an initial experiment to ensure the ability of DAPI to detect cell membrane damage. In this experiment, we treated the cells with a membrane detergent (Triton X) to cause membrane damage. Then, we incubated these cells for 30 min with 2 µM DAPI to check the dye intensity in the cellular nucleus. As expected, intense blue nuclear fluorescence was detected in all the damaged cells (Figure 40B).

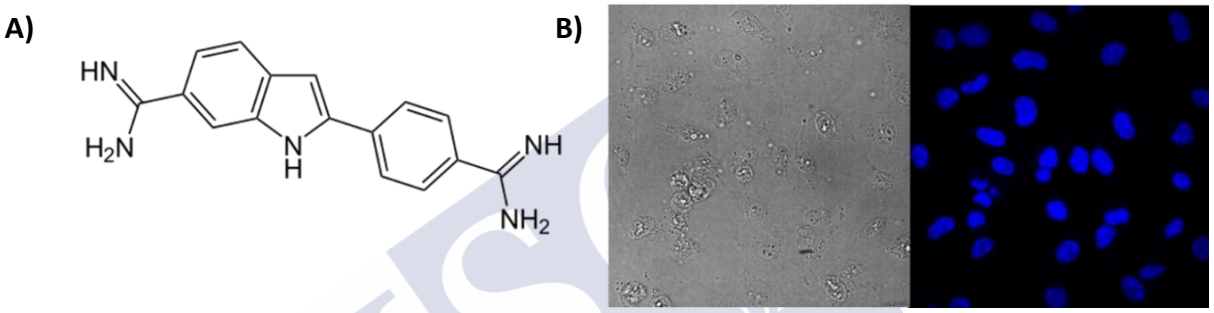

Figure 40. A) Chemical structure of DAPI, this dye produces nuclear staining in case of membrane damage. B) Confocal micrographs of membrane-damaged HeLa cells showing blue nuclear fluorescence of DAPI (2µM).

Once we demonstrated the ability of DAPI to detect cell membrane damage. We carried out the pyranine transport experiment where we incubated pyranine (5 µM) with $^{Tm}\boldsymbol{R_4}$**C** (5 µM) for 30 min with HeLa cells. Cells were washed with HKR buffer several times, and subsequently, we incubated the cells for 30 min with 2 µM DAPI to check membrane integrity. We evaluated the cells under confocal microscopy and no DAPI nuclear fluorescence in the cells loaded with pyranine was found (Figure 41). Therefore, this experiment indicated that there is not permeabilization of the cell membrane during pyranine transport.

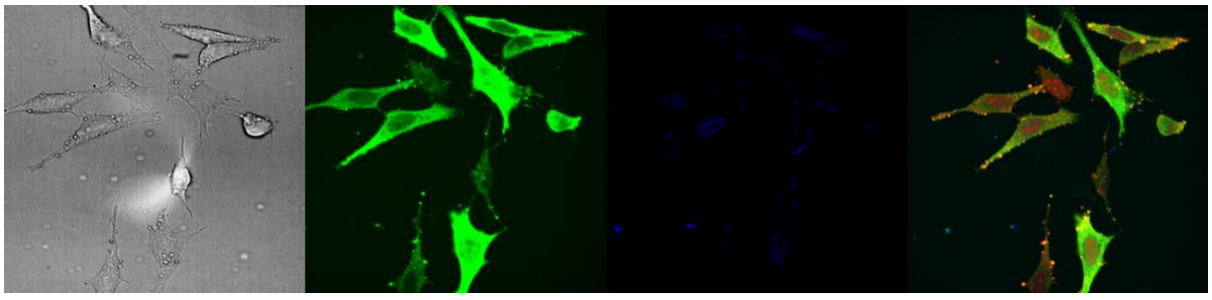

Figure 41. Demonstration of membrane integrity by DAPI in pyranine-loaded HeLa cells. Confocal micrographs of HeLa cells incubated with $^{Tm}\boldsymbol{R_4}$ (5 µM) and Pyranine (5 µM), followed by washes (3x) with HKR and, then, incubated with 2 µM DAPI. Left panel: BF; second panel: pyranine (green); third panel: DAPI (blue); right panel: merge of fluorescence channels [Pyranine emission (green) + TAMRA emission (red) + DAPI emission (blue)].

We then confirmed by propidium iodide the membrane integrity. This probe produces red (λ_{ex} = 493 nm and λ_{em} = 636 nm) nuclear staining in the case of membrane damage. In this experiment, we carried out a sequential addition of pyranine and $^{Ac}\boldsymbol{R_4}\mathbf{C}$ to Vero cells. First, cells were incubated for ten minutes with pyranine before the dropwise addition of $^{Ac}\boldsymbol{R_4}\mathbf{C}$ to a final concentration of 10 µM for 30 minutes at 37 ºC. Then, cells were washed with HKR several times and were incubated with propidium iodide for 10 minutes. This experiment also showed non-membrane permeabilization of pyranine-loaded cells. Interestingly, in Figure 42, we can compare a death cell with membrane damage which shows a red nucleus, with many healthy cells loaded with pyranine without fluorescence detected in the nucleus of cells.

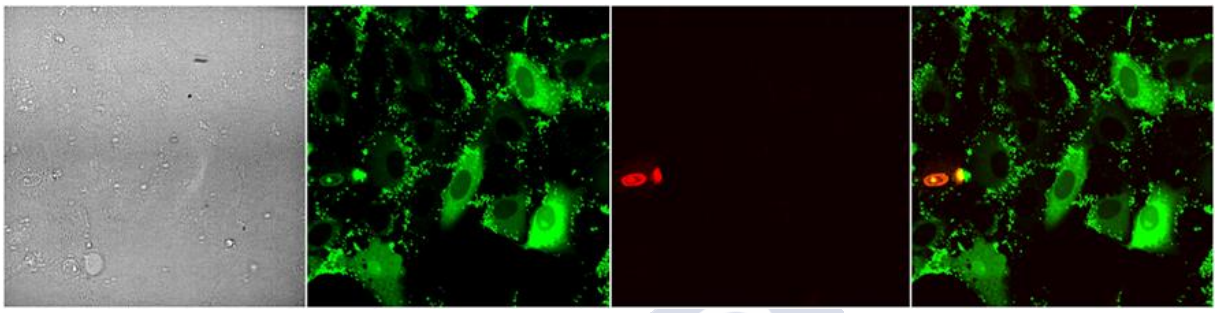

Figure 42. Demonstration of membrane integrity by propidium iodide in pyranine-loaded Vero cells. Confocal micrographs of Vero cells incubated with pyranine before the addition of $^{Ac}\boldsymbol{R_4}\mathbf{C}$ to a final concentration of 10 µM. Then, cells were washed with HKR and incubated with propidium iodide. Left panel: BF; second panel: pyranine (green); third panel: propidium iodide (red); right panel: merge of fluorescence channels [Pyranine emission (green) + Propidium iodide emission (red)].

6.2.Membrane integrity by competition assays

Subsequently, we wondered if the peptide-carrier system would be capable of selectively internalizing pyranine when co-incubated with other structurally-similar probes while maintaining the membrane integrity. With this purpose, we carried out competition experiments between pyranine and TAMRA mixed in the extracellular medium. First, we carried out two different internalization experiments with TAMRA alone and with $^{Ac}\boldsymbol{R_4}\mathbf{C}$ and TAMRA at low concentration (Figure 43). In these experiments, we demonstrated that TAMRA alone and in the presence of $^{Ac}\boldsymbol{R_4}\mathbf{C}$ is not able to cross the cell membrane (Figure 43). Moreover, we carried out a titration experiment by fluorescence to study the interaction between $^{Ac}\boldsymbol{R_4}\mathbf{C}$ and TAMRA and we found that this probe does not interact with $^{Ac}\boldsymbol{R_4}\mathbf{C}$ (Figure 43). Once we demonstrated that TAMRA alone and in the presence of $^{Ac}\boldsymbol{R_4}\mathbf{C}$ is not able to cross the plasma membrane and neither to interact with $^{Ac}\boldsymbol{R_4}\mathbf{C}$, we decided to carry out competition experiments using TAMRA and pyranine. Therefore, if the carrier would have a high preference for pyranine, it would selectively capture and would introduce only this probe inside cells (Figure 43).

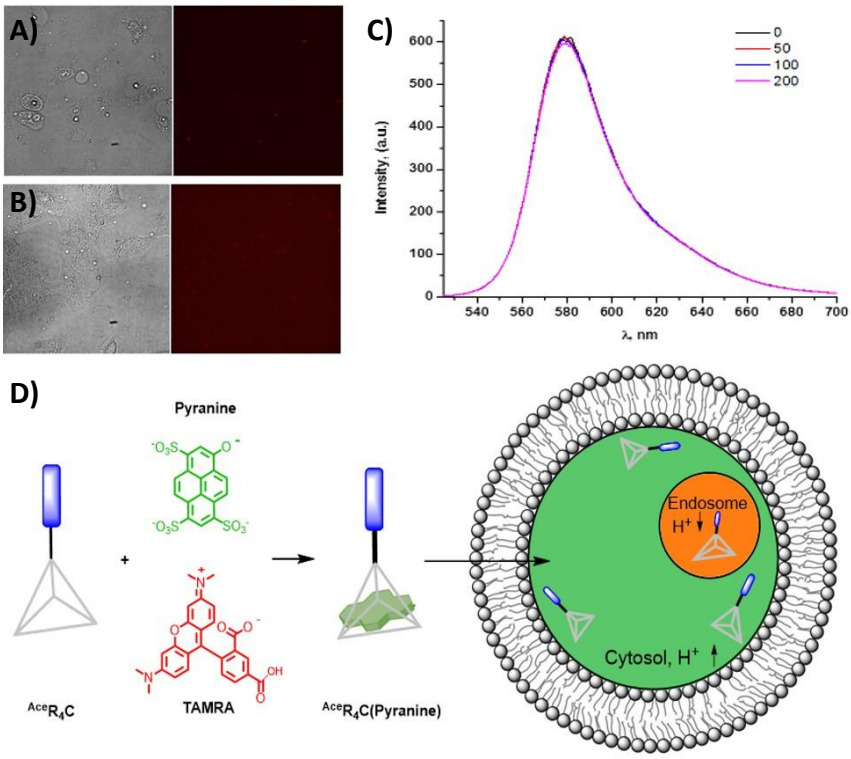

Figure 43. A and B) Confocal micrographs of Vero cells incubated in HKR buffer for 30 min at 37 ^{0}C with: A) only TAMRA (20 µM, red channel). B) ^{Ac}***R*$_4$C** (10 µM) in the presence of TAMRA (20 µM, red channel). Left panels correspond to DIC images. C) Fluorescence spectra of the titration of 30 nM TAMRA fluorophore with increasing equivalents (50, 100, and 200) of ^{Ac}***R*$_4$C**. No evidence of interaction could be found. D) Schematic representation of the competition experiment showing pyranine, TAMRA, and the peptide-cage carrier (^{Ac}***R*$_4$C**).

To carry out this experiment, we co-incubated Vero cells with ^{Ac}***R*$_4$C** (10 µM) and with pyranine and TAMRA (20 µM each) for 30 min (Figure 44). Importantly, we found the internalization of pyranine (green fluorescence) but not TAMRA uptake (red fluorescence). This experiment demonstrated the carrier selectivity for pyranine when co-incubated with other structurally-similar probe and the absence of membrane permeabilization.

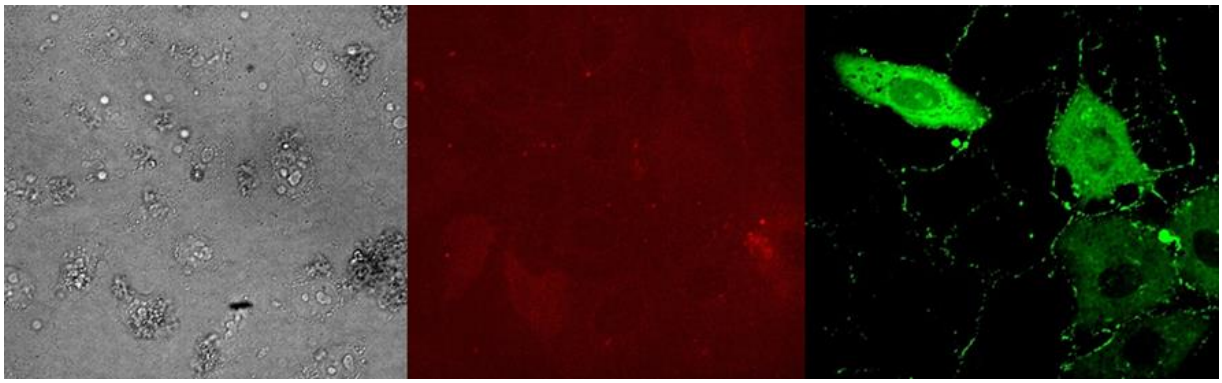

Figure 44. TAMRA competition experiments in Vero cells. Confocal micrographs of Vero cells incubated in HKR for 30 min at 37 ^{0}C with ^{Ac}***R*$_4$C** (10 µM) mixed with pyranine (20 µM, green) in the presence of TAMRA (20 µM, red). Left panel: BF; second panel: TAMRA (red); right panel: Pyranine emission (green).

7. Study of the mechanism of internalization using endocytosis inhibitors

Previous confocal microscopy experiments (Figure 38) showed that beyond the general cytosolic distribution of both pyranine and carrier, a fraction of the peptide-cage carrier was able to colocalize with the probe in the endosomes. Therefore, we hypothesized that the peptide-cage hybrid/pyranine complex was being internalized inside the cells following the endocytic pathway.

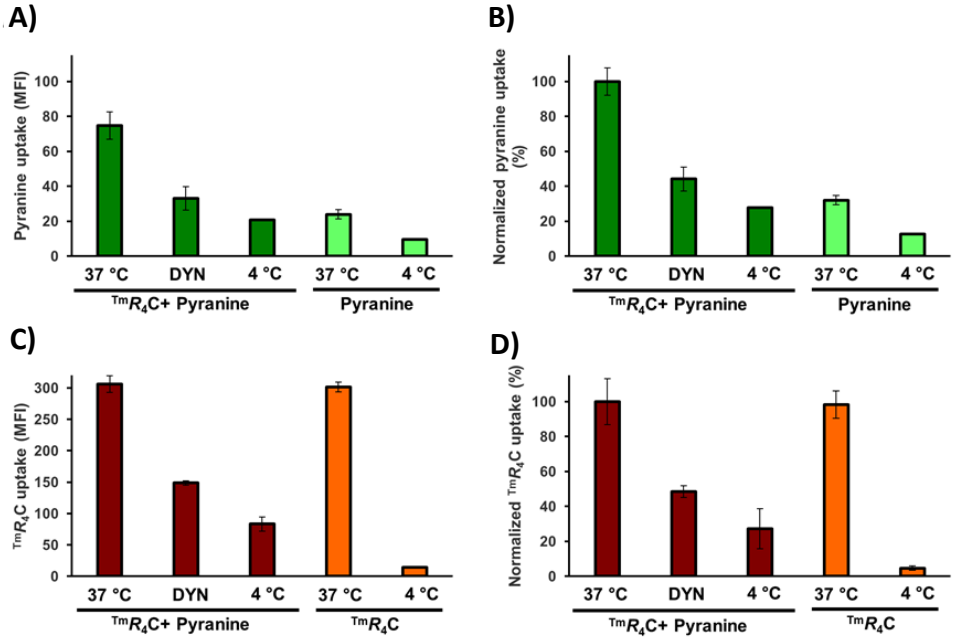

Figure 45. Quantification of the uptake of **$^{Tm}R_4$C** (15 µM) and pyranine (15 µM) in Vero cells under different conditions: 37 ºC (control), DYN (dynasore, 80 µM), and 4 ºC. A) and C) median fluorescence intensity (MFI) corresponding to pyranine fluorescence (A) or **$^{Tm}R_4$C** (C). B) and D) uptake normalized to the control of **$^{Tm}R_4$C** with pyranine incubated at 37 ºC, corresponding to pyranine (B) or **$^{Tm}R_4$C** (D). The last two bars in all charts indicate the uptake of pyranine (A, B) or **$^{Tm}R_4$C** (C, D) when incubated alone. Error bars indicate the SD of three replicates.

To investigate the mechanism of entry of the complex, we decided to perform cell transport experiments using endocytosis inhibitors. For this, we quantified the internalization of **$^{Tm}R_4$C** and pyranine by cell cytometry experiments in the presence of dynasore (DYN) endocytic inhibitor and at low temperature (Figure 45). The low-temperature experiments completely inhibit the energy-dependent uptake and dynasore is an inhibitor of macropinocytosis and all internalization pathways which depend on dynamin. Therefore, if the complex is entering inside the cells following the endocytic pathway, at low temperature and in the presence of dynasore, a reduction of the uptake of **$^{Tm}R_4$C** would be shown. To carry out this experiment, we incubated Vero cells with **$^{Tm}R_4$C** (15 µM) and pyranine (15 µM) and **$^{Tm}R_4$C** (15 µM) alone at low temperatures, with the dynasore inhibitor, and at 37ºC. Interestingly, we found a reduction of the uptake of **$^{Tm}R_4$C**, with or without pyranine, at low temperature (4ºC) and in the presence of dynasore (Figure 45). These results suggest that the internalization of the **$^{Tm}R_4$C** and the **$^{Tm}R_4$C/pyranine** complex is mediated by an energy-dependent endocytosis mechanism.

Based on all previous results, we propose that the complex is entering inside the cell by an endocytosis mechanism, followed by an escape from the endosomes and, then, reach the cell

cytosol. The nucleolar distribution of the peptide also confirmed that the peptide is capable to escape from the endosome (Figure 38). A similar internalization mechanism for the acetylated peptide can also be proposed based on the analogous results showed by this carrier.

8. Interaction and intracellular delivery of different anionic fluorophores

Once we delivered pyranine inside different cell lines using the designed peptide-cage carriers. We wondered if we would be able to internalize new fluorophores with similar structures to pyranine. We first studied the interaction between peptide-cage carriers $^{Ac}R_4C/^{Tm}R_4C$ and various anionic fluorophores with potential biological interest. First, we decided to study the ability of the peptide-cage carrier ($^{Ac}R_4C$) to interact with **carboxyfluorescein** (CF). With this purpose, we carried out titration experiments of this fluorophore with increasing concentrations of $^{Ac}R_4C$ in phosphate buffer at pH 7 (Figure 46). These experiments allowed the calculation of the dissociation constant K_d = 16.2 µM for $^{Ac}R_4C$. Interestingly, when labeled, $^{Tm}R_4C$ also reduced its affinity with pyranine K_d = 51.5 µM (Figure 54).

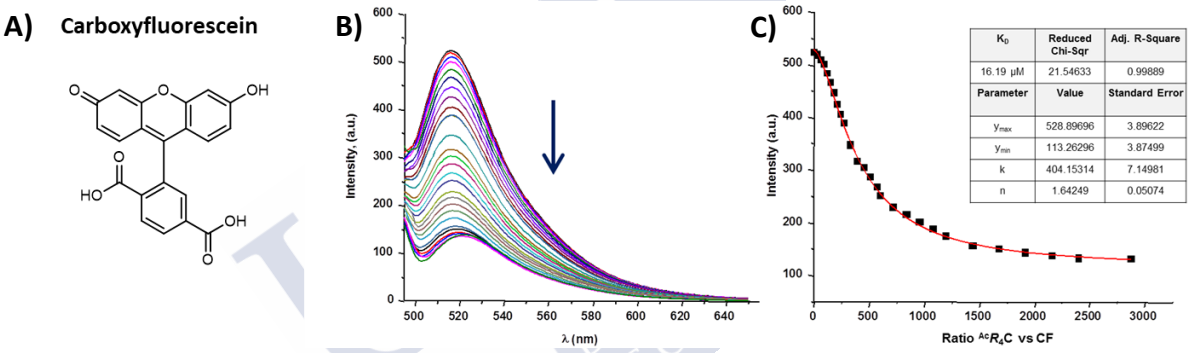

Figure 46. A) Chemical structure of carboxyfluorescein (CF). B) Fluorescence spectra of the titration of CF with $^{Ac}R_4C$ in phosphate buffer (pH 7). Arrow indicates the decrease of CF fluorescence with increasing amounts of the peptide. C) 516 nm fluorescence emission and curve fit for the titration of CF with $^{Ac}R_4C$ in phosphate buffer (pH 7). The best fit to the data using nonlinear analysis with Origin 8.5 to the Hill 1 equation.

Encouraged by the interaction between CF and $^{Ac}R_4C$, we decided to study the potential recognition of the peptide cage hybrid with different Alexa fluorophores. We carried out different titration studies with $^{Ac}R_4C$ and the different Alexa probes (Figure 47) and we found the interaction of $^{Ac}R_4C$ with all the probes with the following binding constants: K_d = 6 µM for Alexa Fluor 488, K_d = 1.37 µM for Alexa Fluor 546, and K_d = 9.5 µM for Alexa Fluor 568.

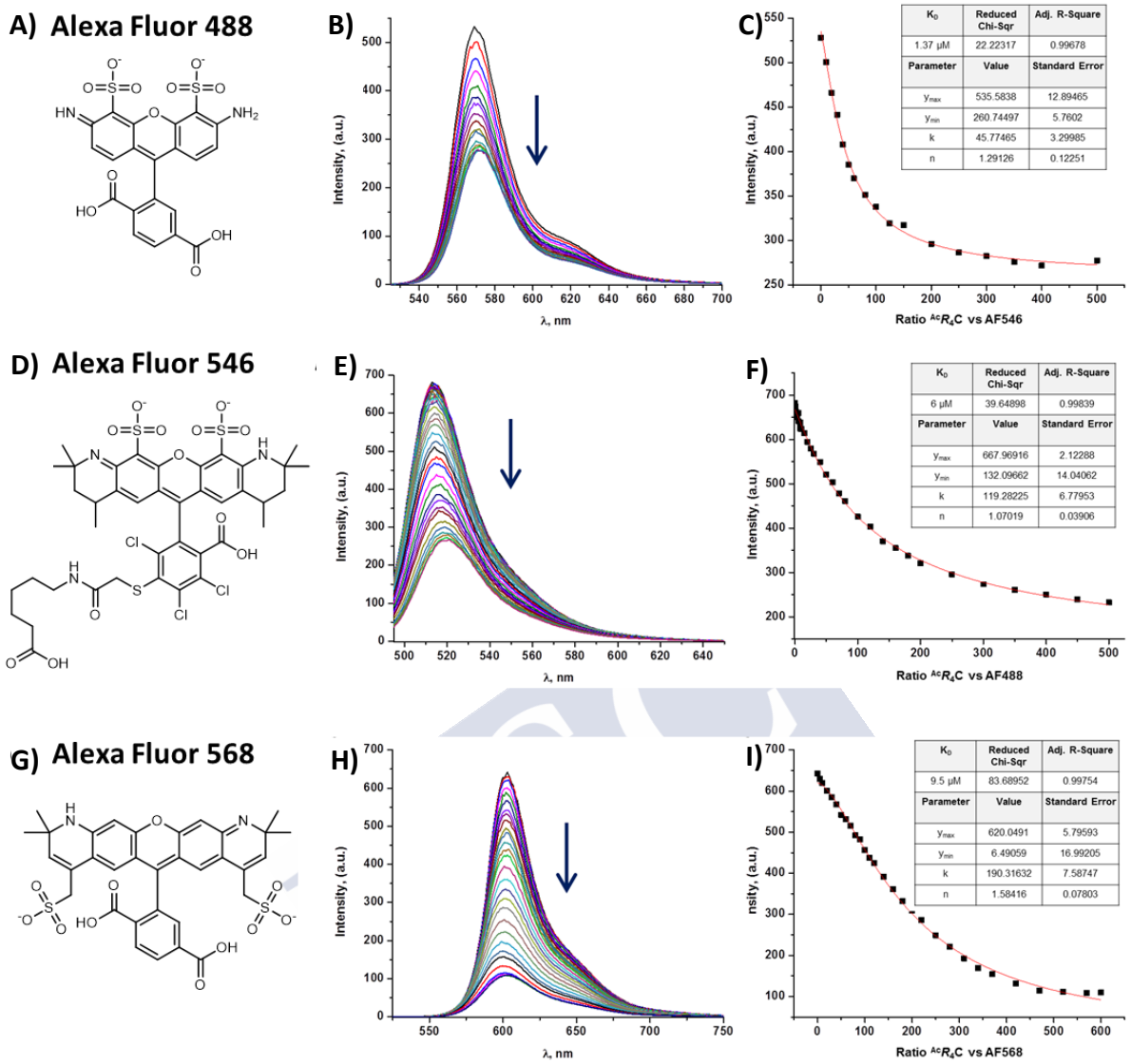

K_D	Reduced Chi-Sqr	Adj. R-Square
1.37 µM	22.22317	0.99678
Parameter	**Value**	**Standard Error**
y_{max}	535.5838	12.89465
y_{min}	260.74497	5.7602
k	45.77465	3.29985
n	1.29126	0.12251

K_D	Reduced Chi-Sqr	Adj. R-Square
6 µM	39.64898	0.99839
Parameter	**Value**	**Standard Error**
y_{max}	667.96916	2.12288
y_{min}	132.09662	14.04062
k	119.28225	6.77953
n	1.07019	0.03906

K_D	Reduced Chi-Sqr	Adj. R-Square
9.5 µM	83.68952	0.99754
Parameter	**Value**	**Standard Error**
y_{max}	620.0491	5.79593
y_{min}	6.49059	16.99205
k	190.31632	7.58747
n	1.58416	0.07803

Figure 47. A), D) and G): Chemical structure of Alexa Fluor 488, 546 and 568, respectively. B, E, and H: Fluorescence spectra of the titration of Alexa Fluor dyes with $^{Ac}\boldsymbol{R_4}$**C**. Arrows indicate the decrease of fluorophore emission with increasing amounts of $^{Ac}\boldsymbol{R_4}$**C**. C), F) and I) Fluorescence emission at the maximum of each fluorophore (513 nm for Alexa Fluor 488, 570 nm for Alexa Fluor 546 and 603 nm for Alexa Fluor 568), and curve fit for the titration with $^{Ac}\boldsymbol{R_4}$**C** in phosphate buffer (pH 7). B), C): Alexa Fluor 488; E), F): Alexa Fluor 546; H), I): Alexa Fluor 568. The best fit to the data using nonlinear analysis with Origin 8.5 to the Hill 1 equation.

Once we discovered that our peptide-cage carrier could encapsulate different anionic/planar fluorescent probes, we decided to use our innovative system to transport these membrane-impermeable fluorophores to the cell interior. First, we demonstrated that $^{Ac}\boldsymbol{R_4}$**C** can transport carboxyfluorescein in two different cell lines such as Vero cells (Figure 48) and HeLa cells (Figure 54). To confirm the potential delivery of the Alexa probes, we incubated Vero cells with the different conditions showed in Figure 48. In these experiments, we have shown that the cage-peptide carrier was able to efficiently deliver into the cytosol of the Vero cells the different Alexa Fluor dyes (Figure 48).

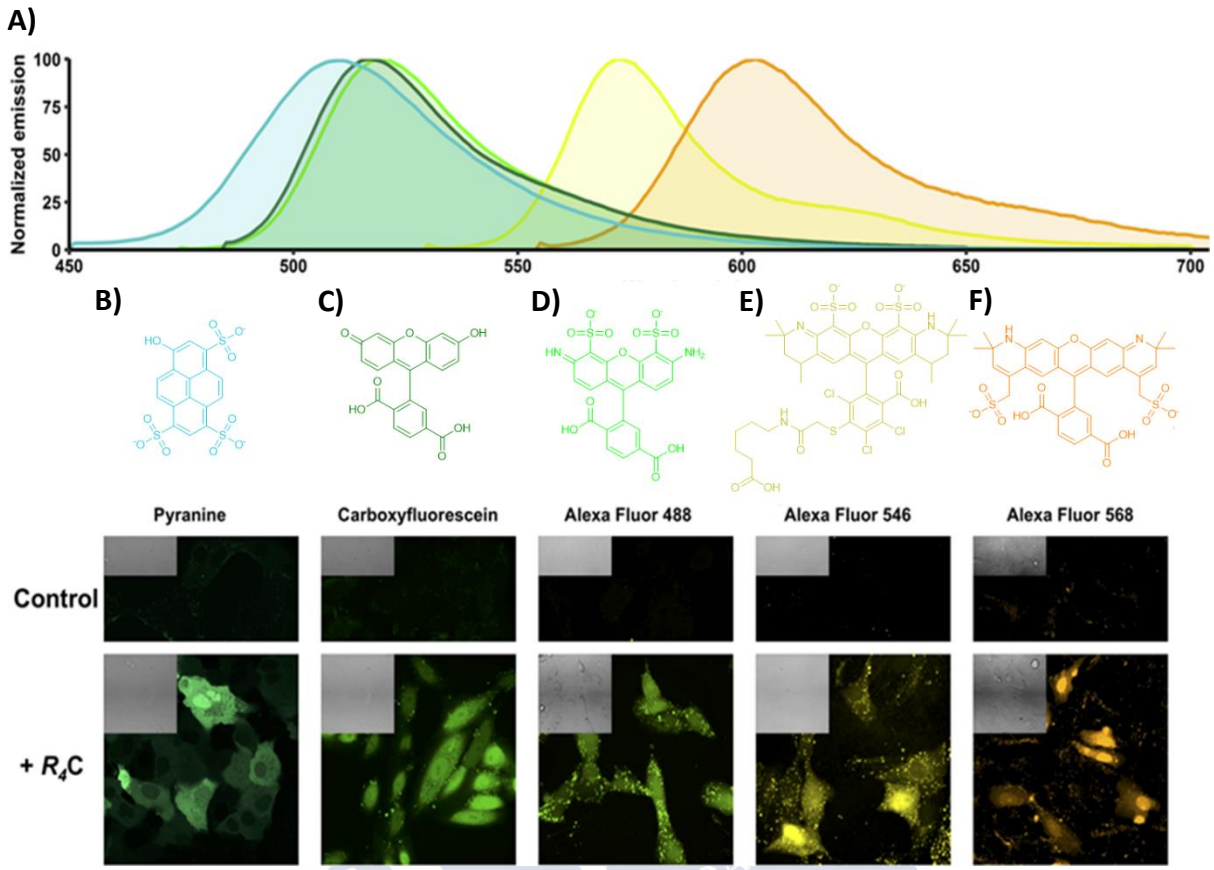

Figure 48. Transport experiments of different anionic fluorophores into Vero cells. A) Emission wavelengths of the different fluorophores. B) to F) Chemical structures and pseudocolored micrographs of Vero cells incubated with the different compounds showed for 30 min and diluted in HKR buffer. B) Pyranine (10 µM) and $^{Tm}\boldsymbol{R}_4\mathbf{C}$ (10 µM). C) CF (10 µM) and $^{Tm}\boldsymbol{R}_4\mathbf{C}$ (10 µM). D) Alexa Fluor 488 (20 µM) and $^{Tm}\boldsymbol{R}_4\mathbf{C}$ (10 µM). E) Alexa Fluor 546 (35 µM) and $^{Ac}\boldsymbol{R}_4\mathbf{C}$ (15 µM). F) Alexa Fluor 568 (25 µM) and $^{Ac}\boldsymbol{R}_4\mathbf{C}$ (15 µM). In all cases, control panels indicate the incubation of the cells with the same amount of dye in the absence of the different peptide-cage hybrid. Insets show DIC images. Excitation and emission wavelengths: pyranine, CF, Alexa Fluor 488: λ_{ex} = 488 nm, λ_{em} = 525/50 nm; Alexa Fluor 546, Alexa Fluor 568: λ_{ex} = 561 nm, λ_{em} = 620/20 nm.

9. pH tracking in living cells

After confirming the ability of peptide/cage hybrids to transport various anionic probes, we investigated the potential of pyranine as a pH-sensitive probe for intracellular ratiometric pH tracking. Pyranine has two ratiometric pH-dependent excitation maxima at 405 nm (protonated) and 450 nm (deprotonated).[240] Interestingly, this property will allow to distinguish the pH of the different cellular organelles.

As previously mentioned in the introduction, the current strategies to efficiently deliver pyranine inside cells such as physical methods have some limitations including cellular toxicity. Therefore, we decided to apply our methodology to carry out cellular pH tracking. For this, we incubated $^{Tm}\boldsymbol{R}_4\mathbf{C}$ (10 µM) and pyranine (10 µM) for 30 min with Vero cells. Interestingly, by just checking the acidic (λ_{exc} = 405 nm) and the basic (λ_{exc} = 488 nm) excitation wavelengths,

[240] C. C. Overly, K. D. Lee, E. Berthiaume, P. J. Hollenbeck, *Proc. Natl. Acad. Sci.* **1995**, *92*, 3156-3160.

we could easily distinguish between the acidic organelles (yellow channel) and the neutral pH of the cytosol (green channel) (Figure 49B and C, respectively).

To explore intracellular pH tracking, we decided to carry out the ratiometric analysis of delivered pyranine in Vero cells. First, we carried out the pH calibration in situ using nigericin-clamped cells (Figure 56 and Figure 57). This approach uses the ionophore nigericin, which exchanges K^+ for H^+ across membranes, in combination with high-potassium buffers of different pH. The high potassium concentration of the buffer outside the cell is assumed to be equal to the intracellular concentration, and under these circumstances, nigericin allows the free flow of protons across the cell membrane until the pH inside the cell is the same as in the buffer outside. After equilibration, images for the protonated (PyrH) and the deprotonated (Pyr-) forms of pyranine-loaded cells were taken by excitation with a 405 nm and a 488 nm lasers, respectively, collecting in both cases the emission at 500-550 nm. The ratio of Pyr-/PyrH pictures was calculated after background subtraction, and the median value per field was used to generate a calibration curve, which was employed to assign the pH values of the rest of the images (Figure 49D). Applying this methodology, we were able to distinguish the pH of different cellular entities such as the moderately acidic pH of the early endosomes (pH: 7.0), the more acidic pH of late endosomes (pH: 6.5), and the neutral pH of cytosol (pH: 7.5).

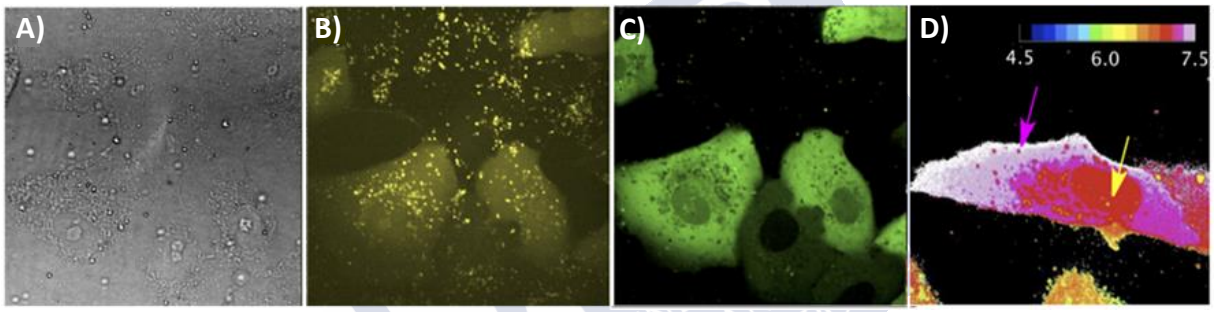

Figure 49. Intracellular pH tracking in Vero cells. Confocal micrographs of cells incubated for 30 min with pyranine (10 μM) and $^{Tm}\boldsymbol{R}_4\mathbf{C}$ (10 μM) in HKR buffer. A) DIC. B) Channel (λ_{ex} = 405 nm and λ_{em} = 525/50 nm) corresponding to the "protonated form" showing higher intensity in the endosomes. C) Channel (λ_{ex} = 488 nm and λ_{em} = 525/50 nm) corresponding to the "deprotonated form" showing higher intensity in the cytosol. D) Ratiometric image of Vero cells after cell calibration. The yellow arrow shows late endosomes and the purple arrow, early endosomes.

Conclusions

USC
UNIVERSIDADE
DE SANTIAGO
DE COMPOSTELA

In this chapter, we have demonstrated that the covalent attachment of a tetraarginine peptide to a membrane-impermeable supramolecular cage, which is capable to encapsulate different anionic/planar dyes, can be applied in the cytosolic delivery of different anionic fluorophores in different cell lines. Furthermore, we have shown that this efficient methodology can be used for ratiometric intracellular pH tracking using the pyranine probe.

In this first chapter,

- We were able to conjugate a membrane-impermeable supramolecular cationic cage with different cell-penetrating peptides of different lengths and we found that only $^{Ac}\boldsymbol{R}_4\mathbf{C}$/$^{Tm}\boldsymbol{R}_4\mathbf{C}$ showed good solubility, biocompatibility, and low cytotoxicity against Hela and Vero cells.
- The supramolecular cage of $^{Ac}\boldsymbol{R}_4\mathbf{C}$ and $^{Tm}\boldsymbol{R}_4\mathbf{C}$ encapsulated the pyranine probe (K_d = 189 nM and K_d = 12.6 µM, respectively**)** and we demonstrated that the peptide-cage hybrid ($^{Ac}\boldsymbol{R}_4\mathbf{C}$) acts as a molecular carrier by *in vitro U*-tube experiments.
- $^{Ac}\boldsymbol{R}_4\mathbf{C}$ and $^{Tm}\boldsymbol{R}_4\mathbf{C}$ were confirmed to deliver pyranine into the cellular cytosol of different cell lines, HeLa, and Vero cells.
- $^{Tm}\boldsymbol{R}_4\mathbf{C}$ was able to specifically transport pyranine and not TAMRA by competition assays. Energy-dependent endocytosis was confirmed as a mechanism of transport inside the cells. The integrity of the cellular membrane was confirmed in the pyranine transport.
- $^{Ac}\boldsymbol{R}_4\mathbf{C}$ showed interaction with the different anionic probes such as carboxyfluorescein and different Alexa probes, which were efficiently transported inside living cells.
- Finally, the developed strategy allowed ratiometric intracellular pH tracking using the pyranine probe.

USC
UNIVERSIDADE
DE SANTIAGO
DE COMPOSTELA

Experimental section

USC
UNIVERSIDADE
DE SANTIAGO
DE COMPOSTELA

1. Chemical structures

A) ^{Tm}A

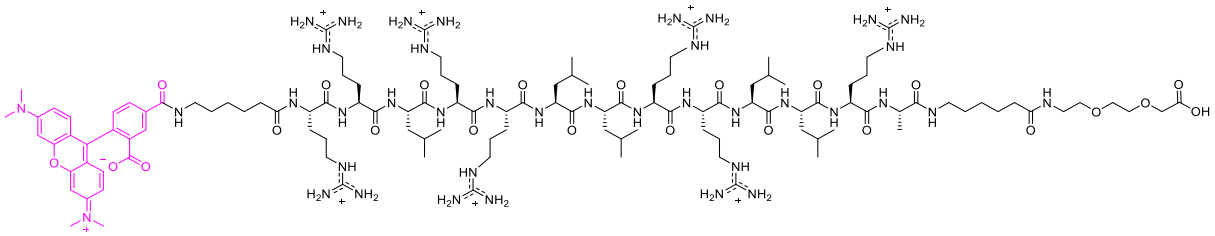

B) $^{Tm}R_8$

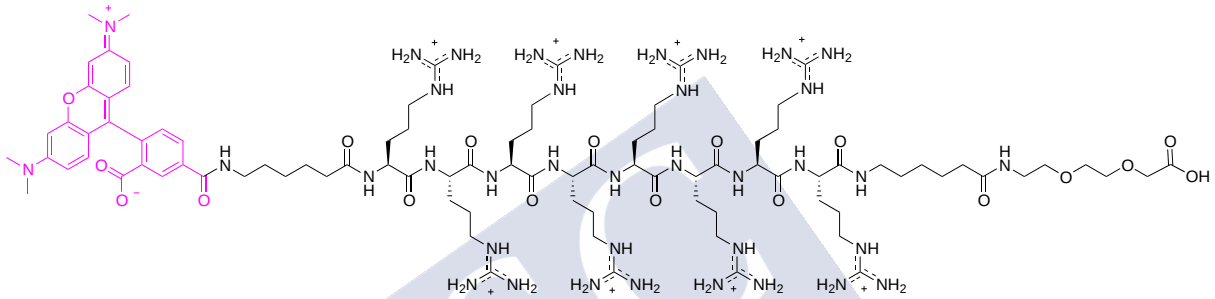

C) $^{Tm}R_4$

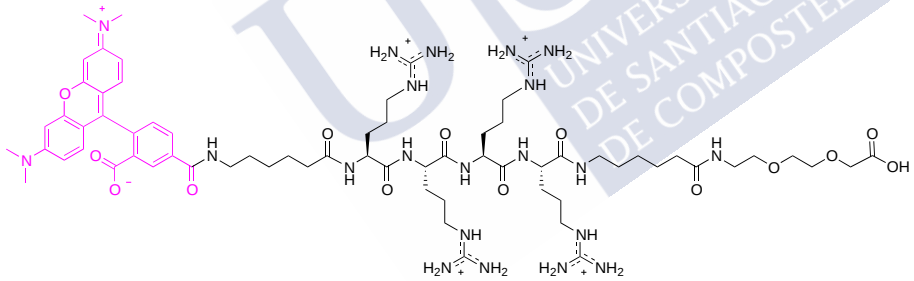

D) $^{Ac}R_4$

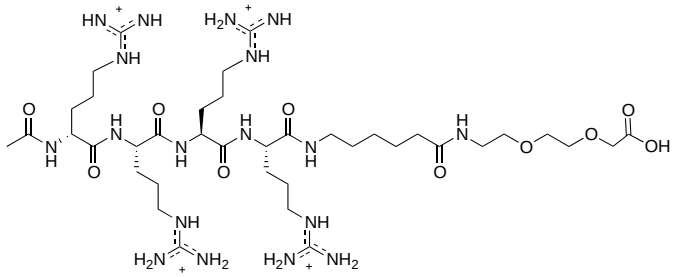

Figure 50. Chemical structures of the peptides A) ^{Tm}**A**, B) ^{Tm}***R*$_8$**, C) ^{Tm}***R*$_4$**, D) ^{Ac}***R*$_4$**.

A) ^{Tm}**AC**

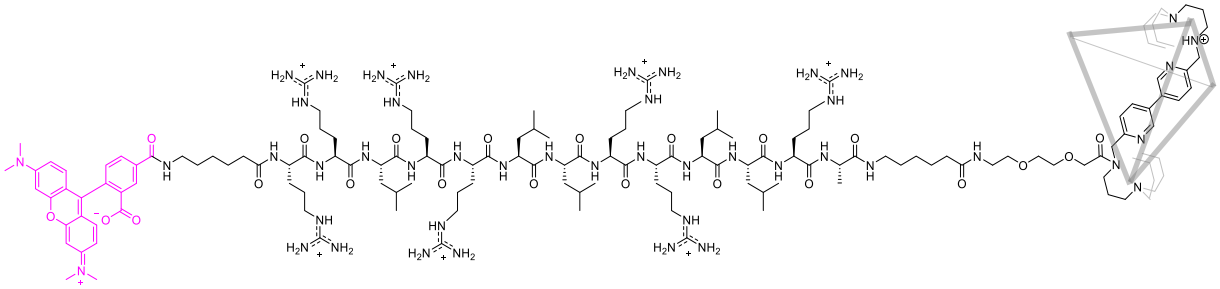

B) ^{Tm}***R*$_8$C**

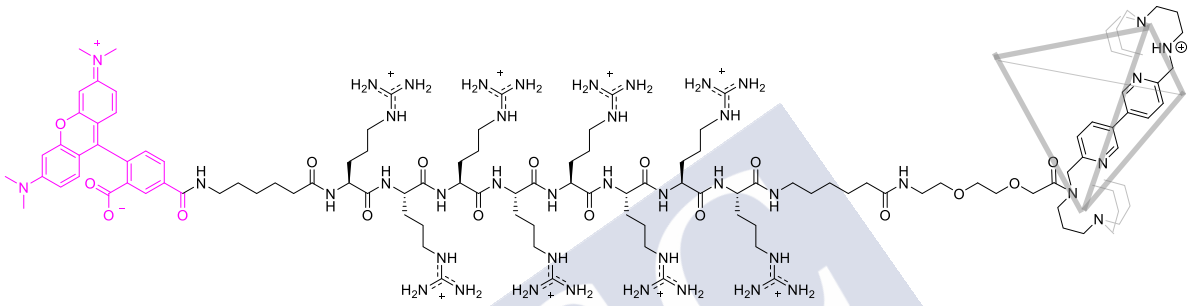

C) ^{Tm}***R*$_4$C**

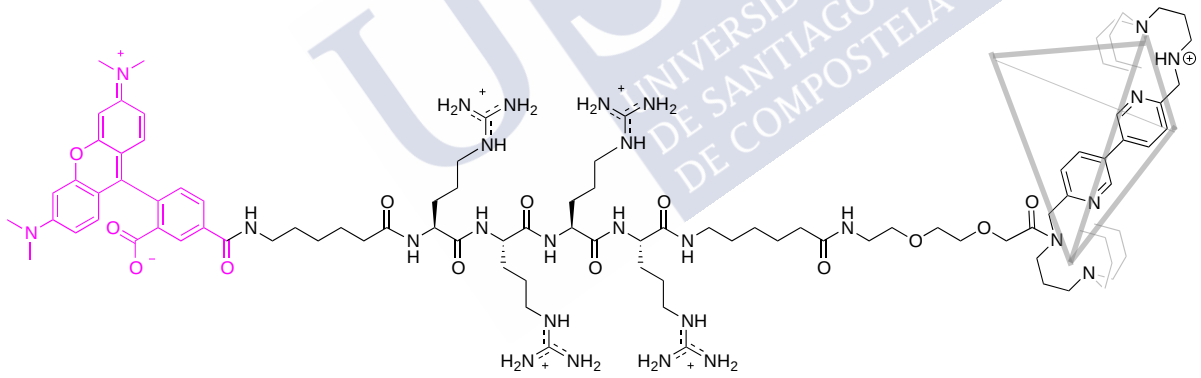

D) ^{Ac}***R*$_4$C**

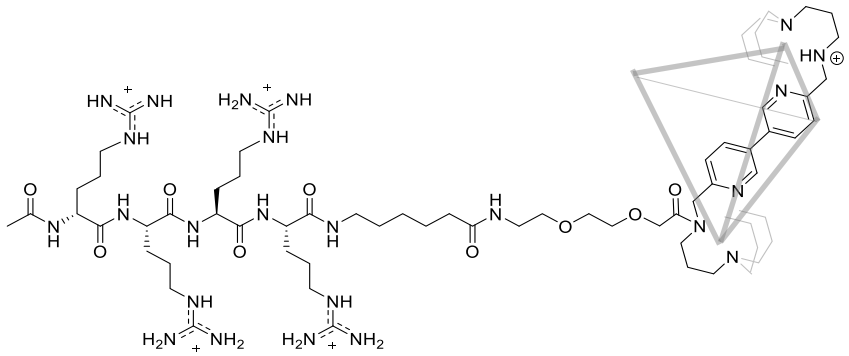

Figure 51. Chemical structures of the peptide-cage hybrids A) ^{Tm}**AC**, B) ^{Tm}***R*$_8$C**, C) ^{Tm}***R*$_4$C**, D) ^{Ac}***R*$_4$C**.

2. Figures

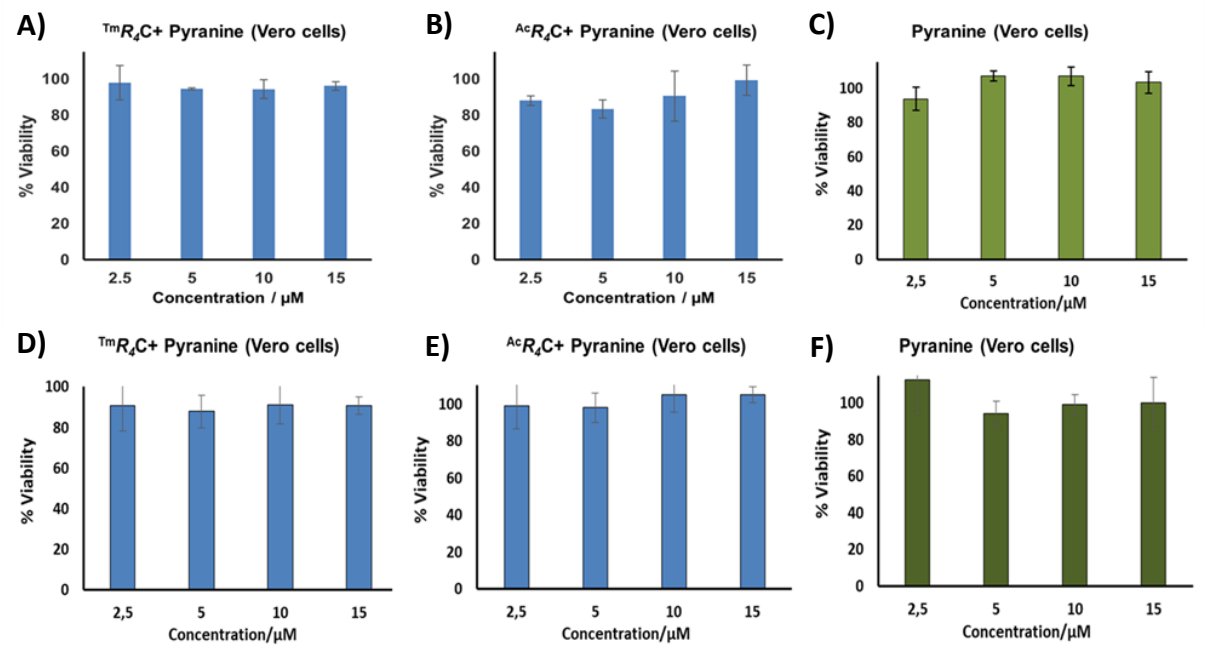

Figure 52. Viability assay in Vero cells with pyranine co-incubated in HKR with $^{Tm}\boldsymbol{R_4C}$ (A, D) or $^{Ac}\boldsymbol{R_4C}$ (B, E) and only pyranine (C, F) at different concentrations after 1 hour incubation time (A, B, C) and after 24 hours incubation time (D, E, F) at 37 ºC. Error bars represent the standard deviation of four replicates.

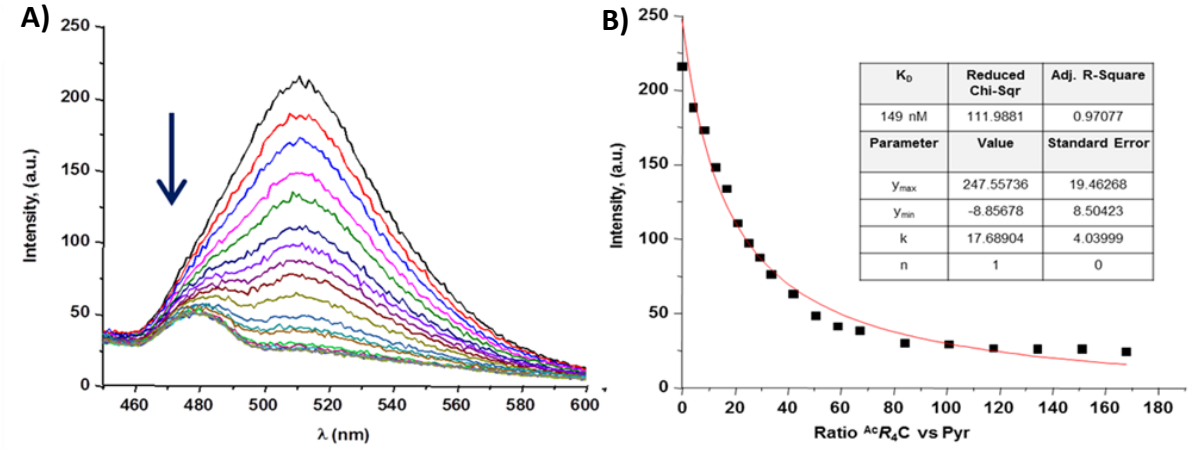

Figure 53. A) Fluorescence titration of pyranine with the peptide/cage $^{Ac}\boldsymbol{R_4C}$ in phosphate buffer (pH 7). Arrow indicates the decrease of pyranine fluorescence with increasing amounts of the peptide. B) 510 nm fluorescence emission and curve fit for the titration of pyranine with $^{Ac}\boldsymbol{R_4C}$ in phosphate buffer pH 7. The best fit to the data using nonlinear analysis with Origin 8.5 to the Hill 1 equation. In B, fitting was done with a fixed value of n = 1, and K_d for $^{Ac}\boldsymbol{R_4C}$ under these conditions was 149 nM. The small peak observed in A) at about 480 nm at the higher concentrations of peptide corresponds to the Raman scattering of water for an excitation wavelength of 415 nm.

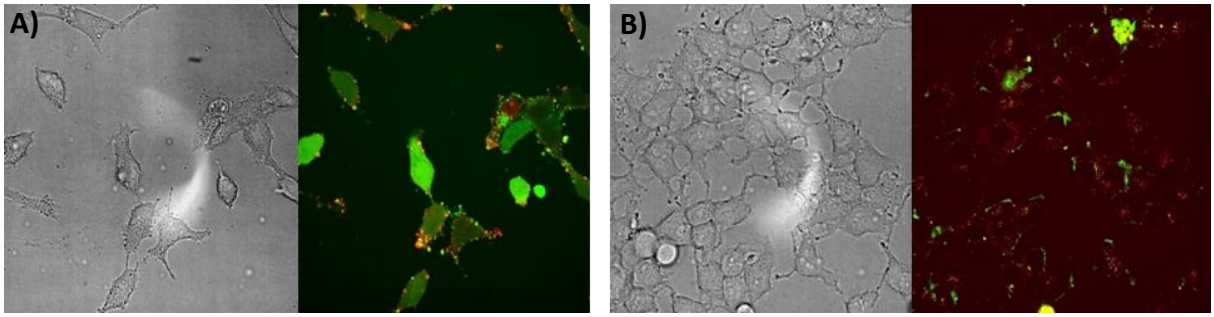

Figure 54. Transport experiments of Carboxyfluorescein (CF) in HeLa cells. Confocal micrographs of HeLa cells incubated with: A) $^{Tm}\boldsymbol{R_4}$**C** (5 µM) and Carboxyfluorescein (5 µM). B) $^{Tm}\boldsymbol{R_4}$ (5 µM) and Carboxyfluorescein (5 µM). DIC on the left and merge channels [Carboxyfluorescein emission (green) + Tm emission (red)] on the right. HeLa cells were incubated with the different components in the HKR buffer for 30 min at 37 ºC. The cells were finally washed (HKR buffer, 3x) and then observed under the confocal microscope.

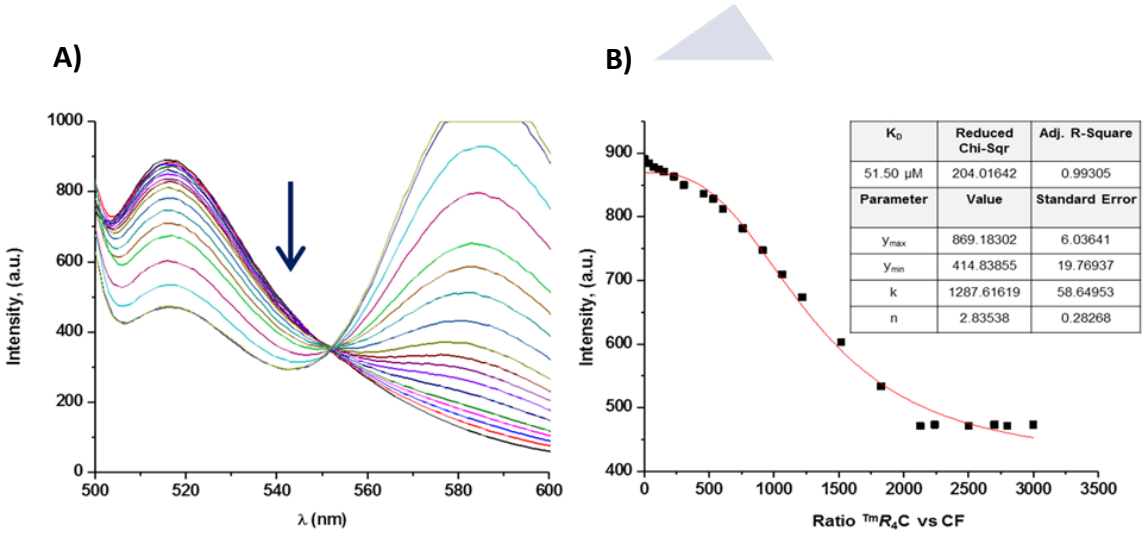

Figure 55**.** A) Fluorescence spectra of the titration of CF with $^{Tm}\boldsymbol{R_4}$**C** in phosphate buffer (pH 7). Arrow indicates the decrease of CF fluorescence with increasing amounts of the peptide. The right peak in C corresponds to the TAMRA emission from $^{Tm}\boldsymbol{R_4}$**C**. B) 516 nm fluorescence emission and curve fit for the titration of CF with $^{Tm}\boldsymbol{R_4}$**C** in phosphate buffer (pH 7). The best fit to the data using nonlinear analysis with Origin 8.5 to the Hill 1 equation.

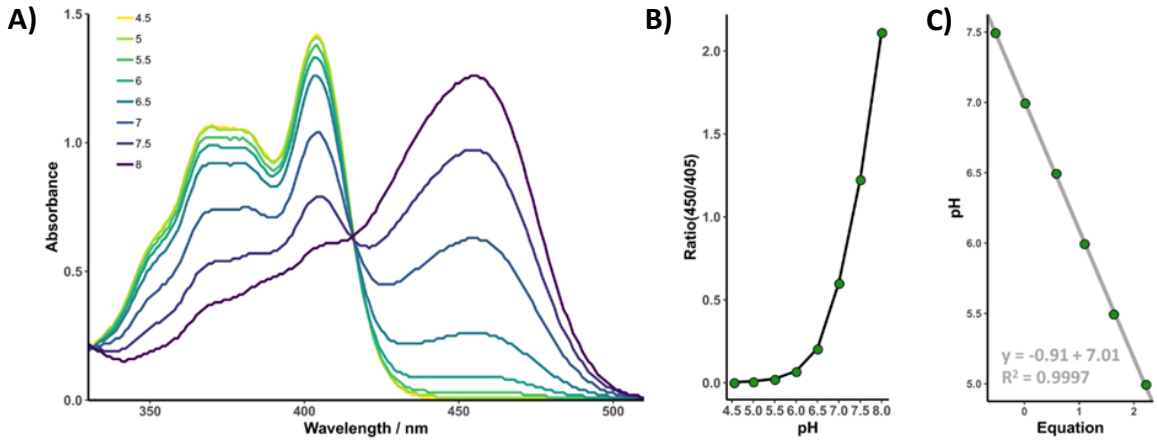

Figure 56. A) Absorption spectra of pyranine in buffers of different pH. B) The ratio of the absorbance at 450 and 405 nm plotted as a function of pH. C) Ratiometric method for determining the pK_a. pK_a = 7.01.

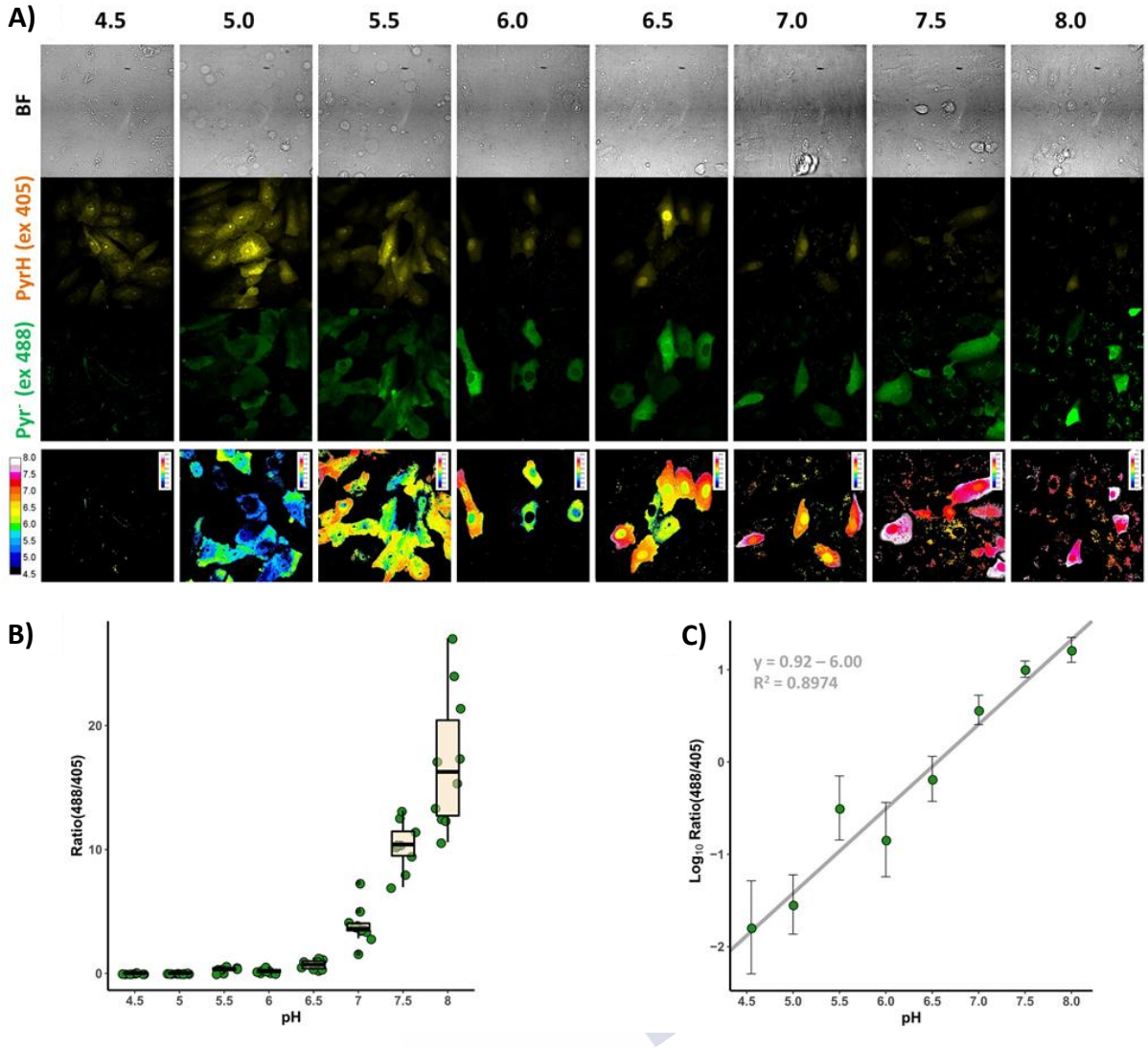

Figure 57. pH studies in Vero cells. A) Ratiometric imaging after pH clamping with nigericin of Vero cells incubated with 10 µM pyranine and 10 µM **$^{Tm}R_4$C**. The top row (BF) shows bright-field images. The second (PyrH) and third (Pyr^-) rows show the emission of pyranine after excitation at 405 nm or 488 nm, respectively. Finally, the bottom row shows the processed images. B) Mean ratio values were obtained for each field and plotted against pH. Box and whisker plot of each dataset, green points represent individual observations. C) Logarithmic conversion of the previous data and linear fit. Error bars indicate SD.

3. Materials and methods

Chemicals were purchased from Carbosynth, Iris Biotech, Sigma Aldrich, Alfa Aesar, Stream Chemicals, and Novabiochem and used without further purification.

Commercially available 2-Chlorotrityl chloride resin, Fmoc-Ahx-OH, Fmoc-O2Oc-OH, Fmoc-*L*-Ala-OH, Fmoc-*L*-Leu-OH, Fmoc-*L*-Arg(pbf)-OH, triisopropylsilane (TIS), Disopropylethyl amine (DIEA), Nigericin and 8-Hydroxypyrene-1,3,6-trisulfonic acid trisodium salt (pyranine) were obtained from Sigma-Aldrich. MTT and MES (2-(N-morpholino)ethanesulfonic acid) were purchased from Alfa Aesar; 5(6)-Carboxyfluorescein (CF) and 5-Carboxytetramethyl rhodamine (TAMRA) were available from Carbosynth. L-α-phosphatidylglycerol (Egg, Chicken) (sodium salt) was purchased from Avanti Polar Lipids and *N*-HATU from Glentham life sciences. *N*-HBTU was obtained from Iris. Hoechst 33342 Trihydrochloride Trihydrate, Alexa Fluor dyes (488, 546 and 594), and Dulbecco's Modified Eagle's Medium (4500 mg/L glucose, L-glutamine, sodium pyruvate, and sodium bicarbonate) were purchased in ThermoFisher. HEPES [4-(2-hydroxyethyl)-1-piperazineethanesulfonic acid)] was purchased from TCI Chemicals.

The solvents for organic synthesis were of reagent grade. Dry solvents were bought from Sigma-Aldrich. *N, N*-dimethylformamide, and trifluoroacetic acid were purchased from Scharlau, dichloromethane from Panreac, and acetonitrile from Merck. Water was deionized and purified on a Millipore Milli-Q Integral system.

The removal of solvents under reduced pressure was carried out on a rotary evaporator Büchi R-210 equipped with a thermostated bath B-491, a vacuum regulator V-850, and a vacuum pump V-700.

Purification of products was accomplished using reversed-phase high-performance liquid chromatography (RP-HPLC) using an Agilent Technologies 1160 Infinity using H_2O (+ 0.1% TFA) and CH_3CN (+ 0.1% TFA) as eluents and a Luna (C18)-Phenomenex column and on Jasco LC-4000 with an Agilent Eclipse XDB-C18 column.

High-performance liquid chromatography coupled with mass spectrometry (HPLC-MS) analyses were carried out on Agilent Technologies 1260 Infinity II associated with a 6120 Quadrupole LC-MS using an Agilent SB-C18 column or on DIONEX Ultimate 3000 U-HPLC$^+$ (Thermo Scientific) with an Acclaim RSLC 120-C18 column with *Solvent A: Solvent B* gradients between 5:95 (*Solvent A*: H_2O with 0.1% TFA; *Solvent B*: CH_3CN with 0.1% TFA).

Fluorescence measurements were performed using a Varian Cary Eclipse fluorometer and UV-Vis spectra were measured in an Agilent 8453 UV-Vis diode-array spectrophotometer or a Biochrom Libra S60 UV-vis spectrophotometer.

For taking confocal microscopy images a Dragonfly confocal spinning-disk system mounted on a Nikon Eclipse Ti-E equipped with an Andor Zyla 4.2 PLUS sCMOS digital camera was used. The 3D reconstructions were obtained from the different individual confocal planes with Imaris bitplane 9.0.0 software.

A Tecan Infinite F200Pro microplate reader was used to measure directly in Costar cell culture 96-well plates UV-Vis absorbance for the MTT viability assays.

Flow cytometry was performed on a Guava easyCyte^{TM} cytometer. Data analysis was performed with InCyte software included in GuavaSoft 3.2 (Millipore).

The "U-tubes" were house-made.

4. General protocol for synthetic procedures

Peptides ^{Tm}**A**, ^{Tm}***R*$_8$**, ^{Tm}***R*$_4$**, and ^{Ac}***R*$_4$** were synthesized according to classic SPPS of peptides and further details are given below. The cage **C** was prepared and purified following the procedure reported in literature.[69,241]

4.1. Synthesis and characterization of the peptides ^{Tm}A, ^{Tm}*R*$_8$, ^{Tm}*R*$_4$ and ^{Ac}*R*$_4$

All peptides were synthesized by manual Fmoc solid-phase peptide synthesis on a 2-Chlorotrityl chloride resin (1.14 mmol/g). The first coupling was performed in CH_2Cl_2 using DIEA as base whereas for the following couplings *N*-HBTU as the activator, DIEA as the base, and DMF as solvent were used. The deprotection of the temporal Fmoc protecting group was performed by treating the resin with 20% piperidine in DMF. 5(6)-carboxytetramethylrhodamine (TAMRA) was coupled using 3 equivalents (0.15 mmol, 64.5 mg), 3 equivalents of *N*-HATU, and 5 equivalents of DIEA 0.2 M in DMF for 60 min. Acetylation of the N-terminal group of ^{Ac}***R*$_4$** was performed by standard Fmoc removal conditions (20% piperidine in DMF) followed by treatment with a solution of acetic anhydride and 2,6- lutidine (1:1, 2 mL) for 30 min.

The cleavage/deprotection step was performed by treatment of the resin-bound peptide for 2 h with the following cleavage cocktail: 900 µL TFA, 50 µL CH_2Cl_2, 25 µL H_2O and 25 µL TIS (1 mL of cocktail/40 mg resin) and peptides were precipitated in Et_2O.

4.1.1. Synthesis and characterization of peptide ^{Tm}A

The synthesis of the peptide ^{Tm}**A** (TAMRA-Ahx-R-R-L-R-R-L-L-R-R-L-L-R-A-Ahx-O2Oc-OH) was performed following the above methodology. ^{Tm}**A** was obtained after RP-HPLC purification [Phenomenex Luna C18(2) 100A column, H_2O (0.1% TFA)/ CH_3CN (0.1% TFA) 95:5→5:95 (5→35 min)] with an overall yield of 12%. R_t 8.0 min [RP-HPLC Agilent SB-C18 column, H_2O (0.1% TFA)/ CH_3CN (0.1% TFA) 95:5→5:95 (0→12 min)] (Figure 58). MS (ESI, H_2O) m/z: calcd for $C_{118}H_{204}N_{39}O_{23}$ $[M+5H]^{5+}$: 507.3, found: 507.5; calcd for $C_{118}H_{203}N_{39}O_{23}$ $[M+4H]^{4+}$: 633.9, found 634.0; calcd for $C_{120}H_{203}N_{39}O_{25}F_3$ $[M+3H+TFA]^{3+}$: 882.9, found: 883.0; calcd for $C_{122}H_{204}N_{39}O_{27}F_6$ $[M+3H+2TFA]^{3+}$: 920.9, found: 920.9; calcd for $C_{122}H_{203}N_{39}O_{27}F_6$ $[M+2H+2TFA]^{2+}$: 1380.8, found: 1380.7.

[69] J. Mosquera, S. Zarra, J. R. Nitschke, *Angew. Chem. Int. Ed.* **2014**, *53*, 1556-1559.
[241] J. Rodríguez, J. Mosquera, J. R. Couceiro, J. R. Nitschke, M. E. Vázquez, J. L. Mascareñas, *J. Am. Chem. Soc.* **2017**, *139*, 55-58.

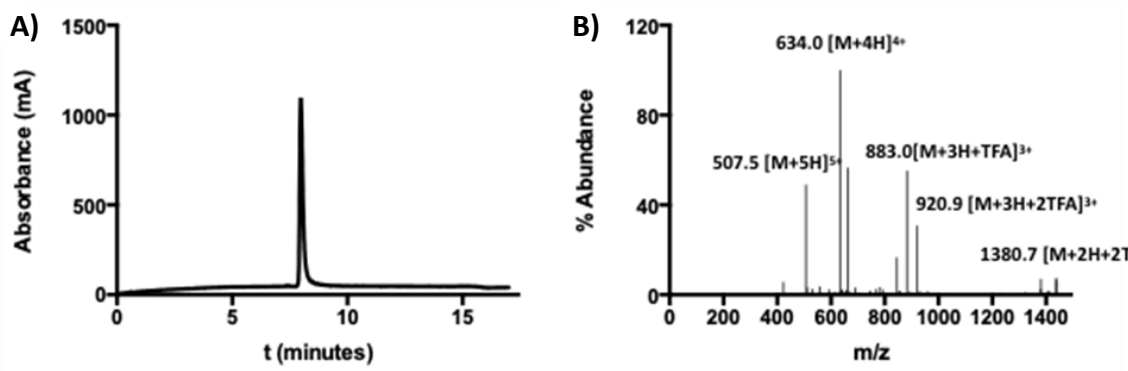

Figure 58. Representation of the HPLC-MS for ^{Tm}**A**. A) HPLC chromatogram (λ_{abs} = 550 nm) of ^{Tm}**A** and B) ESI-MS recorded at 8.0 min of ^{Tm}**A**.

4.1.2. Synthesis and characterization of peptide $^{Tm}R_8$

The synthesis of the peptide $^{Tm}R_8$ (TAMRA-Ahx-R-R-R-R-R-R-R-R-Ahx-O2Oc-OH) was performed following the above methodology. $^{Tm}R_8$ was obtained after RP-HPLC purification [Phenomenex Luna C18(2) 100A column, H_2O (0.1% TFA)/ CH_3CN (0.1% TFA) 95:5→5:95 (5→35 min)] with an overall yield of 12%. R_t 10.9 min [RP-HPLC Agilent SB-C18 column, H_2O (0.1% TFA)/ CH_3CN (0.1% TFA) 75:5→5:75 (0→21 min)] (Figure 59). MS (ESI, H_2O) m/z: calcd for $C_{91}H_{156}N_{37}O_{18}$ $[M+5H]^{5+}$: 411.0, found: 411.3; calcd for $C_{93}H_{156}N_{37}O_{20}F_3$ $[M+4H+TFA]^{4+}$: 542.1, found: 542.3; calcd for $C_{93}H_{155}N_{37}O_{20}F_3$ $[M+3H+TFA]^{3+}$: 722.4, found: 722.9; calcd for $C_{95}H_{156}N_{37}O_{22}F_6$ $[M+3H+2TFA]^{3+}$: 760.4, found: 760.6; calcd for $C_{97}H_{156}N_{37}O_{24}F_9$ $[M+2H+3TFA]^{2+}$: 1197.1, found: 1197.6.

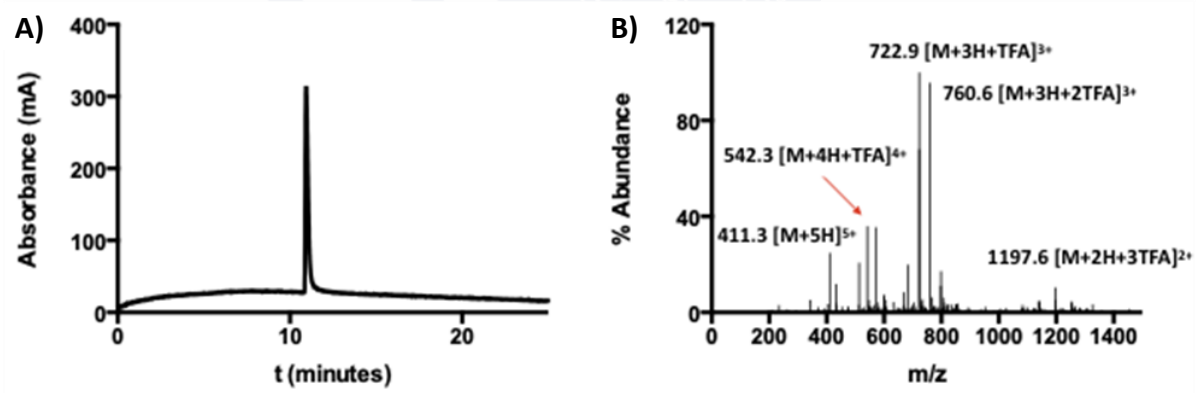

Figure 59. Representation of the HPLC-MS for $^{Tm}R_8$. A) HPLC chromatogram (λ_{abs} = 550 nm) of $^{Tm}R_8$ and B) ESI-MS recorded at 10.9 min of $^{Tm}R_8$.

4.1.3. Synthesis and characterization of peptide $^{Tm}R_4$

The synthesis of the peptide $^{Tm}R_4$ (TAMRA-Ahx-R-R-R-R-Ahx-O2Oc-OH) was performed following the above methodology. $^{Tm}R_4$ was obtained after RP-HPLC purification [Phenomenex Luna C18(2) 100A column, H_2O (0.1% TFA)/ CH_3CN (0.1% TFA) 95:5→5:95 (5→35 min)] with an overall yield of 12%. R_t 11.1 min [RP-HPLC Agilent SB-C18 column, H_2O (0.1% TFA)/ CH_3CN (0.1% TFA) 75:5→5:75 (0→21 min)] (Figure 60). MS (ESI, H_2O)

m/z: calcd for $C_{67}H_{107}N_{21}O_{14}$ $[M+4H]^{4+}$: 357.5, found: 357.8; calcd for $C_{67}H_{106}N_{21}O_{14}$ $[M+3H]^{3+}$: 476.3, found: 476.5; calcd for $C_{67}H_{105}N_{21}O_{14}$ $[M+2H]^{2+}$: 713.9, found: 714.0.

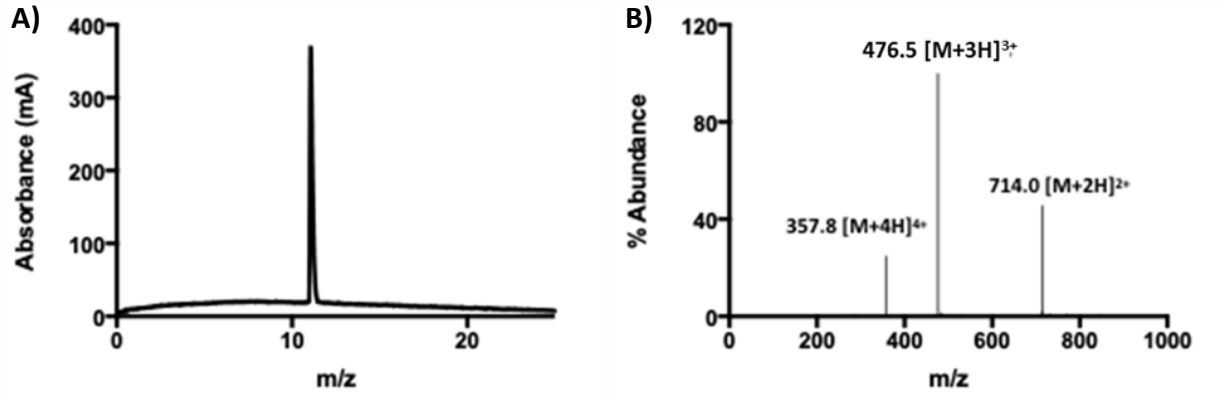

Figure 60. Representation of the HPLC-MS for $^{Tm}\boldsymbol{R_4}$. A) HPLC chromatogram (λ_{abs} = 550 nm) of $^{Tm}\boldsymbol{R_4}$ and B) ESI-MS recorded at 11.1 min of $^{Tm}\boldsymbol{R_4}$.

4.1.4. Synthesis and characterization of peptide $^{Ac}\boldsymbol{R_4}$

The synthesis of the peptide $^{Ac}\boldsymbol{R_4}$ (Ac-R-R-R-R-Ahx-O2Oc-OH) was performed following the above methodology. $^{Ac}\boldsymbol{R_4}$ was obtained after RP-HPLC purification [Phenomenex Luna C18(2) 100A column, H_2O (0.1% TFA)/ CH_3CN (0.1% TFA) 95:5→5:95 (0→5 min)] with an overall yield of 12%. R_t 2.9 min [RP-HPLC Agilent SB-C18 column, H_2O (0.1% TFA)/ CH_3CN (0.1% TFA) 95:5→5:95 (0→5 min)] (Figure 61). MS (ESI, H_2O) m/z: calcd for $C_{38}H_{77}N_{18}O_{10}$ $[M+3H]^{3+}$: 315.2, found: 315.3; calcd for $C_{38}H_{76}N_{18}O_{10}$ $[M+2H]^{2+}$: 472.3, found: 472.4; calcd for $C_{38}H_{75}N_{18}O_{10}$ $[M+H]^{+}$: 943.6, found: 943.6; calcd for $C_{40}H_{77}N_{18}O_{12}F_3$ $[M+2H+TFA]^{2+}$: 529.3, found: 529.4.

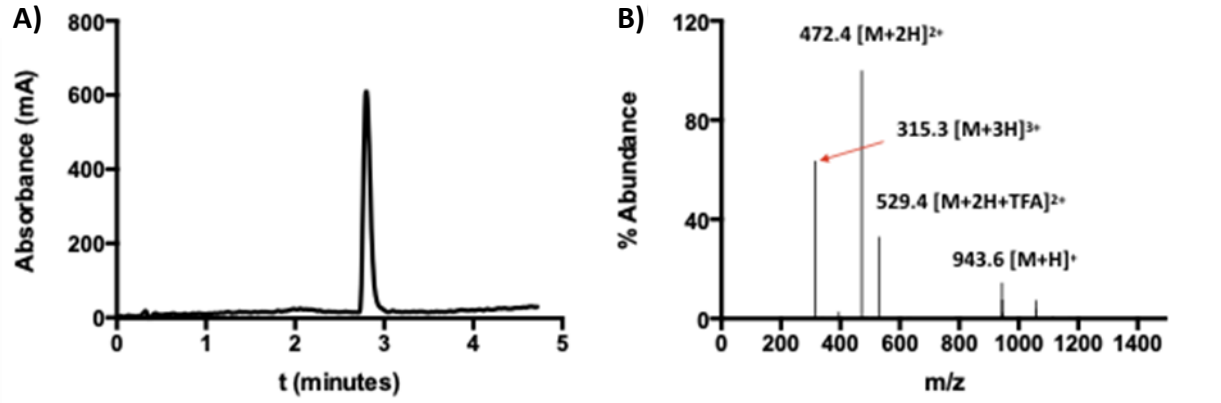

Figure 61. Representation of the HPLC-MS for $^{Ac}\boldsymbol{R_4}$ A) HPLC chromatogram (λ_{abs} = 222 nm) of $^{Ac}\boldsymbol{R_4}$ and B) ESI-MS recorded at 2.9 min of $^{Ac}\boldsymbol{R_4}$.

4.2. Synthesis and characterization of the peptides ^{Tm}AC, ^{Tm}*R*$_8$C, ^{Tm}*R*$_4$C, and ^{Ac}*R*$_4$C

For the synthesis of the supramolecular carriers the ^{Tm}**A**, ^{Tm}***R*$_8$**, ^{Tm}***R*$_4$**, and ^{Ac}***R*$_4$** peptides were solved in DMF (0.1 mM, 100 µL) before *N*-HATU (1 equiv) and DIEA (10 equiv) were added to the solution. This solution was added to a 0.1 mM solution of the cage **C**, adding 1 equiv of the peptide to 1 equiv of **C**, and the reaction mixture was left stirring overnight.

4.2.1. Synthesis and characterization of peptide ^{Tm}AC

^{Tm}**A** was solved in 100 µL of DMF (10 mg, 0.004 mM) before *N*-HATU (6 mg, 0.016 mmol, 4 equiv) and DIEA (6.91 µL, 0.040 mmol, 10 equiv) were added to the solution of the cage **C** in 164 µL of DMF (7.3 mg, 0.004 mmol, 1 equiv). The reaction was left stirring overnight and the resulting reaction mixture was purified by RP-HPLC [Phenomenex Luna C18(2) 100A column, H_2O (0.1% TFA)/ CH_3CN (0.1% TFA) 85:15→55:45 (30 min)]. ^{Tm}**AC** was obtained after sample lyophilization as a purple solid (2 mg, 12 %). R_t 18.7 min (Figure 62). MS (ESI, H_2O) m/z: calcd for $C_{234}H_{356}N_{67}O_{32}F_{12}$ $[M+7H+4TFA+2H_2O]^{7+}$: 692.4, found: 690.9 $[M+7H+4TFA+2H_2O]^{+7}$; calcd for $C_{230}H_{356}N_{67}O_{29}F_6$ $[M+7H+2TFA+3H_2O]^{7+}$:662.4, found: 662.4.

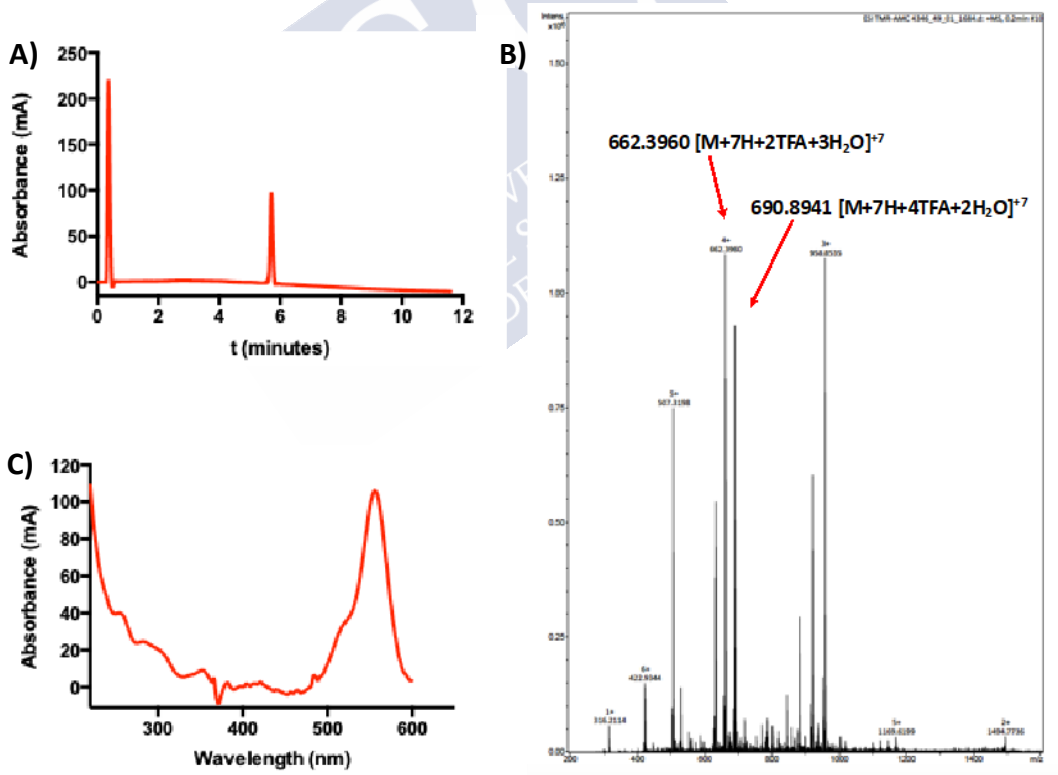

Figure 62. Representation of the HPLC-MS for ^{Tm}**AC**. A) HPLC chromatogram (λ_{abs} = 550 nm) of ^{Tm}**AC** and B) ESI-MS recorded at 5.73 min of ^{Tm}**AC**. C) UV-Vis spectrum at 5.73 minutes corresponding to ^{Tm}**AC**.

4.2.2. Synthesis and characterization of peptide $^{Tm}R_8C$

$^{Tm}R_8$ was solved in 100 µL of DMF (10 mg, 0.005 mM) before *N*-HATU (7.4 mg, 0.019 mmol, 4 equiv) and DIEA (8.5 µL, 0.05 mmol, 10 equiv) were added to the solution of the cage **C** in 225 µL of DMF (9.0 mg, 0.005 mmol, 1 equiv). The reaction was left stirring overnight and the resulting reaction mixture was purified by RP-HPLC.$^{Tm}R_8C$ was obtained after RP-HPLC purification [Phenomenex Luna C18(2) 100A column, H_2O (0.1% TFA)/ CH_3CN (0.1% TFA) 85:15→55:45 (30 min)] with an overall yield of 13% (2.5 mg). R_t 14.3 min (Figure 63). MS (ESI, H_2O) m/z: calcd for $C_{201}H_{310}N_{65}O_{22}F_3$ $[M+10H+TFA+3H_2O]^{10+}$: 404.5, found: 404.0 $[M+10H+TFA+3H_2O]^{+10}$; calcd for $C_{201}H_{308}N_{65}O_{22}F_3$ $[M+8H+TFA+3H_2O]^{8+}$: 505.4, found: 504.8; calcd for $C_{201}H_{306}N_{65}O_{22}F_3$ $[M+6H+TFA+3H_2O]^{6+}$: 673.6, found: 672.7; calcd for $C_{203}H_{300}N_{65}O_{21}F_6Na$ $[M+5H+2TFA+Na]^{5+}$: 824.7, found: 824.7.

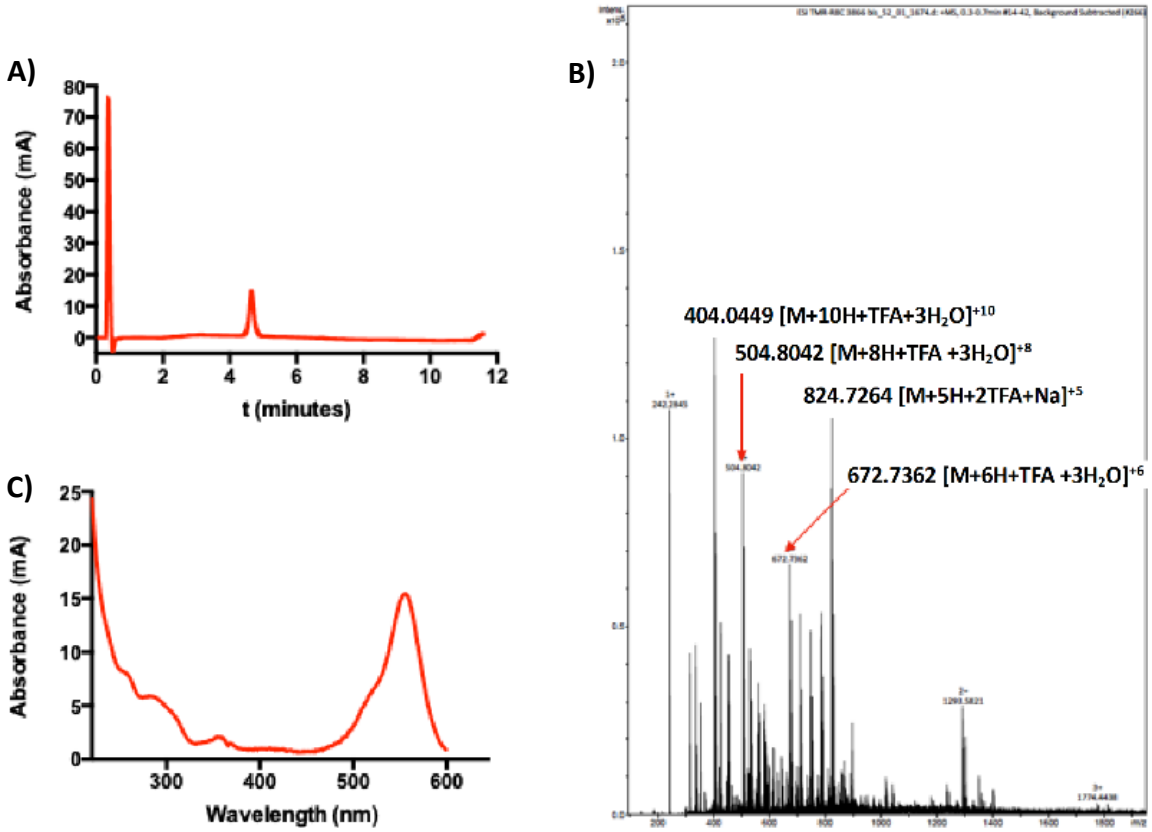

Figure 63. Representation of the HPLC-MS for $^{Tm}R_8C$ A) HPLC chromatogram (λ_{abs} = 550 nm) of $^{Tm}R_8C$ and B) ESI-MS recorded at 4.65 min of $^{Tm}R_8C$. C) UV-Vis spectrum at 4.65 minutes corresponding to $^{Tm}R_8C$.

4.2.3. Synthesis and characterization of peptide $^{Tm}R_4C$

$^{Tm}R_4$ was solved in 100 µL of DMF (12.9 mg, 0.007 mM) before *N*-HATU (10.7 mg, 0.028 mmol, 4 equiv) and DIEA (12.3 µL, 0.07 mmol, 10 equiv) were added to the solution of the cage **C** in 368 µL of DMF (9.0 mg, 0.005 mmol, 1 equiv). The reaction was left stirring overnight and the resulting reaction mixture was purified by RP-HPLC.$^{Tm}R_4C$ was obtained after RP-HPLC purification [Phenomenex Luna C18(2) 100A column, H_2O (0.1% TFA)/ CH_3CN (0.1% TFA) 85:15→55:45 (30 min)] with an overall yield of 13% (2.5 mg). R_t 11.9

min (Figure 64). MS (ESI, H_2O) m/z: calcd for $C_{175}H_{249}N_{49}O_{13}$ $[M+4H]^{4+}$: 811.5, found: 812.4; calcd for $C_{179}H_{259}N_{49}O_{18}F_6$ $[M+10H+2TFA+H_2O]^{10+}$: 349.8, found: 349.7; calcd for $C_{183}H_{259}N_{49}O_{22}F_{12}$ $[M+8H+4TFA+H_2O]^{8+}$: 465.5, found: 465.3.

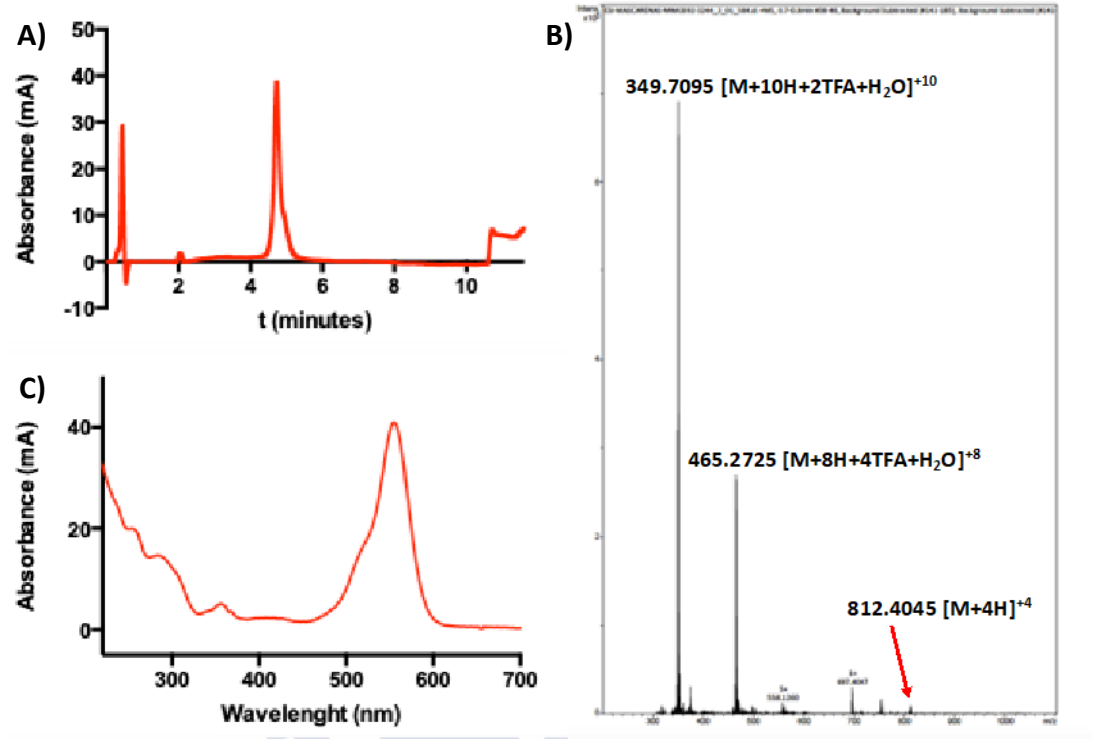

Figure 64. HPLC-MS spectra of $^{Tm}\boldsymbol{R_4}$**C**, A) chromatogram observed for λ=550 nm, B) ESI-MS spectrum corresponding to t = 4.73 minutes which corresponds to $^{Tm}\boldsymbol{R_4}$**C**, and C) UV-Vis spectrum at 4.73 minutes corresponding to $^{Tm}\boldsymbol{R_4}$**C**.

4.2.4. Synthesis and characterization of peptide $^{Ac}\boldsymbol{R_4}$C

$^{Ac}\boldsymbol{R_4}$ was solved in 100 µL of DMF (10.3 mg, 0.011 mM) before *N*-HATU (4 mg, 0.011 mmol, 1 equiv) and DIEA (14.1 µL, 0.109 mmol, 10 equiv) were added to the solution of the cage **C** in 368 µL of DMF (20 mg, 0.011 mmol, 1 equiv). The reaction was left stirring overnight and the resulting reaction mixture was purified by RP-HPLC. $^{Ac}\boldsymbol{R_4}$**C** was obtained after RP-HPLC purification [Luna C18(2) 100A column, H_2O (0.1% TFA)/ CH_3CN (0.1% TFA) 85:15→55:45 (30 min)] with an overall yield of 10% (3.1 mg). R_t 10.5 min (Figure 65). MS (ESI, H_2O) m/z: calcd for $C_{152}H_{227}N_{46}O_{15}F_9$ $[M+8H+3TFA]^{8+}$: 388.6, found: 387.5; calcd for $C_{154}H_{225}N_{46}O_{17}F_{12}$ $[M+5H+4TFA]^{5+}$: 644.0, found: 645.1.

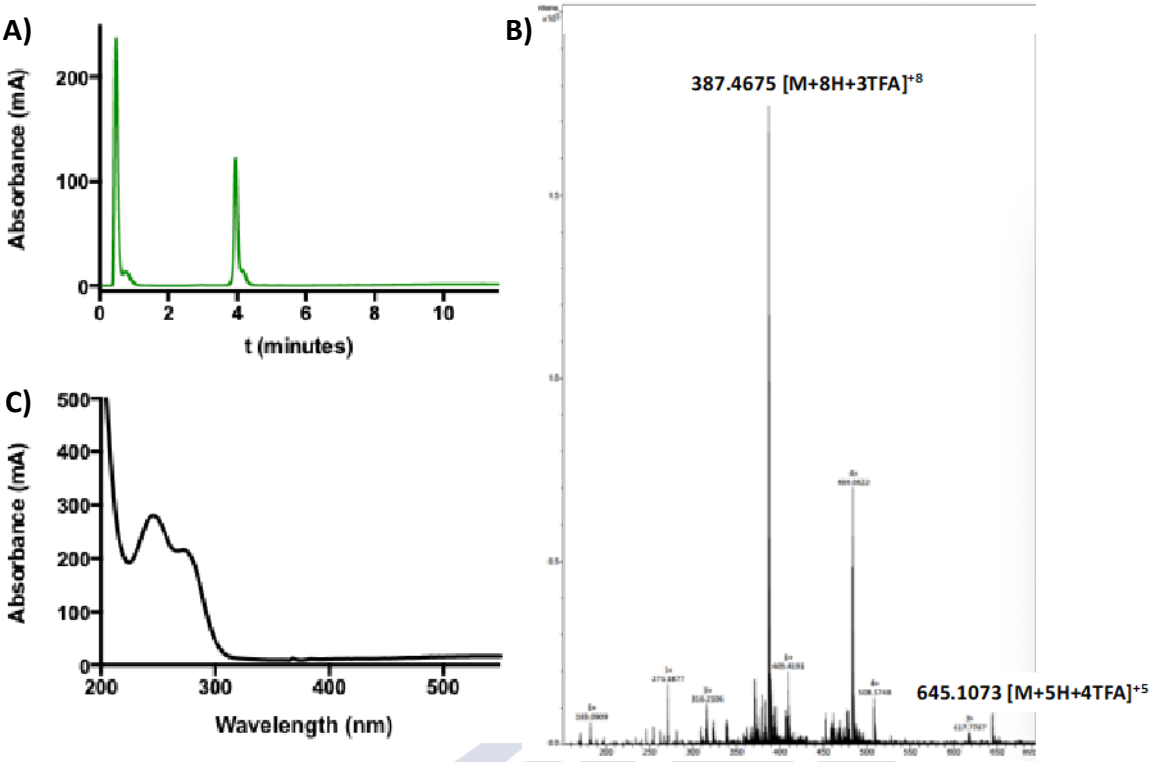

Figure 65. HPLC-MS spectra of $^{Ac}\boldsymbol{R_4}$**C**, A) chromatogram observed for λ=222 nm, B) ESI-MS spectrum corresponding to t = 4.01 minutes which corresponds to $^{Ac}\boldsymbol{R_4}$**C**, and C) UV-Vis spectrum at 4.01 minutes corresponding to $^{Ac}\boldsymbol{R_4}$**C**.

5. Fluorescence titrations

For the spectroscopic studies, a solution of the dye in phosphate buffer (10 mM, pH 7) was prepared and diluted into a quartz Hellma® fluorescence cuvette with a path-length 14 x 10 mm (chamber volume 1.4 mL) to reduce the concentration of dye to the desired concentration in phosphate-buffered solution (pH 7). Measurements were performed using a Varian Cary Eclipse fluorometer using the following settings: increment, 1.0 nm; integration time, 0.2 s; excitation slit width, 5.0 nm; emission slit width, 20.0 nm. The fluorescence emission of the titrations was plotted and fitted by nonlinear regression equations (Hill 1) to obtain the apparent K_d for each experiment. Data were fitted using nonlinear analysis with Origin 8.5 to the Hill 1 equation:

$$y = y_{max} + (y_{min} - y_{max}) \cdot \frac{x^n}{k^n + x^n}$$

In which y_{max} and y_{min} are the maximal and minimal fluorescence values, x is the ratio of concentrations between the indicated peptide and fluorophore, n is the Hill coefficient and k is the ratio of concentrations that correspond to the K_d. From this value, K_d is calculated using the following equation:

$$K_d = k \cdot c$$

In which k is the previously calculated ratio and c is the concentration of the fluorophore. A free value for Hill coefficient (n) was selected for most of the analysis, to account for the

possibility that more than one fluorophore molecule interacts with the cage.[69] Fitting using a 1:1 model gave a similar K_d value.

To 1.0 mL of an 8.4 nM solution of pyranine, 40 nM solution of carboxyfluorescein (CF), 30 nM solution of TAMRA, 50 nM solution of Alexa Fluor 488, 30 nM solution of Alexa Fluor 546, or 50 nM solution of Alexa Fluor 568, in phosphate buffer (10 mM, pH 7), aliquots of a 19 μM stock solution of $^{Ac}\boldsymbol{R}_4\mathbf{C}$ were sequentially added to the corresponding fluorophore solution and the fluorescence spectrum was recorded after each addition. Emission measurements were carried out by using an excitation wavelength of 415 nm for pyranine, 490 nm for CF, 488 nm for Alexa Fluor 488, and 520 nm for TAMRA, Alexa Fluor 546, and Alexa Fluor 568. The emission spectra were recorded at room temperature from 450 to 600 nm for pyranine, from 495 to 700 nm for CF and Alexa Fluor 488, and from 525 to 700 nm for TAMRA, Alexa Fluor 546, and Alexa Fluor 568. The fluorescence emission maxima of the titrations, at 510 nm for pyranine, at 516 nm for CF, at 513 nm for Alexa Fluor 488, at 570 nm for Alexa Fluor 546, and at 603 nm for Alexa Fluor 568, were plotted and fitted by nonlinear regression equations (Hill 1) to achieve the apparent K_d for each experiment. For titrations with $^{Tm}\boldsymbol{R}_4\mathbf{C}$**,** to a 60 nM solution of pyranine or a 40 nM solution of CF, aliquots of a 19 μM stock solution of the peptide were sequentially added and the spectra recorded under the same conditions described for $^{Ac}\boldsymbol{R}_4\mathbf{C}$.

6. *U*-tube experiments

U-tube experiments were carried out following previously described procedures[246] with minimal modifications. The *cis* phase (0.46 mL; 0.200 mM pyranine, 10 mM Na_mH_nPO4, 100 mM NaCl, pH 7.4) containing additional solution of EYPG (10 mM) was vortexed with $CHCl_3$ (0.5 mL). Then, 40 μL of $^{Ac}\boldsymbol{R}_4\mathbf{C}$, 40 μL of $^{Ac}\boldsymbol{R}_4$, or 40 μL of **C** of a 1 mM aqueous solution were added, and the mixture was vortexed again. Both the organic and aqueous layers were added carefully to the *U*-tube containing $CHCl_3$ (1 mL) and the *trans* phase (0.5 mL) from the sampling side. The organic layer was stirred at 700 rpm at room temperature. Aliquots (13.5 μL) were taken from the *trans* phase as a function of time and diluted to 150 μL with a buffer (10 mM $Na_mH_nPO_4$, 100 mM NaCl, pH 7.4). Measurements were carried out using a Varian Cary Eclipse fluorometer with the following settings: integration time, 0.2 s; excitation slit width, 5.0 nm; emission slit width, 20.0 nm; excitation wavelength, 460 nm. The emission spectra were recorded from 470 to 600 nm at 20 °C.

7. Cell lines and culture

HeLa and Vero cell lines were maintained at 37 °C, 5% CO_2, 95 % humidity, in Dulbecco's Modified Eagle's Medium (4500 mg/L glucose, L-glutamine, sodium pyruvate, and sodium bicarbonate), supplemented with 10% fetal bovine serum and 1% of Penicillin-Streptomycin-Glutamine Mix, and kept in an INCO108 incubator (Memmert).

[69] J. Mosquera, S. Zarra, J. R. Nitschke, *Angew. Chem. Int. Ed.* **2014**, *53*, 1556-1559.
[246] N. Sakai, S. Matile, *J. Am. Chem. Soc.* **2003**, *125*, 14348-14356.

8. Cell transport experiments

HeLa or Vero cells seeded the day before on glass-bottom dishes were washed with HEPES-Krebs-Ringer (HKR) buffer (5 mM HEPES, 137 mM NaCl, 2.68 mM KCl, 2.05 mM $MgCl_2$, 1.8 mM $CaCl_2$, pH 7.4) and incubated for 30 min with 1 µM Hoechst 33342 (ThermoFisher) in HKR to stain the nucleus. This solution was removed and cells were incubated for another 30 min with pyranine (or other fluorescent probes such as TAMRA, CF, or Alexa Fluor dyes) in combination with the peptide, cage, or peptide-cage hybrids at the concentrations indicated in the legend of the figures. After this incubation time, cells were washed twice with HKR and examined on the confocal microscope. In some cases, the step of nuclear staining with Hoechst was omitted. To check membrane integrity, after incubation with the complexes, cells were washed with HKR and further incubated with 2 µM of DAPI diluted in HKR buffer for 30 min or 0.5 µg/mL of propidium iodide for 10 min, before washing with HKR and imaging. To investigate the possibility of the *in situ* capture of the pyranine into the cage of the carrier, Vero cells were incubated with 12.5 µM pyranine in HKR for 10 min before adding, dropwise, a solution of **$^{Ac}R_4C$** in HKR to a final concentration of both peptide and pyranine of 10 µM and incubated for 30 min at 37 °C before imaging.

9. *In vitro* pH measurements

To confirm pH sensitivity of the dye in the calibration buffers used for *in situ* calibrations (10 mM MES, 10 mM HEPES, 20 mM glucose, 1 mM $CaCl_2$, 1 mM $MgCl_2$, 135 mM KCl, 20 mM NaCl; pH adjusted with KOH), absorption spectra of pyranine in the different buffers were obtained. Pyranine was diluted at 70 µM in each buffer and absorbance between 330-510 nm was measured in a Libra S60 spectrophotometer. The ratio between absorbances at 450 and 405 nm were calculated, and then transformed using the following equation:

$$log_{10}\left(\left(\frac{R_{max}-R}{R-R_{min}}\right)\cdot\left(\frac{A^{basic}_{405\,nm}}{A^{acidic}_{405\,nm}}\right)\right)$$

in which R represents the ratio A_{450}/A_{405}, R_{max} and R_{min} the maximal and minimal ratio values, and $A^{basic}{}_{405}$ and $A^{acidic}{}_{405}$ the absorbance of the pyranine at the highest and lowest pH tested. Data were fitted to a linear model. Intercept (7.01) corresponds to the pK_a under these conditions.

10. pH studies in cells

For pH ratiometric measurements, Vero cells were incubated with 10 µM pyranine and 10 µM **$^{Tm}R_4C$** peptide for 30 min in HKR buffer. Cells were then washed twice with HKR and imaged. A control with no pyranine was also prepared to quantify the background. To prepare a calibration curve, cells were first incubated with pyranine and **$^{Tm}R_4C$** under standard conditions (30 min, pH = 7.4). Subsequently, the cells were washed twice with high-potassium pH calibration buffers (10 mM MES, 10 mM HEPES, 20 mM glucose, 1 mM $CaCl_2$, 1 mM $MgCl_2$, 135 mM KCl, 20 mM NaCl; pH adjusted with KOH) at each indicated pH. The cells were then incubated at the corresponding pH for 20 min with the calibration buffers containing 10 µg/mL of the ionophore nigericin for pH clamping before imaging. Images were acquired

with a Zyla 4.2 PLUS camera mounted on a Dragonfly spinning disk confocal microscope (Andor), by excitation with 405 nm (protonated form, PyrH) and 488 nm (deprotonated form, Pyr^-) lasers, and detecting the fluorescence at 500-550 nm. Images from the pyranine channels were processed with FIJI,[248] as follows: the background was subtracted from both channels and then image 488 was divided by image 405. Mean values per field were obtained (Figure 57B) and data was linearized by logarithmic conversion and adjusted to a linear model (Figure 57C). The linear fit was then used to assign estimated values of pH to the images.

11. Flow cytometry

To further investigate the uptake mechanisms of the supramolecular complex formed by pyranine and $^{Tm}\boldsymbol{R}_4\mathbf{C}$, Vero cells seeded the day before at 10.000 cells/well of a 96-well plate, were treated for 30 min with dynasore (80 µM) diluted in DMEM without serum or antibiotics. Cells were then washed with HKR and incubated with 15 µM $^{Tm}\boldsymbol{R}_4\mathbf{C}$ and 15 µM pyranine for 30 min at 37 °C with the same concentration of the inhibitor in HKR buffer. For the incubation at low temperature (4 °C), cells were placed on ice before the incubation, and ice-cold solutions were used for the washes and incubations. Controls with 15 µM $^{Tm}\boldsymbol{R}_4\mathbf{C}$ alone and 15 µM pyranine alone were also performed. After 30 min of incubation, cells were washed with HKR and trypsinized. Trypsin was neutralized with 2 % FBS in PBS with 5 mM EDTA and cell fluorescence was measured on a Guava EasyCyte™ cytometer using two lasers: a blue laser (488 nm) with emission collected at 512/18 nm (pyranine) and a green laser (532 nm) collecting the emission at 575/25 nm (TAMRA). Cells with typical FSC and SSC parameters were selected and the median fluorescence intensity (MFI) was calculated for each sample. Each condition was done in triplicate. Fluorescence values were normalized to the uptake of each untreated control (100%) after blank subtraction. In all cases, data analysis was performed with InCyte software included in GuavaSoft 3.2 (Millipore).

12. Cell viability

Cell viability was measured by MTT assay. To evaluate the toxicity of the treatment of cells with $^{Tm}\boldsymbol{R}_4\mathbf{C}$, $^{Ac}\boldsymbol{R}_4\mathbf{C}$, and pyranine, Vero and HeLa cells were submitted to an MTT assay 1 hour and 24 h after the incubation. One day before the assay, a suspension of HeLa and Vero cells were plated in 96-well tissue culture plates by adding 100 µL (~10.000 cells) per well. The next day, the medium was removed and cells were incubated in HKR in the presence of $^{Tm}\boldsymbol{R}_4\mathbf{C}$, $^{Ac}\boldsymbol{R}_4\mathbf{C}$, and pyranine at different concentrations (50 µL/well) during 1 hour of incubation at 37 °C. After the incubation, HKR with the compounds was removed and pre-warmed DMEM containing 10 % FBS was added to the wells. To evaluate the toxicity at 1 hour, MTT (5 mg/mL in PBS, 10 µL/well) was added and the cells were further incubated for 4 h. To evaluate the toxicity at 24 h, cells were incubated for 24 h before adding the MTT. The cells were further incubated for 4 h in the presence of MTT. The supernatant was removed and the water-insoluble formazan salt was dissolved in DMSO (100 µL/well). The absorbance at 570 nm was measured. Data points were collected in triplicate and expressed as normalized values for untreated as control cells (100%) after blank subtraction.

[248] J. Schindelin, I. Arganda-Carreras, E. Frise, V. Kaynig, M. Longair, T. Pietzsch, S. Preibisch, C. Rueden, S. Saalfeld, B. Schmid, et al., *Nat. Methods* **2012**, *9*, 676-682.

USC
UNIVERSIDADE
DE SANTIAGO
DE COMPOSTELA

Chapter II:
Peptide integration and exchange into AuNPs mediated by host-guest molecular recognition

USC
UNIVERSIDADE
DE SANTIAGO
DE COMPOSTELA

Introduction

USC
UNIVERSIDADE
DE SANTIAGO
DE COMPOSTELA

1. Nanoparticles as a tool for nanomedicine

Since the advent of Nanotechnology, nanosystems with diagnostic and/or therapeutic capabilities have been regarded as a new promising paradigm that could improve in a significant manner therapeutical problems such as cancer.[249] This has led to a vast research effort in order to understand how fundamental physicochemical properties, such as size, charge, and chemical composition, can be addressed in order to improve the pharmacokinetic capabilities and biodistribution.[250] In fact, many limitations, such as limited delivery to target tissues are still major hurdles for the development of safe and efficient therapies.[251] Regardless of these difficulties, several nanomedicines are currently on different stages of clinical trials. Up to 2016, the U.S. Food and Drug Administration had approved 51 nanomedicines, with 77 products in clinical trials.[252] An analysis of the nanocarrier category revealed that soft nanoparticles (e.g. micelles, polymers) had more importance in comparison with hard carriers (e.g. metallic nanoparticles). At first sight, this data suggest some inertia towards the successful use of nanoparticle systems in real therapeutic applications, but also it might reflect a pluralistic approach towards the delivery problem, i.e. a single vehicle might not be well suited for different delivery therapeutic problems. Therefore, it seems plausible that different strategies towards the preparation of nanosystems could expand the possible applications in nanomedicine.

In this context, the diversity of structure and function accessible through supramolecular assembly holds promise as a versatile tool for the preparation of nanomedicine tools, including micellar, nanotubular, or nanoparticle-like systems.[188] Here we will focus on the use of host-guest recognition and its integration on nanosystems intended for therapeutic applications.

2. Nanoparticles built up by using host-guest molecular recognition

The use of host-guest molecular recognition offers the possibility to functionalize or even fully assemble nanoparticles by stable, yet reversible interactions. In the latter case, the term supramolecular nanoparticles (SNPs) has often been coined to indicate the formation of particles of nanometric size built fundamentally by non-covalent interactions. One of the simplest examples of the preparation of SNPs is the condensation, driven by electrostatic interactions, between polyanions (e.g. DNA) and positively charged lipids or polymers, which have been traditionally used for DNA delivery.[253] On the other hand, supramolecular interactions can be used for the reversible functionalization with motifs that impart certain functionality. The scaffolds used to build these systems can be either soft or hard, which have important consequences in their physicochemical properties and the therapeutic function. Here we will discuss examples of nanoparticles that integrate host-guest elements according to this classification.

---

[249] R. van der Meel, E. Sulheim, Y. Shi, F. Kiessling, W. J. M. Mulder, T. Lammers, *Nat. Nanotechnol.* **2019**, *14*, 1007-1017.
[250] B. Li, L. A. Lane, *Wiley Interdiscip. Rev. Nanomed. Nanobiotechnol.* **2019**, *11*, e1542.
[251] S. Wilhelm, A. J. Tavares, Q. Dai, S. Ohta, J. Audet, H. F. Dvorak, W. C. W. Chan, *Nat. Rev. Mater.* **2016**, *1*, 16014.
[252] D. Bobo, K. J. Robinson, J. Islam, K. J. Thurecht, S. R. Corrie, *Pharm. Res.* **2016**, *33*, 2373-2387.
[188] M. J. Webber, R. Langer, *Chem. Soc. Rev.* **2017**, *46*, 6600-6620.
[253] O. Boussif, F. Lezoualc'h, M. A. Zanta, M. D. Mergny, D. Scherman, B. Demeneix, J. P. Behr, *Proc. Natl. Acad. Sci.* **1995**, *92*, 7297-7301.

2.1. Soft supramolecular nanoparticles for delivery of therapeutics based on host-guest molecular recognition

2.1.1. Delivery of therapeutic nucleic acids

A particularly successful example of SNPs that has moved from fundamental research to clinical trials is the work of Mark E. Davis group. Since the end of the 90´s, this group has developed targeted SNPs that can deliver small interfering RNA (siRNA) to inhibit tumor growth.[254] These SNPs consist of three different building blocks (Figure 66A): a linear cyclodextrin-containing polymer (CDP), an adamantane-polyethylene glycol conjugate (Ad-PEG), and the targeting moiety transferrin linked to an adamantane moiety (Ad-PEG-Tf). The self-assembly of these three components into a hybrid polymer is driven by host-guest processes. The resulting conjugate is mixed with siRNA, which is subsequently captured by electrostatic interactions between the positively charged polymer and the negatively charged nucleic acid (Figure 66B). This four-component cocktail finally yields soft nanoparticles of around 70 nm size. The vehicle remained stable into the bloodstream and was able to enter into tumor tissues due to the EPR effect. Enhanced delivery efficiency in tumor cells was achieved due to the recognition between anchored transferrin and its receptor (TfR) which is overexpressed in certain types of tumor cells (Figure 66C).[254,255] This therapeutic product named CALAA-01 was evaluated in phase I clinical trials in human patients with solid tumors, administrated by intravenous systemic dosing. Although some adverse effects were observed (fatigue, chill), these studies indicated that this nanosystem could be safely used in humans.[256] This illustrative example was the inspiration for intensive research in the area of gene delivery by using host-guest systems. While Davis group work relied on the incorporation of the host into cationic polymers, many groups have exploited the chemical functionalization of the host as a way for designing homogeneous gene delivery vectors, which are in consequence "preorganized" towards interactions with nucleic acids.[257] In this context, remarkable examples include calixarenes[258] and cyclodextrins[259] hosts.

In the examples above, the size of the soft nanoparticles was a consequence of the interaction between the nucleic acid and the host polymer/molecules, and no size-tuning was reported. However, control over nanoparticle size is desirable, since many cell-nanoparticle interactions are strongly influenced by their contact surface, (e.g. determining the number of receptor-antigen interactions).[260] Remarkably, the group of prof. Tseng developed size-controllable SNPs based on the self-assembly of three different molecular building blocks (Figure 66D): i) multivalent host poly(ethylene imine) functionalized with β-CD (CD-PEI), ii) multivalent guest, Ad-poly(amidoamine) dendrimer (Ad-PAMAM) and iii) monovalent guest linked to a steric stabilizer, Ad-PEG. The beauty of this work is that tuning of the nanoparticle size is achieved simply by changing the mixing ratio of the different building blocks. Importantly, it was shown that this strategy can be a promising strategy for the preparation of

[254] M. E. Davis, *Mol. Pharm.* **2009**, *6*, 659-668.
[255] M. E. Davis, J. E. Zuckerman, C. H. J. Choi, D. Seligson, A. Tolcher, C. A. Alabi, Y. Yen, J. D. Heidel, A. Ribas, *Nature* **2010**, *464*, 1067-1070.
[256] J. E. Zuckerman, M. E. Davis, *Nat. Rev. Drug Discov.* **2015**, *14*, 843-856.
[257] C. Ortiz Mellet, J. M. Benito, J. M. García Fernández, *Chem. Eur. J.* **2010**, *16*, 6728-6742.
[258] F. Sansone, M. Dudič, G. Donofrio, C. Rivetti, L. Baldini, A. Casnati, S. Cellai, R. Ungaro, *J. Am. Chem. Soc.* **2006**, *128*, 14528-14536.
[259] L. Gallego-Yerga, J. M. Benito, L. Blanco-Fernández, M. Martínez-Negro, I. Vélaz, E. Aicart, E. Junquera, C. Ortiz Mellet, C. Tros de Ilarduya, J. M. García Fernández, *Chem. Eur. J.* **2018**, *24*, 3825-3835.
[260] N. Hoshyar, S. Gray, H. Han, G. Bao, *Nanomedicine* **2016**, *11*, 673-692.

NPs with sizes between 30 nm and 100 nm and with a good polydispersity. Interestingly, the size of the SNPs was easily tuned by increasing the quantity of multivalent guest, while keeping constant the concentration of the host and the stabilizer.[261] The control over the assembly and subsequent size distribution were further tuned by modulation of the mixing regimes in microfluidic chips.[262,263] These soft SPNs were used for the intracellular delivery of DNA. SPNs combined with DNA and the targeting ligand RGD (Figure 66E) were used to efficiently deliver DNA inside living cells.[264] Moreover, using this strategy, an intact artificial transcription factor (TF) (GAL4-VP16) was encapsulated into SPNs leading to the targeted delivery of an intact TF. In this work, a DNA plasmid (pG5E4T-Fluc) equipped with five tandem copies of GAL4-VP16 matching recognition sequences ($K_d \approx 10$ nM) was used to improve the incorporation of the TF into the SPN by the formation of an anionic TF/DNA complex.[265] Further examples of the use of these platforms in delivery include the controlled release of the anticancer drug camptothecin[266] or intradermal release of ketoconazole -an antifungal drug- in mice models.[267]

[261] H. Wang, S. Wang, H. Su, K.-J. Chen, A. L. Armijo, W.-Y. Lin, Y. Wang, J. Sun, K. Kamei, J. Czernin, et al., *Angew. Chem. Int. Ed.* **2009**, *48*, 4344-4348.
[262] K. Liu, H. Wang, K.-J. Chen, F. Guo, W.-Y. Lin, Y.-C. Chen, D. L. Phung, H.-R. Tseng, C. K. F. Shen, *Nanotechnology* **2010**, *21*, 445603.
[263] K. Liu, Y.-C. Chen, H.-R. Tseng, C. K.-F. Shen, R. M. van Dam, *Microfluid. Nanofluidics* **2010**, *9*, 933-943.
[264] H. Wang, K.-J. Chen, S. Wang, M. Ohashi, K. Kamei, J. Sun, J. H. Ha, K. Liu, H.-R. Tseng, *Chem. Commun.* **2010**, *46*, 1851-1853.
[265] Y. Liu, H. Wang, K. Kamei, M. Yan, K.-J. Chen, Q. Yuan, L. Shi, Y. Lu, H.-R. Tseng, *Angew. Chem. Int. Ed.* **2011**, *50*, 3058-3062.
[266] K.-J. Chen, L. Tang, M. A. Garcia, H. Wang, H. Lu, W.-Y. Lin, S. Hou, Q. Yin, C. K. F. Shen, J. Cheng, et al., *Biomaterials* **2012**, *33*, 1162-1169.
[267] F. Wang, P. Yang, J. Choi, P. Antovski, Y. Zhu, X. Xu, T.-H. Kuo, L.-E. Lin, D. N. H. Kim, P.-C. Huang, et al., *ACS Nano* **2018**, *12*, 6851-6859.

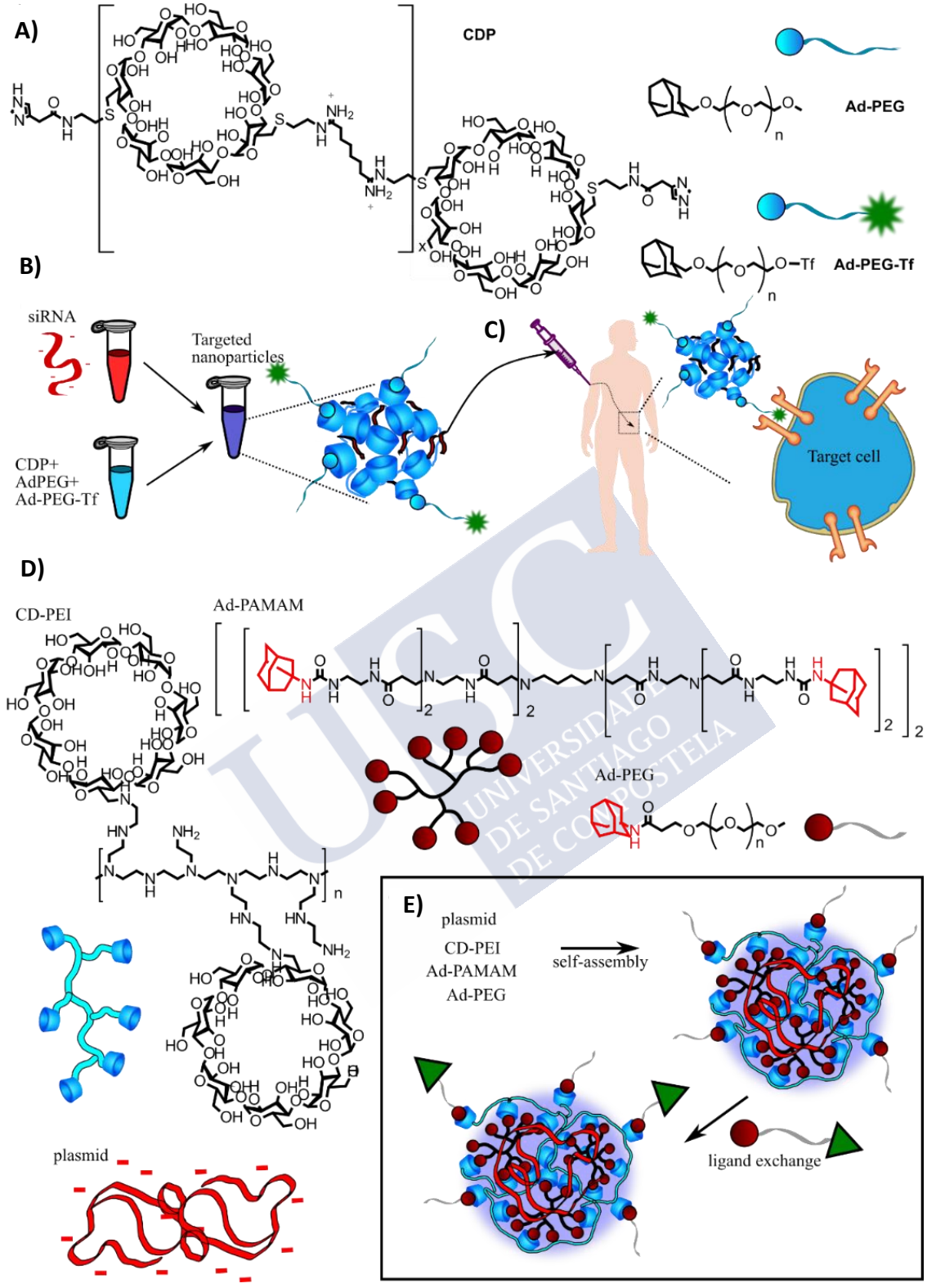

Figure 66. A) Host-guest components of the CALAA1 delivery system.[254] B) Formulation by premixing of the host-guest components, followed by mixing with the therapeutic nucleic acid yields supramolecular nanoparticles.[254] C) These nanoparticles can be administrated systemically in order to reach the specific tumor tissue.[254] D) Molecular components exploited in Tseng's group supramolecular nanoparticle preparation with size control.[261] E) Example of the self-assembly of a gene delivery system where the targeting ligands can be added by simple host-guest exchange.[264]

2.1.2. Delivery of small drugs

Cyclodextrin-based supramolecular nanoparticles have been applied to deliver a variety of small therapeutic and diagnostic molecules. This type of design takes advantage of the ability of *β*-CDs to form inclusion complexes with different hydrophobic drugs such (e.g. antitumoral drugs such as doxorubicin or camptothecin) to build up new supramolecular materials with improved cellular delivery capabilities.[268,269,270,271] Additionally, *β*-cyclodextrin-based SPNs have also been used to deliver diagnostic agents such as ^{64}Cu or Gd complexes.

An inspiring example of these hybrid platforms was developed by the group of Prof. Davis. The structural design consists of SPNs formed by cyclodextrin-containing linear polyethylene glycol (PEG) polymers covalently attached to the drug camptothecin (CPT) (Figure 67A).[272,273,274,275] CPT is an anticancer drug, which acts as an inhibitor of topoisomerase I, an enzyme crucial for DNA replication and cell survival. Unfortunately, under physiological conditions, this drug is transformed from its lactone active form, which is hydrophobic, into its inactive open form, which is more hydrophilic. Interestingly, it was shown that the formation of the inclusion host-guest complex between CPT with *β*-CDs kept this drug in its lactone active form.[272,273] Moreover, due to the PEG chains, the resulting SNPs, presented high water solubility and long-circulating times. Studies in living cells showed that CPT incorporated into these SNPs was released inside of the cell due to the acidic hydrolysis of the CPT-polymer linker.[273] Interestingly, *in vivo* assays have shown entry into tumor tissue through the EPR effect and have demonstrated impressive high efficacy, improved pharmacokinetics, and low side effects in animals[273] and humans.[274,275] This product, named CRLX101, was recently moved to Phase II clinical trials.[276]

Supramolecular nanoparticles have been applied for the delivery of amiodarone (Figure 67B).[277] Amiodarone is used for the prevention and treatment of cardiac arrhythmias. However, it presents important side effects due to its accumulation in off-target tissues. To avoid this undesired effect, a potential solution is a site-specific delivery to cardiac macrophages. The delivery vector designed consisted of L-lysine cross-linked succinyl-*β*-cyclodextrin polymers, which has demonstrated high macrophage affinity.[277] Then, amiodarone was incorporated into the vehicle through the formation of the *β*-cyclodextrin cavitate (Figure 67B). The authors claimed selective delivery of amiodarone into the cardiac tissue via macrophages while the off-target tissue accumulation was reduced.[277]

[268] H. Yao, M. Qi, Y. Liu, W. Tian, *Chem. Eur. J.* **2016**, *22*, 8508-8519.
[269] Q.-D. Hu, G.-P. Tang, P. K. Chu, *Acc. Chem. Res.* **2014**, *47*, 2017-2025.
[270] C. Y. Ang, S. Y. Tan, Y. Zhao, *Org. Biomol. Chem.* **2014**, *12*, 4776-4806.
[271] G. Yu, X. Zhao, J. Zhou, Z. Mao, X. Huang, Z. Wang, B. Hua, Y. Liu, F. Zhang, Z. He, et al., *J. Am. Chem. Soc.* **2018**, *140*, 8005-8019.
[272] J. Cheng, K. T. Khin, G. S. Jensen, A. Liu, M. E. Davis, *Bioconjug. Chem.* **2003**, *14*, 1007-1017.
[273] J. Cheng, K. T. Khin, M. E. Davis, *Mol. Pharm.* **2004**, *1*, 183-193.
[274] M. E. Davis, *Adv. Drug Deliv. Rev.* **2009**, *61*, 1189-1192.
[275] A. J. Clark, D. T. Wiley, J. E. Zuckerman, P. Webster, J. Chao, J. Lin, Y. Yen, M. E. Davis, *Proc. Natl. Acad. Sci.* **2016**, *113*, 3850-3854.
[276] J. E. Zuckerman, M. E. Davis, *Nat. Rev. Drug Discov.* **2015**, *14*, 843-856.
[277] M. S. Ahmed, C. B. Rodell, M. Hulsmans, R. H. Kohler, A. D. Aguirre, M. Nahrendorf, R. Weissleder, *Bioconjug. Chem.* **2019**, *30*, 733-740.

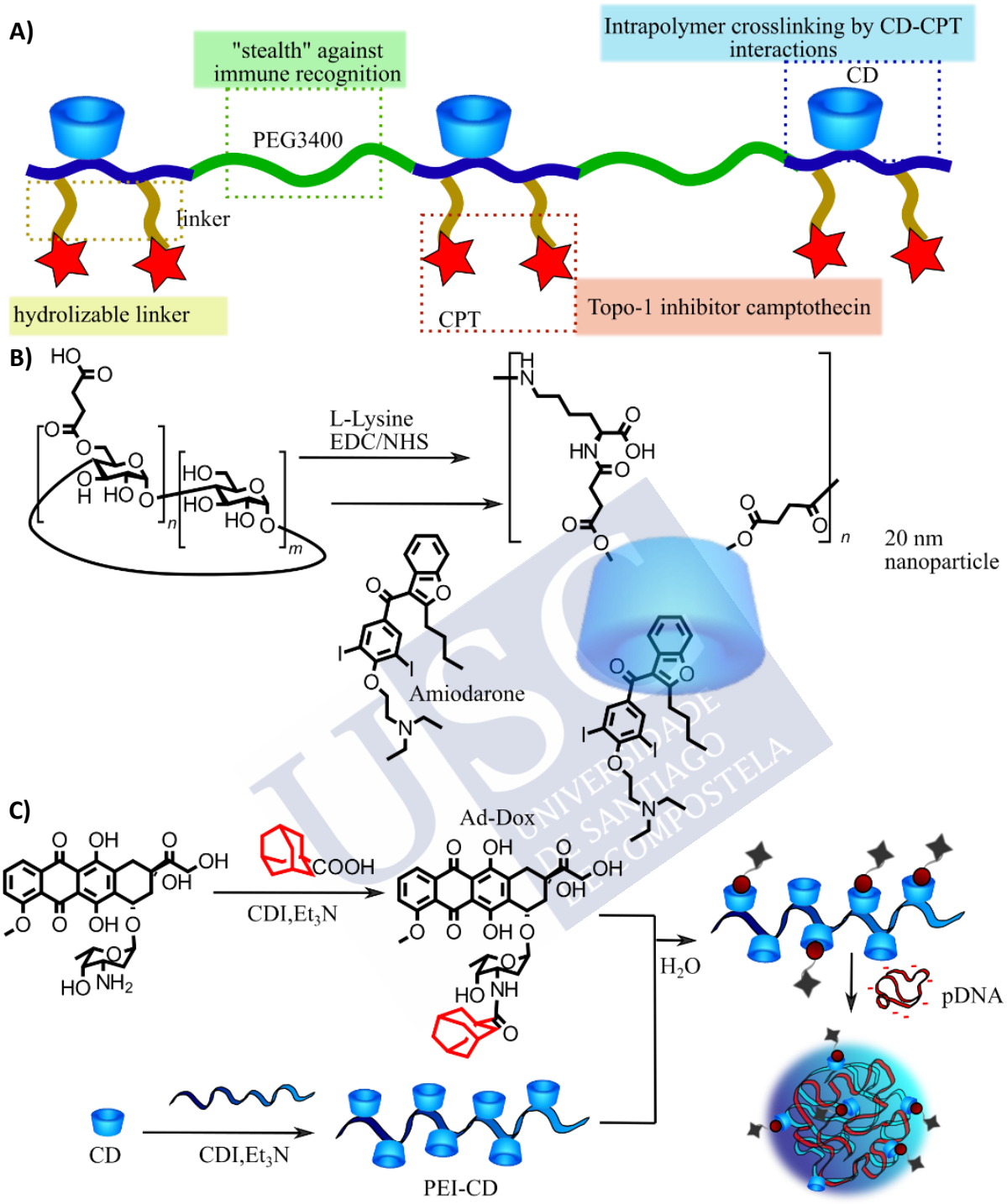

Figure 67. A) Schematic representation of the different components forming CRLX101 and self-assembly into SPNs.[275] B) Schematic representation of the preparation of CDNPs loaded with amiodarone for intravenous injection.[277] C) Schematic illustration of the synthesis of Ad-Dox/PEI-CD and self-assembly of SNPs with DNA plasmid.[279]

2.1.3. Co-delivery of therapeutic molecules

The incorporation of the host-guest entities into nanoparticles could be used for the construction of systems capable of intracellular co-deliver of several therapeutic molecules. For example, co-delivery of therapeutic nucleic acids and anticancer drugs achieved synergistic effects of chemotherapy and gene therapy.[278] In this context, Fan *et al*. synthesized cyclodextrin-containing SNPs for co-delivering doxorubicin and a plasmid encoding TRAIL (Figure 67C).[279] TRAIL (tumor necrosis factor-related apoptosis-inducing ligand) is a protein that has shown to promote apoptosis of human cancer cells. The delivery platform consisted of i) *β*-cyclodextrin-anchored branched polyethylenimine (PEI), ii) adamantine modified doxorubicin, and a plasmid encoding TRAIL (pTRAIL). The formed SPNs demonstrated efficient delivery of both drug and gene, showing enhanced apoptosis in chemoresistant human ovarian cancer cells SKOV-3c and the reduction of the tumor proliferation and growth in mice models.[279]

In another example, co-delivery of adamantyl-modified paclitaxel drug and a small hairpin RNA (shRNA) that silences survivin expression has been also achieved.[280] Survivin is a target protein in anticancer therapy because it inhibits apoptosis. The system was constituted by adamantyl-modified paclitaxel complexed in *β*-CD-PEI polymers by supramolecular interactions. As in previous examples, shRNA was incorporated driven by electrostatic interactions between the polymer and the nucleic acids. Co-delivery was demonstrated *in vitro* by confocal microscopy experiments and a synergistic effect on apoptosis experiments was shown in SKOV-3 cells and *in vivo*, it was shown that the inhibition of tumor growth in mice is about 3.5 fold higher than free paclitaxel.[280]

2.2. Host-functionalized metallic nanoparticles

Metallic nanoparticles are a key component in Nanotechnology and a well-known scaffold in the development of drug delivery systems in Nanomedicine. In particular, gold nanoparticles (AuNPs) have shown promising applications not only in biomedicine[281] but also in catalysis[282] or as sensors.[283] Additionally, they present excellent optical properties, and their plasmonic properties have paved the way for photothermal approaches to therapeutics.[284] A crucial factor for the development of safe and efficient therapies is to gain access to functionalization strategies that could allow multicomponent decoration of their surface, preferably in a regioselective manner.[285,286] While one of the most exploited strategies is covalent

[278] Y. Wang, S. Gao, W.-H. Ye, H. S. Yoon, Y.-Y. Yang, *Nat. Mater.* **2006**, *5*, 791-796.
[279] H. Fan, Q.-D. Hu, F.-J. Xu, W.-Q. Liang, G.-P. Tang, W.-T. Yang, *Biomaterials* **2012**, *33*, 1428-1436.
[280] Q. Hu, W. Li, X. Hu, Q. Hu, J. Shen, X. Jin, J. Zhou, G. Tang, P. K. Chu, *Biomaterials* **2012**, *33*, 6580-6591.
[281] E. C. Dreaden, A. M. Alkilany, X. Huang, C. J. Murphy, M. A. El-Sayed, *Chem. Soc. Rev.* **2012**, *41*, 2740-2779.
[282] P. Hervés, M. Pérez-Lorenzo, L. M. Liz-Marzán, J. Dzubiella, Y. Lu, M. Ballauff, *Chem. Soc. Rev.* **2012**, *41*, 5577-5587.
[283] K. Saha, S. S. Agasti, C. Kim, X. Li, V. M. Rotello, *Chem. Rev.* **2012**, *112*, 2739-2779.
[284] P. Singh, S. Pandit, V. R. S. S. Mokkapati, A. Garg, V. Ravikumar, I. Mijakovic, *Int. J. Mol. Sci.* **2018**, *19*, 1979.
[285] R. Mout, D. F. Moyano, S. Rana, V. M. Rotello, *Chem. Soc. Rev.* **2012**, *41*, 2539-2544.
[286] G. Chen, K. J. Gibson, D. Liu, H. C. Rees, J.-H. Lee, W. Xia, R. Lin, H. L. Xin, O. Gang, Y. Weizmann, *Nat. Mater.* **2019**, *18*, 169-174.

functionalization of the nanoparticle corona, recent works of Kay's group[287,288] have shown reversible dynamic covalent functionalization of gold nanoparticles. However, full reversibility is reachable by exploiting supramolecular interactions; for example, the combination of supramolecular macrocyclic receptors and AuNPs. Importantly, the use of non-covalent interactions allows the construction of complicated systems by facile mixing in solution of the different building blocks. Moreover, this strategy avoids tedious synthetic steps and difficult purifications of the final systems. During the last years, AuNPs functionalized with different macrocyclic hosts such as cucurbiturils, calixarenes, or cyclodextrins (CDs) have been synthesized.[289]

One of the first cavitand-decorated nanoparticle system was reported by Kaifer *et al.*[290] Here, cyclodextrins were attached to the surface of AuNPs by sulfur-gold bonds. The ability to promote specific host-guest recognition was demonstrated by the generation of cross-linked networks constituted by the interaction of host nanoparticles and ferrocene dimers (Figure 68A).[290] Since this discovery, cyclodextrin-modified AuNPs have been explored and this type of hybrid nanomaterials has found interesting applications.[291,292,293] While these reports highlighted the potential of supramolecular interactions as a viable approach for the generation of more complex nanostructures, biofunctionality was implemented later. Interestingly, direct functionalization of cavitands, such as CBs or CAs, has also been reported.[294,295]

2.2.1. Delivery of therapeutic molecules

During the last years, different applications have been shown for the host-functionalized gold nanoparticles such as biosensors or drug delivery vectors. Interestingly, the combination of supramolecular macrocyclic receptors and AuNPs has demonstrated great potential in drug delivery and theranostics.[296] These platforms can be decorated by using both covalent and non-covalent interactions. For instance, the covalent conjugation of targeting ligands such as biotin[297] or anti-epidermal growth factor receptor (anti-EGFR) antibody[298] has been explored to improve the properties of the delivery system of several cavitand nanoparticles.

Heo *et al*. reported a multifunctional cyclodextrin-modified AuNPs to achieve the targeted delivery of the antitumoral drug paclitaxel to A549 lung, HeLa breast, and MG63 osteosarcoma cancer cells (Figure 68B).[297] This multicomponent device was integrated over a *β*-CD@AuNP scaffold covalently functionalized with biotin targeting moiety and PEG as a colloidal

[287] W. Edwards, N. Marro, G. Turner, E. R. Kay, *Chem. Sci.* **2018**, *9*, 125-133.
[288] F. della Sala, E. R. Kay, *Angew. Chem. Int. Ed.* **2015**, *54*, 4187-4191.
[289] V. Montes-García, J. Pérez-Juste, I. Pastoriza-Santos, L. M. Liz-Marzán, *Chem. Eur. J.* **2014**, *20*, 10874-10883.
[290] J. Liu, S. Mendoza, E. Román, M. J. Lynn, R. Xu, A. E. Kaifer, *J. Am. Chem. Soc.* **1999**, *121*, 4304-4305.
[291] Y. Zhao, Y. Huang, H. Zhu, Q. Zhu, Y. Xia, *J. Am. Chem. Soc.* **2016**, *138*, 16645-16654.
[292] Y. Xie, X. Wang, X. Han, W. Song, W. Ruan, J. Liu, B. Zhao, Y. Ozaki, *J. Raman Spectrosc.* **2011**, *42*, 945-950.
[293] N. Zhang, Y. Liu, L. Tong, K. Xu, L. Zhuo, B. Tang, *Analyst* **2008**, *133*, 1176-1181.
[294] Q. An, G. Li, C. Tao, Y. Li, Y. Wu, W. Zhang, *Chem. Commun.* **2008**, 1989-1991.
[295] A. Wei, *Chem. Commun.* **2006**, 1581-1591.
[296] H. Li, Y.-W. Yang, *Chinese Chem. Lett.* **2013**, *24*, 545-552.
[297] D. N. Heo, D. H. Yang, H.-J. Moon, J. B. Lee, M. S. Bae, S. C. Lee, W. J. Lee, I.-C. Sun, I. K. Kwon, *Biomaterials* **2012**, *33*, 856-866.
[298] C. Park, H. Youn, H. Kim, T. Noh, Y. H. Kook, E. T. Oh, H. J. Park, C. Kim, *J. Mater. Chem.* **2009**, *19*, 2310-2315.

stabilizer. Biotin is required by cancer cells to maintain their fast proliferation.[299] Therefore, it has been demonstrated that biotin receptors are overexpressed in cancer cells when compared to normal cells.[300] Then, the drug was loaded in the cyclodextrin cavities by host-guest molecular recognition and used to carry out cell assays. These experiments indicated that the nanosystem was taken up by cells via receptor-mediated endocytosis. The authors proposed that the release of the nanoparticles into the cytoplasm triggers the particle disassembly due to disulfide oxidation in the presence of glutathione. Control experiments in the presence and absence of the biotin tag showed an increased cellular uptake and a higher apoptosis effect when the tag was present. Importantly, these NPs, when incubated with fibroblast normal NIH3T3 cells, demonstrated lower cytotoxic effects than against the cancer cells.[297] In a similar approach, Park *et al.* reported the targeted delivery of the anticancer drug *β*-Lapachone to human lung cancer cells (A549).[298] This system consisted of an analogue cavitand-functionalized NP and steric stabilizer but using an anti-EGFR antibody as targeting ligand. In a similar strategy, the cyclodextrin cavities were used for the complexation of *β*-Lapachone, whose encapsulation association constant (K_a) was estimated as 1.23 x 10^3 M^{-1}. Intracellular delivery of the drug-CD@AuNPs complex was observed by *in vitro* experiments and the release of the *β*-Lapachone from the surface of AuNP was shown to be mediated by intracellular glutathione. Control experiments in the presence or absence of targeting ligand showed an increase in the cellular uptake and a higher apoptosis effect against lung cancer cells in the presence of the formers.[298]

An important limitation of the previous examples is that the amount of drug loading is defined by the thermodynamic binding constant between the drugs and the cyclodextrin pocket. Indeed, low binding constants might result in a poor loading, a situation that can get worse with the dilution. In an extreme situation, certain drugs might not be able to fit at all in the hydrophobic pocket. Therefore, Shi *et al.* circumvented the problem by chemical functionalization of the drug with a strong binding guest.[301] In their approach, the authors prepared a pro-drug consisting of adamantyl-modified oxaliplatin (a prodrug Pt(IV) of the anticancer drug, cisplatin Pt(II)). This pro-drug was efficiently incorporated into CD@AuNPs driven by the specific receptor affinity. The interaction was studied by ICP-MS experiments, obtaining an association constant K_a of 1.4 × 10^3 M^{-1}. Interestingly, the intracellular delivery of this prodrug driven by CD@AuNPs was observed and NPs cluster formation was found in the nucleus of cancer cells. The prodrug loaded NPs demonstrated a cytotoxic effect against human neuroblastoma cells. However, this system showed lower cytotoxicity than free cisplatin. The authors suggest that this fact is due to the low efficiency of the reduction of the prodrug Pt(IV) to Pt(II) species inside living cells, a required step in this type of prodrugs.[301]

In the previous examples, targeting ligands or PEG has been incorporated by the formation of covalent bonds, while the drugs were loaded by the formation of host-guest inclusion complexes. Interestingly, Chen *et al.* were able to incorporate two different functionalities, the drug and targeting ligand, by the exclusive use of host-guest molecular recognition.[302] In this

[299] G. Russell-Jones, K. McTavish, J. McEwan, J. Rice, D. Nowotnik, *J. Inorg. Biochem.* **2004**, *98*, 1625-1633.
[300] W. Yang, Y. Cheng, T. Xu, X. Wang, L. Wen, *Eur. J. Med. Chem.* **2009**, *44*, 862-868.
[297] D. N. Heo, D. H. Yang, H.-J. Moon, J. B. Lee, M. S. Bae, S. C. Lee, W. J. Lee, I.-C. Sun, I. K. Kwon, *Biomaterials* **2012**, *33*, 856-866.
[298] C. Park, H. Youn, H. Kim, T. Noh, Y. H. Kook, E. T. Oh, H. J. Park, C. Kim, *J. Mater. Chem.* **2009**, *19*, 2310-2315.
[301] Y. Shi, J. Goodisman, J. C. Dabrowiak, *Inorg. Chem.* **2013**, *52*, 9418-9426.
[302] W.-H. Chen, Q. Lei, G.-F. Luo, H.-Z. Jia, S. Hong, Y.-X. Liu, Y.-J. Cheng, X.-Z. Zhang, *ACS Appl. Mater. Interfaces* **2015**, *7*, 17171-17180.

work (Figure 68C), multifunctional CD@AuNPs for targeted cancer therapy were constructed by the incorporation of both adamantane-hydrazone-doxorubicin (Ad-Hyd-DOX) and adamantane-modified-PEG_8-GRGDS (Ad-PEG_8-GRGDS), playing the roles of anticancer drug and targeting moiety respectively.[302] The GRGDS peptide sequence has shown the ability to target cancer cells that overexpress $\alpha_v\beta_3$ integrin.[264] On the other hand, the inclusion of the hydrazone bond enabled the proton-mediate hydrolysis of the linker, resulting in the release of the drug at acidic pH values. The authors showed that these multifunctional nanoparticles were able to be selectively internalized by cancer cells via receptor-mediated endocytosis. Moreover, this nanosystem showed cancer cell apoptosis due to the release of doxorubicin at lysosomal pH values. Overall, one of the most remarkable features of this work is the exclusive use of host-guest molecular recognition and the use of a pH-responsive therapeutic agent.[302]

[302] W.-H. Chen, Q. Lei, G.-F. Luo, H.-Z. Jia, S. Hong, Y.-X. Liu, Y.-J. Cheng, X.-Z. Zhang, *ACS Appl. Mater. Interfaces* **2015**, *7*, 17171-17180.
[264] H. Wang, K.-J. Chen, S. Wang, M. Ohashi, K. Kamei, J. Sun, J. H. Ha, K. Liu, H.-R. Tseng, *Chem. Commun.* **2010**, *46*, 1851-1853.

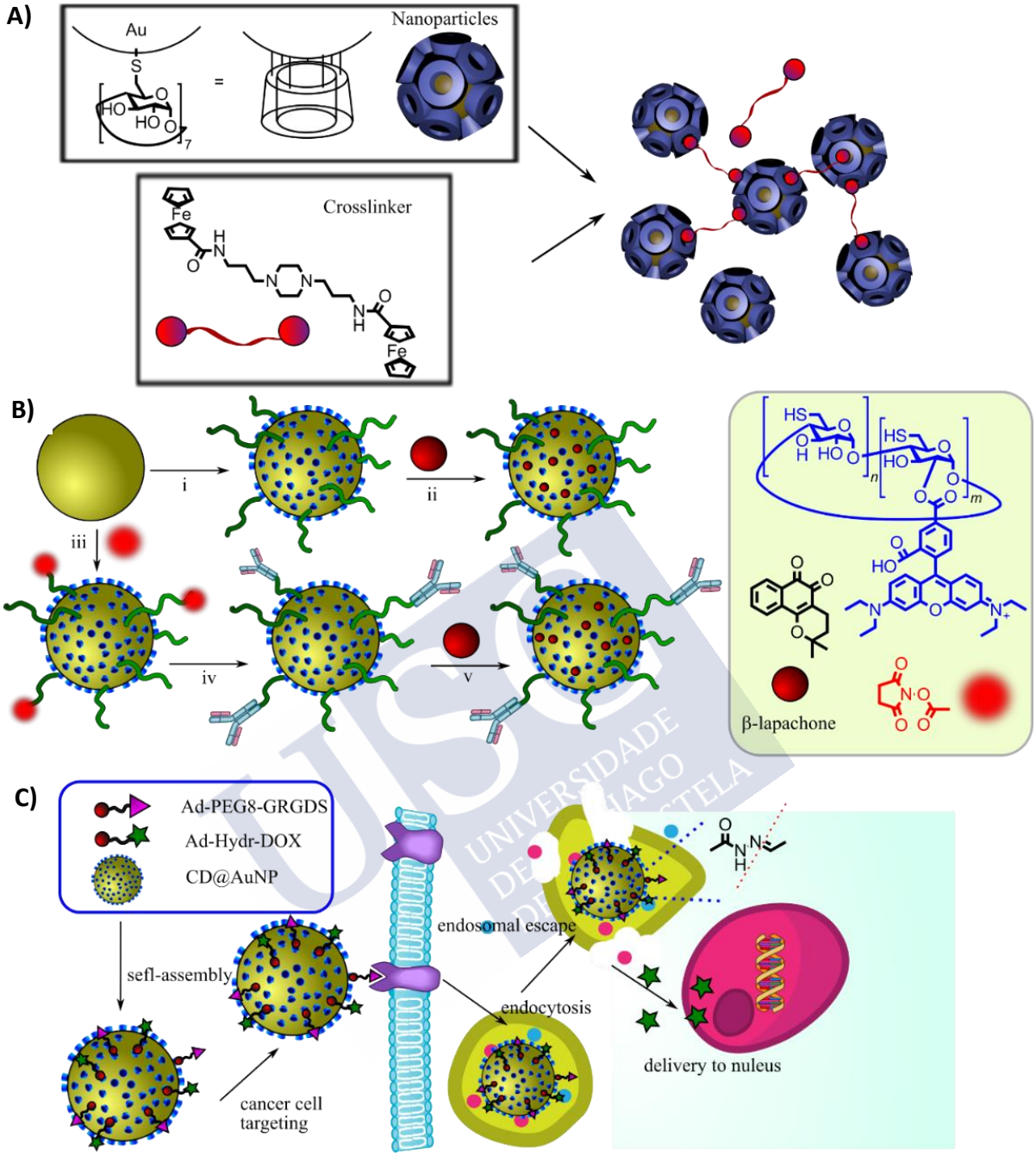

Figure 68. A) Left. Schematic and structural representation of the ferrocene dimer and the perthiolated cyclodextrin attached to the surface of the AuNPs. Right. Formation of the supramolecular network between ferrocene dimer and cyclodextrin-functionalized AuNPs.[290] B) Schematic representation of the preparation of non-targeted and targeted CD@AuNPs for *β*-Lapachone intracellular delivery. Incorporation of building blocks into AuNPs i) SH-CD and PEG-SH ii) *β*-Lapachone, iii) SH-CD, PEG-SH, and NHS-PEG-SH, iv) anti-EGFR and v) *β*-Lapachone.[298] C) Schematic representation of building blocks and self-assembly of multifunctional host-guest CD@AuNPs for targeted anticancer therapy, internalization mechanism, and pH-mediated intracellular release of doxorubicin.[302]

2.2.2. Achieving therapeutic response by changes in physical/catalytic properties

In addition to the incorporation of bioactive drugs, the use of hard nanoparticles decorated with host cavities can additionally exploit supramolecular processes in order to regulate a therapeutic response based on the physical or catalytic properties of the nanoparticles. A pioneering report of Rotello's group showed how dynamic exchange of guests in living cells could be used for triggering a cytotoxic response.[303] In particular, diaminohexane-functionalized gold nanoparticles were capped with CB[7] guests. These particles were readily internalized in MFC-7 cells. Addition of 1-adamantylamine -a guest with a higher binding affinity towards CB[7] in comparison to diaminohexane- to the cell media triggered adamantane uptake and guest exchange in cells. Uncapped gold nanoparticles were able to promote endosomal escape and induce cell death.[303] Sketching a similar concept, the use of redox-responsive guests have been exploited to trigger intracellular nanoparticle aggregation.[304] In this report, CD-coated gold nanoparticles and oxidized divalent ferrocene crosslinkers were co-delivered to HepG2 cells. Flow cell cytometry revealed increased cell toxicity when nanoparticles and crosslinkers were delivered at the same time in comparison with the individual components. As a mechanistic proposal, the authors claimed that intracellular Fc+ was reduced in the presence of intracellular glutathione, initiating nanoparticle aggregation by crosslinking. Quantitative ICP-MS revealed that the presence of the crosslinker resulted in higher Au retention in cells. This accumulation could induce apoptosis in cells.[304]

On the other hand, Rotello's group has shown the regulation of the enzymatic activity of nanoparticle based-nanoreactors.[305] The design is composed of AuNPs coated with N-Benzyl-N,N-dimethyloligoethylenglycol ligands. These can encapsulate transition metal catalysts and hold them by supramolecular capping between CB[7] hosts and the ligands. Catalysts can be exposed to the media by releasing the host cap via competition with endocytosed adamantylamine. Once liberated, the catalytic activity is activated, which was demonstrated by the N-deacylation of an N-alkylated 5-fluorouracil prodrug. This triggered the toxic response of the drug.[305]

[303] C. Kim, S. S. Agasti, Z. Zhu, L. Isaacs, V. M. Rotello, *Nat. Chem.* **2010**, *2*, 962-966.
[304] Y. Wang, H. Li, Q. Jin, J. Ji, *Chem. Commun.* **2016**, *52*, 582-585.
[305] G. Y. Tonga, Y. Jeong, B. Duncan, T. Mizuhara, R. Mout, R. Das, S. T. Kim, Y.-C. Yeh, B. Yan, S. Hou, et al., *Nat. Chem.* **2015**, *7*, 597-603.

Objectives

USC
UNIVERSIDADE
DE SANTIAGO
DE COMPOSTELA

The use of metallic host-guest based-nanoparticles as motifs for nanotherapeutic applications has raised a great deal of interest. In this sense, the reversibility of the host-guest complexes has been traditionally used in the solubilization and integration of different hydrophobic drugs into nanoparticle systems. However, most of these strategies have been focused on the release and exchange of hydrophobic hosts cargos and, to the best of our knowledge, the release and dynamic exchange between host decorated nanoparticles and hydrophilic peptide guests has not been explored. Here, a potential challenge is the chemical complexity of peptides, which might promote unspecific interactions by electrostatic or van der Waals forces with NPs or any other component. On the other hand, the coating of nanoparticle surfaces with hydrophilic (cationic or anionic) peptides has been mostly approached by using covalent and electrostatic coating protocols, while examples using supramolecular recognition are scarce, with little information reporting the effect of progressive coating to control nanoparticle size and surface potential. This is essential to understand the critical parameters that determine nanoparticle stability. Therefore, in this second chapter, we will explore the incorporation of different guest-bearing hydrophilic peptides, such as polyarginine or oligoglutamic peptides, into *β*-cyclodextrin-functionalized gold nanoparticles (***β*-CD@AuNPs**) driven by host-guest molecular recognition (Figure 69). Moreover, we will construct multi-component nanoparticles with the incorporation of hydrophilic stabilizers such as polyethylene glycol chains. Finally, we will show the facilitated uptake of membrane-impermeable hydrophilic peptides driven by the formation of supramolecular peptide/***β*-CD@AuNP** hybrids. We hypothesized that the functional dynamic guest exchange of hydrophilic biomolecules would be possible inside living cells based on the higher affinity of a multivalent guest, exploiting either statistical rebinding or multivalent binding processes.

The specific objectives of this chapter would be:

- The synthesis of ***β*-CD@AuNPs** by incorporation of per-thiolated-*β*-CD at the AuNP surface and their characterization by TEM, DLS, UV-Visible, and TGA experiments.
- The synthesis of a small library of oligoarginine peptides bearing mono- (**AdR$_4$** and **AdR$_8$**) or divalent (**Ad$_2$R$_4$** and **Ad$_2$R$_8$**) adamantane guests attached. We will exploit the alcoxyamine-aldehyde condensation between peptide and guest respectively. Furthermore, mono- (**AdPEG**) and divalent (**Ad$_2$PEG**) PEG moieties will be also prepared following a similar strategy.
- The integration of these elements into multicomponent nanoparticles and their characterization by size and surface potential measurements. The later will be used to quantify the binding constants between functionalized peptides and ***β*-CD@AuNPs**.
- The exploration of the *in cellulo* guest-bearing peptide exchange due to affinity differences based on guest valency. This will be carried out by first assessing the peptide exchange *in vitro* using fluorescence spectroscopy and later inside living cells by imaging (confocal microscopy experiments) and cell cytometry assays.

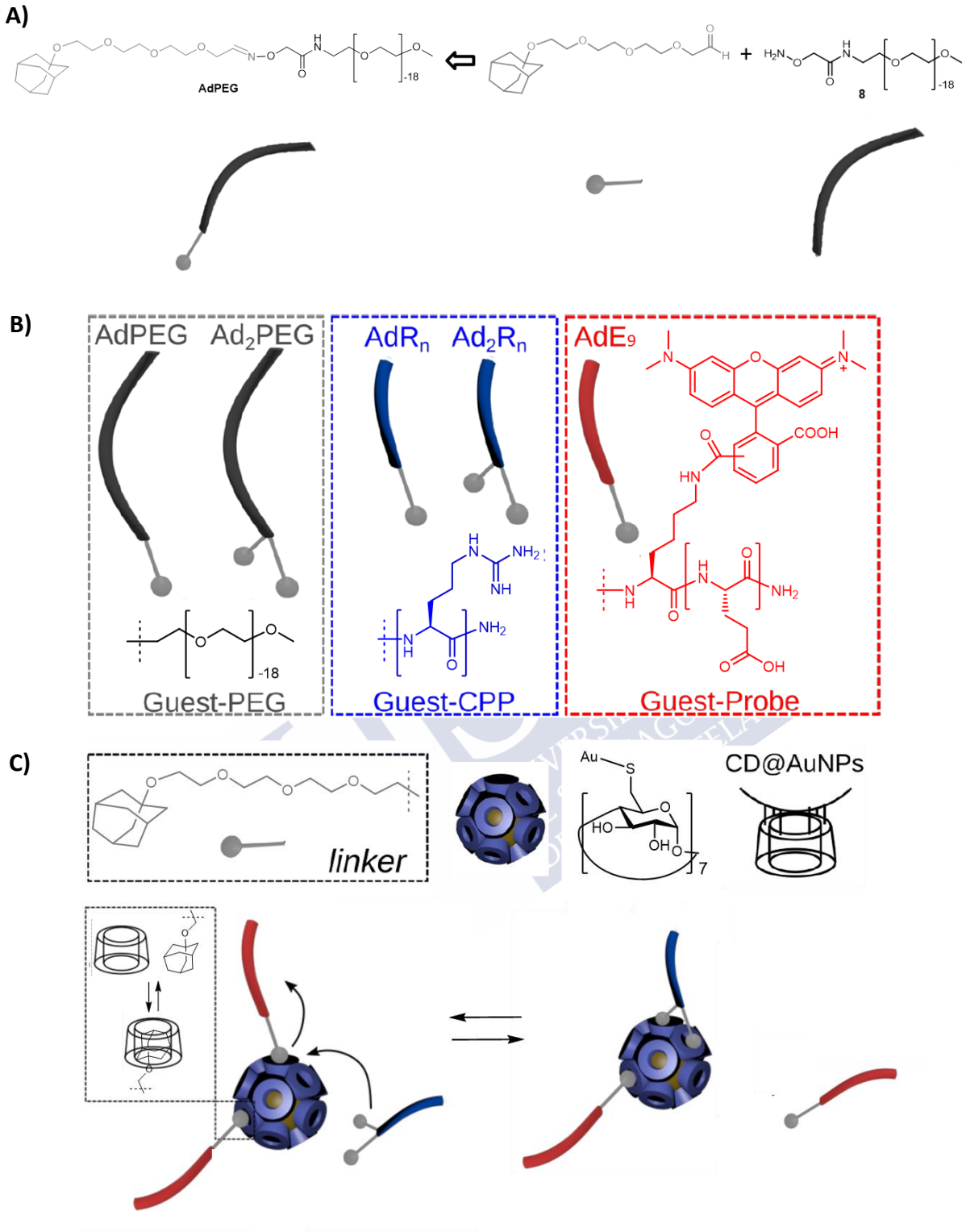

Figure 69. A) Retrosynthetic strategy for the preparation of **AdPEG** exploiting the alcoxyamine-aldehyde condensation between PEG and guest respectively. B) Guest pool composed of monovalent/divalent CPPs (tetra and octarginine based), monovalent/divalent PEG moieties, and monovalent model cargo oligoglutamic peptide (**AdE$_9$**). C) Schematic representation of the incorporation of a monovalent peptide cargo **AdE$_9$** into ***β*-CD@AuNP** leading to the formation of the peptide/***β*-CD@AuNP** supramolecular complex and dynamic exchange between guests according to their valence.

Results and discussions

USC
UNIVERSIDADE
DE SANTIAGO
DE COMPOSTELA

1. Synthesis and characterization of *β*-cyclodextrin-functionalized gold nanoparticles

We started this project by optimizing the conditions for the preparation of the NPs. The ***β*-CD@AuNPs** were prepared following a slightly modified methodology described in the literature.[306] In our procedure, we added a solution of $NaBH_4$ (reducing agent) and per-thiolated-*β*-cyclodextrin[307] in dry DMSO to a solution of $HAuCl_4$ in dry DMSO (Figure 70). During this period, the Au(III) cations were reduced to elementary, coalescing Au(0). Then, nanoparticles were precipitated by adding acetonitrile and collected after centrifugation. Finally, the particles were suspended in water and freeze-dried.

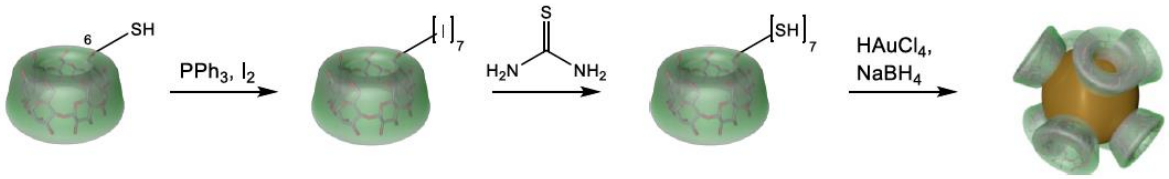

Figure 70. Synthetic pathway for the preparation of ***β*-CD@AuNPs**.

To characterize the ***β*-CD@AuNPs**, we carried out a range of measurements intended to provide information about the physical properties of the particles, as well as the degree of functionalization of the host molecule on the surface. First, we studied the size of the ***β*-CD@AuNPs** by TEM and DLS. TEM micrographs showed the spherical shape and low polydispersity of ***β*-CD@AuNPs** (Figure 71). Image analysis of the particle size distribution evidenced an average nanoparticle size of 2-3 nm (inset Figure 71). DLS experiments of ***β*-CD@AuNPs** suspended in Milli-Q water showed a hydrodynamic diameter of around 8 nm (Figure 71). This discrepancy is based on the fact that DLS measurements are influenced by diffusion factors, such as solvation layers. The UV spectra of ***β*-CD@AuNPs** dispersed in Milli-Q water showed the typical plasmon absorption band for well-dispersed ***β*-CD@AuNPs**.[306] Finally, we used thermogravimetric analysis (TGA) to quantify the amount of organic material at the surface of the prepared ***β*-CD@AuNPs**. The mass loss up to 100°C was attributed to water evaporation, while the weight loss attributed to organic components were observed between 280-320°C. This indicates about 13 % organic material, which would correspond to approximately 20 *β*-cyclodextrins covering each gold nanoparticle (Figure 71). This is in agreement with previous reports.[306]

[306] R. Mejia-Ariza, J. Huskens, *J. Mater. Chem. B* **2014**, *2*, 210-216.
[307] M. T. Rojas, R. Koeniger, J. F. Stoddart, A. E. Kaifer, *J. Am. Chem. Soc.* **1995**, *117*, 336-343.

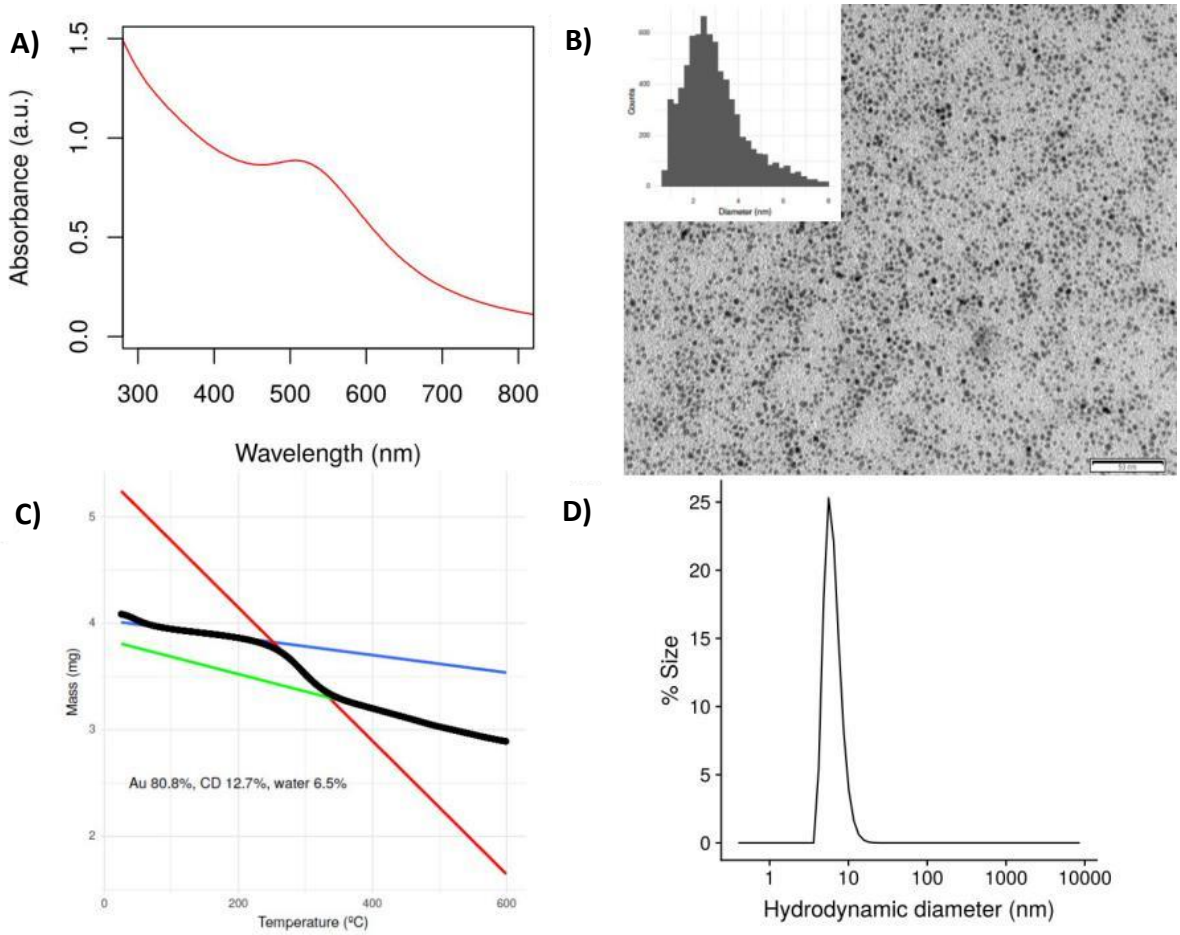

Figure 71. Characterization of ***β*-CD@AuNPs** prepared by the reduction of $HAuCl_4$ in the presence of per-thiol-*β*-CD. A) UV spectra of suspended ***β*-CD@AuNP** in Milli-Q water showing the typical plasmonic absorption band. B) TEM micrographs of the ***β*-CD@AuNPs**. The insert shows the size distribution obtained after image analysis. C) TGA experiments in O_2/N_2 atmosphere of ***β*-CD@AuNPs**. The straight lines were used to calculate the weight changes at different temperatures. D) DLS experiments showing the hydrodynamic diameter of ***β*-CD@AuNPs** expressing the distribution as size percentage.

2. Synthesis of guest-bearing hydrophilic peptides and PEG moieties

Once we prepared and characterized the *β*-CD-functionalized AuNPs, we decided to study the incorporation of mono and divalent guest-bearing hydrophilic peptides and PEG pendants into the surface of these AuNPs. We selected the adamantane (**Ad**) guest due to its high binding constant to *β*-CD receptors.[308] Furthermore, mono- and divalent **Ad** motives were prepared to adjust binding and control dynamic exchange by statistical or multivalent effects. The synthesis of the adamantane-equipped peptides and PEGylated guests was carried out by reaction between guest-bearing aldehydes and the alcoxyamine-modified counterparts (Figure 72). An oxime connection was selected due to its synthetic simplicity and excellent stability at physiological conditions,[309] which gives the possibility to prepare structural modifications with

[308] M. V. Rekharsky, Y. Inoue, *Chem. Rev.* **1998**, *98*, 1875-1918.
[309] J. Kalia, R. T. Raines, *Angew. Chem. Int. Ed.* **2008**, *47*, 7523-7526.

reduced synthetic effort.[90] Monovalent (**2)** and divalent (**4)** aldehydes were synthesized including tetraethylene glycol chains to improve the solubility of the hydrophobic adamantane guests (Figure 72).

Aldehyde **2** was prepared by oxidation of the corresponding alcohol[310] using Swern conditions.[310] Alternatively, aldehyde **4** was prepared by reduction of the nitrile precursor[310] with DIBAL-H, followed by aqueous hydrolysis. Octaarginine and tetraarginine peptides bearing an alcoxyamine moiety (**5** and **6**) were prepared by solid-phase synthesis (Figure 77A) purified by preparative HPLC and condensed with aldehydes **2** and **4** in DMSO at 60 ºC for 2 hours, then purified by precipitation in diethyl ether. This procedure afforded monovalent **AdR$_4$** and **AdR$_8$** and divalent **Ad$_2$R$_4$** and **Ad$_2$R$_8$** peptides (Figure 72B and Figure 77). PEG biocompatible guests (MW ~ 800 Da) were prepared by reaction between the Boc-protected alcoxyamine acetic acid to α-amino ω-methoxy PEG (**7**) followed by carbamate removal in TFA to give **8**. Subsequent coupling of **8** to aldehydes **2** and **4** gave monovalent **AdPEG** and divalent **Ad$_2$PEG** peptide/adamantane hybrids respectively (Figure 72C). Finally, a fluorescently labeled oligoglutamic peptide bearing the adamantane guest moiety (**AdE$_9$**) was synthesized by following the previously described protocol for **AdR$_4$** and **AdR$_8$** (Figure 72D and Figure 77B). Acetylated control peptides **AcR$_4$**, **AcR$_8$**, and **AcE$_9$** were also prepared by standard solid-phase synthesis (Figure 72E).

[90] C. Gehin, J. Montenegro, E. K. Bang, A. Cajaraville, S. Takayama, H. Hirose, S. Futaki, S. Matile, H. Riezman, *J. Am. Chem. Soc.* **2013**, *135*, 9295-9298.
[310] A. Mulder, S. Onclin, M. Péter, J. P. Hoogenboom, H. Beijleveld, J. ter Maat, M. F. García-Parajó, B. J. Ravoo, J. Huskens, N. F. van Hulst, et al., *Small* **2005**, *1*, 242-253.

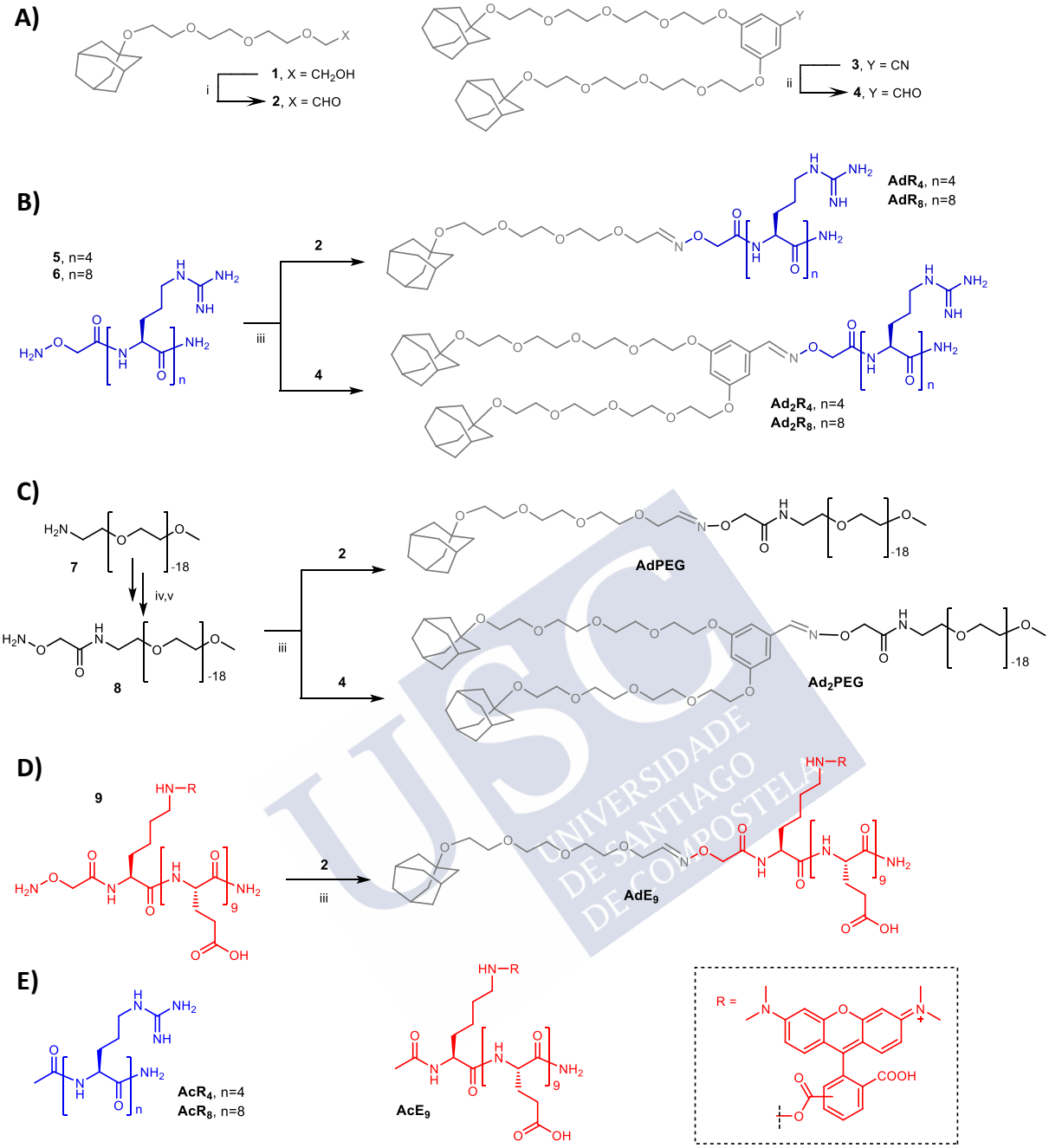

Figure 72. Synthetic scheme for the preparation of peptides and stabilizers incorporated into nanoparticles. A) Preparation of monovalent and divalent adamantane guests bearing an aldehyde function; B) preparation of polyarginine guests by condensation between alcoxyamine-bearing peptides and monovalent and divalent guests; C) preparation of polyethylene glycol stabilizers; D) synthesis of a fluorescently labeled polyglutamic peptide bearing a monovalent guest moiety. R denotes a TAMRA fluorophore; E) control peptides used in this study. Reaction conditions: i) Oxalyl chloride, DMSO, Et_3N, DCM, -70 ºC → r.t., 28 %; ii) DIBAL-H, DCM, silica gel, -40 ºC → 0 ºC, 36 %; iii) Aldehyde, DMSO, 60 ºC, 35-19%; iv) [*tert*-butoxycarbonyl]aminoxy acetic, EDC, DIEA, DMF, r.t., 56%; v) TFA-DCM 1:1, r.t., quantitative.

3. Incorporation of mono and divalent hydrophilic peptides into *β*-CD@AuNPs by using host-guest molecular recognition

Once we prepared and fully characterized the *β*-CD-functionalized AuNPs and the hydrophilic peptides and PEG moieties, first, we decided to study the incorporation of mono and divalent hydrophilic peptides into the surface of these AuNPs. We started the characterization of the host/guest supramolecular system by titrations of the nanoparticle suspensions with the oligoarginine cationic peptides (**AdR$_4$**, **Ad$_2$R$_4$**, **AdR$_8$**, and **Ad$_2$R$_8$**) and following the changes in the surface potential (Figure 73). Control peptides, tetrapeptide **5** and octapeptide **6**, which lack of adamantane moieties, were also included to rule out the unspecific contribution of electrostatic interactions between the prepared negatively charged ***β*-CD@AuNPs** (*ζ*-potential ~ -15 mV at pH ca 7) and the cationic peptides. Thus, the resulting *ζ*-potential data of ***β*-CD@AuNPs** ([*β*-CD] = 10 μM) with increasing concentrations of peptides are shown in Figure 73. The control peptides (**5**, **6**) did not significantly change the surface potential at the concentration range studied, which suggested a minor contribution of unspecific electrostatic interactions (Figure 73, grey points). However, titration of nanoparticles with the adamantyl-modified peptides showed the progressive *ζ*-potential increased from negative to positive values and reaching a plateau, close to +20 mV, at a guest concentration between 10-50 μM. These transitions correlate with the gradual coating of the positively charged peptides at the surface of the nanoparticle. Higher *ζ*-potentials are achieved for octaarginine (**R$_8$**) than tetraargine (**R$_4$**) derivatives, which indicated a higher charge density in the plateau region. However, regardless of the length of the oligoarginine peptide, the *ζ*-potential transition was more pronounced and achieved at lower concentrations when using divalent adamantane binders (e.g. Figure 73A, red *vs* black points), which is consistent with the enhanced affinity of divalent guests.

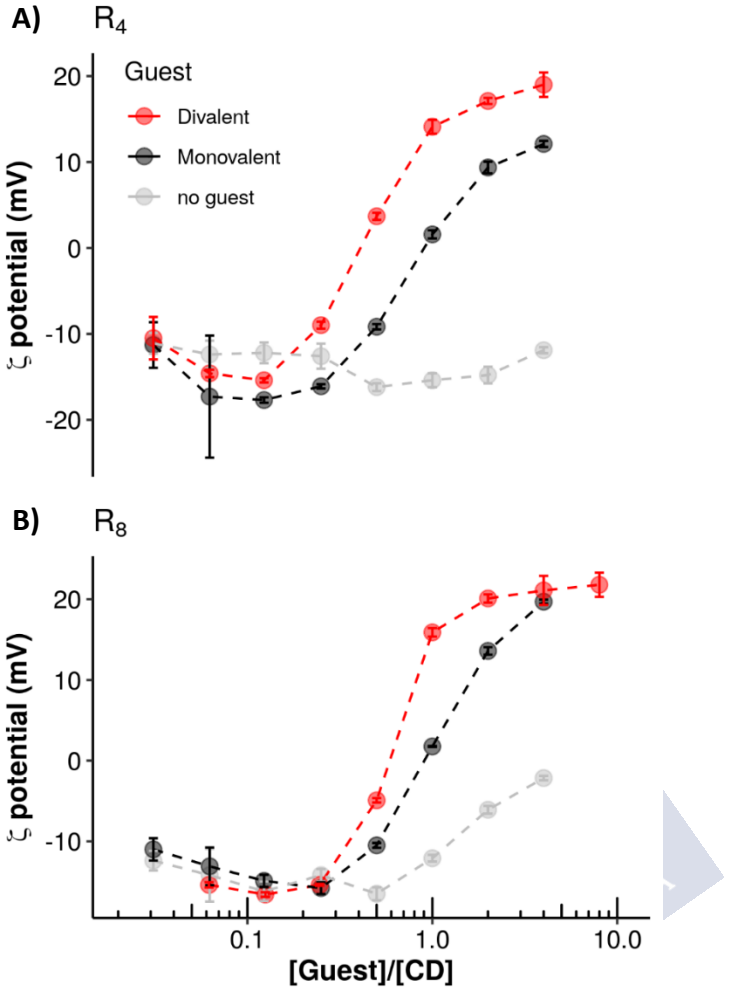

Figure 73. Surface potential measurements of compounds **5**, **6**, **AdR$_4$**, **AdR$_8$**, **Ad$_2$R$_4$**, and **Ad$_2$R$_8$** in the presence of ***β*-CD@AuNPs** at a concentration of 10 μM of *β*-CD in water. Evolution of nanoparticle *ζ*-potential change upon A) addition of **5** (grey circles), **AdR$_4$** (black circles) and **Ad$_2$R$_4$** (red circles) and B) addition of **6** (grey), **AdR$_8$** (black) and **Ad$_2$R$_8$** (red). Error bars denote the standard deviation of 3 measurements.

In order to achieve an estimation of the binding affinity, we fitted the data to a binding model assuming a linear increase of *ζ*-potential with peptide coverage and disregarding potential aggregation effects. Thus, binding affinities of peptides to host surfaces using monovalent and multivalent thermodynamic models could be calculated (Figure 83).[311,312] Table 2 shows the fitting parameters obtained, *K* (*β*-CD/Ad binding constant), C_{ef} the effective molarity,[311], and ζ_{max}, the maximum predicted total charge at full peptide coverage. For monovalent peptides, **AdR$_4$** and **AdR$_8$**, the predicted binding constants (2.0 x 10^5 and 3.5 x 10^4 M^{-1}) diverge from the in-solution *β*-CD/Ad binding constant (in the order of 10^5 M^{-1}) in less than one order of magnitude.[308] Fitting of **Ad$_2$R$_4$** and **Ad$_2$R$_8$** gave plausible individual binding constants (4.5 x 10^4 and 9.3 x 10^4 M^{-1}) with low C_{ef} values (< 0.01 M). The presence of intermolecular electrostatic repulsions could explain this decrease of individual binding

[311] J. Huskens, L. Prins, R. Haag, J. Ravoo, *Multivalency: Concepts, Research and Applications*; Wiley: **2018**.
[312] J. Huskens, A. Mulder, T. Auletta, C. A. Nijhuis, M. J. W. Ludden, D. N. Reinhoudt, *J. Am. Chem. Soc.* **2004**, *126*, 6784-6797.
[308] M. V. Rekharsky, Y. Inoue, *Chem. Rev.* **1998**, *98*, 1875-1918.

affinities. Despite nonlinear effects and aggregation, these fittings strongly support a robust adamantane-*β*-CD@AuNP binding enhanced for the corresponding divalent guests.

Entry	Guest	Model	K (M^{-1})	C_{ef} (M)	ζ_{max} (mV)
1	**AdR_4**	Monovalent	2.0×10^5	-	35
2	**AdR_8**	Monovalent	3.5×10^4	-	63
3	**Ad_2R_4**	Divalent	4.5×10^4	0.001	40
4	**Ad_2R_8**	Divalent	9.3×10^4	2×10^{-5}	44
5	**Ad_2R_4**	Monovalent	1.6×10^6	-	35
6	**Ad_2R_8**	Monovalent	6.4×10^5	-	38

Table 1. Thermodynamic data obtained after fitting the ***β*-CD@AuNP** *ζ*-potential to a monovalent/multivalent thermodynamic model on surfaces. For entries 1, 2, 5, and 6, K and ζ_{max} were used as fitting parameters. In entries 3 and 4, C_{ef} was added as well. Models for entries 3-6 take into account statistical effects.

The reversibility of the binding was tested by the addition of free *β*-CD to the peptide-***β*-CD@AuNP** hybrid particles (Table 2). A drop in the positive *ζ*-potential of the particles, which was especially pronounced for the monovalent guests, confirmed the displacement of the host/guest supramolecular equilibrium.

Conditions	*ζ* -potential (mV)	Sample
without free *β*-CD	19.7	AdR_8
with free *β*-CD	7.7	AdR_8
without free *β*-CD	21.8	Ad_2R_8
with free *β*-CD	15.6	Ad_2R_8

Table 2. *ζ*-potential measurements in the presence or absence of free competing *β*-cyclodextrin. Conditions: 5 mM *β*-CD in HEPES 100 mM; 40 μM peptide, 10 μM *β*-CD as nanoparticles.

4. Multicomponent host-guest *β*-CD@AuNPs by the inclusion of PEG moieties

After studying and confirming the incorporation of mono and divalent hydrophilic peptides into the surface of ***β*-CD@AuNPs** driven by host-guest processes, we next sought to perform a systematic characterization of the multicomponent host/guest supramolecular functionalization of nanoparticle surface by using two different hydrophilic pendants (peptide and PEG) equipped with mono or divalent adamantyl moieties in competition for the particle cyclodextrin hosts at the particle surface (Figure 74).

Biocompatible polymers such as polyethylene glycol (PEG) are frequently employed to prevent particle surface coating with proteins present in the biological medium.[313] To test the effect of PEG pendants in the ***β*-CD@AuNPs**, we synthesized a ~ 700 Da molecular weight PEG that we equipped with mono and divalent adamantane guest moieties. To study the size and surface charge properties of the colloid suspensions of ***β*-CD@AuNPs** we performed titrations with different molar ratios of the peptide (**AdR_8** and **Ad_2R_8**) and the PEG (**AdPEG** and **Ad_2PEG**) hydrophilic pendants. These hydrophilic guest components were mixed at different stoichiometric proportions at a fixed *β*-CD concentration (in the surface of the nanoparticles) and allowed to equilibrate for at least one hour. Dynamic light scattering and *ζ*-

[313] B. Pelaz, P. del Pino, P. Maffre, R. Hartmann, M. Gallego, S. Rivera-Fernández, J. M. de la Fuente, G. U. Nienhaus, W. J. Parak, *ACS Nano* **2015**, *9*, 6996-7008.

potential measurements were carried out on these mixtures. The resulting data of this systematic analysis allowed us to draw several conclusions (Figure 74). First, we observed two potential molar fractions areas where the *β*-CD nanoparticles are coated with the cationic peptide with reduced NP aggregation, which correspond to the addition of low equivalents of cationic peptides ([Peptide]/[CD] < 0.3, Figure 74A, all panels), or addition of higher amounts of the divalent adamantane guest peptide **Ad$_2$R$_8$** ([Peptide]/[CD] > 1, Figure 74A, panel top right). While in the first case little changes on surface potential and size are observed (ζ < 0), in the second, a positive surface potential (> +15 mV) is reached. These stability zones are strongly correlated with a surface potential threshold of ζ < -10 mV and ζ > +15 mV (Figure 74), and particles allocated below this threshold experienced uncontrolled aggregation. From this we conclude that the generation of highly charged particles in equilibrium conditions was required, although not sufficient, to achieve colloidal stable particle suspensions. It was also confirmed that higher guest valence (di > mono) had a beneficial impact on the stabilization of the ***β*-CD@AuNPs**. In the absence of the PEG stabilizer, **AdR$_8$** failed to achieve particle suspension stabilization even at higher concentrations of the peptide, while increasing concentrations of **Ad$_2$R$_8$** stabilized the nanoparticle suspensions (Figure 74A). In comparison, the contribution of PEG stabilizers showed a less marked impact; for example, competition between **AdR$_8$** and **Ad$_2$PEG** revealed that although the surface charge of the nanoparticle is modulated by the stoichiometric amount of **Ad$_2$PEG**, aggregation is observed at all concentrations of **AdR$_8$** (see Figure 74A bottom left block, Figure 79). This suggests that steric stabilization plays a minor role. Importantly, only when colloidal stabilization is achieved by electrostatics, the addition of PEG pendants could be employed to modulate the aggregation of the particle suspensions (Figure 74B, C, extracted from values from the right top panel). For example, when the molar ratio of divalent peptide guest against cyclodextrin host is close to 2 ([**Ad$_2$R$_8$**]/[CD] = 1.8), the addition of one equivalent of the monovalent polyethylene glycol ([**AdPEG**]/[CD] = 1) allows the decrease of the size of colloidal aggregates (56 nm to 23 nm, Figure 74B, purple line). Note that in all these points, the ζ-potential always remains above + 15 mV. On the other hand, at a low molar ratio of the divalent peptide guest against cyclodextrin [**Ad$_2$R$_8$**]/[CD] = 0.1 and with more than 2 equivalents of the monovalent PEG ([**AdPEG**]/[CD] = 2.5), the hydrodynamic radius is also decreased, while the ζ-potential becomes less negative that nanoparticles in the absence of PEG, which indicates PEG incorporation on the peptide ***β*-CD@AuNPs** (Figure 74B-C, green and red line). Importantly, the previously described strategy allowed us to control the size of nanoparticle clusters, which were in a good range (10-100 nm) to trigger cell internalization and nanoparticle uptake by endocytic mechanisms.

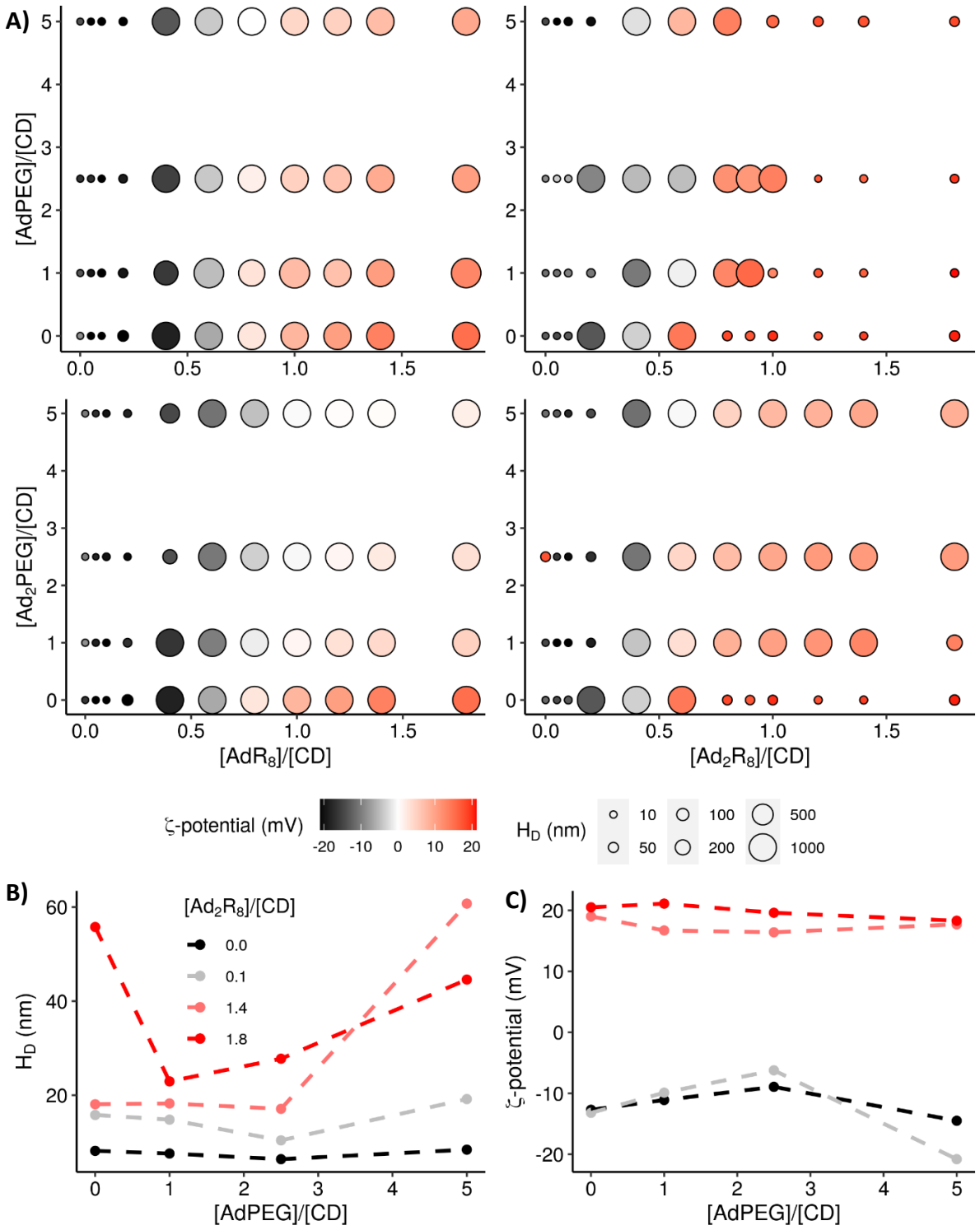

Figure 74. A) Comparative plots showing hydrodynamic diameter and nanoparticle surface potential upon the formation of multicomponent ***β*-CD@AuNPs** by the combination of **AdPEG**, **Ad$_2$PEG**, **AdR$_8$**, and **Ad$_2$R$_8$**. Point size is scaled to the nanoparticle size, while point fill color represents the surface potential. The total concentration of *β*-CD in solution is 10 µM; modulation of B) hydrodynamic diameter and C) ***ζ*-potential of *β*-CD@AuNPs** (10 µM in *β*-CD) at different concentrations of **Ad$_2$R$_8$** and **AdPEG** in colloidal stability zones.

5. Guest exchange *in vitro* and inside living cells

As we have previously mentioned in the introduction of this chapter, the control over the physicochemical properties of the nanoparticle suspensions in terms of size, charge, and ligand distribution can be employed to modulate cellular uptake, biocompatibility, and drug release. To test host/guest dynamic exchange at the surface of nanoparticles in aqueous environment and inside living cells, we employed a strongly anionic membrane-impermeable oligoglutamic peptide **AdE$_9$** equipped with a monovalent adamantane guest and a TAMRA fluorophore (Figure 77 and Figure 72). In this model cargo, the probe fluorescence would be quenched/dequenched upon binding/debinding of the peptide (**AdE$_9$**) to the gold nanoparticles (***β*-CD@AuNPs**).[298]

In vitro control fluorescence experiments showed that the addition of increasing amounts of ***β*-CD@AuNPs** to a solution of **AdE$_9$** at constant concentration resulted in a decrease of the TAMRA emission band (Figure 75C). Additionally, DLS analysis of the **AdE$_9$⊂*β*-CD@AuNP** complexes showed a slight increase of hydrodynamic diameter (from ~ 8 to 10 nms) and a decrease of ***ζ*-potential** (from ~ -12 to -20 mVs), which supports the coating of the nanoparticle surface with the anionic peptide (Figure 75A and B). Furthermore, analogous DLS experiments in DMEM indicated the stability of the resulting colloidal complexes **AdE$_9$⊂*β*-CD@AuNP** in suitable media for cell experiments. On the other hand, to test the peptide exchange capabilities of the system, *in vitro* control fluorescence experiments were carried out. In these experiments, we found that the addition of increasing concentrations of **Ad$_2$R$_8$** to a constant solution of the preformed complex **AdE$_9$⊂*β*-CD@AuNP** resulted in an increase of the TAMRA fluorescence, which is attributed to **AdE$_9$** peptide displacement from its binding to the nanoparticle (Figure 75D). Comparatively, the addition of control peptide **AcR$_8$** did not result in fluorescence increase, but a decrease that might be due to particle aggregation (Figure 81).

[298] C. Park, H. Youn, H. Kim, T. Noh, Y. H. Kook, E. T. Oh, H. J. Park, C. Kim, *J. Mater. Chem.* **2009**, *19*, 2310-2315.

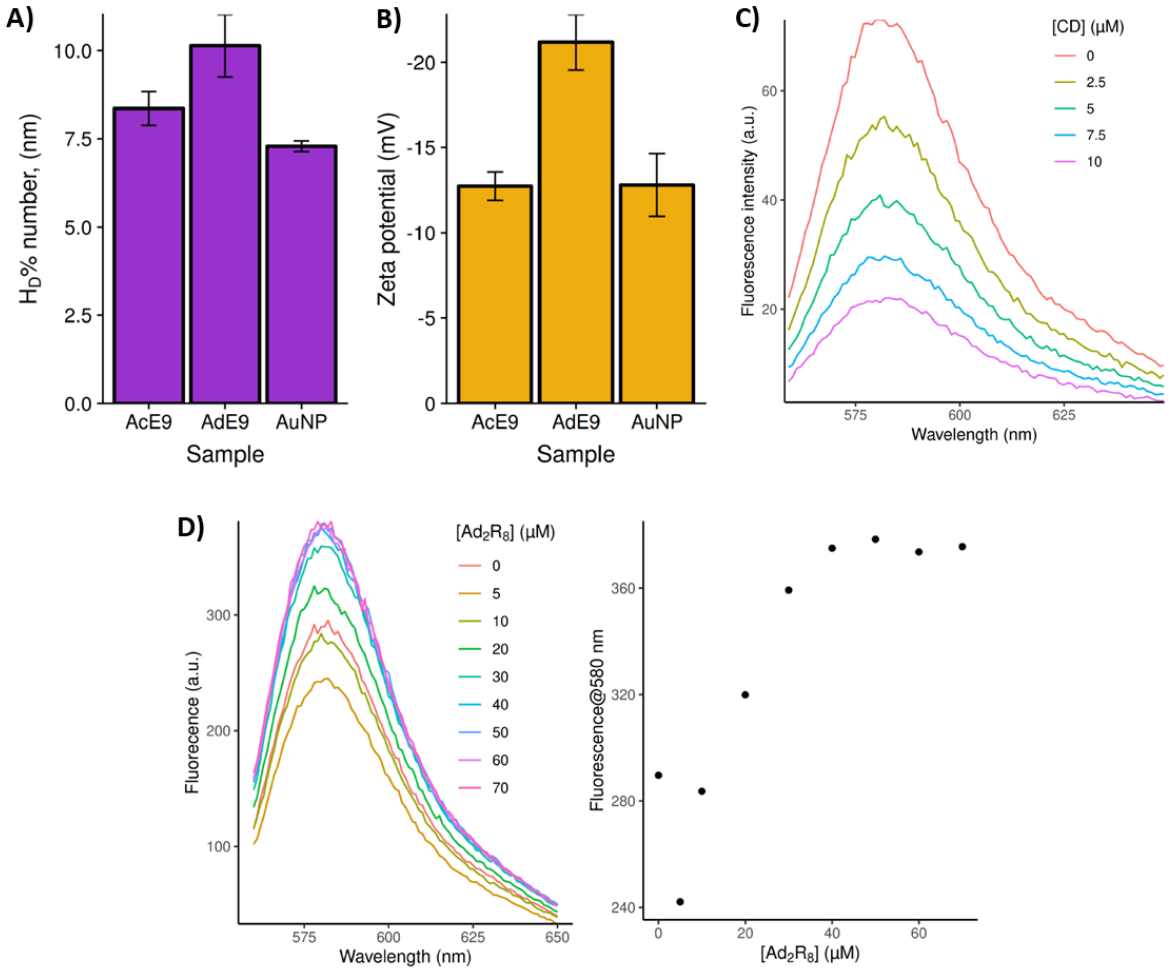

Figure 75. *In vitro* peptide/***β*-CD@AuNPs** complex formation and exchange experiments. A) DLS and B) ***ζ***-potential of nanoparticles formed between compounds **AdE$_9$** and control peptide **AcE$_9$** and ***β*-CD@AuNP**. The concentration of *β*-CD and peptides were 10 μM. Data represent the average of 3 measurements, where the error bars denote the standard deviation. C) Addition of ***β*-CD@AuNPs** to **AdE$_9$** at a concentration of 10 μM. λ_{ex} = 553 nm. D) Exchange of peptide **AdE$_9$** at ***β*-CD@AuNP** (concentration in *β*-CD and **AdE$_9$** was 5 μM) by peptide **Ad$_2$R$_8$.**

Once we confirmed *in vitro* the **AdE$_9$⊂*β*-CD@AuNPs** complex formation and peptide exchange, we decided to explore the potential ***β*-CD@AuNPs**-mediated peptide delivery and exchange in living cells (Figure 76A, B, and C). We initially confirmed that the oligoglutamic peptide **AdE$_9$** in the absence of ***β*-CD@AuNPs** was not capable of crossing the cell membrane (Figure 76D). As it would be expected, the corresponding fluorescence confocal images showed a very low internalization of the anionic **AdE$_9$** in the absence of the nanoparticle vehicle (Figure 76D). However, confocal micrographs of HeLa cells revealed that, when the **AdE$_9$** peptide was incubated with the cyclodextrin bearing nanoparticles (***β*-CD@AuNPs**), the resulting host/guest supramolecular complexes were readily internalized into cells (Figure 76D). Fluorescence signal accumulated mostly in endosomes confirmed the energy-mediated uptake of the nanosized host/guest complexes (Figure 76D). Having confirmed the controlled internalization of the supramolecular peptide/particle complexes, we tested the potential dynamic exchange of the peptide guests inside cells. HeLa cells were first incubated with the peptide/particle complexes and after confirming the uptake of the **AdE$_9$⊂*β*-CD@AuNP** complexes, the cells were washed and incubated with a penetrating peptide equipped with two

adamantane guests **Ad_2R_4** or **Ad_2R_8**. Confocal microscopy and flow cytometry evidenced the strong increase of fluorescence signal confirming the cationic peptide internalization and selective dynamic guest displacement inside cells (Figure 76C, D, and experiments in the absence of cells in Figure 75). The addition of the acetylated control peptide **AcR_8** without adamantane moiety did not result in fluorescence increase, which ruled out electrostatics and confirmed the dynamic host/guest supramolecular exchange of peptide pendants inside living cells (Figure 76F, control experiments in the absence of cells in Figure 81). The corresponding MTT assays revealed negligible toxicity in all cases (Figure 82) that discharges the potential toxicity interference. Increasing concentrations of the penetrating peptides **Ad_2R_4** or **Ad_2R_8** confirmed a dose-response effect in the increase of the fluorescence signal, as shown by confocal fluorescence images (Figure 76D) and flow cytometry experiments (Figure 76F). Again control experiments with the acetylated cationic peptide **AcR_8** showed a minor increase of fluorescence (Figure 76F).

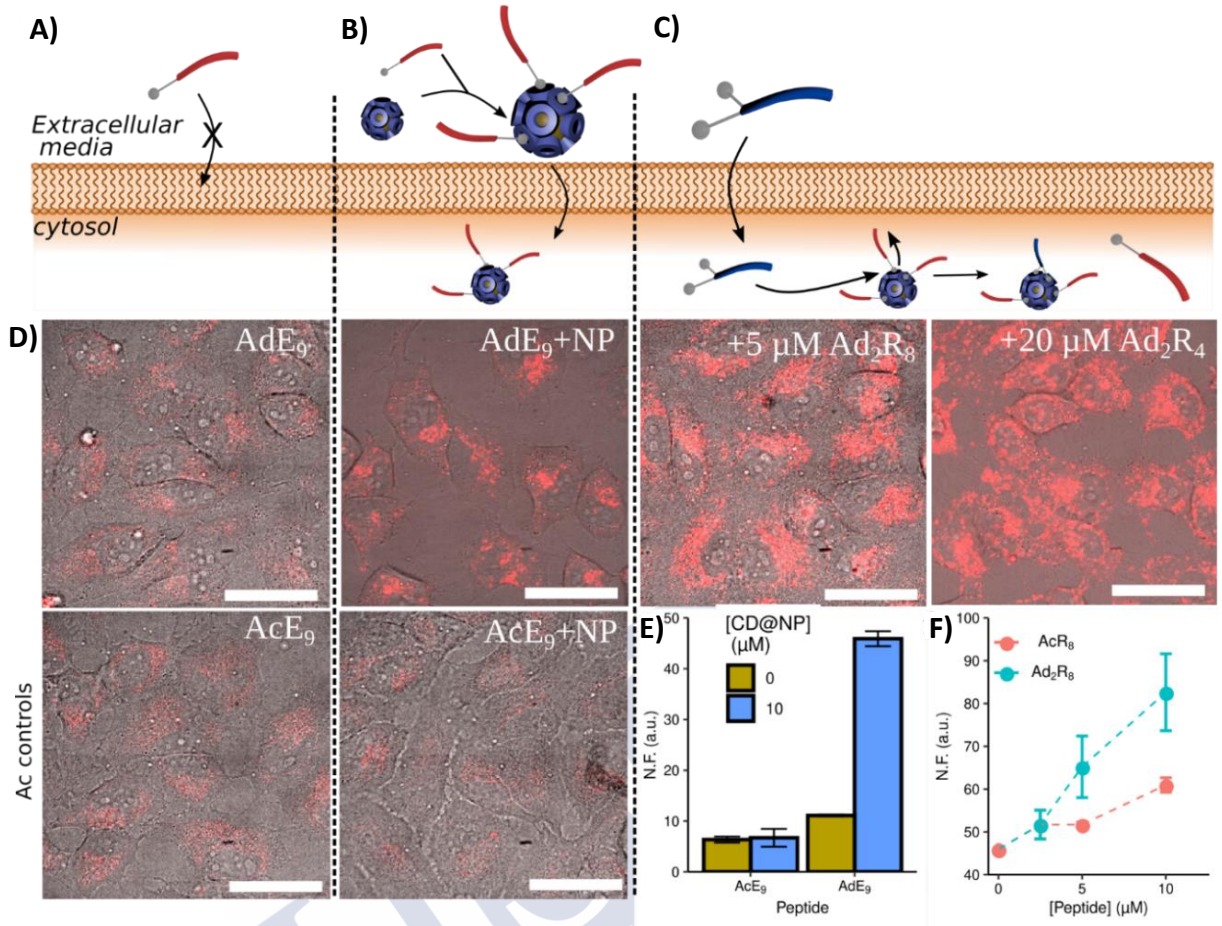

Figure 76. Uptake and exchange of guests inside living cells. Uptake experiments were carried out in the absence of serum. A) bare **AdE$_9$** was not uptaken by the cell. B) Uptake of **AdE$_9$** was triggered by the addition of ***β*-CD@AuNPs** to the cell medium containing the monovalent guest molecule; C) after uptake, a second divalent peptide (**Ad$_2$R$_8$**) was added and displaced the equilibria to the release of the first peptide inside the cell; D) Confocal images of cells after incubation with peptides **AdE$_9$** and **AcE$_9$** in the presence or absence of ***β*-CD@AuNPs**, as well as after the addition of **Ad$_2$R$_8$**. Scale bars denote 40 µm; E) Flow cytometry of HeLa cells populations after internalization of peptides **AdE$_9$** and control peptide **AcE$_9$** in the presence (blue bars) or absence (yellow bars) of ***β*-CD@AuNPs** at a concentration of 10 µM in the *β*-CD moiety. Fluorescence of control cells was substracted to all measurements; F) Cell cytometry after the addition of peptide (**Ad$_2$R$_8$**, blue points) and control peptide (**AcR$_8$**, red points) to cells containing uptaken **AdE$_9$⊂*β*-CD@AuNP** complexes. In all conditions, data is plotted as an average of three wells and error bars denote their standard deviation. Dashed lines are added for eye guidance only.

USC
UNIVERSIDADE
DE SANTIAGO
DE COMPOSTELA

Conclusions

USC
UNIVERSIDADE
DE SANTIAGO
DE COMPOSTELA

In this chapter, we have developed a supramolecular strategy for the incorporation of hydrophilic (cationic and anionic) peptides into ***β*-CD@AuNPs** by using host-guest supramolecular processes. We have shown that the incorporation of neutral guests (**AdPEG** and **Ad$_2$PEG**) can be used to modulate the nanoparticle properties within formulation stability zones. Moreover, applying this strategy, we were able to promote the intracellular delivery of membrane-impermeable anionic peptides by the formation of supramolecular **peptide⊂CD@AuNP** hybrids and to carry out the dynamic exchange of hydrophilic peptides inside living cells using cationic penetrating peptides equipped with higher valence guest.

In this second chapter,

- We prepared ***β*-CD@AuNPs** showing a hydrodynamic diameter of around 8 nm bearing an average of 20 *β*-CD per nanoparticle and we synthesized a library of hydrophilic mono (**AdR$_4$** and **AdR$_8$**) and divalent ligands bearing CPPs (**Ad$_2$R$_4$** and **Ad$_2$R$_8$**).
- We studied the incorporation of these mono and divalent peptides into ***β*-CD@AuNPs** by *ζ*-potential experiments and we found that specific host-guest interaction is the main driving force for the binding of polyarginine peptides composed of 4 or 8 arginine units, where peptides lacking guest moieties did not show important coating at the working concentrations. We also quantified the binding constants between guest-functionalized peptides and ***β*-CD@AuNPs**, where apparent binding constants suggest rather a statistical rebinding or internanoparticle interactions than a purely multivalent binding.
- We synthesized and characterized mono and divalent PEG moieties and we constructed multicomponent nanoparticles formed by guest-functionalized peptides and PEG. Their characterization was performed by size and surface potential measurements. We found that the incorporation of these PEG moieties allowed a controlled aggregation effect when used in the corresponding electrostatically stable zones.
- Finally, we demonstrated the cellular internalization of the membrane-impermeable anionic peptide (**AdE$_9$**) after complexation with ***β*-CD@AuNPs**. We confirmed the exchange of the hydrophilic peptide **AdE$_9$** with peptides with higher valence guests such as **Ad$_2$R$_8$** not only *in vitro* using fluorescence experiments but also inside living cells by using confocal microscopy experiments and cell cytometry assays. These findings suggest that multivalent competition could be used as a strategy for the release of cargos within cells in dynamic host-guest nanomaterials.

USC
UNIVERSIDADE
DE SANTIAGO
DE COMPOSTELA

Experimental section

USC
UNIVERSIDADE
DE SANTIAGO
DE COMPOSTELA

1. Experimental procedures

1.1. Materials and methods

Reagents were acquired from Fluka, Aldrich, Iris Biotech, or TCI. Chemical shifts (δ) are reported in ppm relative to TMS ($\delta = 0$). All spectra were normalized with respect to the residual solvent signal. Infrared spectra were acquired in a PerkinElmer Spectrum Two ATR. Analytical HPLC was carried out in an Agilent 1260 Infinity II equipped with an Agilent SB-C18 column and connected to a 6120 Quadrupole LCMS. HR-MS was acquired in a Bruker Microtof. Derivatives **1** and **3** were prepared as described in the literature.[310]

Synthesis of *β*-CD covered gold nanoparticles (*β*-CD@AuNPs). ***β*-CD@AuNPs** were prepared following an adapted procedure.[306] To a solution of $HAuCl_4$ (100 mg, 255 μmol) in dry DMSO (10 mL), a solution of $NaBH_4$ (133 mg, 3.5 mmol) and per-thiol-*β*-CD[307] (33 mg, 26 μmol) in dry DMSO (10 mL) was quickly added. The reaction turned dark immediately and the mixture was stirred overnight. Nanoparticles were precipitated by adding acetonitrile (40 mL) and the particles were collected after centrifugation, followed by washing with acetonitrile-DMSO 1:1 (40 mL, × 3), then the particles were suspended in water and freeze-dried.

Thermogravimetric analysis. For thermogravimetric analysis, 6-7 mg of freeze-dried ***β*-CD@AuNPs** were used for combustion. Samples were analyzed in a TGA Q5000 (TA instruments) using the following parameters: temperature ramp: 10 °C/min; temperature range: 25-600 °C; gas flow of a mixture of air (50 mL/min) and nitrogen (10 mL/min) flow.

Dynamic Light Scattering and *ζ*-potential measurements. DLS measurements were carried out in a Malvern Zetasizer Nano. Buffers were filtered through a 0.45 μm syringe filter. Size measurements were carried out with the following specification: sampling time, automatic; number of measurements, 3 per sample; medium viscosity, 1.054 cP; scattering angle, 173 °; temperature, 25 °C. Values were given as a number distribution of the major population.

Fluorescence spectroscopy experiments. Fluorescence measurements were carried out in a Varian Cary Eclipse fluorescence spectrophotometer. Fluorescence spectra were acquired at 20 °C with an averaging time of 0.5 s.

1.2. Cell experiments

Cell lines and culture. HeLa cell line was maintained at 37 °C, 5% CO_2, 95 % humidity, in Dulbecco's Modified Eagle's Medium (4500 mg/L glucose, L-glutamine, sodium pyruvate, and sodium bicarbonate), supplemented with 10% fetal bovine serum and 1% of Penicillin-Streptomycin-Glutamine Mix, and kept in an INCO108 incubator (Memmert).

Cell uptake and exchange experiments. HeLa cells seeded the day before on glass-bottom dishes were washed with DMEM (Dulbecco's Modified Eagle's Medium (DMEM, 4500 mg/L glucose, L-glutamine, sodium pyruvate, and sodium bicarbonate) without serum, antibiotics, and phenol red and incubated for 30 min with 10 μM ***β*-CD@AuNPs** in combination with 10 μM of the guest-anchored peptide in DMEM. This solution was removed and cells were

[310] A. Mulder, S. Onclin, M. Péter, J. P. Hoogenboom, H. Beijleveld, J. ter Maat, M. F. García-Parajó, B. J. Ravoo, J. Huskens, N. F. van Hulst, et al., *Small* **2005**, *1*, 242-253.
[306] R. Mejia-Ariza, J. Huskens, *J. Mater. Chem. B* **2014**, *2*, 210-216.
[307] M. T. Rojas, R. Koeniger, J. F. Stoddart, A. E. Kaifer, *J. Am. Chem. Soc.* **1995**, *117*, 336-343.

washed two times with DMEM. Then, cells were incubated for another 30 min with the peptide in DMEM at the concentrations indicated in the corresponding Figure. Later, cells were washed once with DMEM and examined on the confocal microscope.

Flow cytometry. HeLa cells seeded the day before at 10.000 cells/well of a 96-well plate, were treated for 30 min with the preformed complex of 10 μM of ***β*-CD@AuNPs** and 10 μM of **AdE$_9$** diluted in DMEM without serum, antibiotics, and phenol red. Cells were then washed (2 ×) with DMEM and incubated with the divalent peptide (**Ad$_2$R$_4$** and **Ad$_2$R$_8$**) for 30 min at the different concentrations in DMEM at 37 °C. After the incubation, cells were washed with DMEM and trypsinized.

As controls, 10 μM ***β*-CD@AuNPs** in the presence or absence of 10 μM **AdE$_9$** or **AcE$_9$** diluted in DMEM were also performed. After 60 min of incubation, cells were washed with DMEM and trypsinized. Trypsin was neutralized with 2 % FBS in PBS with 5 mM EDTA and cell fluorescence was measured on a Guava EasyCyteTM(Millipore) cytometer using a green laser (532 nm) collecting the emission at 575/25 nm (TAMRA).

Cells with typical FSC and SSC parameters were selected and the median fluorescence intensity (MFI) was calculated for each sample. Each condition was done 4 times. In all cases, data analysis was performed with InCyte software included in GuavaSoft 3.2 (Millipore).

Toxicity quantification by MTT assays. To evaluate the toxicity of the treatment of cells with ***β*-CD@AuNPs** (10 μM) and **AdE$_9$** (10 μM) and the following incubation with the different peptides in DMEM without serum, antibiotics, and phenol red. HeLa cells were submitted to an MTT assay 1 hour after the incubation. One day before the assay, a suspension of HeLa were plated in 96-well tissue culture plates by adding 100 μL (10.000 cells) per well. The day after, the medium was removed and cells were incubated in DMEM in the presence of different conditions at different concentrations (50 μL/well) during 1 hour of incubation at 37 °C. After the incubation, DMEM with the compounds was removed, pre-warmed DMEM containing 10 % FBS, and MTT (5 mg/mL in PBS, 10 μL/well) was added to the wells and the cells were further incubated for 2 h. The supernatant was carefully removed and the water-insoluble formazan salt was dissolved in DMSO (100 μL/well). The absorbance at 570 nm was measured with an Infinite F200Pro Plate reader. Data points were collected 4 times and expressed as normalized values for untreated as control cells (100%) after blank subtraction.

1.3.Synthesis of new derivatives

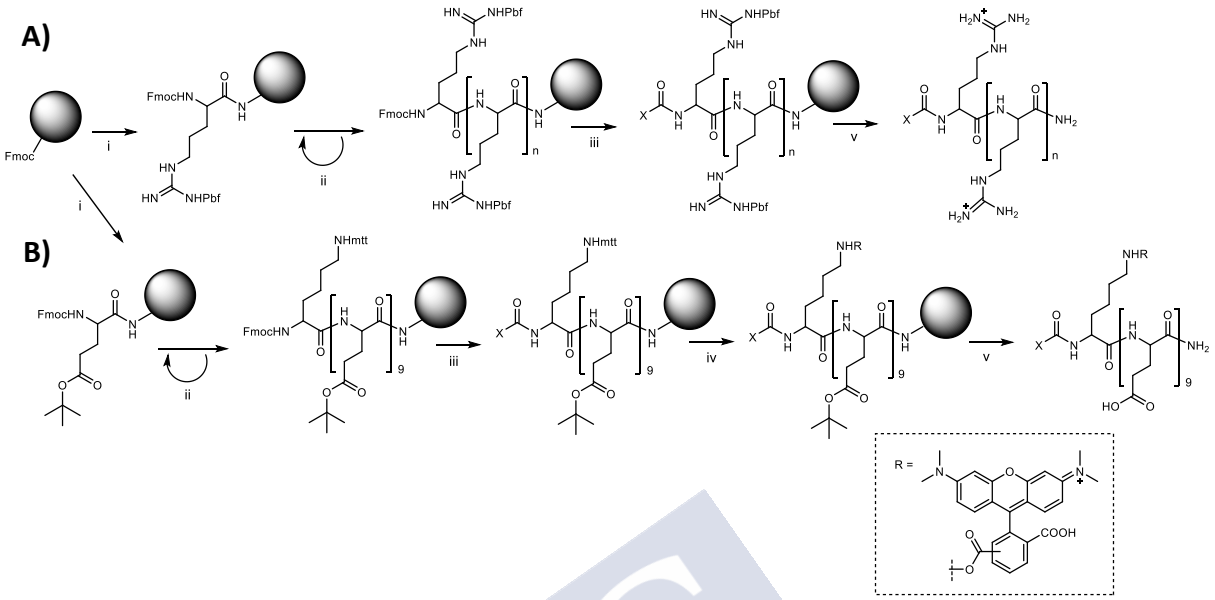

Figure 77. Schematic representation of solid-phase synthesis of peptides used in this study. A) Preparation of polyarginine derivatives with n = 3 or 7); B) Preparation of labeled polyglutamic derivatives. Reagent and conditions: i) 1) piperidine/DMF (20%), 10 min, 2) aminoacid, *N*-HBTU, DIEA, DMF, 30 min; ii) 1) piperidine/DMF (20%), 10 min, 2) aminoacid, *N*-HBTU, DIEA, DMF, 30 min, repeated sequentially; iii) 1) piperidine/DMF (20%), 10 min, 2) BocHNOCH$_2$COOH , *N*-HATU, DIEA, 45 min (→ X = CH$_2$ONHBoc) or 2) acetic anhydride-1,6-lutidine 1:1, 45 min (→ X = CH$_3$); iv) 1) DCM/HFIP/TFE/TIS (6.5:2:1:0.5), 1 h. ×2, 2) 5-Carboxytetramethylrhodamine, *N*-HBTU, DIEA, DMF, 45 min.; v) TFA-DCM-H$_2$O-TIS 0.9:0.05:0.025:0.025, 2 h (→ X = CH$_2$ONH$_2$ or CH$_3$).

General procedure for the preparation of linear peptides. Peptides were prepared manually by solid-phase synthesis as depicted in Figure 77. Fmoc-Rink Amide AM resin (135 mg, 0.1 mmol, 0.74 mmol/g loading) were soaked in DMF (3 mL) for 30 min. The Fmoc group was removed by treatment with piperidine/DMF (1:4, 2-3 mL) for 10 min. The resin was washed with DMF (6 mL) and then treated with a solution of Fmoc-protected amino acid (0.3 mmol), *N*-HBTU (113 mg, 0.3 mmol), and DIEA (100 μL, 0.6 mmol) in DMF (3 mL). The resin was shaken for 30 min and then washed with DMF (3 mL × 3). After the coupling of the last amino acid, the Fmoc was removed as described above, and a solution of (Boc-aminoxy)acetic acid (96 mg, 0.5 mmol) and *N*-HATU[314](188 mg, 0.5 mmol) in DMF (1 mL) was added to the resin followed by the dropwise addition of DIEA (84 μL, 0.5 mmol) in DMF (1 mL). The resulting mixture was mechanically shaken for 45 min and finally, the resin was washed with DMF (3 ×, 3 mL).

For acetylation, the resin was treated with 2,6-lutidine-acetic anhydride 1:1 (2 mL) for 45 min, then the resin was washed with DCM (3 ×) and DMF (3 ×).

For the selective removal of the 4-methyltrityl group, the resin was washed with DCM (3 ×, 4 mL) and then treated with a mixture of DCM/HFIP/TFE/TIS (6.5:2:1:0.5, 3 mL). After shaking for 1 h., the mixture was filtered off and washed with DCM (3 ×, 3 mL). This process was repeated in the same conditions and finally, the resin was washed with DCM (3 ×, 3 mL) and DMF (3 ×, 3 mL). For the coupling of TAMRA fluorophore, was carried out by dissolving

[314] A. El-Faham, F. Albericio, *Chem. Rev.* **2011**, *111*, 6557-6602.

5-Carboxytetramethylrhodamine (52 mg, 1.2 mmol, 1.2 equiv.), *N*-HBTU (44 mg, 1.2 mmol, 1.2 equiv), and 20 μL DIEA (1.2 mmol, 1.2 equiv.) in 3 mL DMF. This was added to the resin, and it was stirred for 45 min. Then the resin was washed with DMF (3 times) and DCM (3 times). The peptide was released from the resin by treatment with a freshly prepared cleavage cocktail (TFA-DCM-H_2O-triisopropylsilane, 0.9:0.05:0.025:0.025, 3 mL) for 2 h and then filtered. The resin was washed with TFA (0.5 mL) and the combined acidic solutions were evaporated to 1-2 mL by bubbling argon. The concentrated solution was added dropwise to cold diethyl ether (10 mL diethyl ether/mL TFA). The resulting precipitate was centrifuged for 10 min at 3000 rpm. The supernatant was discarded, then fresh diethyl ether was added and the suspension was sonicated for 1 min and centrifuged. The sample was dried with a stream of air and dissolved in Milli-Q water and purified by semipreparative HPLC using a C18 column.

General procedure for the condensation between aldehydes and oximes. The corresponding alcoxyamine and aldehyde (1.2-2 equiv) were mixed in 100 μL DMSO in an eppendorf. The solution was stirred at 60 °C for 2 h. Then the solution was cooled down, and diethyl ether was added (≈ 2 mL) and vigorously shaken. The precipitated was centrifuged and the solution discarded. Fresh diethyl ether was added and the mixture was sonicated for 10 min, then centrifuged and decanted. This procedure was repeated 3 times. Then, the powder was dried at high vacuum. The yield was between 35-19% Compounds **AdPEG** and **Ad$_2$PEG** were purified by preparative HPLC using a gradient of H_2O-ACN (0.1 % TFA) 50:50 → 0:100 in 20 min.

Synthesis of 2. Oxalyl chloride (0.5 mL, 6 mmol, 1.3 equiv.) was dissolved in dry DCM (7 mL) and cooled down to -70 °C under Ar atmosphere. Then DMSO (0.9 mL) in DCM (4 mL) was added dropwise and the reaction mixture was stirred for 30 min below -65 °C. Compound **1** (1.5 g, 4.5 mmol) in DCM (18 mL) was slowly added and the reaction was further stirred 1 h below -65 °C. Finally, Et_3N (3.5 mL, 25 mmol, 5.6 equiv.) was added and the reaction was stirred for 2 h at -65 °C then allowed to heat up to room temperature. Over the course of the reaction, a white precipitated was formed. Water (10 mL) was added and the mixture was stirred until the salts were dissolved. The organic layer is decanted and the aqueous phase was extracted with DCM (3 ×). The combined organic layers were washed with water, then dried ($MgSO_4$), filtered, and concentrated to give a yellow solid. The crude was purified by column chromatography in AcOEt-petroleum ether 3:1 to give a colorless oil. Yield: 410 mg (28 %). ^{1}H NMR (300 MHz, $CDCl_3$, 298 K) δ: 9.73 (s, 1 H), 4.17 (s, 2 H), 3.80-3.55 (m, 12 H), 2.14 (s, 3 H), 1.75 (bs, 6 H), 1.62 (bs, 6 H); ^{13}C NMR (300 MHz, $CDCl_3$, 298 K) δ: 201.0, 76.8, 72.3, 71.3, 71.2, 70.7, 70.6, 70.5, 59.2, 41.4, 36.4, 30.5; HR-MS calculated for $C_{18}H_{31}O_5^+$: 327.2166, found: 327.2166.

Synthesis of 4. Glassware was dried in the oven overnight. A solution of **3** (50 mg, 0.07 mmol) in freshly distilled DCM was cooled down to -70 °C. Then DIBAL-H (0.73 mL, 1 M in methylene chloride, 0.073 mmol, 1.1 equiv.) was added dropwise. The solution was allowed to warm to -40 °C over a period of 1 h. Hydrolysis was effected by slowly adding a homogeneous mixture of 100 mg silica gel and 1 mL water. After stirring for 1 h at 0 °C, K_2CO_3 and $MgSO_4$ were added, the solids were filtered off and rinsed thoroughly with dichloromethane and diethyl ether. The solvents are evaporated under reduced pressure. The residue is purified by column chromatography (AcOEt-petroleum ether 3:1 → AcOEt). The compound was a colorless oil. Yield: 18 mg (36 %); ^{1}H NMR (300 MHz, $CDCl_3$, 298 K) δ: 9.89 (s, 1 H), 7.03 (d, 2 H, *J*H,H = 3 Hz), 6.76 (bt, 1 H), 4.16 (t, 4 H, *J*H,H = 6 Hz), 3.87 (t, 4 H, *J*H,H = 6 Hz), 3.75-3.50 (m, 26 H), 2.13 (bs, 6 H), 1.74 (m, 12 H), 1.61 (m, 12 H); ^{13}C NMR (300 MHz, $CDCl_3$, 298 K) δ:

191.8, 160.4, 138.3, 108.3, 108.0, 72.2, 71.3, 70.9, 70.7, 69.6, 67.9, 59.3, 41.5, 36.5, 30.5; HR-MS calculated for $C_{43}H_{66}O_{11}Na^+$: 781.4492, found: 781.4498.

Preparation of AcR$_4$. Sample was purified by preparative HPLC using a gradient of water-ACN (0.1 % TFA) 100:0 → 50:50 in 35 min; uHPLC: gradient water-ACN (0.1 % TFA) 100:0 → 50:50 in 21 min; *Rt* = 7.21 min; ^{1}H NMR (300 MHz, D_2O, 298 K) δ: 4.29-4.16 (m, 4 H), 3.14 (t, 8 H, *J*H,H = 6 Hz), 1.96 (s, 3 H), 1.85-1.48 (m, 16 H); HR-MS calculated for $C_{26}H_{55}O_{17}N_{52}^+$: 342.7278, found: 342.7284.

Preparation of AcR$_8$. Sample was purified by preparative HPLC using a gradient of water-ACN (0.1 % TFA) 100:0 → 50:59 in 35 min.; uHPLC: gradient water-ACN (0.1 % TFA) 100:0 → 50:50 in 21 min; *Rt* = 6.82 min; ^{1}H NMR (300 MHz, D_2O, 298 K) δ: 4.32-4.10 (m, 8 H), 3.14 (t, 16 H, *J*H,H = 6 Hz), 1.97 (s, 3 H), 1.87-1.48 (m, 32 H); HR-MS calculated for $C_{50}H_{103}O_{33}N_{92}^+$: 654.9291, found: 654.9310.

Preparation of 5. Peptide was prepared as described above. Sample was purified by preparative HPLC using a gradient of water-ACN (0.1 % TFA) 100:0 → 70:30 in 20 min. Yield: 12.1 mg (17 %); uHPLC: gradient water-ACN (0.1 % TFA) 100:0 → 75:25 in 15 min; *Rt* = 6.9 min; ^{1}H NMR (300 MHz, D_2O, 298 K) δ: 4.50 (s, 2 H), 4.38-4.25 (m, 4 H), 3.19 (t, 8 H, *J*H,H = 6.0 Hz), 1.90-1.50 (m, 16 H); HR-MS calculated for $C_{26}H_{55}N_{18}O_6^+$: 715.4540, found: 714.4542.

Preparation of 6. Peptide was prepared as described above. Sample was purified by preparative HPLC using a gradient of water-ACN (0.1 % TFA) 100:0 → 50:50 in 20 min; Yield: 16.7 mg (12 %); uHPLC: gradient water-ACN (0.1 % TFA) 100:0 → 75:25 in 15 min; *Rt* = 8.5 min; ^{1}H NMR (300 MHz, D_2O, 298 K) δ: 4.40 (s, 2 H), 4.31 (m, 8 H), 3.18 (t, 16 H, JH,H = 6Hz), 1.80-1.50 (m, 32 H); HR-MS calculated for $C_{50}H_{104}N_{34}O_{102}^+$: 670.4319 , found: 670.4341.

Preparation of AdR$_4$.Yield: 3.1 mg (35 %); uHPLC: gradient water-ACN (0.1 % TFA) 95:5 → 5:95 in 21 min; *Rt* = 12.3 min; 1H NMR (300 MHz, D2O, 298 K) δ: 4.57 (s, 2 H), 4.43 (s, 1 H), 4.26 (m, 4 H), 4.16 (d, 1 H, *J*H,H = 6 Hz), 3.66 (m, 14 H), 3.15 (bt, 8 H), 2.08 (s, 3 H), 1.80-1.50 (m, 28 H); HR-MS calculated for C44H83N18O10+: 1023.6522, found: 1023.6534

Preparation of AdR$_8$. Yield: 1.1 mg (19 %); uHPLC: gradient water-ACN (0.1 % TFA) 95:5 → 5:95 in 21 min; *Rt* = 12.0 min; ^{1}H NMR (300 MHz, D_2O, 298 K) δ: 4.57 (s, 2 H), 4.43 (s, 1 H), 4.26-4.16 (m, 10 H), 3.63 (m, 14 H), 3.15 (bt, 16 H), 2.07 (s, 3 H), 1.90-1.40 (m, 44 H); HR-MS calculated for $C_{68}H_{132}N_{34}O_{142}^+$: 824.5311, found: 824.5330.

Preparation of Ad$_2$R$_4$. Yield: 3.2 mg (20 %); uHPLC: gradient water-ACN (0.1 % TFA) 95:5 → 5:95 in 21 min; *Rt* = 18.6 min; ^{1}H NMR (300 MHz, D_2O, 298 K) δ: 8.74 (s, 1 H), 7.30 (d, 2 H, *J*H,H = 3 Hz), 7.12 (bt, 1 H), 5.16 (m, 2 H), 4.9-4.7 (m, water overlapped), 4.63 (bt, 4 H, *J*H,H = 6 Hz), 4.32 (bt, 4 H, *J*H,H = 6 Hz), 4.19-4.09 (m, 16 H), 4.04 (s, 8 H), 3.6 (m, 8 H), 2.58 (bs, 6 H), 2.40-2.00 (m, 40 H) ; HR-MS calculated for $C_{69}H_{119}N_{18}O_{16}^+$: 1455.9021, found: 1455.9045.

Preparation of Ad$_2$R$_8$. Yield: 1.9 mg (25 %); uHPLC: gradient water-ACN (0.1 % TFA) 95:5 → 5:95 in 21 min; *Rt* = 13.2 min; ^{1}H NMR (300 MHz, D_2O, 298 K) δ: 8.30 (s, 1 H), 6.87 (d, 2 H, *J*H,H = 2.3 Hz), 6.71 (t, 1 H), 4.71 (m, water overlapped), 4.28 (m, 8 H), 4.19 (m, 4 H), 3.89 (m, 4 H), 3.80-3.60 (m, 16 H), 3.56 (m, 8 H), 3.12 (m, 16 H), 2.05 (bs, 6 H), 1.89-1.50 (m, 56 H); HR-MS calculated for $C_{93}H_{168}N_{34}O_{202}^+$: 1041.1581, found: 1041.1594.

Preparation of 7. To a solution of [*tert*-butoxycarbonyl]aminoxy acetic acid (36 mg, 0.2 mmol, 1.5 equiv), EDC (36 mg, 0.2 mmol, 1.5 equiv.) and DIEA (32 μL, 0.2 mmol, 1.5 equiv) in DMF (1 mL), *α*-amino-*ω*-methoxy polyethylene glycol (MW ≈ 800, 100 mg) was added in portions. The reaction mixture was stirred at room temperature for 6 h. The solvent was removed under reduced pressure, and the residue was dissolved in DCM (10 mL). The organic layer was washed with water (50 mL, 3×) and NaOH 2 M (10 mL, 3×). Then the organic phase was dried, filtered, and concentrated. The residue was precipitated by dissolving it in a minimal amount of DCM and adding to diethyl ether (15 mL), then cooling the solution to -32 °C. The solution was separated from the solids using a syringe while the solvent is very cold (eventual warming up led to the dissolution of the product). 70 mg of a waxy solid were obtained (70 mg, 56%). ^{1}H NMR (300 MHz, $CDCl_3$, 298 K) *δ*: 4.28 (s, 2 H), 3.67-3.50 (m, 83 H), 3.34 (s, 3 H), 1.44 (s, 9 H).

Preparation of 8. **7** (70 mg, ≈ 70 μmol) was dissolved in a mixture of TFA-DCM 1:1 (1 mL) and the mixture was stirred at room temperature for 2 h. Then, TFA was evaporated, and the crude was dissolved in DCM (5 mL). The organic phase was washed with saturated $NaHCO_3$ (×2) and water (×2). The organic phase was filtered, dried, and concentrated. The compound was used without further purification (70 mg, quantitative). ^{1}H NMR (300 MHz, $CDCl_3$, 298 K) *δ*: 4.11 (s, 2 H), 3.6 (m, 84 H), 3.35 (s, 3 H).

Preparation of AdPEG. A solution of **2** (8.6 mg, 0.3 mmol, 2 equiv.) and **8** (21 mg) in acetonitrile (1 mL) were stirred at room temperature for 4 h. The residue solution was diluted with 1 mL water and purified by preparative HPLC using a gradient of water-acetonitrile (0.1 % TFA) 50:50 → 0:100 in 20 min; Yield: 7.4 mg (29 %); uHPLC: gradient water-ACN (0.1 % TFA) 95:5 → 5:95 in 21 min; *Rt* = 14.1 min; ^{1}H NMR (300 MHz, $CDCl_3$, 298 K) *δ*: 4.55 (s, 2 H), 4.37 (d, 1 H, *J*H,H = 3 Hz), 4.14 (m, 2 H), 3.65 (m, 98 H), 3.39 (s, 3 H), 2.86 (bs, 5 H), 2.14 (s, 3 H), 1.75-1.72 (m, 12 H).

Preparation of Ad$_2$PEG. A solution of **4** (20 mg, 0.3 mmol, 2 equiv.) and **8** (21 mg) in acetonitrile (1 mL) were stirred at room temperature for 4 h. The residue solution was diluted with 1 mL water and purified by preparative HPLC using a gradient of water-acetonitrile (0.1 % TFA) 50:50 → 0:100 in 20 min; Yield: 5.6 mg (18 %); uHPLC: gradient water-ACN (0.1 % TFA) 95:5 → 5:95 in 21 min; *Rt* = 19.1 min; ^{1}H NMR (300 MHz, $CDCl_3$, 298 K) *δ*: 8.1 (s, 1 H), 6.75 (bd, 2 H, *J*H,H = 3 Hz), 6.54 (bt, 1 H), 4.66 (s, 2 H), 4.12 (t, 4 H, *J*H,H = 6 Hz), 3.66 (t, 4 H, *J*H,H = 6 Hz), 3.65 (m, 114 H), 3.39 (s, 3 H), 2.14 (bs, 6 H), 1.75 (m, 12 H), 1.61 (m, 12 H).

Preparation of AcE$_9$. Sample was purified by preparative HPLC using a gradient of water-ACN (0.1 % TFA) 100:0 → 50:50 in 20 min; uHPLC: gradient water-ACN (0.1 % TFA) 95:5 → 5:95 in 21 min; *Rt* = 13.3 min; 1H NMR (300 MHz, DMSO - d6 , 298 K) *δ*: 12.05 (bs, 6 H), 8.84 (m, 1 H), 8.67 (m, 1 H), 8.27 (m, 1 H), 8.01 (m, 7 H), 7.88 (t, 2 H, *J*H,H = 6.5 Hz), 7.54 (m, 1 H), 7.23 (m, 1 H), 7.01 (m, 4 H), 6.49 (m, 2 H), 4.19 (m, 9 H), 2.96 (bs, 6 H), 2.70 (s, 2 H), 2.25 (m, 18 H), 1.83-1.00 (m, 24 H); HR-MS calculated for $C_{78}H_{98}N_{14}O_{332}^-$: 879.3201, found: 879.3209.

Preparation of 9. Sample was purified by preparative HPLC using a gradient of water-ACN (0.1 % TFA) 100:0 → 50:50 in 20 min; uHPLC: gradient water-ACN (0.1 % TFA) 95:5 → 5:95 in 21 min; *Rt* = 12.8 min; ^{1}H NMR (300 MHz, DMSO - d_6, 298 K) *δ*: 11.90 (bs, 6 H), 8.85 (m, 1 H), 8.69 (m, 1 H), 8.29 (m, 1 H), 8.03 (m, 7 H), 7.90 (m, 2 H), 7.56 (m, 1 H), 7.25 (m, 1 H), 7.03 (m, 4 H), 6.51 (m, 2 H), 4.21 (m, 8 H), 2.98 (bs, 6 H), 2.72 (s, 2 H), 2.26 (m, 18 H), 1.85-1.00 (m, 24 H); HR-MS calculated for $C_{78}H_{103}N_{15}O_{34}^{2-}$: 896.8375, found: 895.8308

Preparation of AdE$_9$. Sample was purified by preparative HPLC using a gradient of water-ACN (0.1 % TFA) 100:0 → 50:50 in 35 min; uHPLC: gradient water-ACN (0.1 % TFA) 95:5 → 5:95 in 21 min; *Rt* = 14.6 min; ^{1}H NMR (300 MHz, D_2O, 298 K) δ: 8.26 (s, 1 H), 8.02 (d, 1 H), 7.65 (t, 1 H), 7.47 (d, 1 H), 7.24 (d, 2 H), 6.96 (d, 2 H), 6.82 (s, 2 H), 4.58-4.10 (m, 16 H), 3.70-3.58 (m, 16 H), 3.23 (s, 12 H), 2.25-1.43 (m, 54 H) HR-MS calculated for $C_{96}H_{127}O_{38}N_{152}^-$: 1048.9221, found: 1049.4159.

2. Figures

2.1. Comparison between R_4 and R_8 peptides

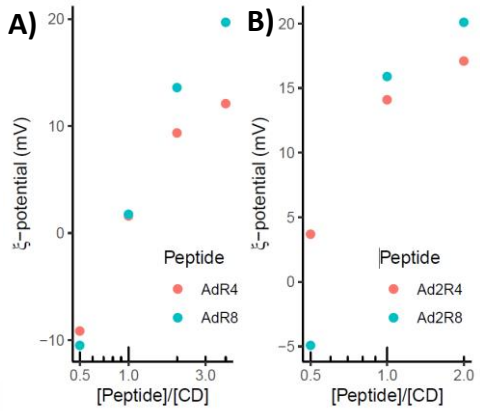

Figure 78. ζ-potential measurements of ***β*-CD@AuNP** (10 μM in *β*-CD) when adding A) **AdR$_4$** and **AdR$_8$**, and B) **Ad$_2$R$_4$** and **Ad$_2$R$_8$**. Results are the average of three measurements

2.2. Stability zones as evidenced by ζ –potentials

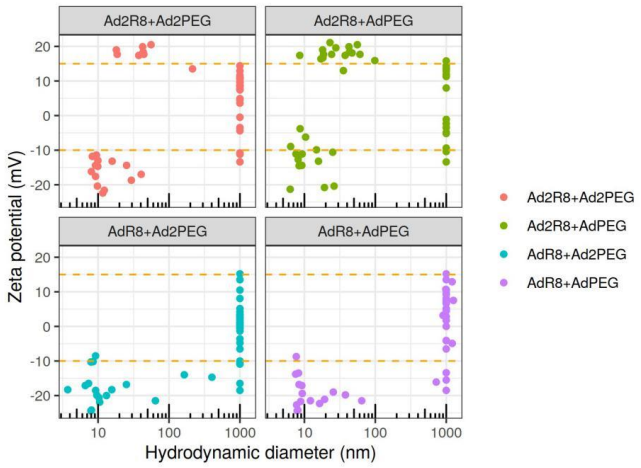

Figure 79. Distribution of sizes as a function of the surface potential for ***β*-CD@AuNP** at a concentration of 10 μM in *β*-CD by mixing compounds **AdR$_8$**, **Ad$_2$R$_8$**, **AdPEG,** and **Ad$_2$PEG**. Orange dashed lines represent suggested surface potential thresholds needed to achieve colloidal stability.

2.3.Host-guest formation in *β*-CD@AuNPs

The presence of a polyethylene glycol stabilizer resulted in the modulation of the surface charge, although it did not prevent nanoparticle aggregation, regardless of the valency of it. Figure 80B shows the ζ-potential at increasing concentration of stabilizer **Ad$_2$PEG** at several fixed concentrations of **Ad$_2$R$_8$**. When there is no **Ad$_2$R$_8$**, increasing concentrations of **Ad$_2$PEG** yields stable, closer to neutrality nanoparticles (Figure 80B, red line). When **Ad$_2$R$_8$** is present, increasing the concentration of **Ad$_2$PEG** gives rise to less charged aggregates, with ζ-potentials that can reach electroneutrality. This decrease of surface potential suggests that binding of the PEG moiety to the nanoparticle is effective, but the equilibrium state reached probably involves the exchange of PEG by the peptide. In this sense, the addition of peptide to equilibrated solutions of ***β*-CD@AuNP** + PEG guests typically leads equally to aggregation.

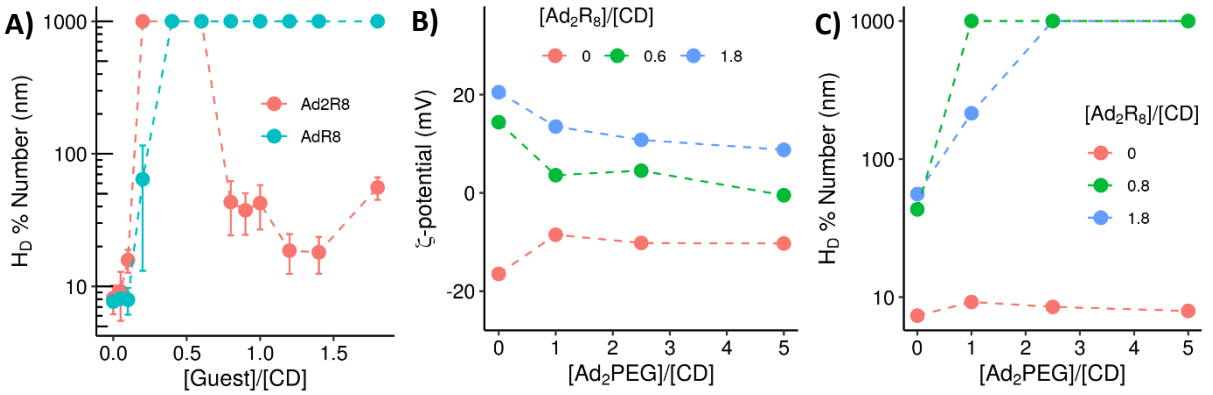

Figure 80. DLS and ζ-potential of nanoparticles formed between compounds **AdR$_8$**, **Ad$_2$R$_8$** and **Ad$_2$PEG** and ***β*-CD@AuNP** at a concentration of 10 μM in *β*-CD. Data represent the average of 3 measurements, where the error bars denote the standard deviation: A) Hydrodynamic diameter in the absence of PEG after the addition of **AdR$_8$** and **Ad$_2$R$_8$**. B) Effect on the surface potential of the addition of **Ad$_2$PEG** to fixed concentrations of **Ad$_2$R$_8$**. C) Effect on the hydrodynamic diameter of the addition of **Ad$_2$PEG** to fixed concentrations of **Ad$_2$R$_8$**.

2.4.Control peptide exchange experiments

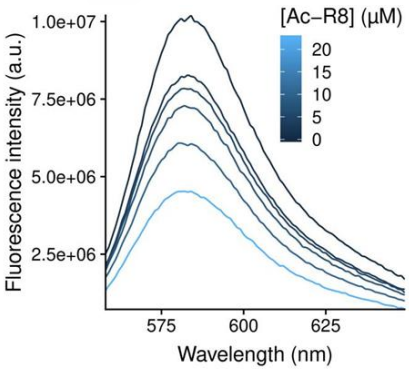

Figure 81. Exchange of peptide **AdE$_9$** at *β*-CD@AuNP (concentration in *β*-CD and **AdE$_9$** was 5 μM) by peptide **AcR$_8$**.

2.5.Toxicity determined by MTT assays

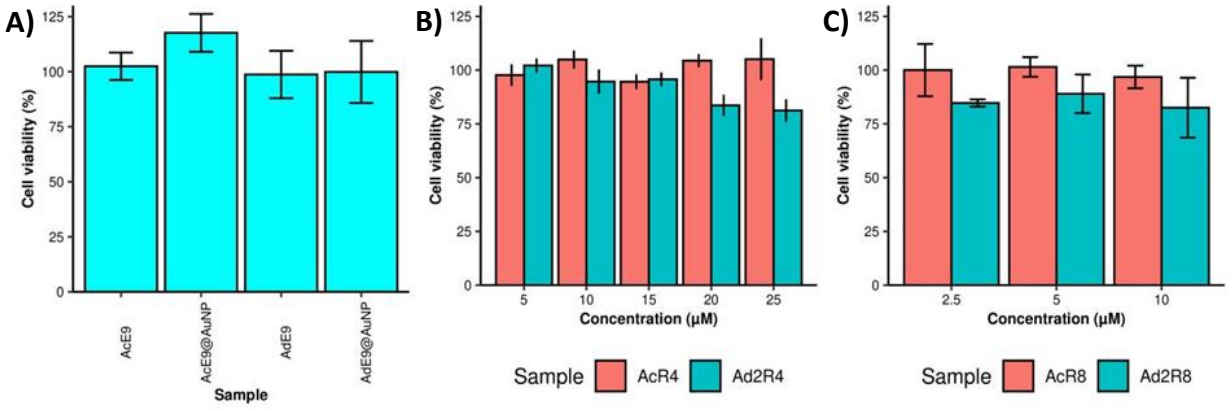

Figure 82. Determination of cell toxicity by MTT assays: A) **AdE$_9$** and **AcE$_9$** in the presence or absence of nanoparticles; after 30 min incubation with **AdE$_9$⊂*β*-CD@AuNP** (10 μM both), then B) **Ad$_2$R$_4$** and **AcR$_4$**; and C) **Ad$_2$R$_8$** and **AcR$_8$**.

3. Fitting *ζ*-potential data to thermodynamic models

In order to evaluate the binding affinity of derivatives **AdR$_4$**, **AdR$_8$**, **Ad$_2$R$_4$**, and **Ad$_2$R$_8$** according to the surface potential measurements shown in Figure 73, we assumed that the ζ-potential of the nanoparticle increases linearly with the coverage of peptide on the surface:

$$\Delta\zeta = \zeta - \zeta\text{min} = \Theta \times \zeta\text{max} \quad \text{(S1)}$$

were ζ is the surface potential of the particle at a particular concentration of guest, ζ_{min} is the minimal value of surface potential observed,[310] Θ is the coverage of host-guest complex in the nanoparticle, and ζmax is the maximum value of ζ achieved when the concentration of guest is infinite.

For a monovalent complexation between a monovalent guest (G) and a host (H), the chemical equilibrium is:

$$[H]+[G] \leftrightarrow [HG] \quad \text{(S2)}$$

where K is the thermodynamic equilibrium constant. Taking [HG] = K[H][G], mass balances of [H] and [G] are given by

$$H = \frac{[H]t}{1+K[G]} \quad \text{(S3)}$$

$$H = \frac{[G]t}{1+K[H]} \quad \text{(S4)}$$

From Equation S1, the increase of the surface potential will be given by

$$\Delta\zeta = \frac{[HG]}{[H]t}\zeta max \quad \text{(S5)}$$

[310] A. Mulder, S. Onclin, M. Péter, J. P. Hoogenboom, H. Beijleveld, J. ter Maat, M. F. García-Parajó, B. J. Ravoo, J. Huskens, N. F. van Hulst, et al., *Small* **2005**, *1*, 242-253.

On the other hand, a divalent binding from **Ad_2R_4** and **AdR_8** to nanoparticles was also evaluated using a thermodynamic model on surfaces.[311,312] For the chemical equilibrium:

$$G_2 + H_s \leftrightarrow (HG)_s - G \text{ (S6)}$$

$$(HG)_s - G + H_s \leftrightarrow (H_2G_2)_s \text{ (S7)}$$

and the concentration of host-guest complexes are given by

$$[(HG)_s - G] = 2K[H_s][G_2] \text{ (S8)}$$

$$[(H_2G_2)_s] = K^2 C_{ef} [G_2] \frac{[Hs]^2}{[Hs]t} \text{ (S9)}$$

from mass balances $[G_2]_t = [G_2]+[(HG)_s-G]+[(H_2G_2)_s]$ and $[H_s]_t = [H_s]+[(HG)_s-G]+2[(H_2G_2)_s]$, the following expressions for $[H_s]$ and $[G_2]$ are deduced:

$$[G2] = \frac{[G2]t}{1+K[Hs](2+\frac{KCef[Hs]}{[H]t})} \text{ (S10)}$$

$$[Hs] = \frac{[Hs]t}{1+2K[G2](1+\frac{KCef[Hs]}{[H]st})} \text{ (S11)}$$

Taking expression S1, the variation of the surface potential will be given by the following expression

$$\Delta\zeta = \frac{[(HG)s-G]+[(H2G2)s]}{[Hs]tot} x\ \zeta max \text{ (S12)}$$

Models were implemented in a spreadsheet as described,[311] and fitting was carried out by minimization of the error between experimental and modeled Δζ values.

[311] J. Huskens, L. Prins, R. Haag, J. Ravoo, *Multivalency: Concepts, Research and Applications*; Wiley: 2018.
[312] J. Huskens, A. Mulder, T. Auletta, C. A. Nijhuis, M. J. W. Ludden, D. N. Reinhoudt, *J. Am. Chem. Soc.* **2004**, *126*, 6784-6797.

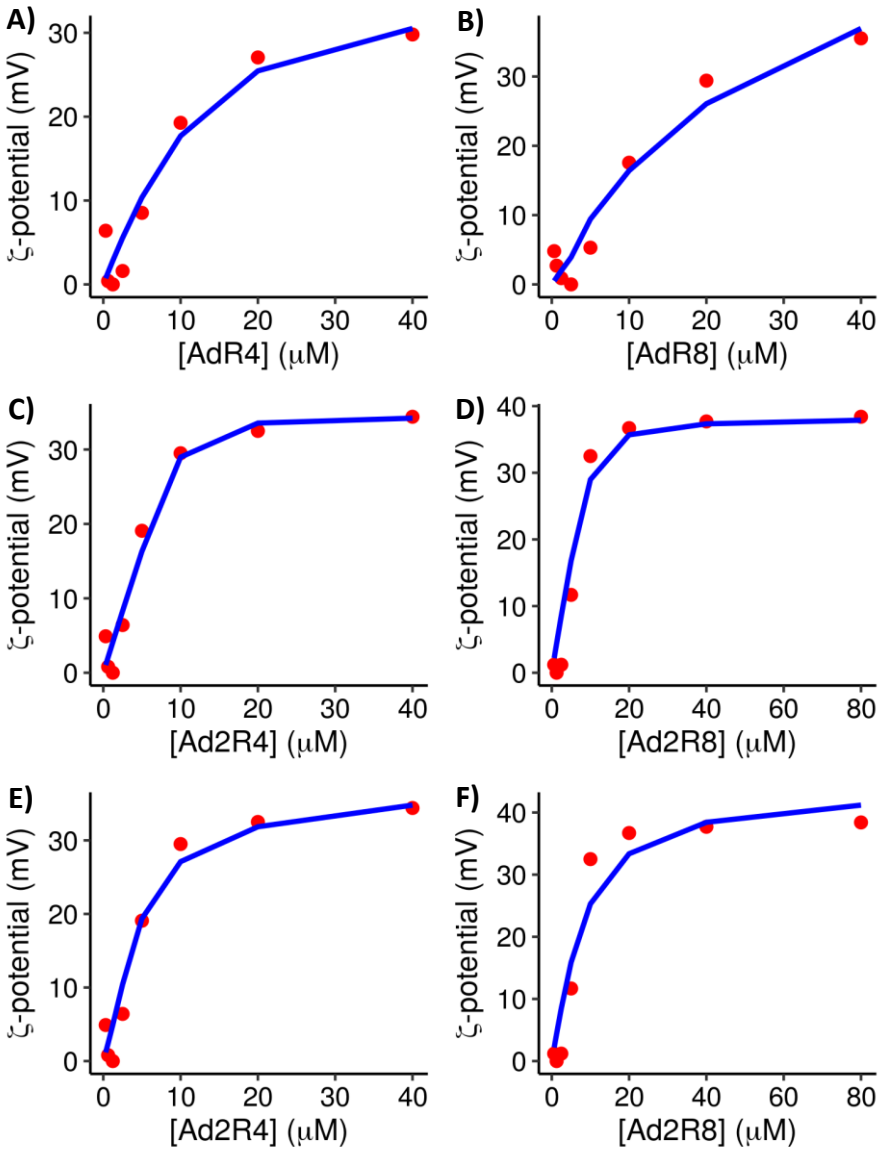

Figure 83. Measured **ζ**-potential for ***β*-CD@AuNP** and fitting to a thermodynamic model. Red points represent experimental data while blue lines indicate best-fitting achieved with the corresponding model. A) Monovalent binding of **AdR$_4$** to ***β*-CD@AuNP**. B) Monovalent binding of **AdR$_8$** to ***β*-CD@AuNP**. C) Divalent binding of **Ad$_2$R$_4$** to ***β*-CD@AuNP**. D) Divalent binding of **Ad$_2$R$_8$** to ***β*-CD@AuNP**. E) Monovalent binding of **Ad$_2$R$_4$** to ***β*-CD@AuNP**. F) Monovalent binding of **Ad2R$_8$** to ***β*-CD@AuNP**. In all cases, the total concentration of *β*-CD was 10 μM.

[Ad$_2$R$_8$]/[CD]	H_D (nm)
1.8	44 ± 21
0.1	277 ± 185

Table 3. Hydrodynamic diameter (H_D measurements carried out to assess the stability of ***β*-CD@AuNP** (10 μM in [*β*-CD] and **Ad$_2$R$_8$** in DMEM media containing serum (10% v/v) without bromophenol red.

4. Characterization of new derivatives

4.1.NMR of derivative 2

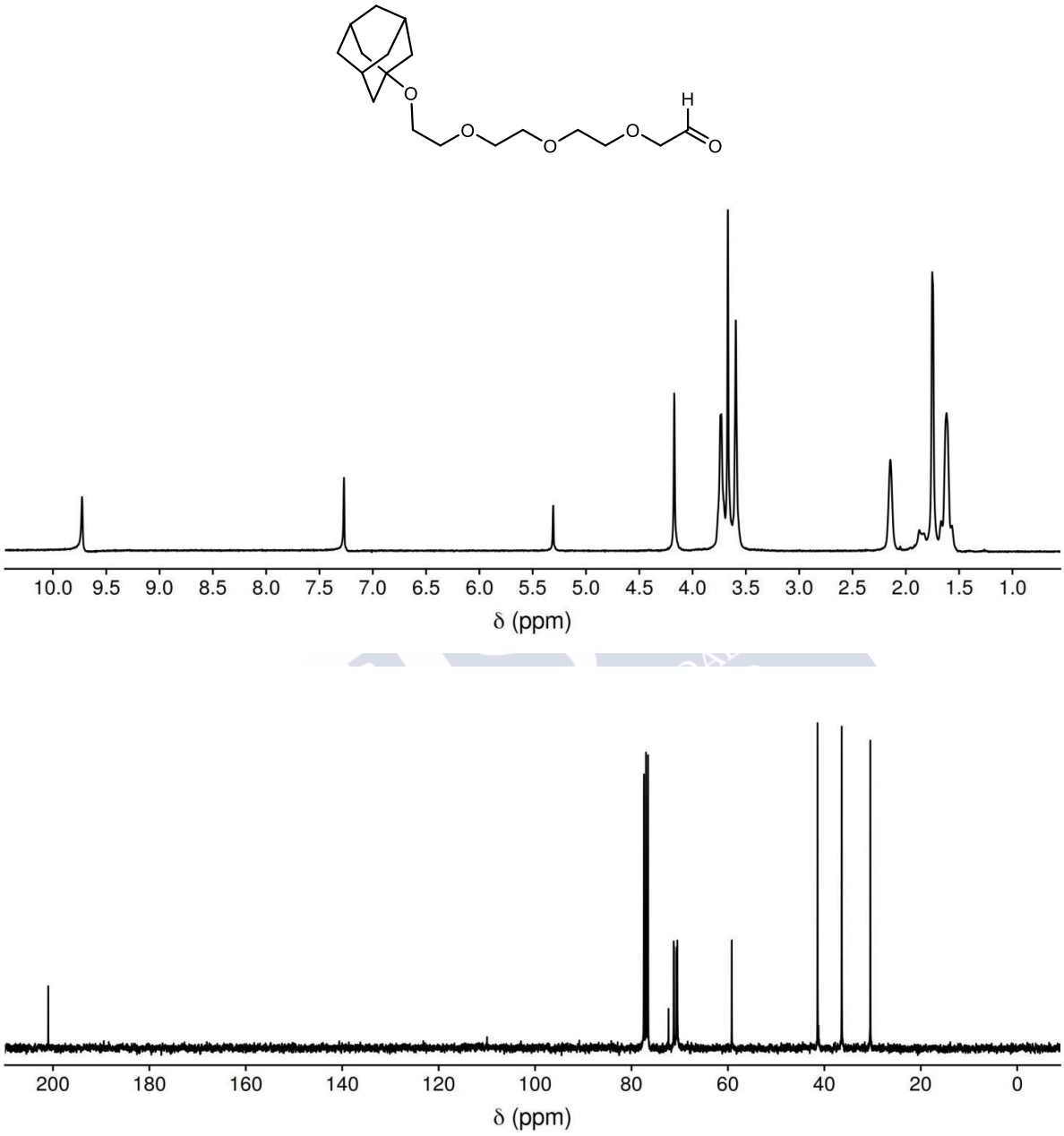

Figure 84.^{1}H NMR (300 MHz, $CDCl_3$, 273K, top) and ^{13}C NMR (75 MHz, $CDCl_3$, 273K, bottom) of derivative **2**.

4.2.NMR of derivative 4

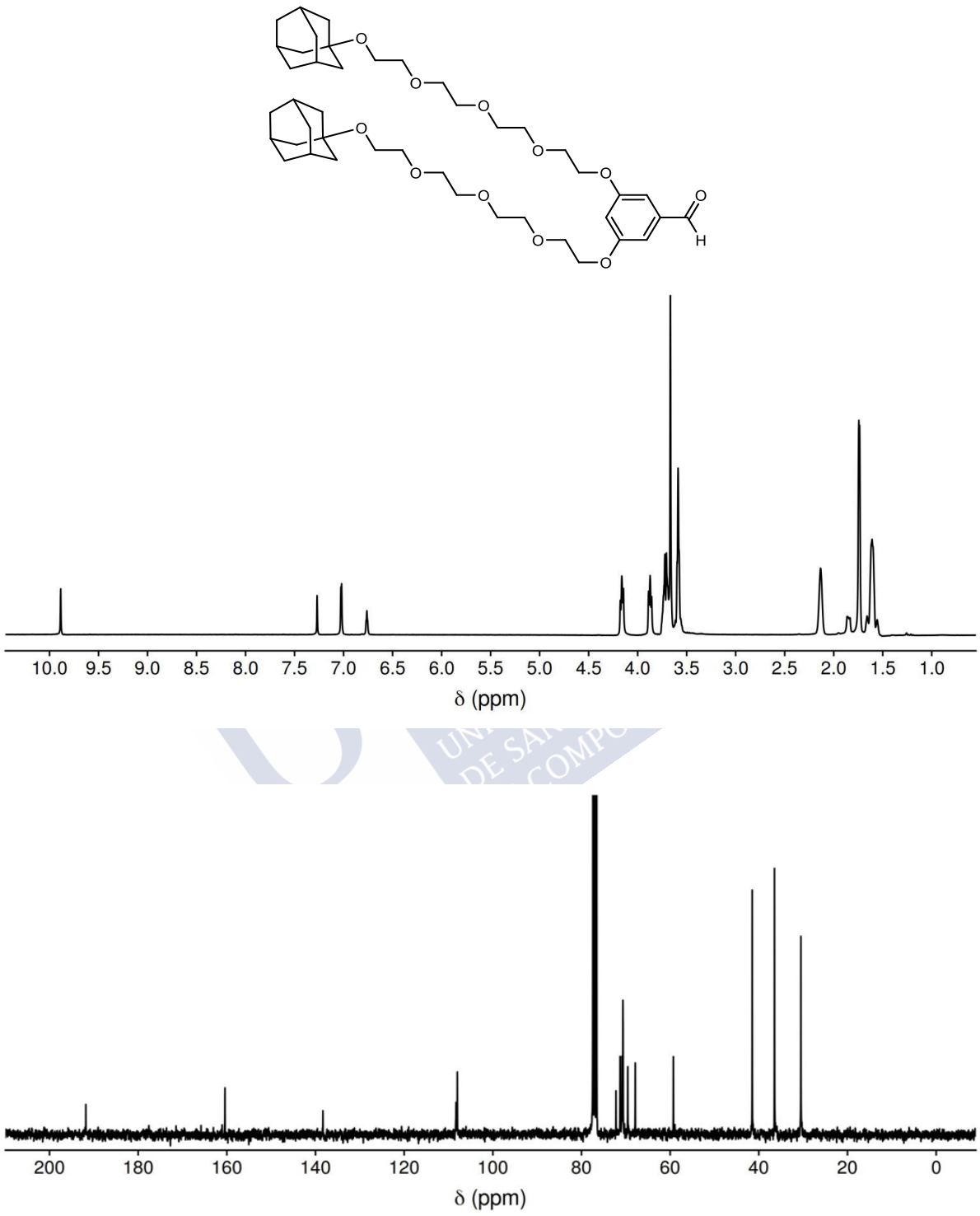

Figure 85. ^{1}H NMR (300 MHz, $CDCl_3$, 273K, top) and ^{13}C NMR (75 MHz, $CDCl_3$, 273K, bottom) of derivative **4**.

4.3.HPLC-MS and ^{1}H NMR spectra of AcR_4

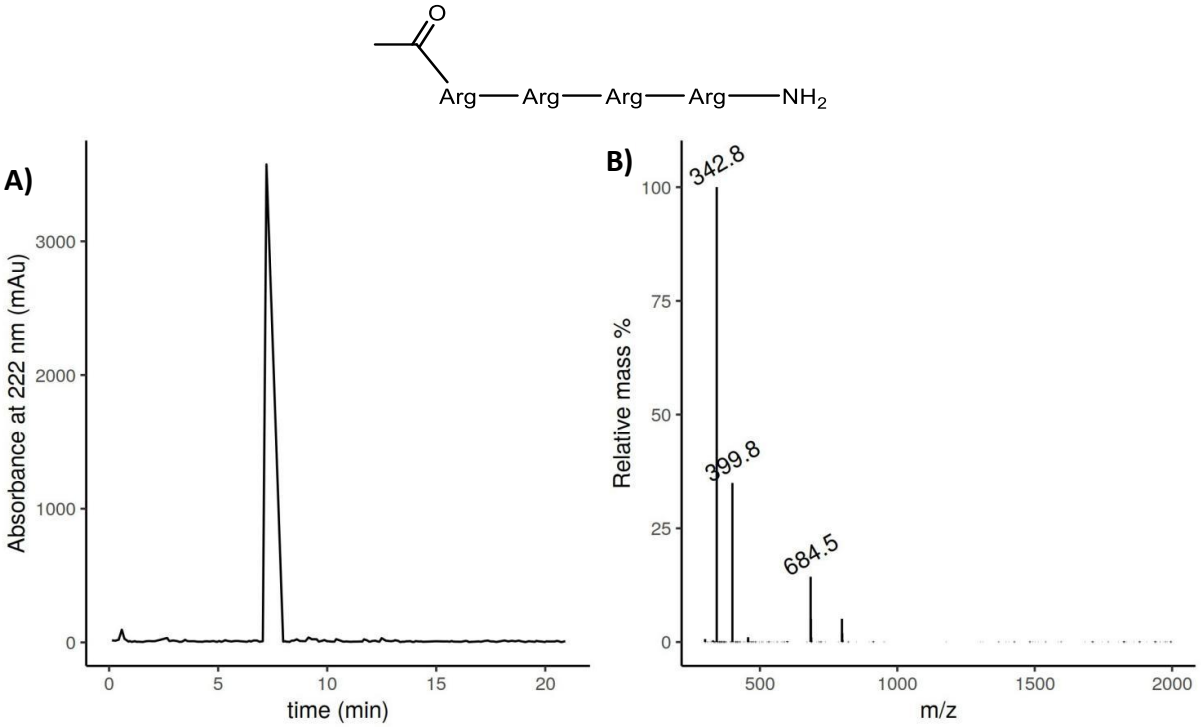

Figure 86. A) HPLC (water-ACN (0.1 % TFA) 100:0 → 50:50 in 21 min) and B) corresponding MS spectra of derivative **AcR_4**.

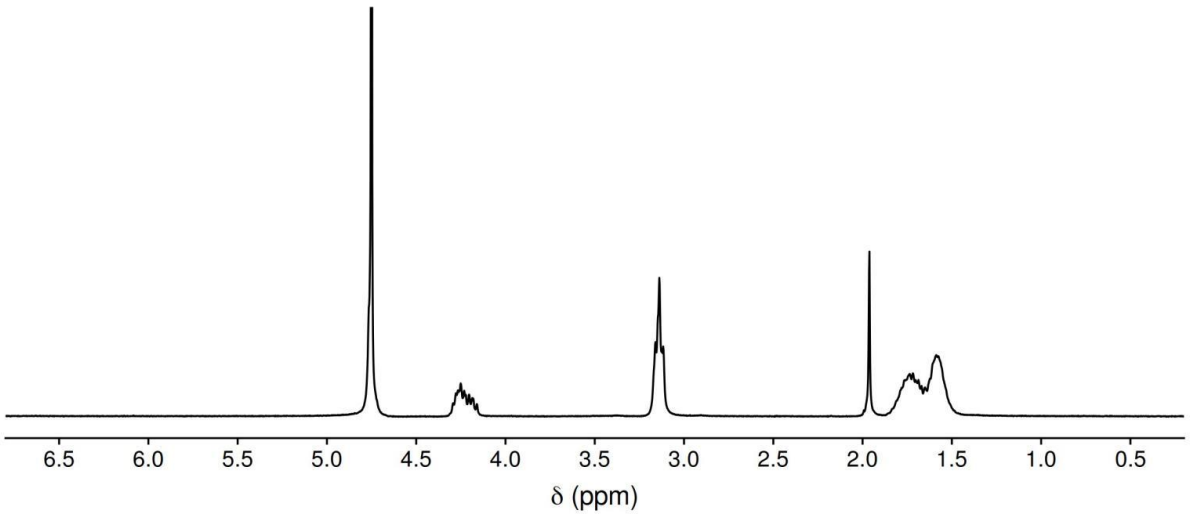

Figure 87. ^{1}H NMR (300 MHz, D_2O, 273K) of derivative AcR_4.

4.4.HPLC-MS and ^{1}H NMR spectra of AcR_8

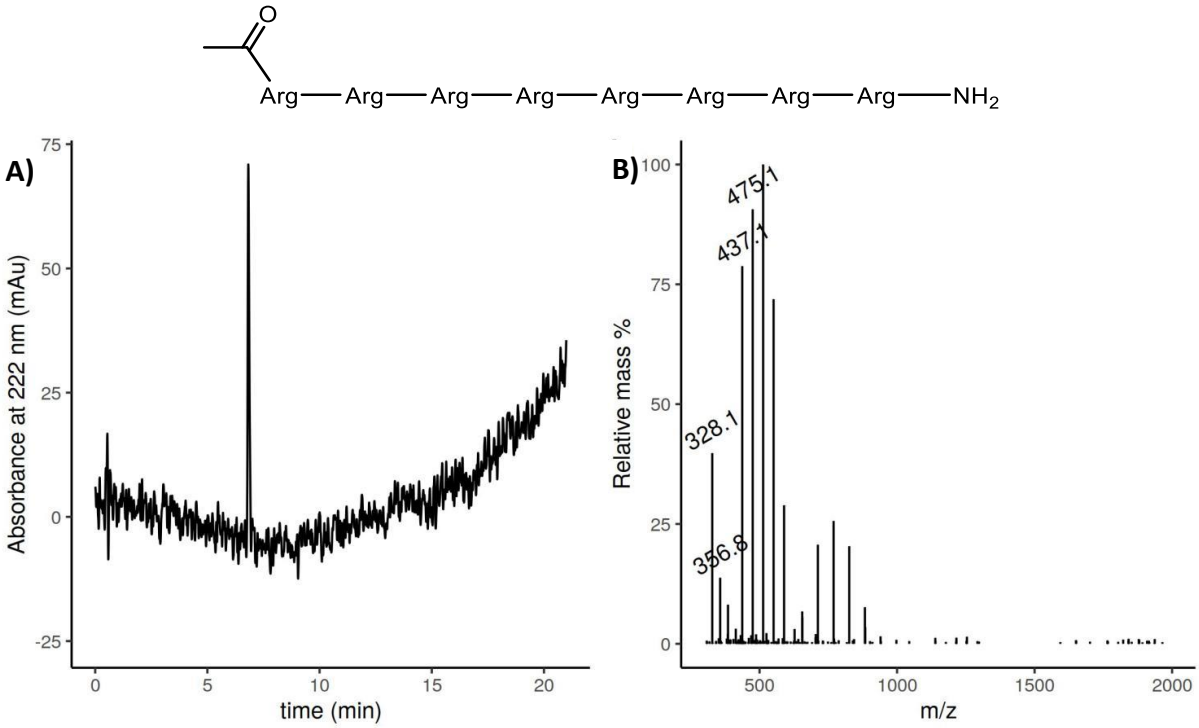

Figure 88. A) HPLC (water-ACN (0.1 % TFA) 100:0 → 50:50 in 21 min) and B) corresponding MS spectra of derivative **AcR_8**.

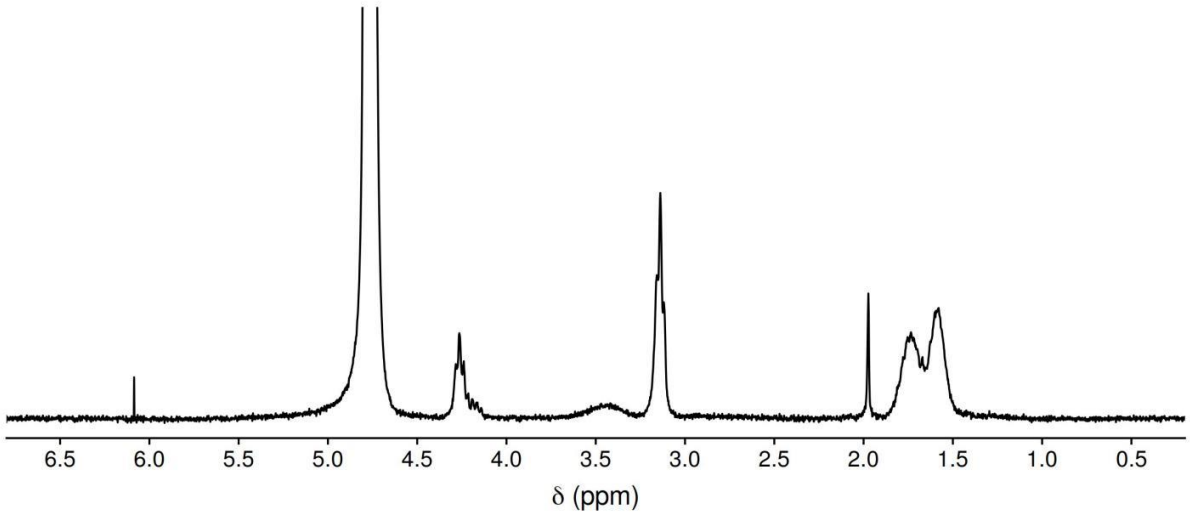

Figure 89. ^{1}H NMR (300 MHz, D_2O, 273K) of derivative **AcR_8**.

4.5.HPLC-MS and ^{1}H NMR spectra of 5

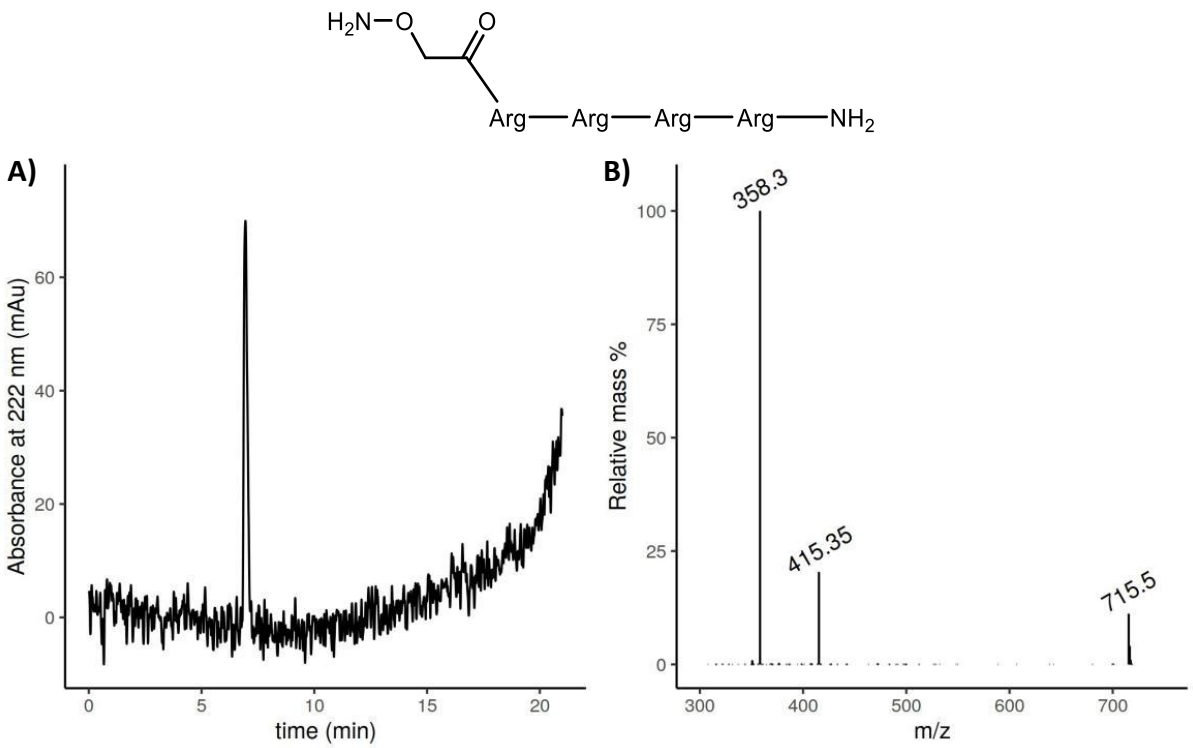

Figure 90. A) HPLC (water-ACN (0.1 % TFA) 100:0 → 75:25 in 15 min) and B) corresponding MS spectra of derivative **5**.

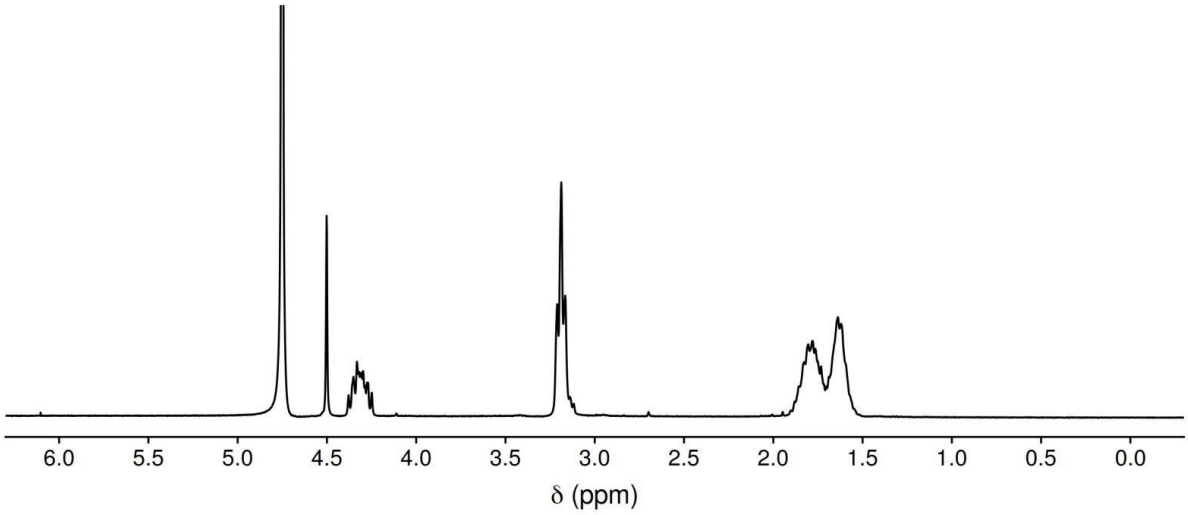

Figure 91. ^{1}H NMR (300 MHz, D_2O, 273K) of derivative **5**.

4.6.HPLC-MS and ^{1}H NMR spectra of 6

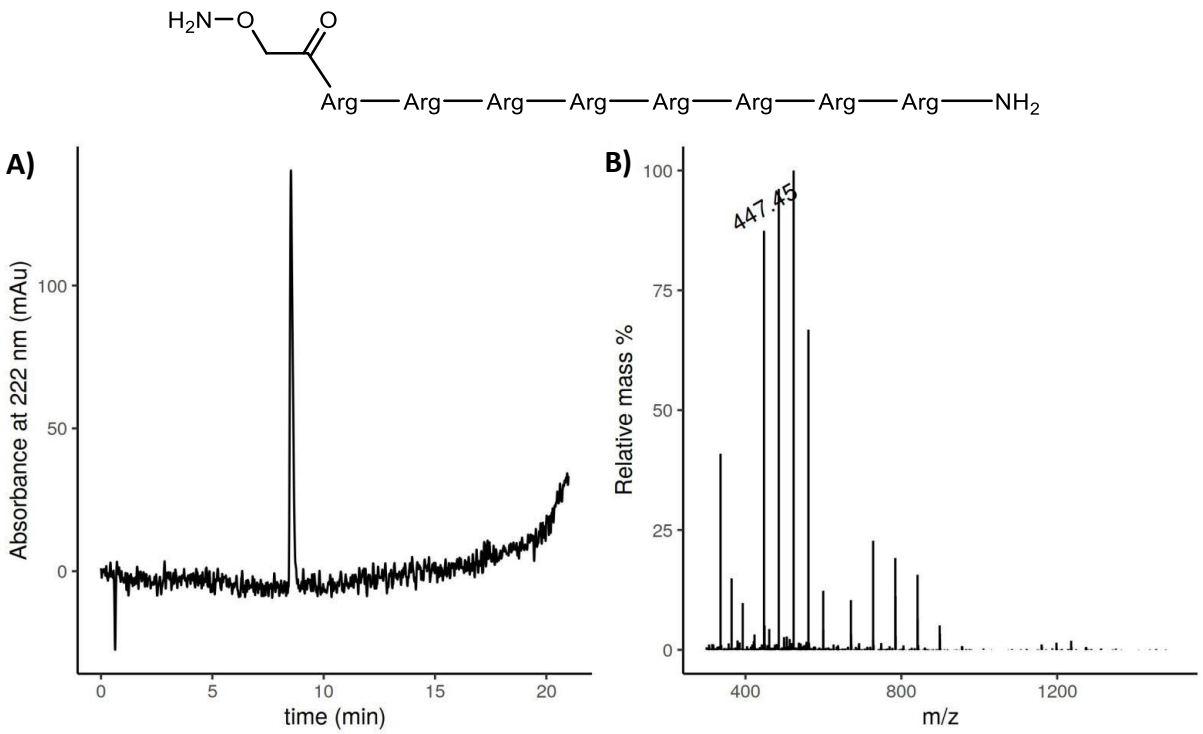

Figure 92. A) HPLC (water-ACN (0.1 % TFA) 100:0 → 75:25 in 15 min) and B) corresponding MS spectra of derivative **6**.

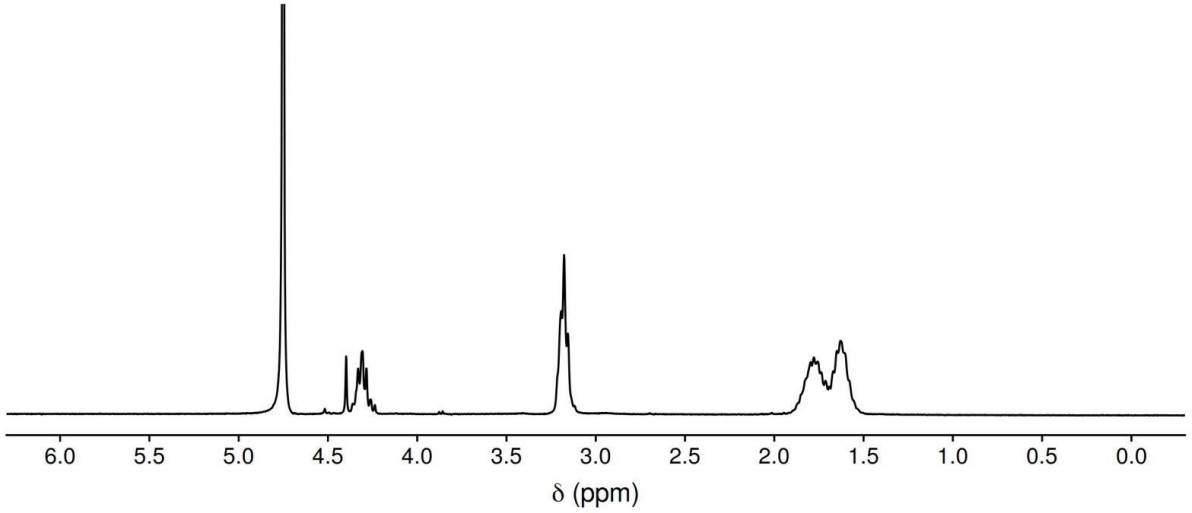

Figure 93. ^{1}H NMR (300 MHz, D_2O, 273K) of derivative **6**.

4.7.HPLC-MS and ^{1}H NMR spectra of AdR$_4$

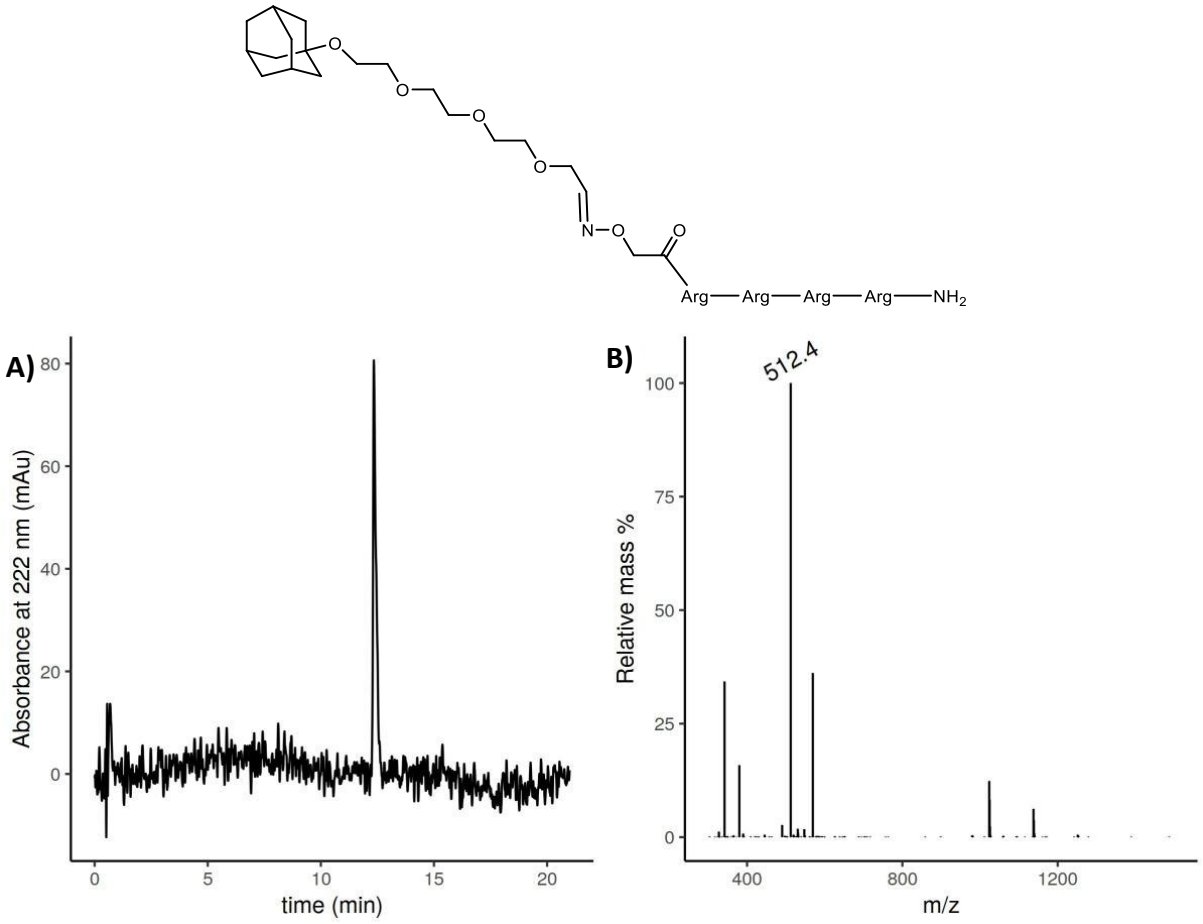

Figure 94. A) HPLC (water-ACN 95:5 → 5:95 in 21 min) and B) corresponding MS spectra of derivative **AdR$_4$**.

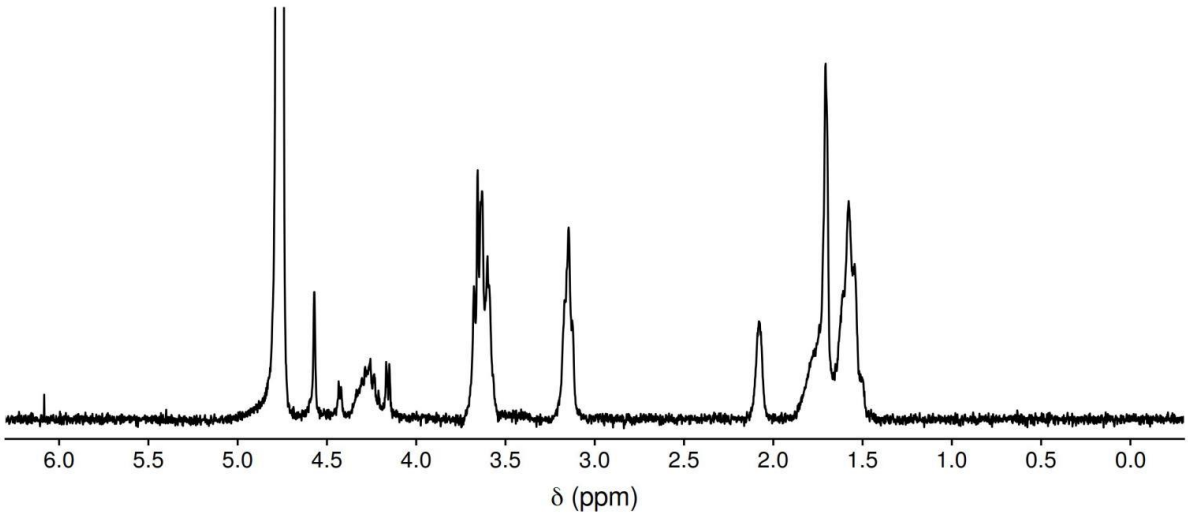

Figure 95. ^{1}H NMR (300 MHz, D_2O, 273K) of derivative **AdR$_4$**.

4.8.HPLC-MS and ^{1}H NMR spectra of AdR_8

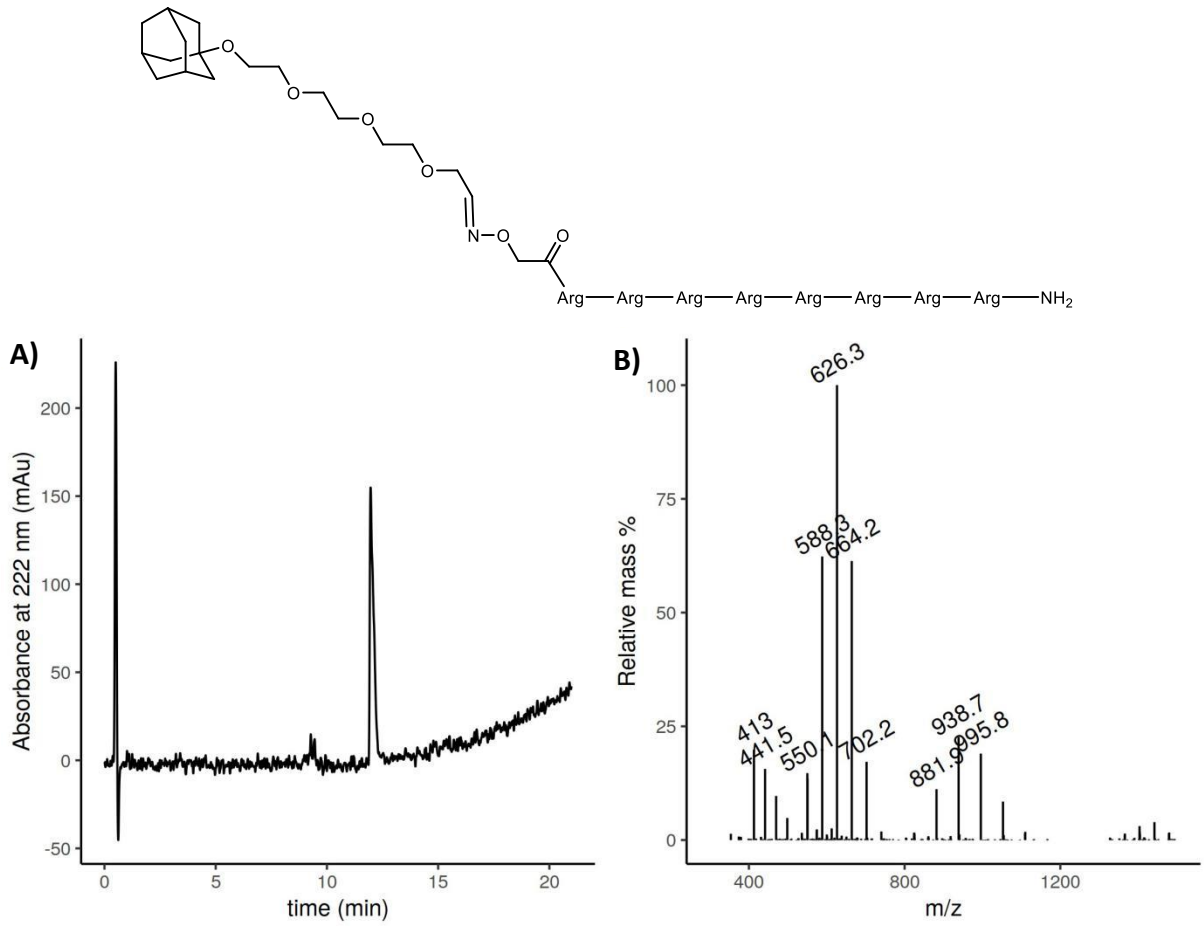

Figure 96. A) HPLC (water-ACN 95:5 → 5:95 in 21 min) and B) corresponding MS spectra of derivative **AdR_8**.

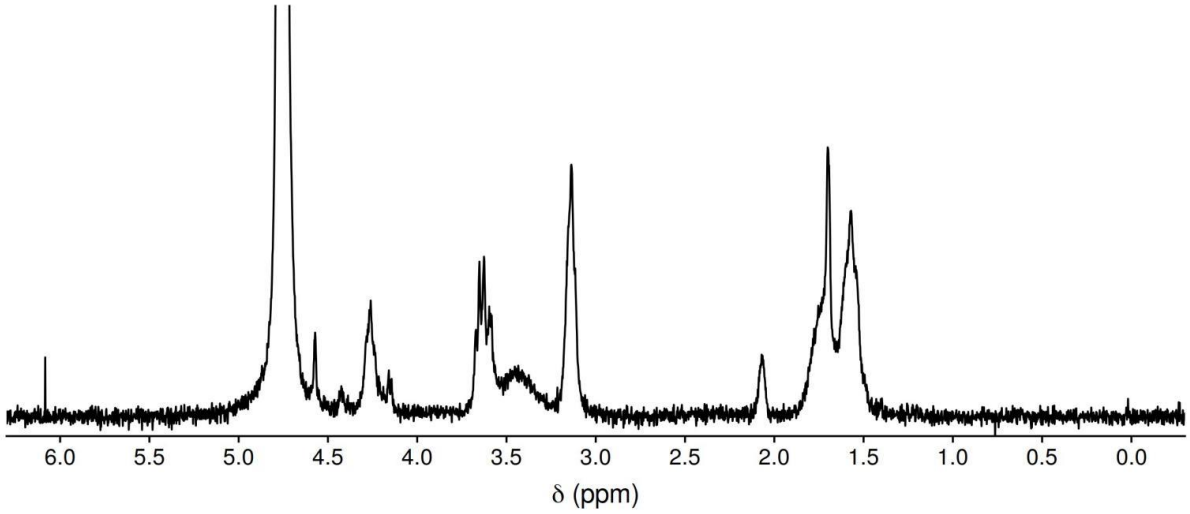

Figure 97. ^{1}H NMR (300 MHz, D_2O, 273K) of derivative **AdR_8**.

4.9.HPLC-MS and ^{1}H NMR spectra of Ad_2R_4

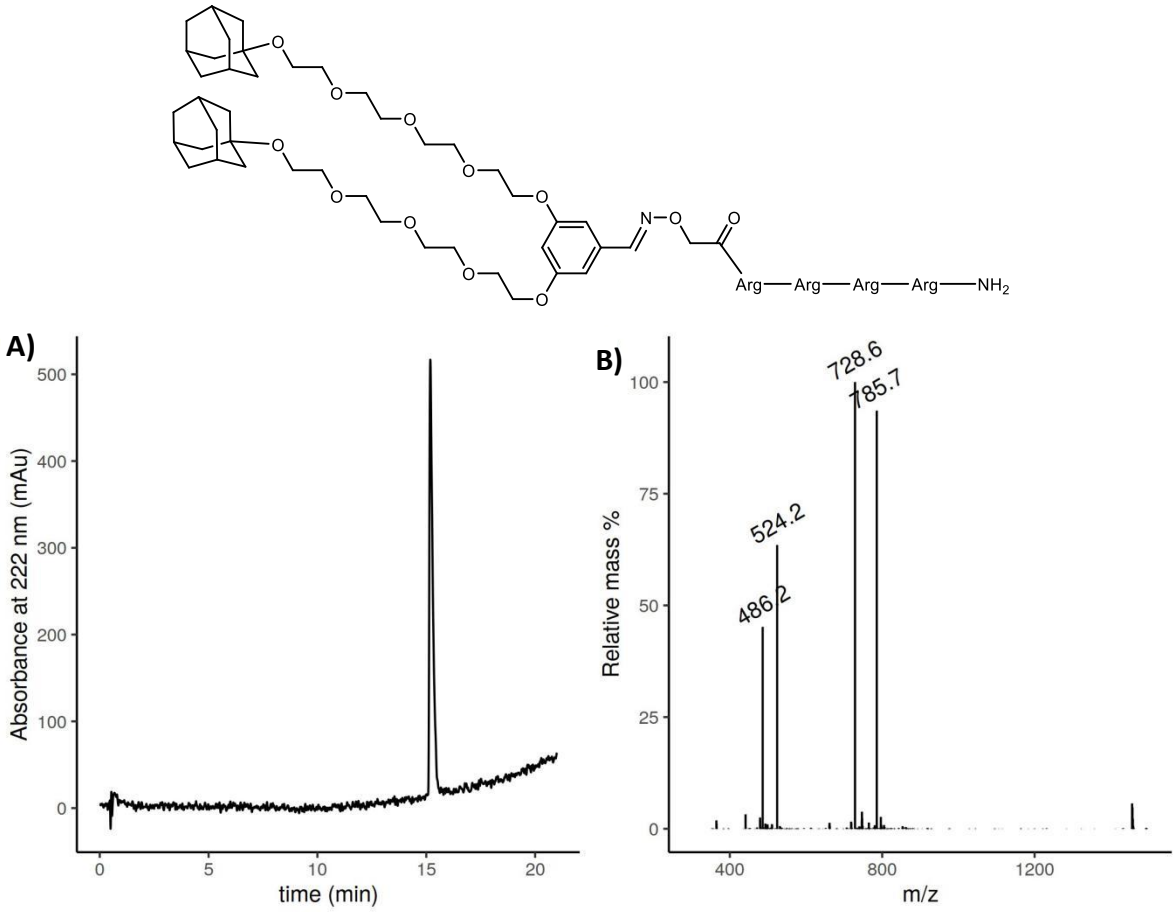

Figure 98. A) HPLC (water-ACN 95:5 → 5:95 in 21 min) and B) corresponding MS spectra of derivative **Ad_2R_4**.

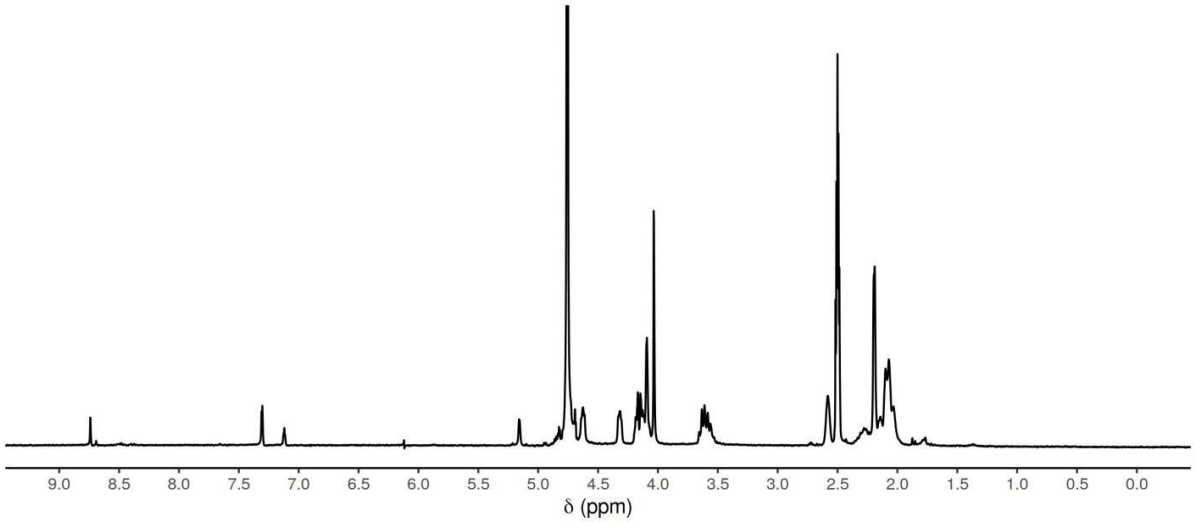

Figure 99. ^{1}H NMR (300 MHz, D_2O, 273K) of derivative **Ad_2R_4**.

4.10. HPLC-MS and ^{1}H NMR spectra of Ad_2R_8

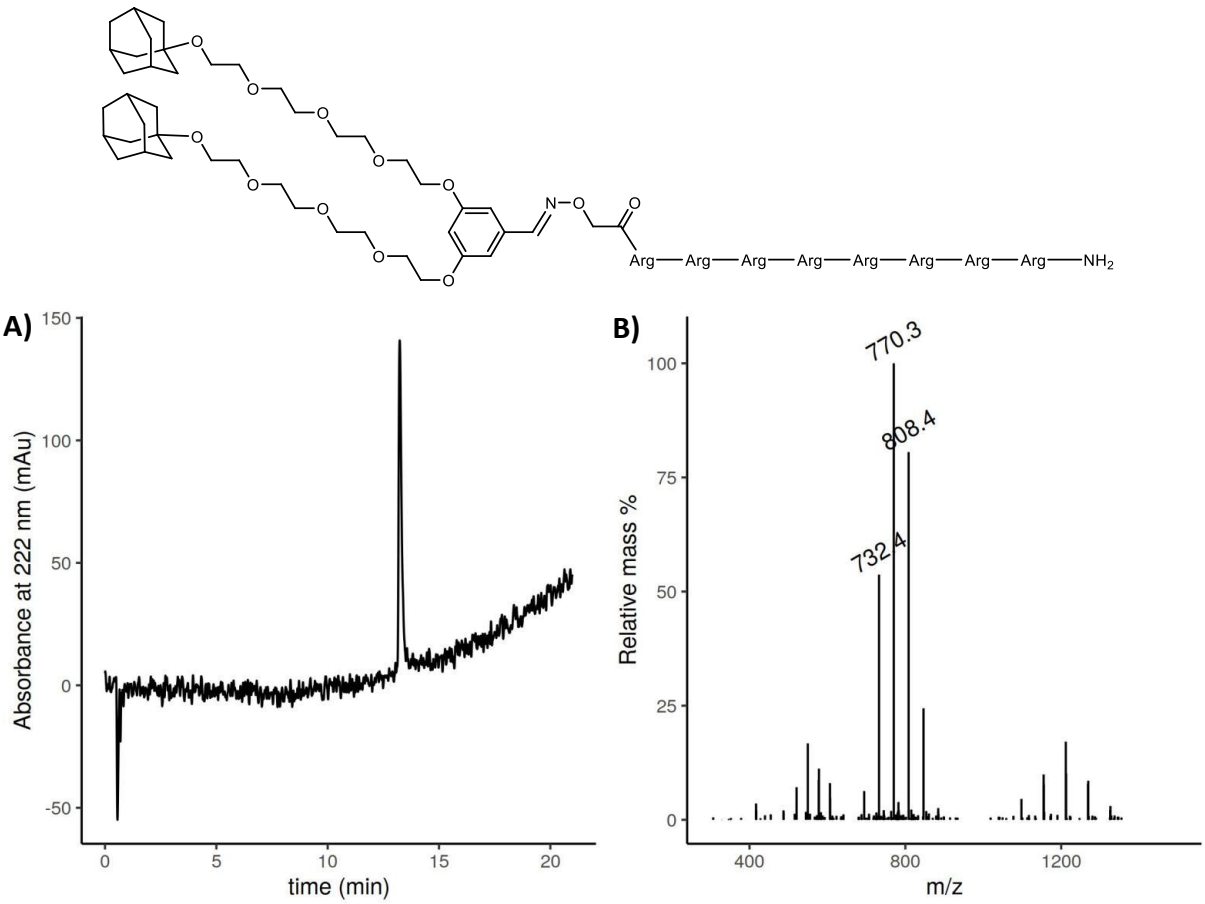

Figure 100. A) HPLC (water-ACN 95:5 → 5:95 in 21 min) and B) corresponding MS spectra of derivative **Ad_2R_8**.

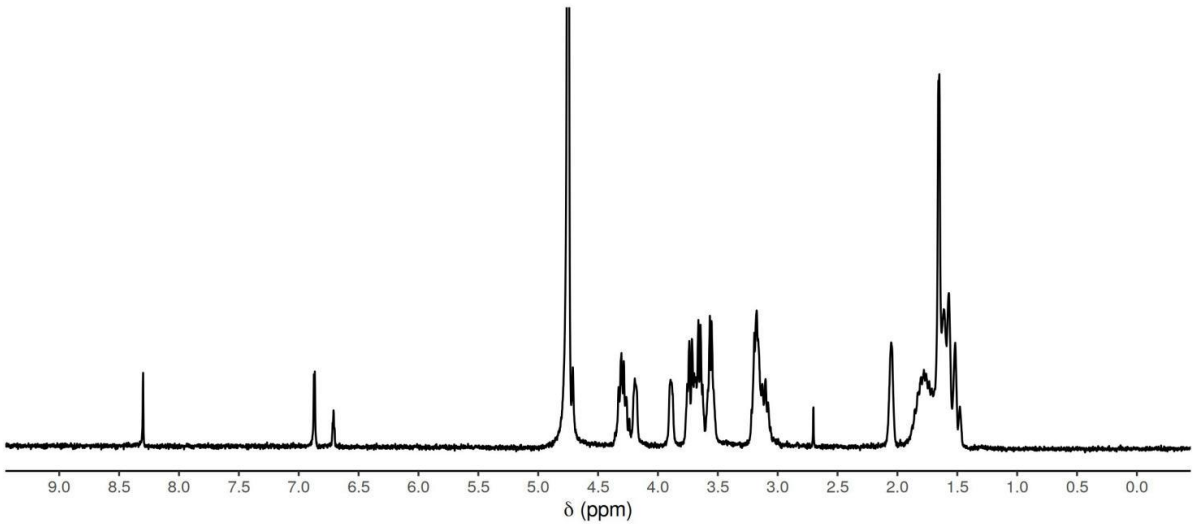

Figure 101. ^{1}H NMR (300 MHz, D_2O, 273K) of derivative **Ad_2R_8**.

4.11. ^{1}H NMR spectra of 7

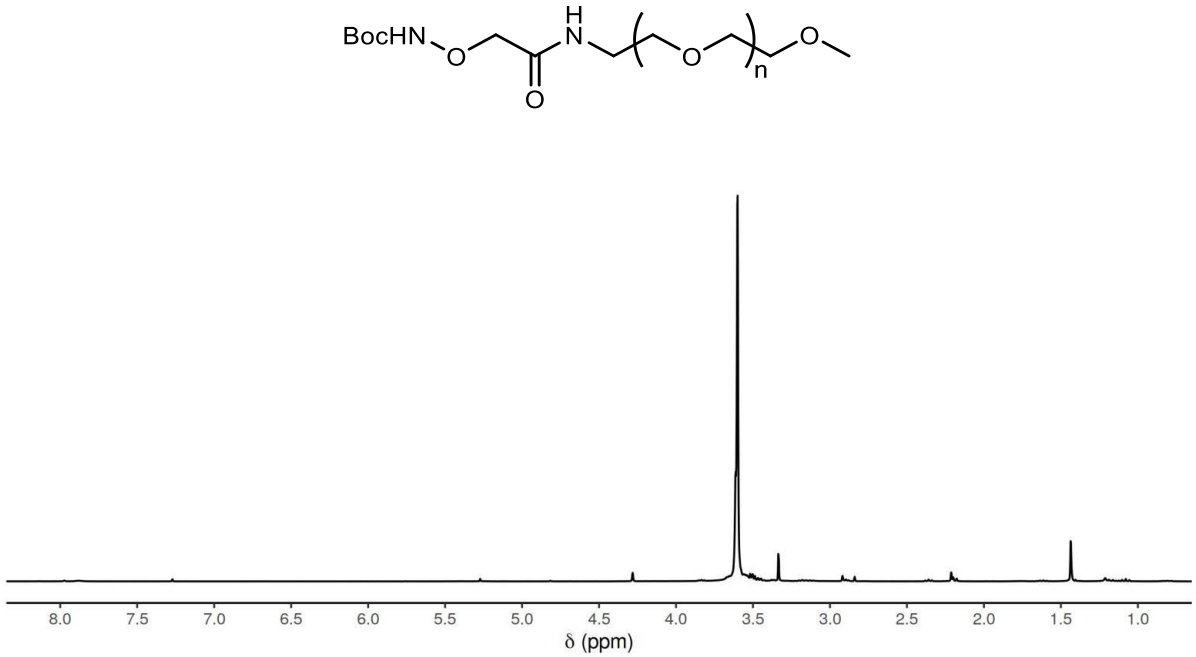

Figure 102. ^{1}H NMR (300 MHz, $CDCl_3$, 273K) of derivative **7**.

4.12. ^{1}H NMR spectra of 8

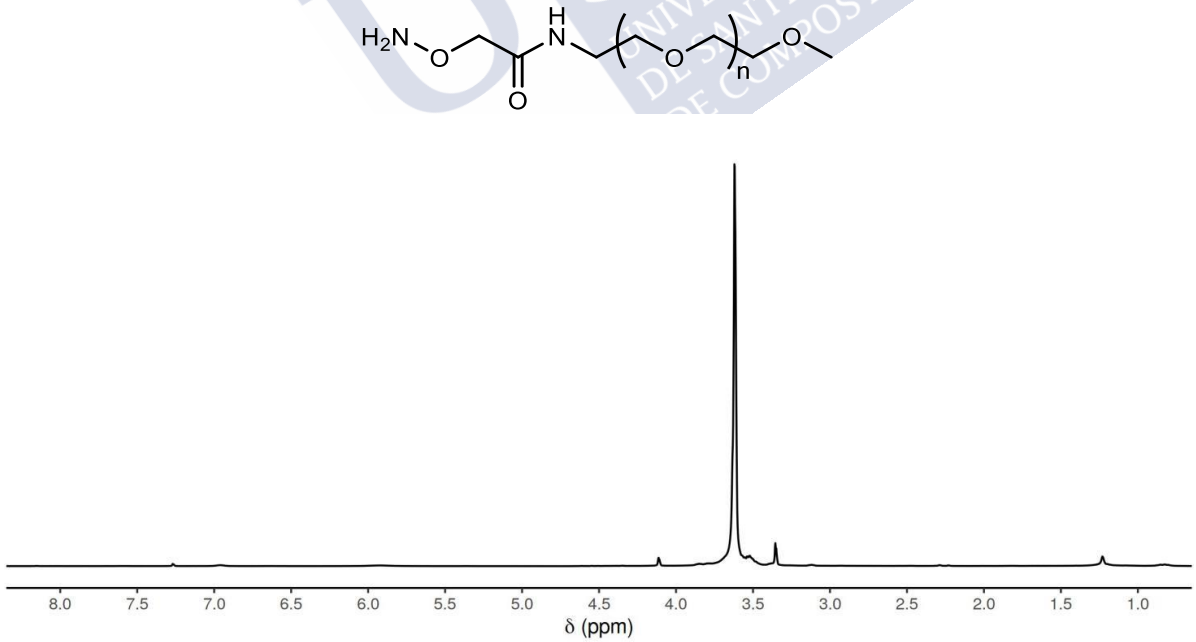

Figure 103. ^{1}H NMR (300 MHz, $CDCl_3$, 273K) of derivative **8**.

4.13. HPLC-MS and ^{1}H NMR spectra of AdPEG

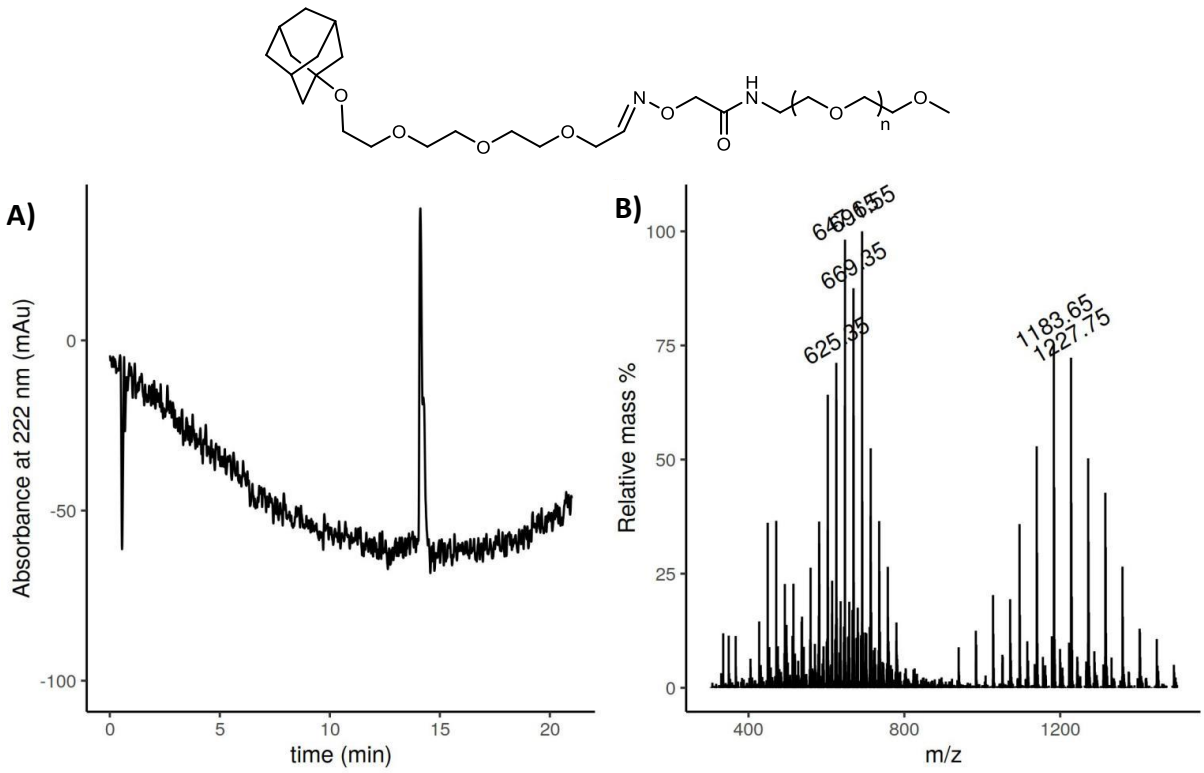

Figure 104. A) HPLC (water-ACN 95:5 → 5:95 in 21 min) and B) corresponding MS spectra of derivative **AdPEG**.

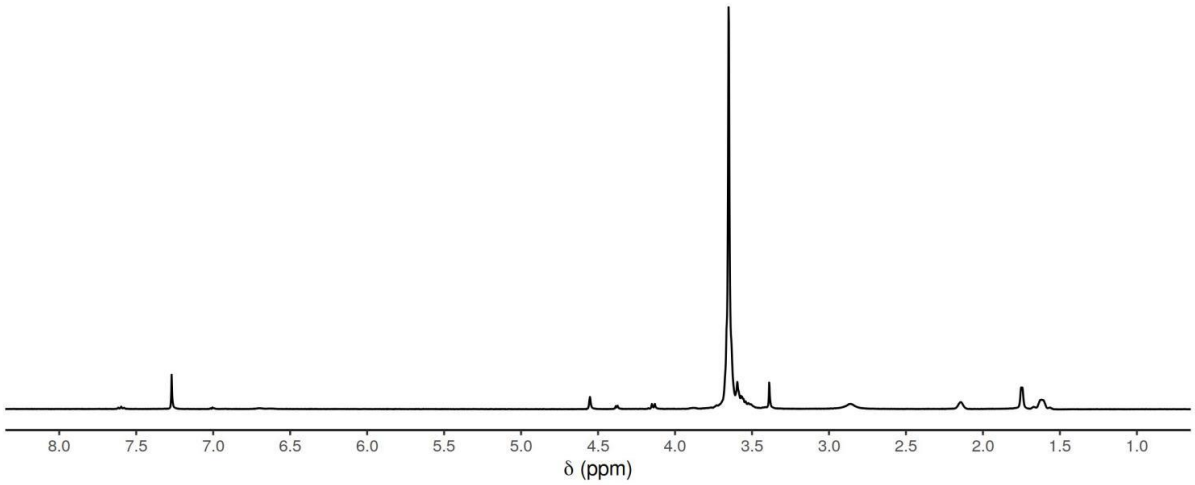

Figure 105. ^{1}H NMR (300 MHz, $CDCl_3$, 273K) of derivative **AdPEG**.

4.14. HPLC-MS and ^{1}H NMR spectra of Ad$_2$PEG

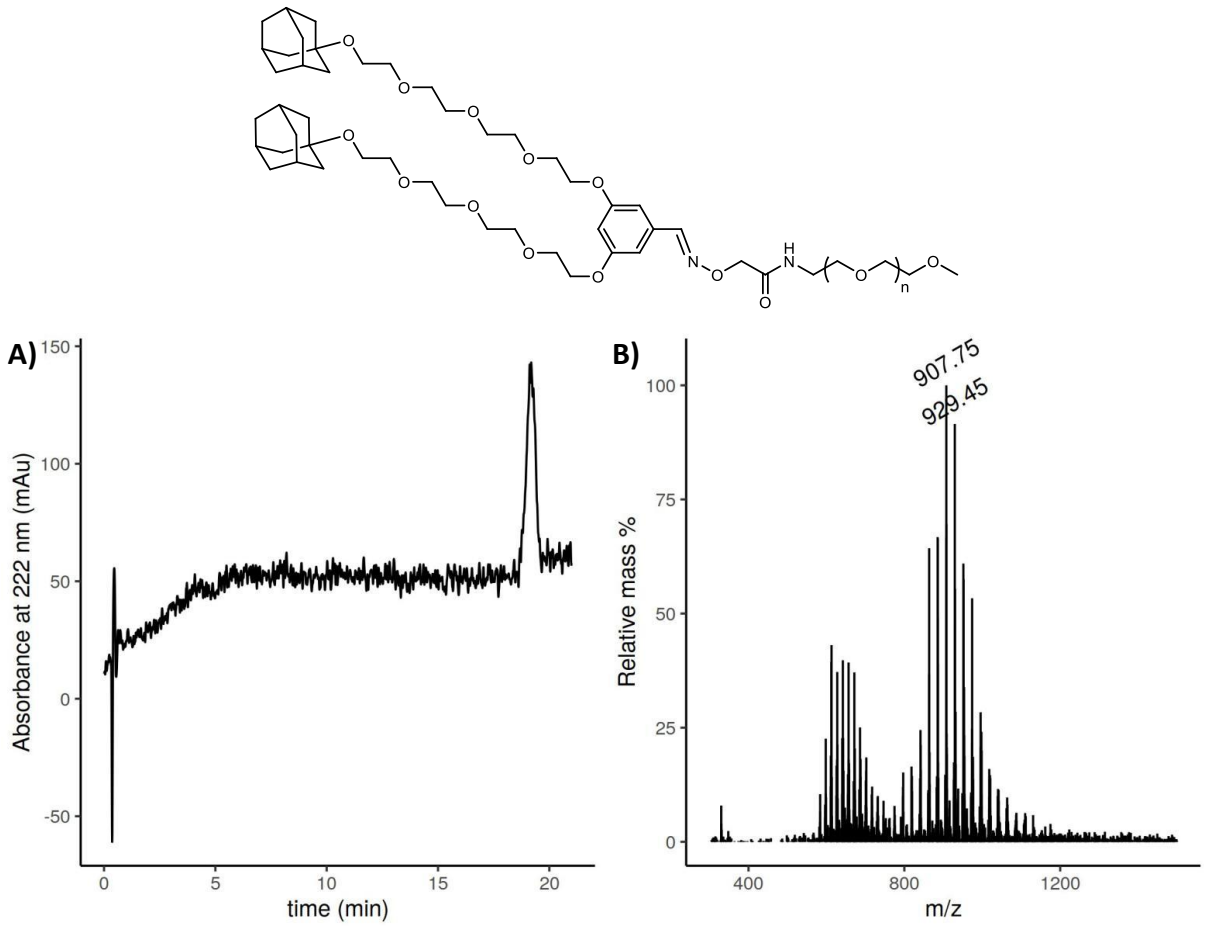

Figure 106. A) HPLC (water-ACN 95:5 → 5:95 in 21 min) and B) corresponding MS spectra of derivative **Ad$_2$PEG**.

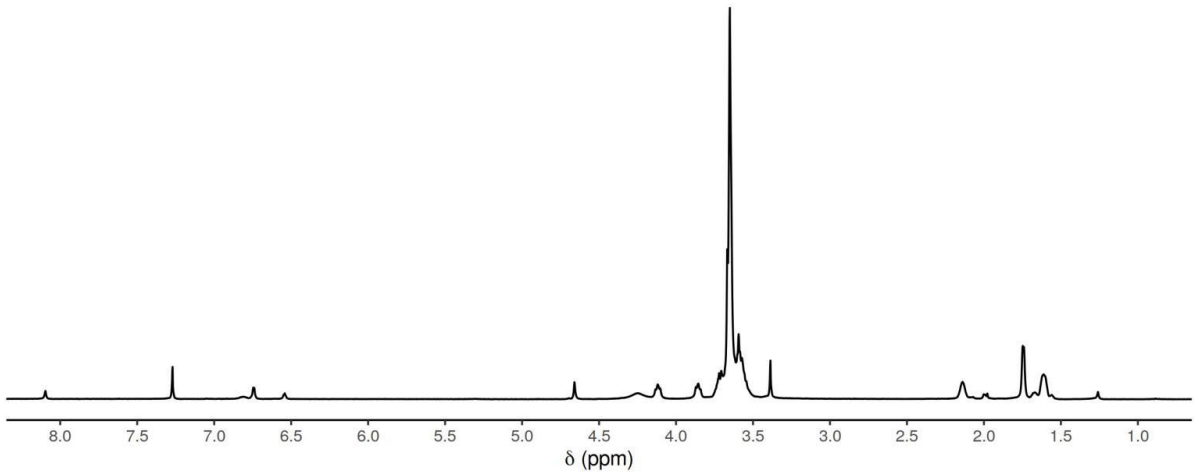

Figure 107. ^{1}H NMR (300 MHz, $CDCl_3$, 273K) of derivative **Ad$_2$PEG**.

4.15. HPLC-MS and ^{1}H NMR spectra of AcE_9

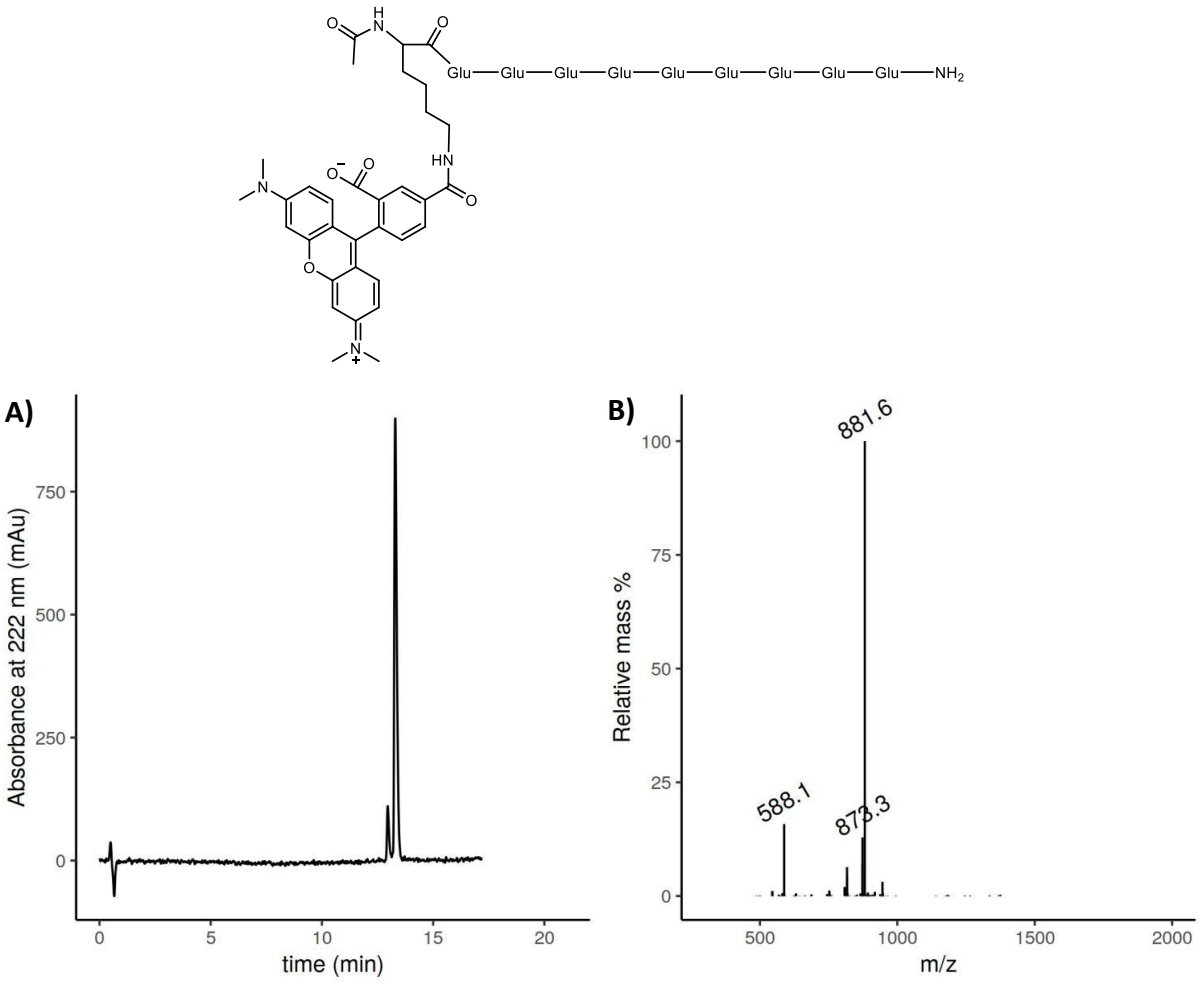

Figure 108. A) HPLC (water-ACN 95:5 → 5:95 in 21 min) and B) corresponding MS spectra of derivative **AcE_9**.

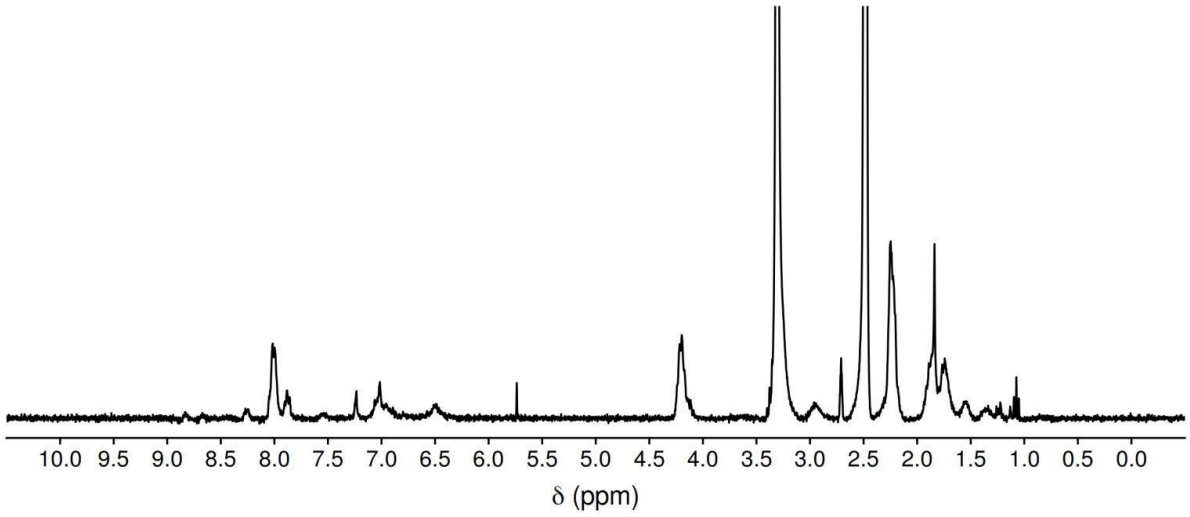

Figure 109. ^{1}H NMR (300 MHz, DMSO - d_6, 273K) of derivative **AcE_9**.

4.16. HPLC-MS and ^{1}H NMR spectra of 9

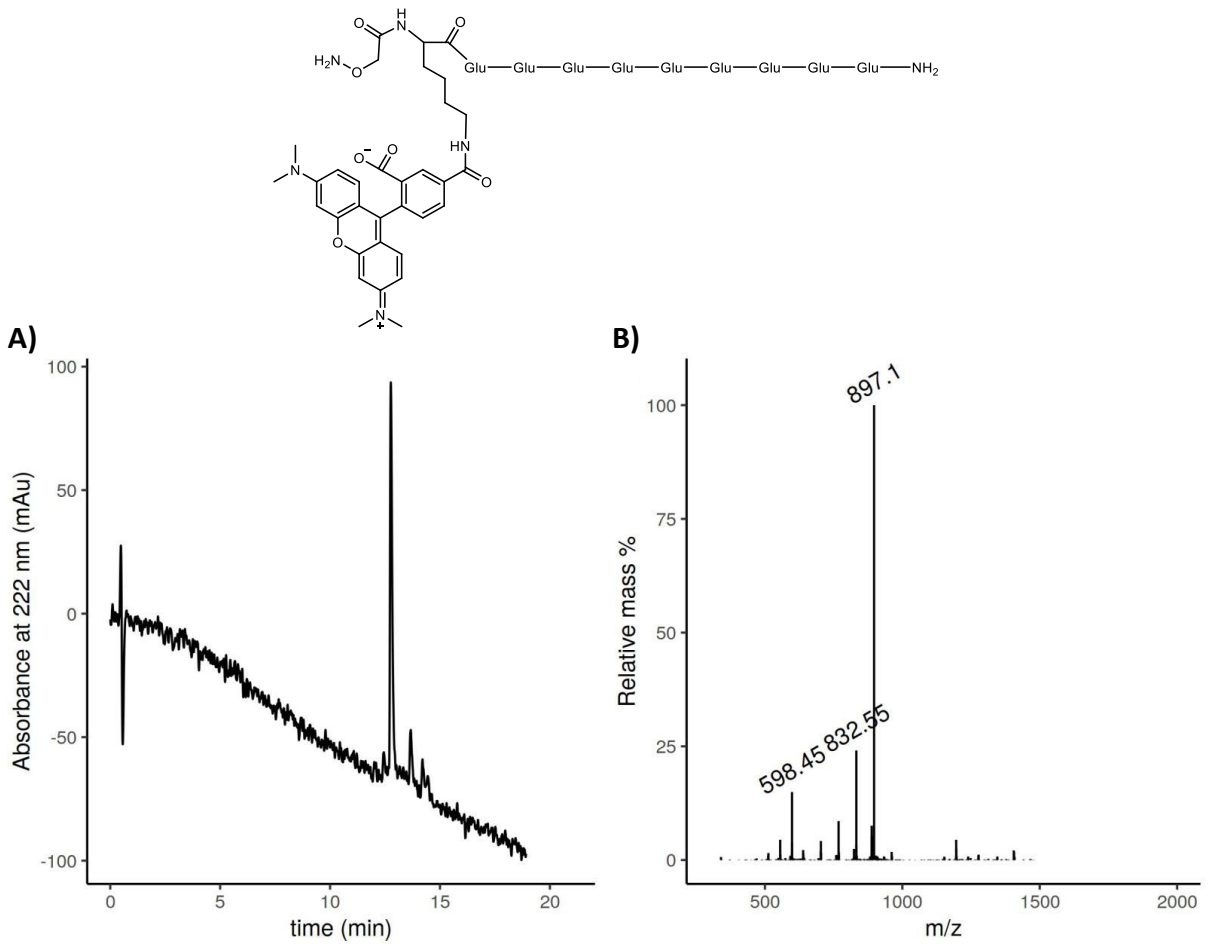

Figure 110. A) HPLC (water-ACN 95:5 → 5:95 in 21 min) and B) corresponding MS spectra of derivative **9**.

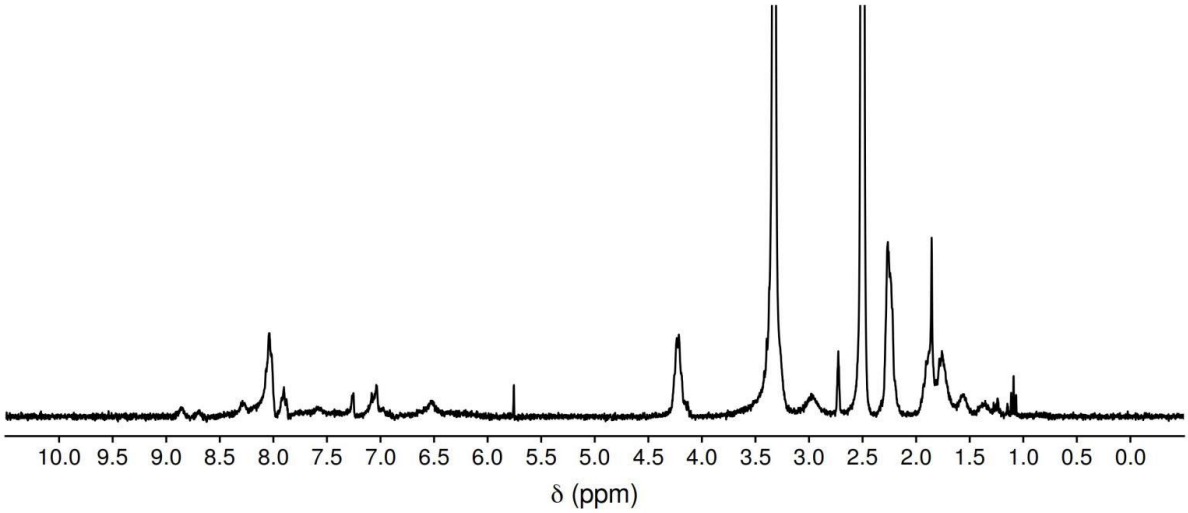

Figure 111. ^{1}H NMR (300 MHz, DMSO - d_6, 273K) of derivative **9**.

4.17. HPLC-MS and ^{1}H NMR spectra of AdE$_9$

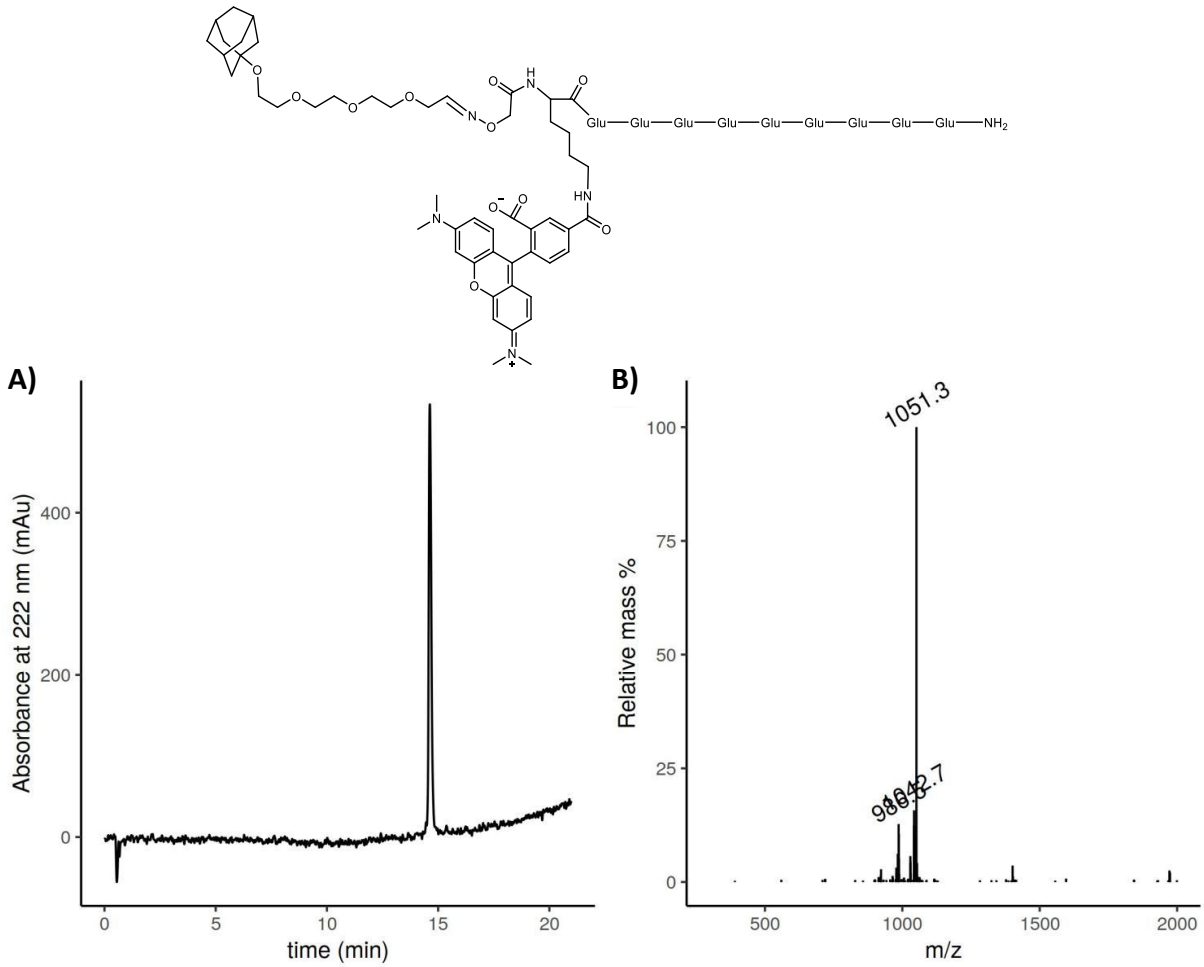

Figure 112. A) HPLC (water-ACN 95:5 → 5:95 in 21 min) and B) corresponding MS spectra of derivative **AdE$_9$**.

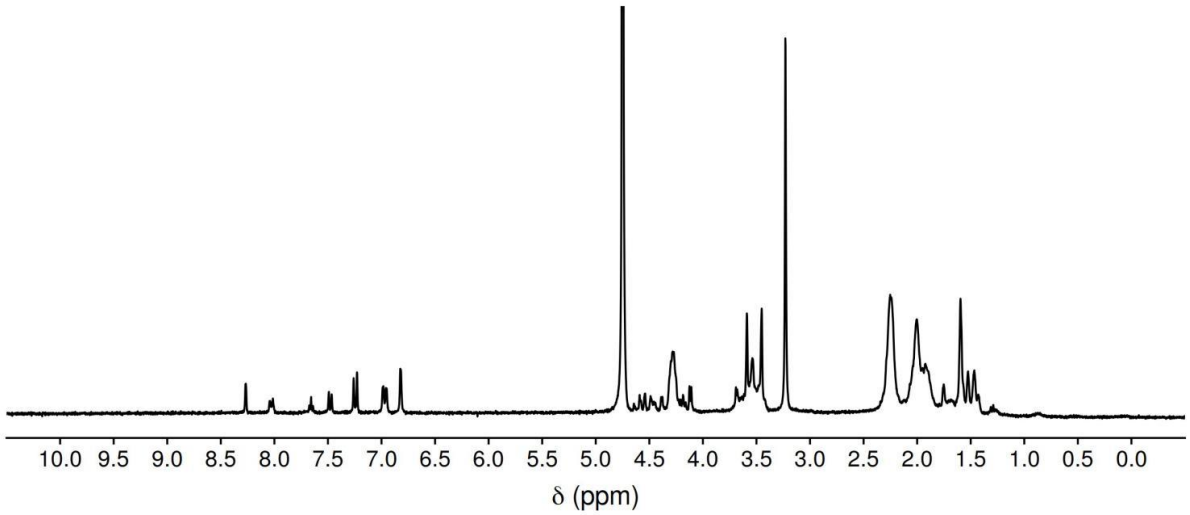

Figure 113. ^{1}H NMR (300 MHz, D_2O, 273K) of derivative **AdE$_9$**.

USC
UNIVERSIDADE
DE SANTIAGO
DE COMPOSTELA

Chapter III:
Design of new thermoresponsive elastin-based cyclic peptides

USC
UNIVERSIDADE
DE SANTIAGO
DE COMPOSTELA

Introduction

USC
UNIVERSIDADE
DE SANTIAGO
DE COMPOSTELA

1. Thermoresponsive systems

The so-called "smart" materials have attracted the attention of the scientific community due to their innovative and excellent responsive capabilities.[315] One of the most prominent groups of "smart" materials are the stimuli-responsive polymers. These materials have the ability to respond to a wide variety of stimuli such as pH, temperature, ionic strength, electric or magnetic field, or light.[316] Among them, thermoresponsive polymers constitute a class of these materials that can respond to the variation of environmental temperature.[317] Such systems have shown promising biomedical applications such as drug delivery, gene therapy, or tissue engineering.[318]

Considering the temperature-driven change of their physicochemical properties, thermoresponsive polymers can be distinguished considering their miscibility gap in two main groups: polymers that show a lower critical solution temperature (LCST) or an upper critical solution temperature (UCST). LCST and UCST behaviors are defined by their phase critical temperature points, *below* or *above*, respectively, on which the polymer is totally miscible with the solvent (Figure 114). The phase transition temperature is defined as the cloud point temperature (T_{CP}) and the values for a variety of different polymers have been reported.[319] For instance, below the T_{CP}, a LCST polymer in water leads to a clear solution (Figure 114) because their chains are hydrated. Heating above the T_{CP} produces the collapse and aggregation of the polymer chains and the release of the water molecules to the bulk water, resulting in a turbid solution. Contrary, a UCST polymer presents the opposite behavior.[320]

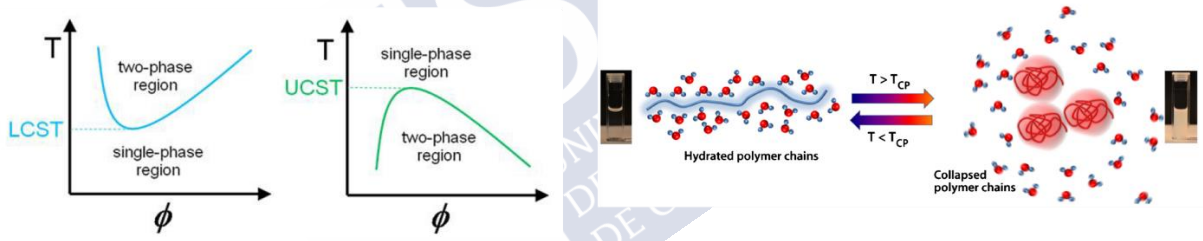

Figure 114. Left. Schematic representation of phase diagrams of LCST (left) and UCST (right) polymers in solution showing temperature against polymer volume fraction Φ. Reprinted from ref. 323 under the terms of the Creative Commons CC-BY license. Left. Schematic representation at the molecular level of reversible phase transition of LCST polymer in water. Reprinted from ref. 320 under the terms of the Creative Commons CC-BY-NC-ND license. Copyright 2015 The Authors. Published by Elsevier Ltd.

Among the vast variety of polymers that show T_{CP} with LCST behavior,[319] poly(*N*-isopropylacrylamide) (PNIPAM) is one of the most used. This material shows a T_{CP} of around 32 °C[321] and consequently, results useful for a wide range of biomedical applications since its T_{CP} is close to the body temperature.[322] Interestingly, the copolymerization of PNIPAM with polar or non-polar moieties allowed to tune the T_{CP} of the resulting copolymer. Other relevant examples of well-studied polymers with thermoresponsive properties are poly(*N*-

[315] Y. Lu, A. A. Aimetti, R. Langer, Z. Gu, *Nat. Rev. Mater.* **2017**, *2*, 16075.
[316] M. Wei, Y. Gao, X. Li, M. J. Serpe, *Polym. Chem.* **2017**, *8*, 127-143.
[317] E. Cabane, X. Zhang, K. Langowska, C. G. Palivan, W. Meier, *Biointerphases* **2012**, *7*, 9.
[318] A. Gandhi, A. Paul, S. O. Sen, K. K. Sen, *Asian J. Pharm. Sci.* **2015**, *10*, 99-107.
[319] D. Roy, W. L. A. Brooks, B. S. Sumerlin, *Chem. Soc. Rev.* **2013**, *42*, 7214-7243.
[320] V. R. de la Rosa, P. Woisel, R. Hoogenboom, *Mater. Today* **2016**, *19*, 44-55.
[321] E. Gil, S. Hudson, *Prog. Polym. Sci.* **2004**, *29*, 1173-1222.
[322] C. de las H. Alarcón, S. Pennadam, C. Alexander, *Chem. Soc. Rev.* **2005**, *34*, 276-285.

vinlycaprolactam) (PVCL) or poly(oligoethyleneglycol) (POEG) which show a LCST between 25 and 35 °C or around 85 °C respectively.[323]

Temperature responsive polymers based on polypeptides and related artificial poly(amino acids) have attracted a great deal of interest in the drug delivery field due to their unique properties such as biocompatibility, biodegradability, and LCST behavior.[324] For instance, since the thermoresponsive behavior of elastin was found, the research of elastin-like polypeptides (ELPs) and synthetic elastin-based polymers have arisen.[319]

2. Elastin

Elastin is a structural protein found in multiple mammalian tissues such as lungs, skin, and ligaments where it acts as an elastomeric material (Figure 115).[325] Tropoelastin is the un-cross-linked precursor protein of elastin, whose primary structure is characterized by repeating pentapeptide sequences. The most commonly occurring is $Val_1Pro_2Gly_3Val_4Gly_5$ or VPGVG, defined as the elastin canonical sequence.[326] The secondary structure of this pentapeptide has been identified as a proline β turn type II and showed LCST thermoresponsive behavior (Figure 115). This property is derived from the temperature-driven conformational change from an expanded form at low temperature to a contracted structure at a high temperature. The extended structure is mainly stabilized by interactions of the dipeptide Pro_2-Gly_3 with a Val_1 C=O --- H-N Val_4 hydrogen bond.[327] The transition temperature of this sequence is approximately 27 °C.[328] Due to this thermoresponsive behavior, during the last years, ELPs and synthetic elastin-based polymers have been developed.[319]

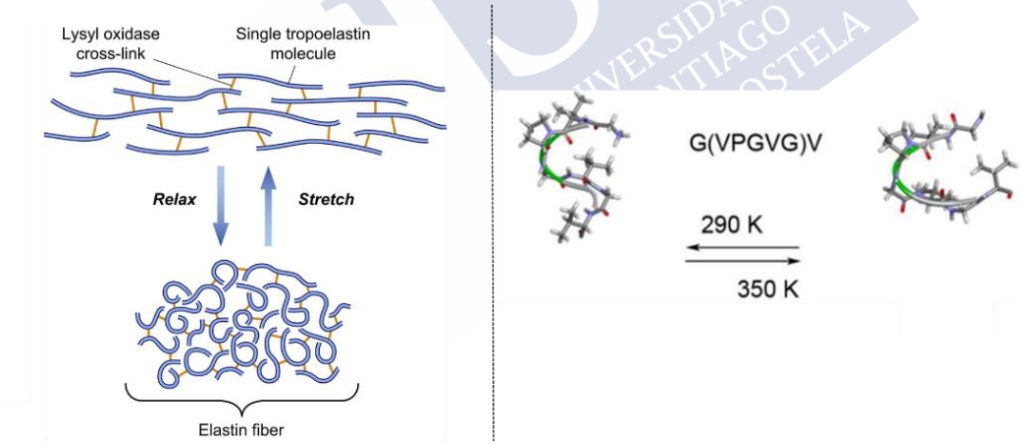

Figure 115. Left. Schematic illustration of elastin protein showing elastic capabilities. Reprinted with permission from ref. 325 Copyright 2012 The Voice Foundation. Published by Elsevier Inc. Right. Conformational change of the elastin moiety from expanded (low temperature) to a contracted form (high temperature). Reprinted with permission from ref. 327. Copyright 2014 American Chemical Society.

[323] M. A. Ward, T. K. Georgiou, *Polymers* **2011**, *3*, 1215-1242.
[324] P. Zarrintaj, M. Jouyandeh, M. R. Ganjali, B. S. Hadavand, M. Mozafari, S. S. Sheiko, M. Vatankhah-Varnoosfaderani, T. J. Gutiérrez, M. R. Saeb, *Eur. Polym. J.* **2019**, *117*, 402-423.
[319] D. Roy, W. L. A. Brooks, B. S. Sumerlin, *Chem. Soc. Rev.* **2013**, *42*, 7214-7243.
[325] J. Moore, S. Thibeault, *J. Voice* **2012**, *26*, 269-275.
[326] J. C. M. van Hest, D. A. Tirrell, *Chem. Commun.* **2001**, *19*, 1897-1904.
[327] N. K. Li, F. G. Quiroz, C. K. Hall, A. Chilkoti, Y. G. Yingling, *Biomacromolecules* **2014**, *15*, 3522-3530.
[328] H. Reiersen, A. R. Clarke, A. R. Rees, *J. Mol. Biol.* **1998**, *283*, 255-264.

2.1.Elastin-like polypeptides (ELPs)

ELPs are linear polymers that consist of a repetition of the elastin canonical sequence or variations of it (i.e. Val-Pro-Gly-X-Gly, where X = any amino acid other than proline). These polymers have been synthesized using recombinant strategies or solid-phase peptide synthesis (SPPS).[329,330] Interestingly, ELPs show reversible LCST behavior.[331] These polymers present high solubility in aqueous solution at low temperatures but aggregate due to the entropically driving dehydration of the valine hydrophobic side chains when heated.[332] ELPs thermoresponsivity is related to the conformational change of the pentamer and intermolecular van der Waals interactions between the different moieties. Interestingly, the transition temperature can be changed by modifying the different residues which constitute the pentapeptide and this can be related to some physical properties of this residue such as its hydrophobicity.[333,334] For instance, by using recombinant technologies, Chilkoti and Quiroz showed that modifying or adding key amino acids in the tropoelastin repeated sequence, the LCST behavior can be changed as a consequence of the modification of its hydropathy.[335]

ELPs have been applied in the biomedical field as substrates for cell adhesion or as drug delivery systems due to their high biocompatibility and LCST behavior. For instance, the group of prof. Chilkoti applied a temperature-responsive ELP attached to doxorubicin to promote temperature-mediated tumor suppression.[336] The hybrid material was used in cancer therapy being able to accumulate the drug in the cell nucleus.

2.2.Elastin-based polymers (EBPs)

Although the linear elastin-like polypeptides showed promising thermoresponsive properties, the synthesis of these polymers, by SPPS or by using recombinant methods, required tedious and not scalable methodologies. Therefore, elastin-based side-chain polymers (EBPs) emerged as an alternative to solve these synthetic limitations.[337] EBPs were defined as artificial polymers with VPGVG peptide sequences as side chains.

Different strategies have been used for the synthesis of LCST EBPs. For instance, the group of prof. van Hest polymerized a methacrylate derivative of VPGVG by atom transfer radical polymerization (ATRP) to obtain polymers with this type of properties.[337] A few years later, the

[329] F. Aladini, C. Araman, C. F. W. Becker, *J. Pept. Sci.* **2016**, *22*, 334-342.
[330] W. Hassouneh, T. Christensen, A. Chilkoti, *Curr. Protoc. Protein Sci.* **2010**, *61*, 6.11.1-6.11.16.
[331] S. R. MacEwan, A. Chilkoti, *Biopolymers* **2010**, *94*, 60-77.
[332] B. Li, D. O. V. Alonso, B. J. Bennion, V. Daggett, *J. Am. Chem. Soc.* **2001**, *123*, 11991-11998.
[333] D. W. Urry, C. H. Luan, T. M. Parker, D. C. Gowda, K. U. Prasad, M. C. Reid, A. Safavy, *J. Am. Chem. Soc.* **1991**, *113*, 4346-4348.
[334] D. W. Urry, D. C. Gowda, T. M. Parker, C.-H. Luan, M. C. Reid, C. M. Harris, A. Pattanaik, R. D. Harris, *Biopolymers* **1992**, *32*, 1243-1250.
[335] F. G. Quiroz, A. Chilkoti, *Nat. Mater.* **2015**, *14*, 1164-1171.
[336] M. R. Dreher, D. Raucher, N. Balu, O. Michael Colvin, S. M. Ludeman and A. Chilkoti, *J. Control. Release*, **2003**, *91*, 31-43.
[337] L. Ayres, M. R. J. Vos, P. J. H. M. Adams, I. O. Shklyarevskiy, J. C. M. van Hest, *Macromolecules* **2003**, *36*, 5967-5973.

group of prof. Cameron developed an improved strategy to prepare EBPs via RAFT polymerization (Figure 116).[338]

Importantly, the behavior in solution of these polymers has been explored and similar self-assembly and LCST properties to ELPs were demonstrated. Interestingly, these polymers also showed dependence of the transition temperature on polymer concentration and molecular weight.[339] However, an important difference was found. These EBPs are not only thermoresponsive but also showed a strong dependence of the transition temperature on the pH of the media due to the presence of the free terminal carboxylic acid on each repeat unit.[340]

More recently, UCST EBPs have also been synthesized. Bergueiro *et al.* prepared an elastin-based side-chain helical poly(phenylacetylene) (EBPPA) having attached the thermoresponsive VPGVG pentapeptide to each phenylacetylene repit.[341] Contrary to all previously reported studies of polymers using this particular sequence, a conformational dependent UCST behavior was found for these helical hybrids (Figure 116).

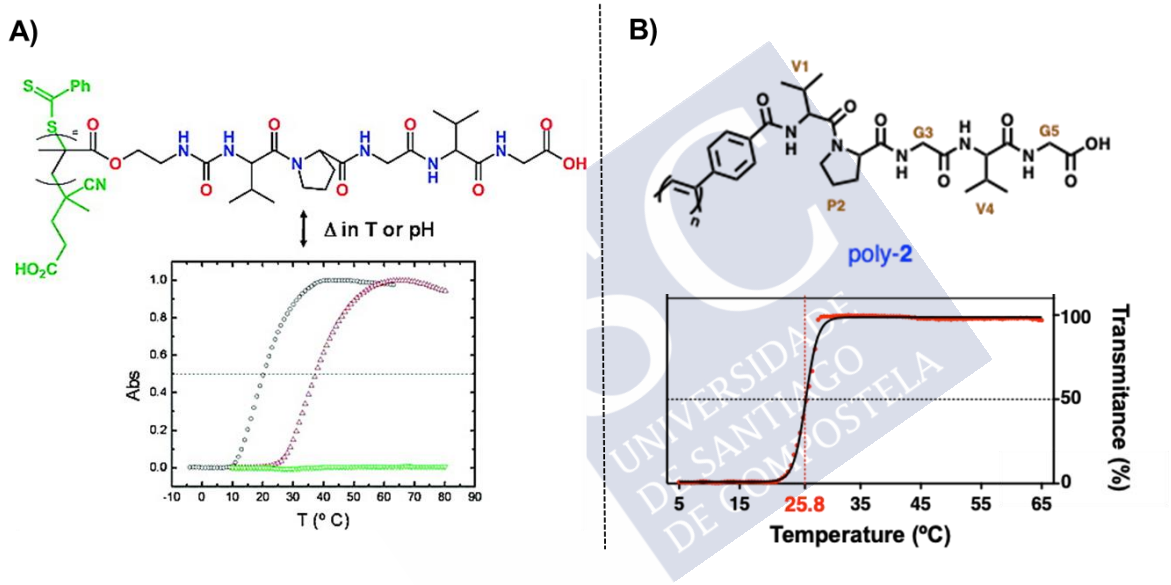

Figure 116. Representative examples of LCST (A) and UCST (B) elastin-based side-chain polymers (EBPs). A) Top, chemical structure of EBP prepared by RAFT polymerization. Bottom, UV-visible spectra of the upper LCST EBP showing an increase of the Absorbance (Abs) with the rise of the temperature (ºC). Reprinted with permission from ref. 338. Copyright 2007 American Chemical Society. B) Top, chemical structure of the elastin moiety incorporated into poly(phenylacetylene) scaffold. Bottom, turbidimetry spectra of the upper UCST polymer EBPPA showing an increase of the transmittance (%) with the increase of the temperature (ºC). Reprinted and adapted from ref. 341 with permission from John Wiley and Sons. Copyright 2017 Wiley-VCH Verlag GmbH & Co. KGaA, Weinheim.

[338] F. Fernández-Trillo, A. Duréault, J. P. M. Bayley, J. C. M. van Hest, J. C. Thies, T. Michon, R. Weberskirch, N. R. Cameron, *Macromolecules* **2007**, *40*, 6094-6099.
[339] L. Ayres, K. Koch, J. C. M. van Hest, *Macromolecules* **2005**, *38*, 1699-1704.
[340] F. Fernández-Trillo, J. C. M. Van Hest, J. C. Thies, T. Michon, R. Weberskirch, N. R. Cameron, *Chem. Commun.* **2008**, 2230-2232.
[341] S. Arias, F. Freire, M. Calderón, J. Bergueiro, *Angew. Chem. Int. Ed.* **2017**, *56*, 11420-11425.

3. Supramolecular polymers as platform for novel thermoresponsive materials

3.1. Supramolecular polymers

Supramolecular polymers have been defined as a type of polymers whose monomeric subunits hold together by using non-covalent interactions. A wide range of non-covalent interactions has been explored to build up supramolecular polymers such as hydrogen bonding, van der Waals interactions, π-π stacking, or metal coordination.[342,343] For instance, a widely explored type of supramolecular polymers is self-assembling cyclic peptide nanotubes (SCPNs).[344]

3.2. Self-assembling cyclic peptide nanotubes (SCPNs)

One of the most commonly applied strategies for the formation of supramolecular nanotubes is the stacking of cyclic units that allows the strict control of the internal diameter of the nanotube.[345] In this sense, self-assembling cyclic peptide nanotubes (SCPNs) have been constructed using *D*,*L*-α-cyclic peptides (*D*,*L*-α-CPs), which consist of an even number of amino acids with alternating chirality. Due to this, the cyclic peptide adopts a flat conformation in which the amide groups (carbonyl and NH) are oriented perpendicular to the ring plane. Cyclic peptides self-assembly is based on the stacking of various units of these molecules through the formation of a network of hydrogen bonds, between the amide groups on one side of the CP with the complementary side of the other CP, which holds adjacent macrocycles together.[346] In this supramolecular entity, the highly uniform internal diameter is defined by the size of the CP used[347] thanks to all the side chains of the amino acids of the CP are oriented outwards of the hollow structure. In addition, this external irradiation of all the residues sides chains define the properties of the external surface of the CP nanotubes.[345]

The initial studies in this field date back to 1974, when De Santis and coworkers showed, through theoretical studies, that cyclic peptides consisting of an even number of α-amino acids with alternating chirality (*D*,*L*-α-CPs) could be used as precursors of CP nanotubes.[348] After this report, different experimental approaches were carried out in the following years, although without success in demonstrating the stacking of these precursors due to the low solubility of the studied CPs.[349]

In 1993, the group of prof. Ghadiri demonstrated the formation of nanotubular structures from *D*,*L*-α-CPs (Figure 117).[350] In this work, the authors demonstrated that the octapeptide *c*-[(*L*-Gln-*D*-Ala-*L*-Glu-*D*-Ala-)$_2$] formed microcrystalline aggregates, starting from a basic aqueous solution, in which the peptide was completely soluble, due to the deprotonation of the

[342] L. Brunsveld, B. J. B. Folmer, E. W. Meijer, R. P. Sijbesma, *Chem. Rev.* **2001**, *101*, 4071-4098.
[343] L. Yang, X. Tan, Z. Wang, X. Zhang, *Chem. Rev.* **2015**, *115*, 7196-7239.
[344] J. Y. Rho, H. Cox, E. D. H. Mansfield, S. H. Ellacott, R. Peltier, J. C. Brendel, M. Hartlieb, T. A. Waigh, S. Perrier, *Nat. Commun.* **2019**, *10*, 4708.
[345] N. Rodríguez-Vázquez, M. Amorín, J. R. Granja, *Org. Biomol. Chem.* **2017**, *15*, 4490-4505.
[346] D. T. Bong, T. D. Clark, J. R. Granja, M. R. Ghadiri, *Angew. Chem. Int. Ed.* **2001**, *40*, 988-1011.
[347] R. Hourani, C. Zhang, R. van der Weegen, L. Ruiz, C. Li, S. Keten, B. A. Helms, T. Xu, *J. Am. Chem. Soc.* **2011**, *133*, 15296-15299.
[348] P. De Santis, S. Morosetti, R. Rizzo, *Macromolecules* **1974**, *7*, 52-58.
[349] L. Tomasic, G. P. Lorenzi, *Helv. Chim. Acta* **1987**, *70*, 1012-1016.
[350] M. R. Ghadiri, J. R. Granja, R. A. Milligan, D. E. McRee, N. Khazanovich, *Nature* **1993**, *366*, 324-327.

Glu residues. It was shown that the reduction of the pH of the medium gave rise to long needles-shaped microcrystals (10-30 μm). The characterization of these nanotubes using microscopic and spectroscopic techniques demonstrated that the nanotubes were composed of stacked cyclic subunits. Furthermore, Fourier transform infrared (FTIR) spectroscopy experiments showed that CPs self-assembly was based on the formation of antiparallel *β*-sheets.

Subsequently, the cyclic peptide *c*-[(*L*-Gln-*D*-Ala-*L*-Glu-*D*-Ala-)$_3$], which presents an additional unit of the Gln and Glu based tetrapeptide than the pristine CP, was studied and shown to form nanotubes. This study allowed to demonstrate that the diameter of the CP nanotube could be controlled simply by modifying the number of residues that form the cyclic peptide.[351]

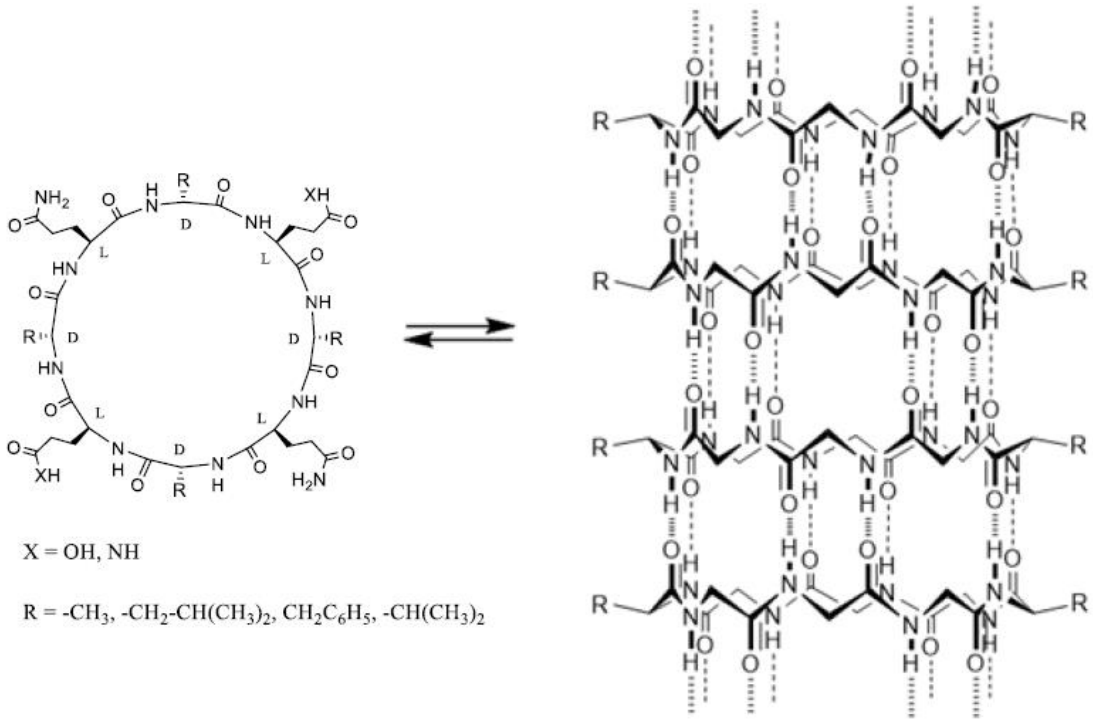

Figure 117. Chemical structure of cyclic peptide subunit and schematic representation of CP nanotube showing hydrogen bond formation between adjacent cyclic peptide subunits. Reprinted and adapted with permission from ref. 350 Copyright 1993 Springer Nature.

A few years later, it was shown that Glu residues were not essential for the formation of SCPNs.[352] CPs were synthesized containing four Gln and showed the ability to dissolve in acidic medium and the self-assembly process occurred, when the solution was basified. Interestingly, the hydrophobic residues were also modified (changing Ala for Leu, Phe, or Val) in order to explore the modulability of the external properties of the SCPNs. Importantly, the best results for nanotube formation were found with the CP equipped with four Leu residues.

Since the discovery of the CP nanotubes, different structural modifications have been carried out and also a wide range of applications have been described.[353] These supramolecular

[351] N. Khazanovich, J. R. Granja, D. E. McRee, R. A. Milligan, M. R. Ghadiri, *J. Am. Chem. Soc.* **1994**, *116*, 6011-6012.
[352] J. D. Hartgerink, J. R. Granja, R. A. Milligan, M. R. Ghadiri, *J. Am. Chem. Soc.* **1996**, *118*, 43-50.
[353] R. J. Brea, C. Reiriz, J. R. Granja, *Chem. Soc. Rev.* **2010**, *39*, 1448-1456.

entities have shown potential properties as analogues of membrane ion channels[354,355] or as ion sensors.[356] Moreover, SCPNs have been used as antibacterial[357] or antiviral agents[358] and also as drug delivery vehicles for antitumoral agents[359] and gene transfections.[360]

Recently, in our research group, a new CP has been designed which showed the ability to form fibers inside vesicles at basic pH.[361] This cyclic peptide was equipped with one Lys and two His residues that allowed to control the self-assembly in nanotubes with the variation of the pH (Figure 118). Furthermore, a Lys group was functionalized with an alcoxyamine moiety and subsequently, the hydrophobic pyrene group was attached, by forming an oxime bond. Interestingly, the basification of the aqueous solutions of this peptide gave rise to the formation of fibers due to the combination of different intermolecular interactions such as the histidine-histidine hydrogen bond formation, hydrophobic effects, and/or π-π interactions. More recently, a microfluidic device has been used to precisely form fibers into the core or at the interface of droplets by using the previously described CP structure.[362]

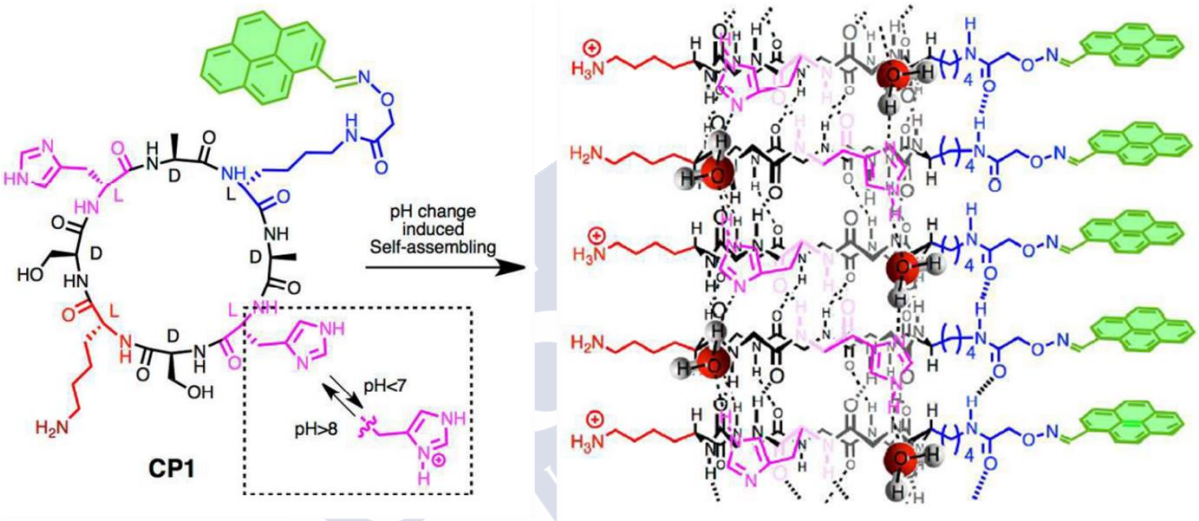

Figure 118. Chemical structure of the cyclic peptide designed to achieve self-assembly into CP nanotubes at basic pH. Reproduced from Ref. 361 with permission from The Royal Society of Chemistry.

Furthermore, a novel cyclic octapeptide with *D,L*-alternating chirality has been recently synthesized and showed for the first time the formation of nanosheets composed by CP nanotube bilayers.[363] This peptide consisted of a hydrophobic domain (Leu-Trp-Leu), two different hydrophilic pH-responsive residues, Glu and His, on either side of the peptide ring,

[354] M. R. Ghadiri, J. R. Granja, L. K. Buehler, *Nature* **1994**, *369*, 301-304.
[355] J. Montenegro, M. R. Ghadiri, J. R. Granja, *Acc. Chem. Res.* **2013**, *46*, 2955-2965.
[356] K. Motesharei, M. R. Ghadiri, *J. Am. Chem. Soc.* **1997**, *119*, 11306-11312.
[357] S. Fernandez-Lopez, H.-S. Kim, E. C. Choi, M. Delgado, J. R. Granja, A. Khasanov, K. Kraehenbuehl, G. Long, D. A. Weinberger, K. M. Wilcoxen, et al., *Nature* **2001**, *412*, 452-455.
[358] W. S. Horne, C. M. Wiethoff, C. Cui, K. M. Wilcoxen, M. Amorin, M. R. Ghadiri, G. R. Nemerow, *Bioorg. Med. Chem.* **2005**, *13*, 5145-5153.
[359] Y. Wang, S. Yi, L. Sun, Y. Huang, S. C. Lenaghan, M. Zhang, *J. Biomed. Nanotechnol.* **2014**, *10*, 445-454.
[360] M. Li, M. Ehlers, S. Schlesiger, E. Zellermann, S. K. Knauer, C. Schmuck, *Angew. Chem. Int. Ed.* **2016**, *55*, 598-601.
[361] A. Méndez-Ardoy, J. R. Granja, J. Montenegro, *Nanoscale Horizons* **2018**, *3*, 391-396.
[362] A. Méndez-Ardoy, A. Bayón-Fernández, Z. Yu, C. Abell, J. R. Granja, J. Montenegro, *Angew. Chem. Int. Ed.* **2020**, *132*, 6969-6975.
[363] I. Insua, J. Montenegro, *J. Am. Chem. Soc.* **2020**, *142*, 300-307.

and a hydrophilic Gln opposite to the Trp residue. This CP structure provided properties that follow a hierarchical organization at physiological pH (7.4) in aqueous media in which first self-assembled into one dimensional (1D) CP nanotubes that subsequently arrange to form nanotubular bilayers generating two dimensional (2D) nanosheets.

3.2.1. Stimuli-responsive SCPNs

Cyclic peptides have been decorated with polymers leading to the preparation of polymer-CP hybrids that can also form nanotubes.[364] Different synthetic strategies, such as click chemistry, have been applied for the construction of these hybrid materials.[365,366] The attachment of polymers to SCPNs allowed not only to improve the control over the nanotube length but also to solubilize SCPNs otherwise not soluble in certain solvents.[367] Interestingly, the incorporation of stimuli-sensitive polymers into SCPNs allowed the synthesis of "smart" supramolecular materials whose properties can be regulated by external stimuli such as the variation of the pH or the temperature.[368]

The incorporation of pH-responsive polymers into the cyclic peptide scaffold provided to supramolecular SCPNs with improved pH-responsive properties. For instance, the use of a pH-sensitive polymer, such as poly(acrylic acid), attached to a CP tuned the assembling properties by the variation of the pH.[369] More recently, the introduction of two arms of the pH-responsive polymer poly(dimethylamino ethyl methacrylate) (pDMAEMA) into a cyclic peptide scaffold also showed pH-responsive behavior of the hybrid nanotubes (Figure 119). In this work, it was shown that the uncharged conjugates self-assemble into bottlebrushes at basic pH that upon reduction of the pH showed a reversible decrease of the aggregation properties.[370]

On the other hand, the group of prof. S. Perrier and prof. K. A. Jolliffe prepared thermoresponsive cyclic peptide nanotubes by using the temperature-responsive polymer, poly(2-ethyl-2-oxazoline).[371] In this work, the degree of polymerization (DP) (20 and 40) was modified to tackle the importance of the polymer length on the nanotube properties. With this purpose, the authors developed a divergent approach in which the different polymers were attached to the cyclic peptide bearing two azido groups via copper-catalyzed azide-alkyne cycloaddition. These conjugates were able to self-assemble into nanotubes in water. Interestingly, when the temperature reaches the cloud point temperature (T_{CP}) of the conjugate, this supramolecular entity is reversibly transformed into microparticles (Figure 119). It was found that the conjugates with the DP 40 showed a T_{CP} at 70 ºC in water.[371] Furthermore, thermoresponsive SCPNs have also demonstrated abilities to form temperature-sensitive channels in phospholipid bilayers and their properties were used to switch the channel open state by temperature changes.[372]

---

[364] J. Couet, J. D. J. S. Samuel, A. Kopyshev, S. Santer, M. Biesalski, *Angew. Chem. Int. Ed.* **2005**, *44*, 3297-3301.
[365] R. Chapman, K. A. Jolliffe, S. Perrier, *Aust. J. Chem.* **2010**, *63*, 1169-1172.
[366] M. A. Gauthier, H.-A. Klok, *Chem. Commun.* **2008**, 2591-2611.
[367] R. Chapman, K. A. Jolliffe, S. Perrier, *Polym. Chem.* **2011**, *2*, 1956-1963.
[368] I. Cobo, M. Li, B. S. Sumerlin, S. Perrier, *Nat. Mater.* **2015**, *14*, 143-159.
[369] R. Chapman, G. G. Warr, S. Perrier, K. A. Jolliffe, *Chem. Eur. J.* **2013**, *19*, 1955-1961.
[370] S. Catrouillet, J. C. Brendel, S. Larnaudie, T. Barlow, K. A. Jolliffe, S. Perrier, *ACS Macro Lett.* **2016**, *5*, 1119-1123.
[371] R. Chapman, P. J. M. Bouten, R. Hoogenboom, K. A. Jolliffe, S. Perrier, *Chem. Commun.* **2013**, *49*, 6522-6524.
[372] M. Danial, C. M. N. Tran, K. A. Jolliffe, S. Perrier, *J. Am. Chem. Soc.* **2014**, *136*, 8018-8026.

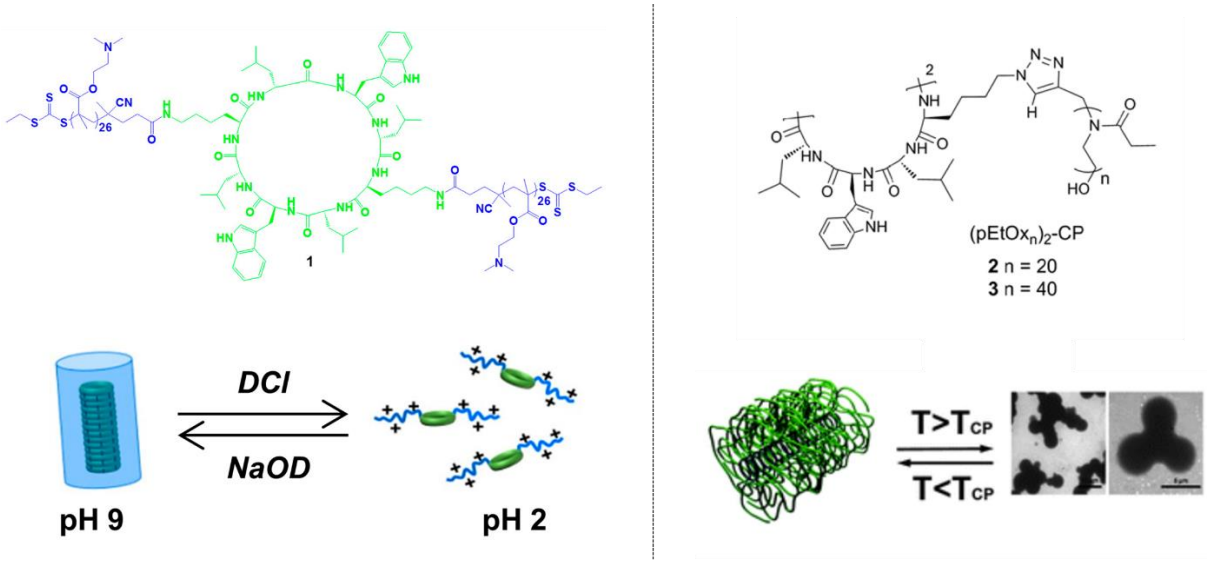

Figure 119. Left. Chemical structure (up) and schematic representation of the pH-responsive behavior of polymer-cyclic peptide conjugates. Reprinted with permission from ref. 370. Copyright 2016 American Chemical Society. Right. Chemical structure (up) and schematic illustration of the temperature-responsive behavior of polymer-cyclic peptide conjugates. Reproduced from Ref. 371 with permission from The Royal Society of Chemistry.

However, the reported approximations based on the attachment of thermoresponsive artificial polymers to cyclic peptides lack of a simple synthetic approximation that allows a deep tuning of the transition temperatures and a detailed study of the temperature effect on the SCPNs self-assembly. Furthermore, these hybrid materials normally show high cytotoxicity for biomedical applications. Therefore, the incorporation of peptide thermoresponsive moieties such as elastin into cyclic peptides would allow to develop fully biocompatible and thermoresponsive supramolecular materials in a simpler and tunable manner.

USC
UNIVERSIDADE
DE SANTIAGO
DE COMPOSTELA

Objectives

USC
UNIVERSIDADE
DE SANTIAGO
DE COMPOSTELA

The combination of supramolecular polymers and thermoresponsive peptidic moieties can lead to innovative approaches in the design of new thermoresponsive materials with improved capabilities. Such designed "smart" materials will have novel properties with potential use in a wide range of applications in the material and biomedical fields.

Therefore, the main objective of this third chapter is to design and synthesize CPs composed of eight amino acid residues with alternating chirality (*D,L*-α-CP) functionalized with a thermoresponsive elastin moiety. The elastin-modified cyclic peptides self-assemble into SCPNs driven by the pH will be studied as well as their thermoresponsive properties and their influence in the assembly process.

More in detail, the specific objectives of this third chapter will be as following:

- Design of different elastin-modified CPs:
  - Selection of building blocks:
    - Elastin sequence and anchoring possibilities
    - CP designs with pH-dependent assembly properties
  - Possible designs of elastin-modified cyclic peptides
- Synthesis of elastin-modified CPs.
  - Full synthesis vs convergent strategy
  - One arm CP by SPPS
- Self-assembly of the elastin-modified CPs
- Thermoresponsive properties of the elastin decorated SCPNs

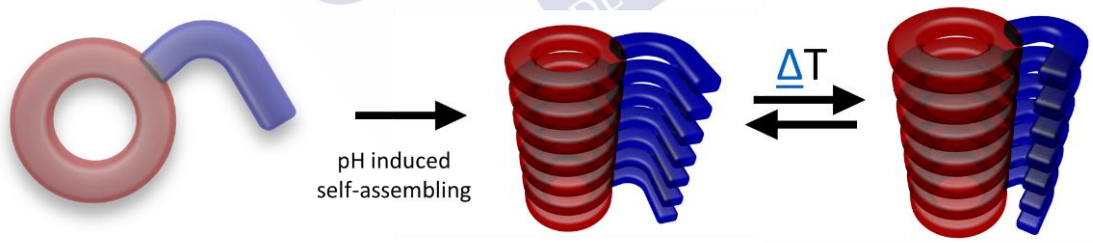

Figure 120. Schematic representation of the pH-driven self-assembly of the elastin-modified cyclic peptides and thermoresponsive behavior of the peptide nanotube.

USC
UNIVERSIDADE
DE SANTIAGO
DE COMPOSTELA

Results and discussions

USC
UNIVERSIDADE
DE SANTIAGO
DE COMPOSTELA

1. Design of elastin-modified cyclic peptides

1.1. Selection of building blocks

1.1.1. Elastin sequence and anchoring possibilities

The elastin canonical sequence can be attached to the CP by using the amino-terminal moiety of either the natural canonical sequence [**H**-(V-P-G-V-G-)OH][373] or its reversed configuration [**H**-(G-V-G-P-V-)OH]. These two approximations respect the proline turn, as well as the terminal free carboxylic acid, and thus both have identical thermoresponsive properties. Alternatively, further modifications of the elastin sequence could be carried out to further tune and study the thermoresponsivity of the assembled system.

Anchoring in Val (natural occurring orientation): The attachment through the terminal Val residue of the elastin sequence [**H**-(V-P-G-V-G-)OH] will allow us to situate the proline turn of the elastin closer to the CP scaffold. This configuration places the elastin's proline turn in close proximity (one residue distance) to the CP backbone and perhaps display a more efficient change in conformational properties that can be translated to the nanotube formation and properties.

Anchoring in Gly (reversed orientation): The attachment through the terminal Gly of the reversed residue of the elastin sequence place the proline turn of the elastin (3 residues) in a more distanced position relative to the CP scaffold but alternatively display the Val side chain more exposed to the aqueous media mediating more efficiently the water order around nanotube structure.

These two conjugation strategies will allow us to study the effect of the steric hindrance produced by the elastin's proline turn in both, the CP assembly process into SCPNs and in the expected thermoresponsive properties of the final assembly.

1.1.2. Cyclic peptide designs with pH-dependent assembly properties

We decided to design a base scaffold cyclic octapeptide (Scheme 1) whose sequence can be modified to adjust the pH-responsive assembly of the final CPs decorated with elastin. The base octapeptide will consist of nanotube forming derivatives composed by α-amino acids of alternating *L*,*D*-chirality. We expect that this design will carry out the assembly properties by adopting the flat conformation in which the amide groups (carbonyl and NH) are perpendicularly oriented perpendicular to the ring plane. At the positions of opposite chirality (D), we chose 2 non-polar residues of Ala to use the hydrophobic interactions to stabilize the nanotube and also 2 polar Ser residues to increase the solubility (Scheme 1).

Elastin anchoring into the cyclic peptide

In our original design, we planned to study the attachment of either one or two elastin arms. One arm elastin-modified cyclic peptides could be designed by attaching one elastin moiety in the R_1 position by using the desired sequence, VPGVG, or the reversed sequence, GVGPV. On the other hand, the two-arms elastin modified cyclic peptides were designed by attaching one elastin moiety in the R_1 position and the other in the opposite side R_3 position.

[373] All peptide sequences are represented from left to right from the N-terminus (**H**-) to the C terminus (-OH).

pH driven self-assembly

At the positions, R_2, R_3, and R_4, different pH-sensitive amino acids, i.e. His, Glu, Asp, or Lys, can be attached to modulate the pH required for the assembly/disassembly requirements.

- **Basic pH response:**

To achieve a basic pH response, we decided to incorporate into the cyclic peptide sequence (**CP1**) three pH-sensitive residues (2 His and 1 Lys). In this structure, the basification of the aqueous media will give rise to the deprotonation of the histidine side chains ($pK_a \approx 6.0$) that will lead to the formation of histidine-histidine hydrogen bonds, most likely mediated by a water molecule.[374] Moreover, the Lys side chains will be deprotonated to minimize the cationic electrostatic repulsions.

- **Neutral pH response:**

Alternatively, we also envisage incorporating into the cyclic peptide sequence (**CP2**) three pH-sensitive residues (2 Lys and 1 Glu). At neutral pH, the Lys side chains ($pK_a \approx 10.5$) will be deprotonated and the Glu side chain ($pK_a \approx 4.2$) will be protonated.[374]

- **Acidic pH response:**

We also planned the incorporation of three Glu residues to the cyclic peptide sequence (**CP3**). The acidification of the aqueous media will give rise to the protonation of the Glu side chains that will lead to the formation of hydrogen bonds.

1.2.Possible designs of elastin-modified cyclic peptides

Considered all the above-mentioned requirements, we have designed a library of elastin-modified cyclic peptides named **CPX** showed in Scheme 1. Moreover, the corresponding control peptides (**CP1**, **CP2,** and **CP3**) having a Glu residue instead of the elastin fragment have been also designed.

[374] D. L. Nelson, M. M. Cox, *Lehninger Principles of Biochemistry*, 5th edition, W. H. Freeman & Company, New York, **2008**.

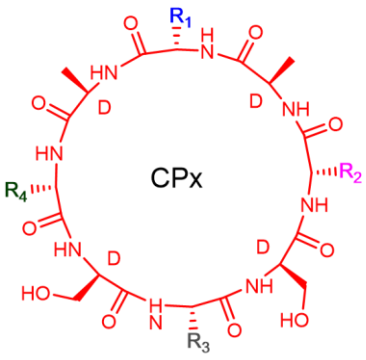

CPX	R1	R2	R3	R4	Self-assembly pH
CP1	-(CH2)2COOH		-(CH2)4NH2		Basic
CP1.1	-(CH2)2CO-VPGVG-OH		-(CH2)4NH2		Basic
CP1.2	-(CH2)2CO-GVGPV-OH		-(CH2)4NH2		Basic
CP2	-(CH2)2COOH	-(CH2)4NH2	-(CH2)2COOH	-(CH2)4NH2	Neutral
CP2.1	-(CH2)2CO-VPGVG-OH	-(CH2)4NH2	-(CH2)2COOH	-(CH2)4NH2	Neutral
CP2.2	-(CH2)2CO-GVGPV-OH	-(CH2)4NH2	-(CH2)2COOH	-(CH2)4NH2	Neutral
CP3	-(CH2)2COOH	-(CH2)2COOH	-(CH2)2COOH	-(CH2)2COOH	Acidic
CP3.1	-(CH2)2CO-VPGVG-OH	-(CH2)2COOH	-(CH2)2COOH	-(CH2)2COOH	Acidic
CP3.2	-(CH2)2CO-GVGPV-OH	-(CH2)2COOH	-(CH2)2COOH	-(CH2)2COOH	Acidic

Scheme 1. Left. General structure of the designed cyclic peptides. Right. Library of possible designs of elastin-modified cyclic peptides.

During the studies addressed in this thesis, we only had time to prepare two different elastin-modified cyclic peptides **CP1.1** and **CP3.1** in which the second number provide the information about the elastin orientation, 1 for the natural elastin segment and 2 for the reversed structure. We hypothesized that **CP1.1** would be able to self-assemble at basic pH while **CP3.1** at acidic pH.

2. Synthesis of elastin-modified cyclic peptides

2.1.Full synthesis vs convergent strategy

For the incorporation of the thermoresponsive elastin moiety to the cyclic peptide scaffold, we considered two different approaches, the full synthesis and also the convergent strategy. The full synthesis by SPPS (Figure 121) in which we could carry out both the attachment (and growth) of the elastin segment and the cyclization of the peptide on the resin in a single SPPS procedure. On the other hand, the convergent strategy (Figure 121) in which, first, we could carry out independently by SPPS the cyclization of peptide and the growth of the elastin segment on the resin in two different SPPS procedures. Then, the attachment of the elastin to the cyclic peptide could be carried out in solution at the last synthetic step leading to the target molecule.

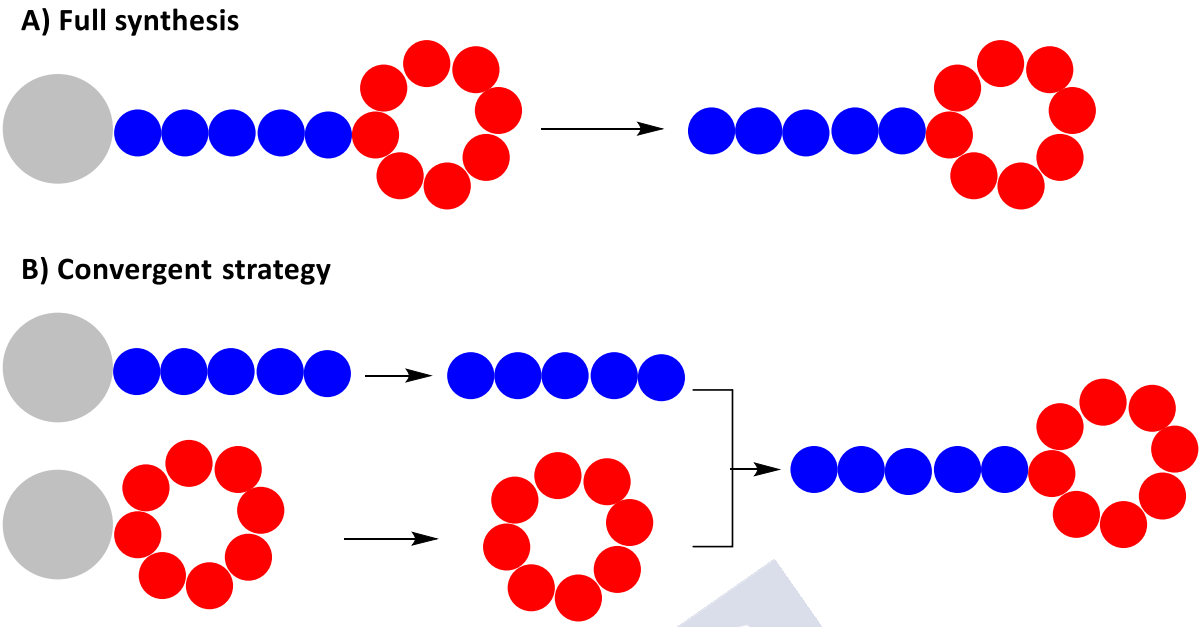

Figure 121. Schematic representation of the proposed strategies, the full synthesis (A), and the convergent strategy (B). Grey dots represent the resin used in SPPS, blue dots depict the amino acids of the thermoresponsive moiety VPGVG or GVGPV, while red dots represent the amino acids of the cyclic peptide.

Importantly, the full synthesis presents several advantages in comparison with the convergent synthesis such as: a) it is a single SPPS procedure that will allow higher yields of the final molecule; b) the cyclization will be more efficient due to the relative distance between the resin and the cyclization point when compared to a classical cyclization approach (cyclization point close to the resin); c) only a single purification step is required. For all these reasons, we decided to carry out a full synthesis by using SPPS instead of using convergent strategies for the preparation of one arm cyclic peptides such as **CP1.1** and **CP3.1**.

2.2.One arm CP by SPPS

One arm cyclic peptides (**CP1.1** and **CP3.1**) were prepared using a simple and elegant full synthesis by Fmoc solid-phase peptide synthesis (SPPS).[375] In general, the synthetic strategy consists in initially growing the linear elastin peptide on the solid support and then continuing growing the CP. With this purpose, a Glu would be attached to the N-terminus of the elastin first residue (Val) through its side chain. In this way, the cyclic peptide precursor could be grown on the resin and then cyclized before cleave form the solid support. The full synthetic methodology used for the synthesis of **CP1.1** and **CP3.1** is illustrated in Figure 122. We used 2-chlorotrityl chloride (CTC) resin because we needed to obtain a carboxylic acid group at the terminal carboxylic end of elastin due to its important role in its thermoresponsivity. For the synthesis, first, we attached the 5 amino acids of the elastin moiety (VPGVG) in the typical sequential way. Once the elastin fragment was finished, the cleavage of a small resin portion confirmed the preparation of the pentamer in high purity. Then, the Glu residue was attached through its lateral chain by using the α-carboxy and amino protected derivative (Fmoc-Glu-OAll). Deprotection of the Glu amino group allowed to grow the rest of the cyclic peptide in

[375] R. Behrendt, P. White, J. Offer, *J. Pept. Sci.* **2016**, *22*, 4-27.

the typical Fmoc/*t*Bu sequential way. This methodology also allowed to perform the cyclization of the linear peptide after the removal of the temporary orthogonal protecting groups (Fmoc and allyl) from the N- (piperidine treatment) and C-terminal ends (palladium π-allyl chemistry) of the peptide. Therefore, the allyl group was selectively removed by reaction with palladium acetate [$Pd(OAc)_2$] and triphenylphosphine (PPh_3), a well-known method for *in situ* generation of Pd(0) complex, and a nucleophile (4-methylmorpholine).[361] Then, the Fmoc protecting group was also removed under standard conditions. The cyclization was carried out by using PyAOP as the coupling reagent to provide the cyclic peptide in reasonable yields as determined by HPLC analysis of the crude mixture. The cyclization process was followed by cleaving small portions of the resin and analyzing the resulting solutions by HPLC-MS. Finally, we deprotected the temporary protecting groups, and we cleavaged the cyclic peptide from the resin obtaining the cyclic peptide modified with elastin.

[361] A. Méndez-Ardoy, J. R. Granja, J. Montenegro, *Nanoscale Horizons* **2018**, *3*, 391-396.

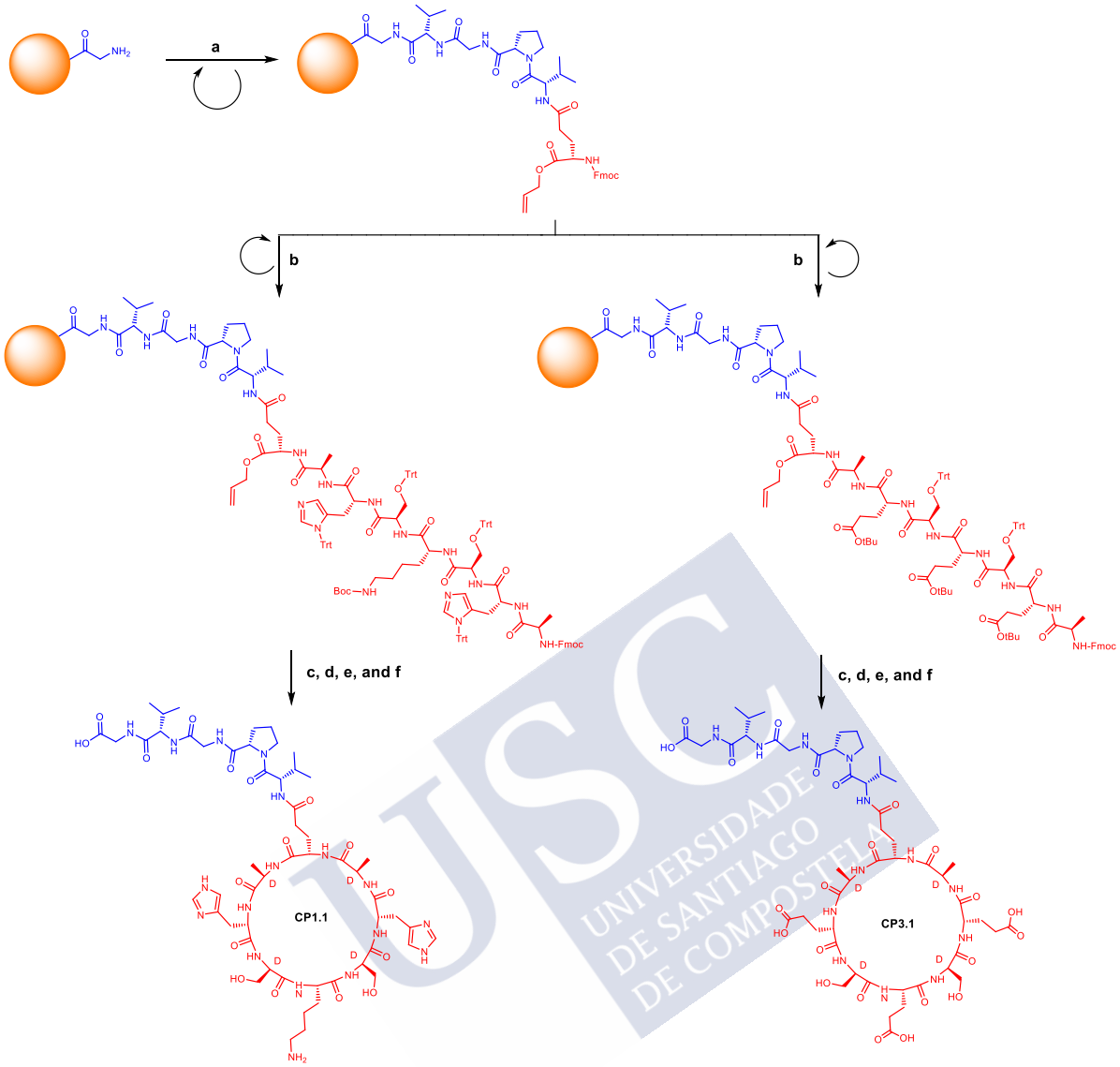

Figure 122. Structure and synthetic scheme for the synthesis of **CP1.1** and **CP3.1** by using direct SPPS. Conditions for the coupling of the first amino acid on CTC resin: *N*-α-(9-Fluorenylmethyloxycarbonyl)-L-glycine, DIEA, DCM, 2 h. a) Repeated cycles of Fmoc deprotection and coupling of the corresponding amino acid for growing the linear elastin moiety. b) Repeated cycles of Fmoc deprotection and coupling of the corresponding amino acid for the elongation of the CP sequence (left, **CP1.1,** and right, **CP3.1**). Fmoc deprotection conditions: piperidine/DMF (1:4), 30 min. Amino acid coupling conditions: amino acid (4 equiv), *N*-HBTU (4 equiv), DIEA, DMF, 45 min. c) Allyl group deprotection, conditions: $Pd(OAc)_2$, PPh_3, 4-methylmorpholine, phenylsilane, DCM, overnight. d) Fmoc group deprotection. e) Cyclization, conditions: PyAOP, DIEA, DMF, overnight. f) Removal of the temporary protecting groups and cleavage of the elastin-modified cyclic peptide from the resin, conditions: TFA-DCM-H_2O-TIS (9:0.5:0.25:0.25).

3. Self-assembly of elastin-modified CPs

Once we have synthesized both peptides **CP1.1** and **CP3.1**, we decided to study the pH-driven self-assembly. The analysis was carried out by using different techniques. We paid special attention to CD measurements, considering that nanotube formation should imply the formation of chiral excitons visible under the circularly polarized light.

- **CP1.1**

Once we have synthesized, purified, and characterized **CP1.1** by HPLC-MS and ^{1}H-NMR, we studied the self-assembly into nanotubes driven by basic pH in aqueous solution. For this, we carried out circular dichroism experiments. We prepared an aqueous solution of **CP1.1** at 1 mM concentration. pH was adjusted by adding small aliquots of NaOH (0.1 M) and HCl (0.1 M). CD measurements at basic and acidic pH and at different temperatures were carried out. We found a CD signal at 230 nm at basic pH but not at acidic pH (Figure 123). Unfortunately, we could not correlate this CD signal with cyclic peptide self-assembly at basic pH. Importantly, further techniques are needed to ensure the presence or the absence of self-assembly such as fluorescence experiments with thioflavin dye or microscopy experiments such as TEM or AFM.

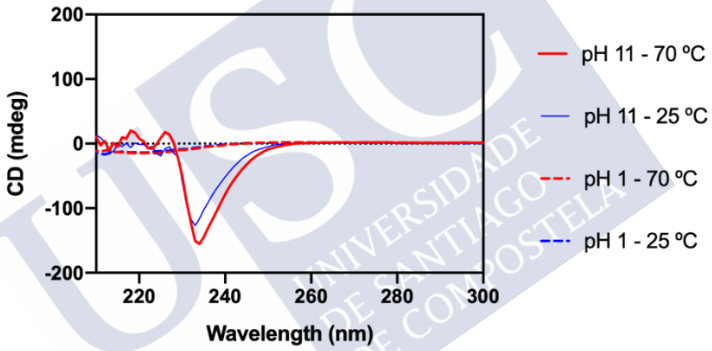

Figure 123. CD spectra of **CP1.1** at different pHs and temperatures.

- **CP3.1**

We tackle the study of the self-assembly of **CP3.1** into nanotubes driven by changing the pH of the media without further purification after the cleavage from the resin. Importantly, we decided to avoid the purification step not only due to the low solubility of this peptide but also because we clearly have a major peak whose molecular weight, as confirmed by HPLC-MS studies, coincide with the mass of the target compound. Therefore, to study the self-assembly of **CP3.1**, we followed the purification procedure described in the literature for the cyclic peptide with a similar sequence but without the elastin moiety.[350] The peptide hybrid was not very soluble under acidic conditions but was soluble at basic pH. Therefore, a small change of the Ghadiri original conditions was developed. Following this procedure, we prepared a suspension of 25 mg/ml of the peptide subunit and we basified adding NaOH to provide a clean and colorless solution. Subsequently, we acidified the solution by the addition of 1% trifluoroacetic in acetonitrile. Following the reported protocol, at this point, nanotube particles started to be formed as a white suspension over a period of hours. Then, the authors were able to collect the nanotubes by centrifugation. However, when we carried out the same procedure,

[350] M. R. Ghadiri, J. R. Granja, R. A. Milligan, D. E. McRee, N. Khazanovich, *Nature* **1993**, *366*, 324-327.

unfortunately, we did not observe the formation of any white precipitate that might suggest the absence of nanotube formation. We hypothesized that **CP3.1** is not able to self-assemble due to the proline turn of the elastin moiety is avoiding the formation of hydrogen bonds between cyclic peptides (Figure 124). However, further investigation is needed to ensure this hypothesis. Unfortunately, the lack of solubility did not allow continuing with the study of the structural properties of the supramolecular nanotubular polymer.

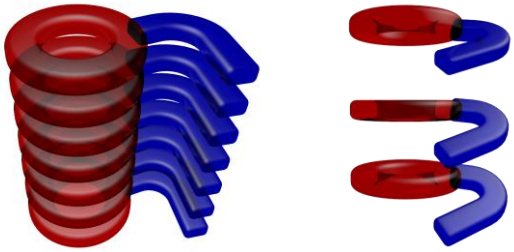

Figure 124. Left. Schematic representation of the self-assembly of **CP3.1** without the interference of the proline turn of elastin. Right. Schematic representation of the disruption of the self-assembly of **CP3.1** driven by the proline turn of elastin.

4. Thermoresponsive properties of the elastin decorated SCPNs

Finally, we decided to study the thermoresponsivity of the CP nanotubes by using turbidimetry experiments**.** We prepared an aqueous solution of **CP1.1** at 1 mM concentration. We adjusted the pH by adding small drops of NaOH (0.1 M). Unfortunately, we did not observe any variation of the % transmittance with the increase of the temperature at basic pH (Figure 125). Therefore, **CP1.1** did not show temperature-responsive behavior at basic pH using turbidimetry experiments. New designs and peptides should be prepared for continuing these studies. Unfortunately, the lack of time did not allow continuing with these studies.

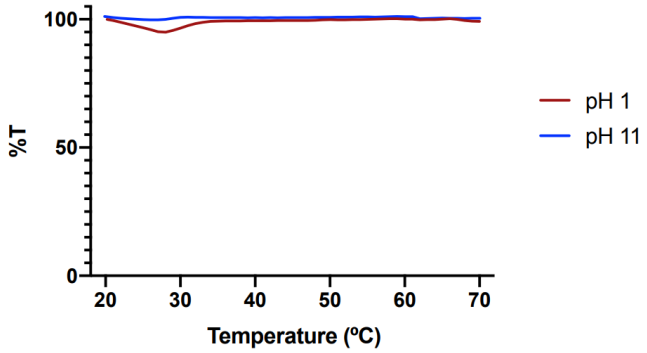

Figure 125. UV spectra of **CP1.1** at 1 mM concentration showing the variation of % transmittance with the temperature.

Conclusions

USC
UNIVERSIDADE
DE SANTIAGO
DE COMPOSTELA

In this third chapter, we have initiated a new program to develop thermoresponsive materials with nanotube shape. With this purpose, we have designed and synthesized two different cyclic peptides (**CP1.1** and **CP3.1**). **CP1.1** and **CP3.1** consisted of eight amino acid residues with alternating chirality (*D,L*-α-CP) functionalized with one thermoresponsive moiety, elastin. Furthermore, we have studied the self-assembly and the thermoresponsiveness of both elastin-modified cyclic peptides.

In this third chapter,

- We have studied the different alternatives to design elastin-modified cyclic peptides that could self-assemble into nanotubular structures driven by the modification of the pH.
- We have synthesized two different elastin-modified cyclic peptides (**CP1.1** and **CP3.1**) by using an elegant full solid-phase peptide synthesis in which the synthesis and cyclization of the *D,L*-fragment and the ramification and growth of the elastin-based fragment were implemented on a trityl resin in good yield. Furthermore, we have characterized **CP1.1** by HPLC-MS and ^{1}H-NMR experiments.
- Evaluation of the self-assembly capabilities of **CP1.1** at basic pH by using CD did not show a clear CD signal that can be correlated with the nanotube formation, further techniques are needed to carefully study the self-assembly of **CP1.1**.
- Preliminary studies of the self-assembly capabilities of **CP3.1** did not show clear evidence of the supramolecular process at acidic pH under previously reported purification conditions.
- Exploration of the thermoresponsiveness of **CP1.1** nanotubes did not give any indication of thermoresponsivity at the different pH and temperatures used at the turbidimetry experiments.

USC
UNIVERSIDADE
DE SANTIAGO
DE COMPOSTELA

Experimental section

USC
UNIVERSIDADE
DE SANTIAGO
DE COMPOSTELA

1. Materials and methods

Chemicals were purchased from Carbosynth, Iris Biotech, Sigma Aldrich, Alfa Aesar, Stream Chemicals, and Novabiochem and used without further purification.

The solvents for organic synthesis were of reagent grade. *N, N*-dimethylformamide, and trifluoroacetic acid were purchased from Scharlau, dichloromethane from Panreac, and acetonitrile from Merck. Water was deionized and purified on a Millipore Milli-Q Integral system.

Purification of products was accomplished using reversed-phase high-performance liquid chromatography (RP-HPLC) using an Agilent Technologies 1160 Infinity using H_2O (+ 0.1% TFA) and CH_3CN (+ 0.1% TFA) as eluents and a Luna (C18)-Phenomenex column.

High-performance liquid chromatography coupled with mass spectrometry (HPLC-MS) analyses were carried out on Agilent Technologies 1260 Infinity II associated with a 6120 Quadrupole LC-MS using an Agilent SB-C18 column with *Solvent A: Solvent B* gradients between 5:95 (*Solvent A*: H_2O with 0.1% TFA; *Solvent B*: CH_3CN with 0.1% TFA).

UV-Vis spectra were measured in a Biochrom Libra S60 UV-vis spectrophotometer. Circular dichroism spectra were acquired in a Jasco J-1100 CD spectrometer.

2. General protocol for the synthesis of elastin-modified cyclic peptides

Cyclic peptides were prepared manually using Fmoc solid-phase peptide synthesis. 2-Chlorotrytil chloride resin (2-CTC, 500 mg) was soaked in freshly distilled DCM (4 mL) for 30 min. The solvent was filtered off, and a solution of Fmoc-Gly-OH (0.4 mmol) and 348 µL of DIEA (2 mmol) in freshly distilled DCM (4 mL) was added to the resin. After 2 h, the solvent was filtered off and the resin was washed with DCM (4 mL). A mixture of DCM-MeOH-DIEA (8.5:1:0.5, 4 mL) was added and the resin was shaken for 1 h, then washed with DCM (3 x 4 mL) and diethyl ether (4 mL). The resin was dried under high vacuum and the loading was determined by quantification of the Fmoc group. For this, a small portion of the resin (ca 10 mg) was treated with a solution of piperidine in DMF (1:4, 2 mL) for 30 min. An aliquot of this solution (20 uL) is diluted to 1 mL DMF and the absorbance was read between 290-301 nm. The concentration of the dibenzofulvene-piperidine adduct is obtained by using the extinction coefficients tabulated in the literature.

A portion of resin (0.1 mmol) was used for the synthesis of the peptide. The Fmoc group was removed by treatment with piperidine/DMF (1:4, 2-3 mL) for 30 min. The resin was washed with DMF (6 mL) and then treated with a solution of Fmoc-protected amino acid (0.4 mmol), *N*-HBTU (151 mg, 0.4 mmol), and DIEA (0.1 mL, 0.6 mmol) in DMF (3 mL). The resin was shaken for 45 min and then washed with DMF (3 mL). The procedure was repeated with each corresponding amino acid. After the coupling of the last amino acid, the resin was washed with DCM (3 x 3 mL) and a solution of PPh_3 (39 mg, 0.15 mmol), N-methylmorpholine (110 µL, 1 mmol), and phenylsilane (120 µL, 1 mmol, 10 equiv) in DCM (2 mL) was added, and the mixture was bubbled with argon for 10 min. Then, a solution of $Pd(OAc)_2$ (6.7 mg, 0.03 mmol) in DCM (0.5 mL) was added dropwise and the resin was further bubbled with Ar for 2 min and the suspension was stirred overnight. The resin was washed with DCM (4 mL), DIEA in DMF (2% v/v, 4 x 4 mL), sodium diethyldithiocarbamate (0.5% w/v in DMF, 4 x 4 mL) and

DMF (4 x 4 mL). The resin was stirred with piperidine/DMF (1:4, 2 mL) for 30 min. Finally, it was washed with DIEA in DMF (2% v/v, 4 x 2 mL) and DMF (4 x 4 mL).

The cyclization was carried out by adding a solution of PyAOP (208 mg, 0.4 mmol) and DIEA (0.1 mL, 0.6 mmol) in DMF (3 mL), and the suspension was stirred for 12 h. After washing with DMF (3 mL), the reaction was repeated twice in the same conditions. Finally, the peptide was released from the resin by treatment with a freshly prepared TFA cocktail (TFA-DCM-H_2O-triisopropylsilane, 0.9:0.05:0.025:0.025, 1 mL/40 mg resin) for 2 h and then filtered. The resin was washed with TFA (0.5 mL) and the combined fractions were evaporated to 1-2 mL by bubbling argon. The concentrated solution was added dropwise to cold diethyl ether. The resulting precipitate was centrifuged for 10 min at 3000 rpm. The supernatant was discarded, then fresh diethyl ether was added, and the suspension was sonicated and centrifuged. The resulting solid was dried under vacuum.[361]

3. Characterization of CP1.1

The synthesis of the **CP1.1** was performed following the above methodology. **CP1.1** was obtained after RP-HPLC purification [Phenomenex Luna C18(2) 100A column, H_2O (0.1% TFA)/ CH_3CN (0.1% TFA) 95:5→5:95 (5→35 min)]. R_t 10.4 min [RP-HPLC Agilent SB-C18 column, H_2O (0.1% TFA)/ CH_3CN (0.1% TFA) 95:5→5:95 (0→21 min)] (Figure 126). ^{1}H-NMR (300 MHz, D_2O) δ: 8.97 (2H, s), 7.65 (2H, bs), 4.96-4.56 (water overlapped, m), 4.40-4.0 (13H, m), 3.88 (2H, q, $J_{H,H}$ = 6.0 Hz), 3.75-3.40 (6H, m), 3.30 (2H, t, $J_{H,H}$ = 7.0 Hz), 2.65-1.9 (42H, m), 1.84-1.44 (12H, m), 1.53 (2H, t, $J_{H,H}$ = 7.1 Hz), 1.29 (14H, m). MS (ESI, H_2O): 420 $[M+3H]^{3+}$, 629,5 $[M+2H]^{2+}$, 1258,6 $[M+1H]^{1+}$.

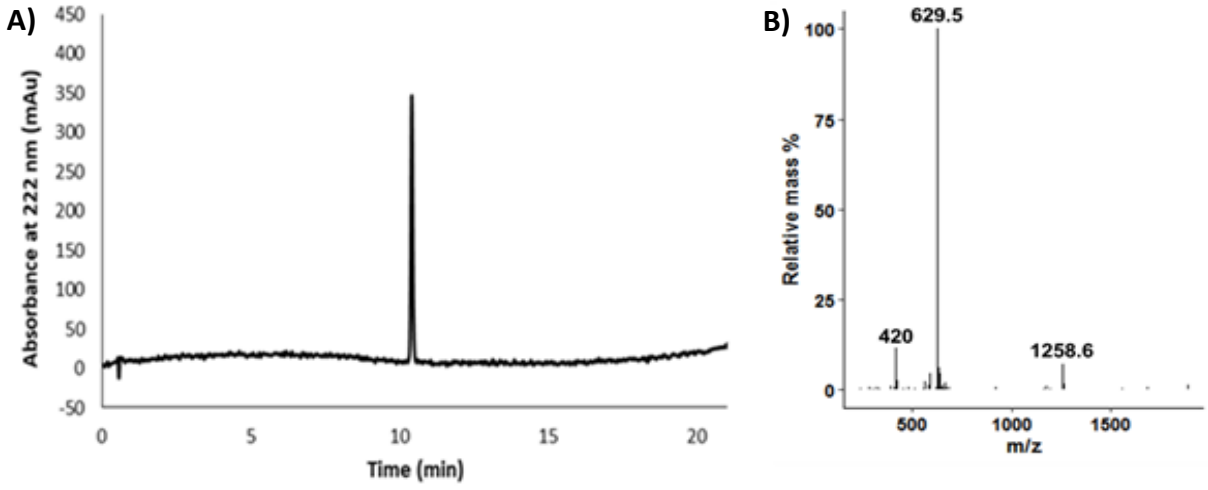

Figure 126. Representation of the HPLC-MS for **CP1.1.** A) HPLC chromatogram (λ_{abs} = 222 nm) and B) ESI-MS recorded at 10.4 min of **CP1.1**.

[361] A. Méndez-Ardoy, J. R. Granja, J. Montenegro, *Nanoscale Horizons* **2018**, *3*, 391-396.

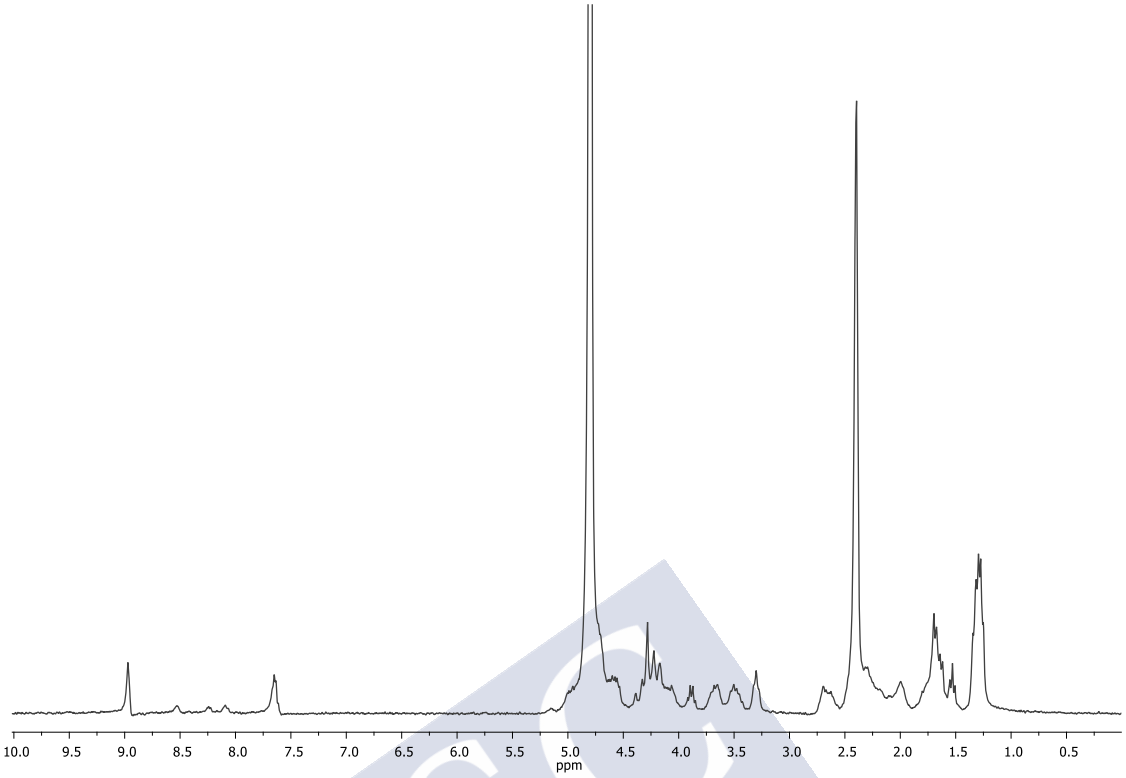

Figure 127. ^{1}H NMR (300 MHz, 273 K) of **CP1.1** in D_2O.

4. Self-assembly of CP3.1.

The self-assembly of **CP3.1** without further purification was carried out following the protocol previously reported in the literature.[350]

5. UV-visible experiments

Data were collected at different temperatures from 20ºC to 70ºC and in a 2 mm light path quartz cuvette after subtraction of the solvent background signal. A concentration of 1 mM **CP1.1** was fixed. pH was adjusted by adding small aliquots of NaOH (0.1 M) and HCl (0.1 M). The pH was measured using a drop pH-meter and solutions were equilibrated for 10 min prior measurements.

6. Circular dichroism experiments

Circular dichroism spectra were acquired in a Jasco J-1100 CD spectrometer. Data was collected at 25ºC and 70ºC in a 2 mm light path quartz cuvette after subtraction of the solvent background signal. In all the experiments, a concentration of 1 mM **CP1.1** was fixed. pH was adjusted by adding small aliquots of NaOH (0.1 M) and HCl (0.1 M).and the pH was measured using a drop pH-meter. Solutions were equilibrated for 10 min prior measurements.

[350] M. R. Ghadiri, J. R. Granja, R. A. Milligan, D. E. McRee, N. Khazanovich, *Nature* **1993**, *366*, 324-327.

USC
UNIVERSIDADE
DE SANTIAGO
DE COMPOSTELA